BIOLUMINESCENCE,

the NATURE of the LIGHT

"Experiment, is the interrogation of Nature" *Robert Boyle 1665*

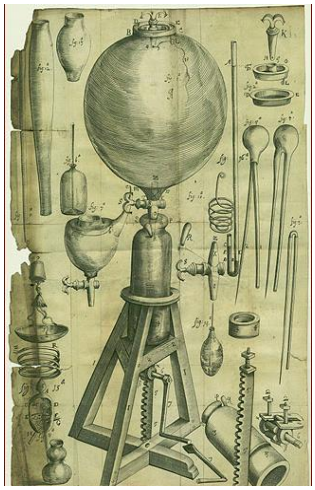

FROM: Robert Boyle. New Experiments Physico-Mechanicall: Touching the Spring of the Air and its Effects (1660)

John Lee

The University of Georgia

2017

This is the fifth update of this book first deposited in 2014 in the digital library collection Atheneum@UGA:

http://athenaeum.libs.uga.edu/xmlui/

The most recent edition can be downloaded here:

http://hdl.handle.net/10724/20031

http://www.bmb.uga.edu/directory/john-lee

National Library of Medicine

http://www.ncbi.nlm.nih.gov/nlmcatalog/?term=101675046

April 2017

CONTENTS

1. **History. Bioluminescence and the Theory of Light**

"*And the angel of the LORD appeared unto him in a flame of fire out of the midst of a bush; and he looked, and, behold, the bush burned with fire, and the bush was not consumed.*" EXODUS 3:2.

Among many speculations about Moses and the "burning bush" one is that the "flame" was from an infection of bioluminescent fungi on the decaying leaves, meaning that Moses should be credited with the first published report (~1450 BCE) of a bioluminescence! Another thousand years passed before the existence of records of the more reliable observations by the natural philosophers of Ancient Greece, many having an intense interest in the nature of visible light, and another two thousand years before Isaac Newton's postulate of the corpuscular theory of light. It was evident to the Ancients that light took many forms, a hot light from the sun, fire, and oil lamps, light without any warmth from the heavenly bodies, and the cold luminescence emanating from many living creatures. Euclid (*Optics*, 300 BCE) disputed an earlier theory that light rays came from the eye, instead insisting that light originated in the object itself, based on his observations that light traveled in straight lines and of the laws of reflection.

In contrast to the highly illuminated environment we inhabit at this present day, even until the last few hundred years most of humanity lived at least a third of the day in darkness. The result of efficient dark adaptation of the eye was to allow ready detection of the self-luminescence from the many terrestrial forms of bioluminescence, fireflies and glow-worms, rotting wood, and of the light from agitated sea-water as well as from many marine creatures. Written reports remained fragmentary up till the time of Aristotle (384-322 BCE), who was the first to recognize the self-luminosity of organisms and that it was not accompanied by heat. Aristotle wrote about the glow from dead fish or flesh now known to be from an infection by bioluminescent bacteria, and the light generated on disturbance of sea-water, and of fireflies and glow-worms.

Pliny the Elder (23-79 CE) in his *Naturalis Historia*, wrote quite detailed descriptions of many bioluminescent animals: glowworms and fireflies, the luminous mollusk *Pholas dactylus* (a Roman delicacy), the purple jellyfish *Pelagia noctilus* common in the Mediterranean, the lantern fish, and the fungi, glowing wood and mushrooms (Fig. 1.1).

In the period following the fall of the Roman Empire (*ca.* 500 CE) very few new reports of bioluminescent organisms can be found. Even though progress in scientific investigation continued elsewhere, in Arabia, India, and China, little interest in the theory of light or particularly the nature of animal light, seems to be evident from any written records. Perhaps the history of science in these areas has not received sufficient attention, even in the scholarly work on the *History of Science in China* by Joseph Needham.

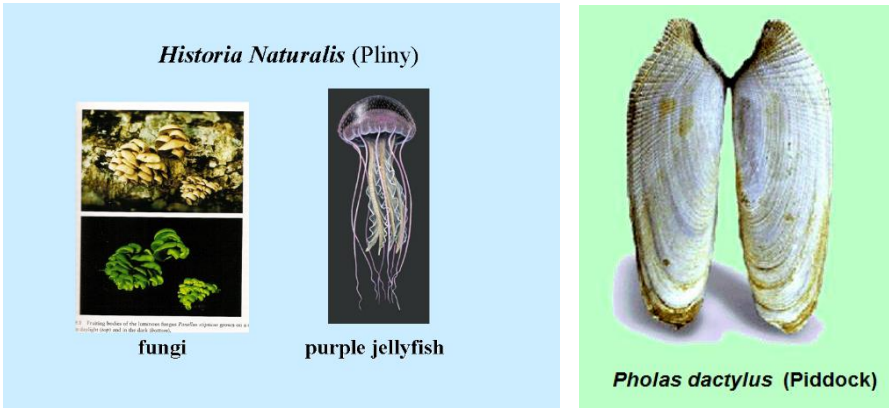

Figure 1.1. Some bioluminescent organisms described by Pliny the Elder (23-79 CE).

The book *De Animalibus* published in1478, was a collection of the works of Albertus Magnus (1206-1280 CE), a German monk, but although he described and cataloged many luminous species, not much was added to Pliny the Elder's earlier list. Of particular interest, Magnus claimed that it was possible to make extracts of fireflies, *Liquor Lucidus* that produced a permanent luminescence. Later investigators in following centuries were unable to reproduce Magnus's results, so cast doubt on his discovery. We have to leave open the attribution of the first *in vitro* extract of bioluminescence therefore, until almost 800 years later, until the experiments of Raphaël Dubois in Paris.

The time of the Renaissance in Europe, in the few hundred years before the end of the 15th Century, saw a revival of learning as well as an increase in maritime exploration and trade. Voyagers brought back reports of "burning seas" probably the phenomenon now called "milky seas" suggested to be due the bioluminescent marine bacteria. Christopher Columbus (1492) referred to mysterious lights in the sea nearby San Salvador, probably from the marine worms *Odontosyllis* known to inhabit these Caribbean waters. Oviedo (1478-1557) in Spain, published extensively on the natural history of the New World. He described the elaterid ("click") beetle *Pyrophorus*, bioluminescent caterpillars, and railroad worms (*Phrixothrix*) (Fig. 1.2). Tropical fireflies in the East Indies were also seen by Sir Francis Drake (1540-1596).

Conrad Gesner (1516-1565), Professor of Natural History and Medicine in Zurich, is credited with writing the first book devoted to luminescence, *De Lunariis* (1555). This book was a collection of all observations going back to ancient times, of bioluminescent animals and also of luminous stones. He listed several marine bioluminescent species and the terrestrial forms, fireflies, caterpillars, luminous wood and flesh. For scholars, the 16th Century was a period of collecting and reporting of natural phenomena such as bioluminescence, with little attempt at explanation. The value of "experimentation" was not yet ready to be realized.

Firefly *Phrixothrix* *Pyrophorus*

Figure 1.2. Representatives of the three families of bioluminescent beetles: Firefly, railroad worm, click beetle. (*V.R.Viviani*).

The 17th Century is known as the age of the "Science Revolution". Up till 1600 CE, as a consequence of the increase in exploration and commerce, there was a demand for reliable and predictive knowledge that required development of an objective methodology for discovery. Also, there were advances in technology, such as the invention of the telescope and the microscope, enabling the astronomical discoveries of Galileo (1564-1642) and of van Leeuwenhoek (1632-1723) in microbiology. The air pump, improved by Boyle (1627-1691) and his able assistant Hooke (1635-1703), led to landmark observations in bioluminescence and many related phenomena.

The foundations of the scientific method at this time were laid by the writings of Sir Francis Bacon (1561-1626) in England and Renee Descartes (1596-1650) in France. Bacon proposed that true knowledge is to be obtained by first collecting a sufficient number of carefully observed and verifiable particulars, or instances. Then one could propose a modest generalization or axiom, from which a direction for collecting more observations would be indicated. He emphasized that it was important to find new instances whereby the axiom could be refuted, because this would suggest that a better axiom was needed. Bacon recorded observations of triboluminescence for example but never developed any theory of light, indeed in the Baconian system, establishing hypotheses is not considered so important. In contrast, the doctrine espoused by Descartes was that a Grand Theory was essential in Science, from which deduction from such a grand Principle is used to arrive at a particular instance. Descartes did propose a theory of light, first he dismissed the idea that space could be a vacuum, instead he imagined it to be a plenum of contiguous particles, all jostling and crowded together. He thus deduced that light originated from the friction of particles rubbing together as observed for triboluminescence, and that light is transmitted by one particle pushing against the next. Light from sea-water he proposed, arose from vigorous disturbance by the oars of the boat, and the light from fish due to particles of salt penetrating the pores. Workers of the French school followed Descarte's generalization and put forward similar explanations for other bioluminescence phenomena.

By the end of the 17th Century the Theory of Light had divided into opposing views, the wave theory of Hooke and Huygens, and that light consisted of particles, an idea more associated with Newton (1642-1727) than Descartes. Due mainly to the dominant reputation of Newton,

his corpuscular theory remained unchallenged for almost 150 years, when it was clearly incompatible with the diffraction experiments of Young and the work of Fresnel.

Kircher (1602-1680), a German Jesuit priest, applying the Baconian principle, collected and tabulated many new observations of bioluminescent phenomena. He noted that in fireflies, the light would dim on handling the insect, and then reappear if left alone. Many of the insects placed together would display "ostentatiously". Kircher conjected (the axiom) that the light was in order to be seen and extended this idea to the function of bioluminescence in fish in the darkness of the ocean, that it was similar to the function in fireflies, for communication. Kircher's suggestions we now know to be essentially correct. He even made experimental observations showing how the luminescence on some organisms such as the clam *Pholas dactylus*, could be rubbed off on a stick. He also was unable through many variations, to produce an indefinitely glowing extract from firefly light organs (photophores), concluding that the *Liquor Lucidus* claim of Magnus was demonstrably false. In 1798, Carradori observed that the firefly photophore could be excised and dried whereupon the emission ceased, but would revive again with water. Later workers reported that the dried material could be kept for long periods and emission could occur on moistening. Perhaps we can give some credit to Magnus for making the first extract of bioluminescence, but not for the claim of a permanent glow.

Robert Boyle was a strong believer in the Baconian system, collecting and categorizing results both positive and negative without intention to formulate any grand theory according to the philosophy of Descartes. Boyle is best known for experiments establishing "Boyle's Law", the inverse relation of pressure and volume of a gas. Unusual for that time, the experimental observations for the first time were published in a table listing the quantitative values of pressures and volumes. Boyle and Hooke constructed an improved version of the air pump for the purpose of investigating the properties of air. Just as Galileo made many discoveries with the newly invented telescope, Boyle utilized state-of-the-art technology to gain novel results and insight into natural phenomena. Boyle was well aware of reports of both inorganic and animal light. With his efficient air pump Boyle recorded that removal of air over iron heated to red hot emission was without effect, whereas for a candle flame or a glowing coal, the luminescence was extinguished and did not recover on readmission of air. A live mouse died in the absence of the air and also did not recover on readmission of the air. In contrast, for a piece of shining wood or a glowworm, the light only dimmed, and then exuberantly generated a glow on readmitting the air into the test chamber. We now know that these last observations are due to the general requirement in bioluminescence reactions of oxygen, which was not identified as a constituent of air for another 100 years. Oxygen is an essential requirement for respiration of living creatures and for bioluminescence. The light from most bioluminescent systems may only dim and not extinguish, because extremely small amounts of oxygen still support the light reaction, and if oxygen is removed for some short period, the reaction precursors build up and produce a burst of reaction to luminescence when the air, or oxygen is reintroduced.

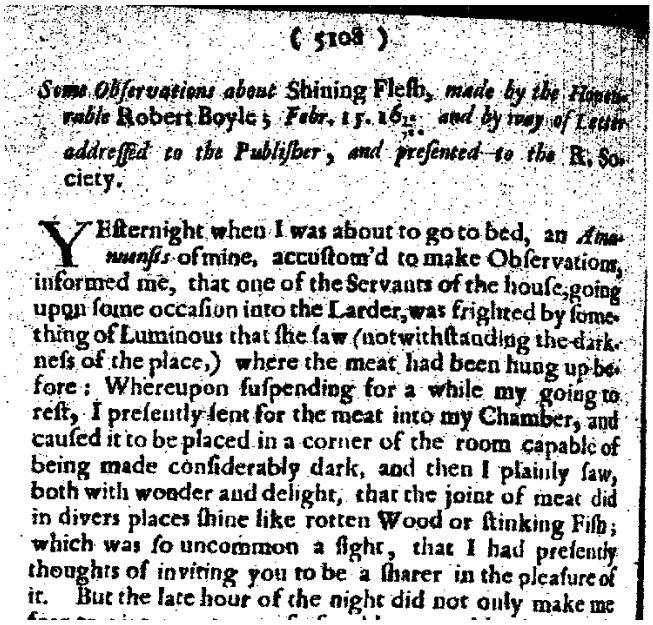

(5108)

Some Obſervations about Shining Fleſh, *made by the Honourable* Robert Boyle; *Febr.* 15. 167⅛. *and by way of Letter addreſſed to the Publiſher, and preſented to the* R. Society.

YEſternight when I was about to go to bed, an *Amanuenſis* of mine, accuſtom'd to make Obſervations, informed me, that one of the Servants of the houſe, going upon ſome occaſion into the Larder, was frighted by ſomething of Luminous that ſhe ſaw (notwithſtanding the darkneſs of the place,) where the meat had been hung up before: Whereupon ſuſpending for a while my going to reſt, I preſently ſent for the meat into my Chamber, and cauſed it to be placed in a corner of the room capable of being made conſiderably dark, and then I plainly ſaw, both with wonder and delight, that the joint of meat did in divers places ſhine like rotten Wood or ſtinking Fiſh; which was ſo uncommon a ſight, that I had preſently thoughts of inviting you to be a ſharer in the pleaſure of it. But the late hour of the night did not only make me

Figure 1.3. *From:* Boyle, Robert. (1672) Some Obfervations about Shining Flefh. Phil. Trans. R. Soc., Lond. 7: 5108-5116.

Boyle performed and published the results of so many seminal experiments that led him to propound the maxim that "Experiment, is the interrogation of Nature". The influence of Boyle's philosophy was such that subsequent scientific work became highly experimental, and the 18th Century became what is called "The Age of Experiment". This period saw investigations into the properties of electricity, magnetism, light and importantly, the discovery of oxygen, attributed to Priestly in England, Lavoisier in France, and Scheele in Germany. At that time, oxygen was called "deflogisticated air" because of a current theory that a chemical substance called "phlogiston", escaped when a compound was burned. In the History of Science, this is regarded as a "dead-end theory" and it was eventually overturned by the precise measurements of mass changes on combustion. This led to insight into the nature of combustion as a chemical reaction with oxygen, and the realization that respiration and bioluminescence could be related processes.

The air pump experiments of Boyle were repeated and the results verified. Forster in Copenhagen, observed control of the firefly flash by removal and readmission of air to the insect. Spallanzi in Italy, showed that removal of air dimmed the light from glowing wood or a bioluminescent squid, and readmission of air caused an even brighter luminescence than before. He found the light to disappear under nitrogen, hydrogen, or carbon dioxide ("fixed air"). He concluded that bioluminescence was in the nature of a slow burning.

In this time period there were two discoveries important to the science of Biology, resulting from studies of bioluminescence. The first was that the luminous material from the clam *Pholas* could be scraped out, made into a paste with flour, kept for a year, then the light reconstituted on adding water. The luminous material from the jellyfish also could be dried and the light returned on adding water. This meant that the principle responsible for light emission was dissociable from the living animal, it was not a *vital* process, and that it was a

reaction able to take place just in water, separate from the organism. Perhaps other vital functions, essential for the living state, might be of the same nature and able to be studied *in vitro*? In other words, this idea later became the foundation of the field of Biochemistry.

Figure 1.4. The sparkling light from sea-water is due to bioluminescent dinoflagellates. *Night Hauling, by Andrew Newell Wyeth (1917-2009). Bowdoin College Museum of Art*.

The second discovery concerned the nature of light in the sea. In the latter half of the century with a plethora of bioluminescent creatures being identified in the top layers of the ocean, jellyfish and other animals down to the size of crustaceans, there was effort given to the study of sea-water samples under magnification. Copepods were found in abundance and other "sea-worms" and eventually, even "sea-insects" were visible under the primitive microscopes available at that time. It was concluded therefore, that the origin of "sea-light" or what is still due to Charles Darwin commonly called "ocean phosphorescence", was indeed from tiny organisms, "animacules". It took another 50 years before this bioluminescence could be proven to be mostly from dinoflagellates and other plankton. These observations around that time, led to the suggestion that other bioluminescence phenomena, in particular that of glowing wood or glowing flesh, might also have a similar microscopic origin.

Modern Science can be said to arise by the beginning of the 19th Century, a result strongly dependent on the Industrial Revolution in Europe and England. Up to this time, observations such as the air pump experiments were still quite controversial, mainly due to the lack of reliable equipment and other technologies that hindered obtaining accurate results. The air pumps leaked and were inefficient, and it was not realized just how small the amounts of oxygen were that could optimize bioluminescence emission. Improvements in fabrication of optical components led to microscopes of higher magnification, and the main source of ocean phosphorescence was finally identified as from dinoflagellates. Physical optics now became the tools of the physicists, with spectroscopic technology, good prisms and diffraction gratings, leading to new approaches to investigating the nature of light. Newton's corpuscular theory was no longer in favor following the interference and diffraction experiments of Thomas Young. Light was instead believed to consist of waves occurring in a space-filling

"ether", the original "plenum" concept of Descartes. It was another 100 years before the concept of the ether was overturned and the wave-particle duality theory of light established.

With increased specialization of investigators, the physicists with their refined optical instruments and the chemists who were starting to uncover the stoichiometry and other properties of chemical reactions, the study of animal luminescence became more the prerogative of the biologists. A number of suggestions were made about the biological function of bioluminescence, for the dinoflagellates their flash on disturbance to deter predators, for fireflies a male-female communication or courtship, ideas that remain substantially correct today. Microscopic observation of dinoflagellates also revealed the bioluminescence to be localized in discrete particles floating in the cytoplasm; in recent times these have been labeled "scintillons". In most organisms bioluminescence could be stimulated in various ways, by shaking, adding chemicals, electrical shock, evidence that their bioluminescence was under neuromuscular control. Classification of bioluminescent organisms was pursued intensively, because it was a highly accessible observational technique especially with the advantage of improved microscopes.

Another major advance in the 19th century was the improved technology of ocean-going vessels. This increased the ability for world exploration and the collection of specimens. Among some well-outfitted scientific cruises probably the most well-known is Charles Darwin's voyages on the *HMS Beagle* (1831-1836) and the expeditions of the *HMS Challenger* (1872-1876).

Most terrestrial bioluminescent organisms were well identified by the 1800's with a few additions from scientific expeditions. It was already evident that the number of bioluminescent marine organisms exceeded those occurring terrestrially, thus stimulating interest in mounting research cruises. Darwin recorded observations of bioluminescence but remarked that it presented a difficulty in his theory of the origin of species by natural selection, since intermediate forms leading to adaptation could not be found, so he conveniently deleted these instances in later editions of his *Origin of Species*. In the latter half of the 19th Century, technologically advanced research cruises had been collecting at greater ocean depths, below 200 m, with a rich harvest of new organisms for investigation. Such probing continues to this day.

Insight into the nature of chemical reactions was developing rapidly in the early 1800's. In 1877, the first glowing chemical reaction was discovered, the chemiluminescent oxidation of an organic compound, lophine. This led to the proposal that bioluminescence was some form of chemiluminescence occurring within the animal. The work of Dubois a few years later in Paris (1885), verified this idea completely. Dubois made a paste of the luminescent material from the clam *Pholas* and suspended this in cold water. He divided the resulting solution into two parts, one part heated until it ceased glowing, then recooled. After waiting for the other part in the cold water to cease glowing, he mixed the two parts together, and light emission started up again. Dubois carried out the same experiment with an extract from the photophore (light organ) of the Jamaican click-beetle *Pyrophorus*, which similarly produced *in vitro* bioluminescence from a hot-water cold-water reaction.

Dubois concluded that the bioluminescence was chemical in nature. Being aware of the studies of fermentation and the notion of "enzymes", he thought that the cold water extract was an enzyme and accordingly, he introduced the name "luciferase", in line with the nomenclature of an enzyme acting on a substrate the heat stable solution, which he named "luciferine". These names became imbedded in the literature, except the substrate name "luciferin" is now used for the active organic molecule being oxidized, whereas the hot water extract of *Pholas* now named "Pholasin", happens also to be a protein, to which the smaller organic molecule, the genuine Pholas luciferin is bound. Dubois' experiment worked because pholasin although a protein, is just more thermally stable than Pholas luciferase. It also is now known that the hot water extract of *Pyrophorus* turned out not to be click-beetle luciferin, which is the same chemical as firefly luciferin, but adenosine triphosphate (ATP), a required coenzyme in the bioluminescence of the beetle family. It is also now realized that these terms luciferase and luciferin are generic, the chemical structures and properties being different among the bioluminescence types, the clam, beetles, jellyfish, etc.

Dubois followed by many others, continued using these techniques of hot-water cold-water extract reactions for many years. Harvey in the early 20th Century, also took up these studies and included a more detailed investigation of the requirement of oxygen. Many types of organisms were investigated. On a microscopic examination of "shining wood", Heller (1853) determined with certainty, that fungal threads (mycelia) growing on the wood were the source of the luminescence. This discovery implied the same origin for the bioluminescence of mushrooms. Heller is also credited with establishing the bacterial origin of "shining flesh" and the luminescence of putrefying fish. He showed that one could wipe off the luminescence and inoculate the skin of a dark fish and render it bioluminescent. In the later part of the 1800s as the field of microbiology developed, pioneers in this field of study, Pluger, Beijerinck, Giard, Ludwig, and others, made many studies of bacterial bioluminescence, classifying and characterizing these bacteria, and identifying their parasitic and symbiotic habitats. In neither of the cases of fungal nor bacterial bioluminescence, was a bioluminescence reaction of hot-cold water extracts, successful at that time.

2. **Bioluminescence to 1950. Biology, Biochemistry, and Physics**

"Those who cannot remember the past are condemned to repeat it". George Santayana (1905).

The study of bioluminescence was not completely left in the hands of the biologists in the 19th Century. Of concern to the physicists was the question of why bioluminescence was a cold light in contrast to the considerable heat accompanying light emission from combustion, as from the gas light or from incandescence. Even though the quality of physical optics was not sufficient for accurate spectral measurement, a prism spectroscope examination of the firefly color was first made by Murray as early as 1826. Spectral experiments (Lehmann, Schnauss, Pasteur) in the1860s, established that the bioluminescence from the click beetle *Pyrophorus*, was composed of a mixture of colors ranging from the purple through red, meaning that it was covering the same visible range as the sensitivity of the human eye. This was confirmed by subsequent workers, with the additional conclusion that there was no contribution at all from ultra-violet or infra-red radiation. As instrumentation became more precise, it was also shown that the broad bioluminescence spectra from different types of beetles differed in spectral maximum, as could be discerned even by the naked eye as a range in color from green through orange. Ludwig (1884) established the bacterial bioluminescence spectrum as also being broad and continuous, with contribution from the violet to yellow. McDermott (1911) absolutely verified an absence of any contribution in the ultra-violet.

A significant practical implication of these spectral results as already indicated by the cold-light property was not lost on the scientific community at that time. Bioluminescence was advertised as a possible remarkably efficient source of illumination, "the cheapest form of light". It can be suggested that in this regard, the phenomenon of bioluminescence played a role in the development of the modern Theory of Light. A young German engineer by the name of Max Planck, was employed to research means of making incandescent light bulbs more efficient. An incandescent source like the light bulb filament or the sun, was known to have a spectral distribution extending from the visible well into the infra-red, the latter contributing the wasteful emission of heat. The incandescent spectral maximum was dependent on the source temperature, and the spectral distribution could be fitted to an equation developed from Maxwell's (1865) monumental theory of electromagnetism. One expression accounting for the variation of the spectral wavelength maximum (λ_{max}) on absolute temperature *T*,

$$\lambda_{max} T = \text{constant},$$

was derived by determining the maximum of the black-body power distribution *B* by differentiation of the Wien Displacement Equation for a so-called "black-body",

$$B(\lambda, T) = A\lambda^{-5}\exp(C\lambda T)^{-1},$$

where A and C are constants. These equations and others similarly derived from the Maxwell theory, accounted quite well for most of the spectral distribution of the black-body spectral curve, but ran into an embarrassing difficulty in that the total energy obtained by integration

over all wavelengths was infinite, certainly not consistent with the obviously limited energy output.

The reader may verify this easily by using an on-line integration calculator to determine the zero to infinity integral. Planck (1900) made the somewhat arbitrary decision to make the equation behave by adjusting it to become zero below a certain short wavelength. On this basis, he derived a new equation that fitted the black-body emission perfectly without the infinity embarrassment.

$$B(\lambda,T) = A\lambda^{-5}\exp[(C\lambda T)^{-1} - 1]^{-1}.$$

The integral zero to infinite wavelength, is complex but may be verified that it comes to a definite value by polynomial expansion. Planck's notion was, that there had to be no light emitted with an energy above a certain value, i.e., implying a specific "packet" size for light from a black-body at temperature T, a reversion to the corpuscle theory of light. He related the energy *E* of the packet or quantum, directly to the energy or frequency of the light *v*, or inversely to the wavelength λ, by the now well-accepted Planck equation:

$$E = hv = hc/\lambda$$

where *h* is "Planck's constant" and *c*, the velocity of light. It is said that Planck did not appreciate the revolutionary nature of his suggestion until a few years later, when Einstein (1905) introduced the concept of the photon as explaining on the basis of Planck's energy packets, the experiments on the photoelectric effect showing that there was a specific minimum energy required for photo-ejection, which could not occur at longer wavelengths even at high light intensity.

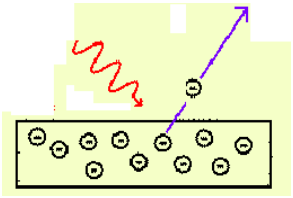

Figure 2.1. The photoelectric effect. A light wave (or photon) impinging on a metal surface may cause an electron (blue) to be ejected only if it has a sufficient minimum energy.

To restate these two ideas, from an incandescent body no light having an energy greater or wavelength shorter, than a certain value is emitted, and the opposite case in photoemission, that the photon energy has to be greater than a certain value to eject an electron. Large numbers of photons of lower energies cannot add up to eject an electron, meaning that there is a one photon-one electron correspondence. This is the basis for the Stark-Einstein Law of Photochemical Equivalence (Chapter 5), relevant to understanding all photon-molecule interactions, especially including the ones in bioluminescence emission.

In 1909 W. Coblentz in the USA, a pioneer in experimental spectroscopy, turned his attention to several questions concerning the properties of the light in bioluminescence. At that time, a

belief still persisted that any emission of light must always be accompanied by heat according to Planck's equation for the black-body. So the question was, where does the bioluminescence energy go? The second concern was about the physiology of the human eye, where the sense of color can be confounded by levels of the light intensity. In other words, a very weak light is visually whitish due to the lack of color sensitivity of the dark-adapted eye. It was agreed that the bioluminescence of different species of fireflies did have different colors, some in the green and others more yellow-orange. Coblentz used a prism spectrometer with photographic detection and importantly, calibrated the spectral sensitivity of detection to absolute photons by thermoelectric methods. He demonstrated that the spectral distribution of various firefly species in fact differed quantitatively, being the source of the color variation. It was not an artifact of human visual sensitivity. The spectral maxima Coblentz published were, for *Pyrophorus noctilucas* 538 nm, *Photuris pennsylvanica* 552 nm, *Photinus pyralis* 567 nm, and *Photinus scintillans* 578 nm. These values are close to those determined recently using more modern instrumentation. Coblentz also rigorously excluded any production of heat, i.e., emission in the infra-red at wavelength longer that 0.7 microns (700 nm).

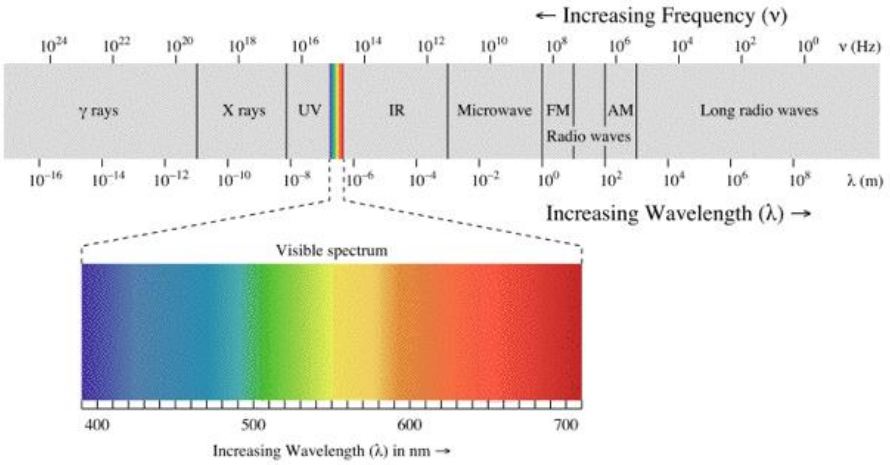

Figure 2.2. The wavelengths and frequencies of electromagnetic radiation. Human visual sensitivity range is from 390-710 nm.

In 1926, Coblentz and Hughes measured the spectral distribution of the bioluminescence of the ostracod crustacean *Cypridina*, again finding a broad smooth spectrum with maximum at 482 nm, and also the same for the green bioluminescence color from a species of fungus, as having a spectral maximum at 520 nm. Later workers reported maxima at 526 and 520 nm for various fungal species. Within the accuracy of measurement, it seems there is no species difference in fungal bioluminescence spectra comparable to the spread of spectral maxima from species of firefly and other beetles.

Bacterial bioluminescence has a range of blue colors, and in this spectral region the human eye has difficulty in sensing color variations. Although early in the century it was agreed that

bacterial bioluminescence spectra extended from the violet to the green, claims as to species variation were easily dismissed, lacking any quantitative measurement. Some workers published color variation at different stages of growth in culture. It is curious that Coblentz did not choose to give attention to bacterial bioluminescence, perhaps because of lower light levels in this case. It was not until 1950, that Spruit-van der Burg showed that the bacterial emission spectrum had no growth dependence and that there was in fact, a type dependence of the absolute spectral distribution, with maxima for *Photobacterium phosphoreum* at 472 nm, *P. splendidum* 489 nm, and *P. fischeri* 496 nm (Fig. 2.3). The spectra were shown to be smooth and not resolvable into multiple contributions, as earlier claimed by others and now attributable mostly to self-absorption in the dense bacterial cultures and distortions due to light scattering.

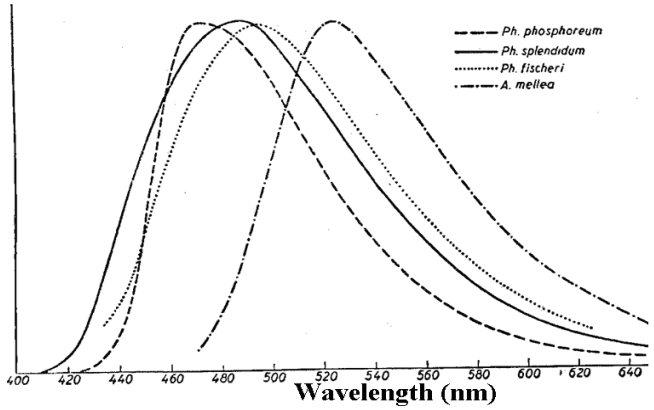

Figure 2.3. The absolute bacterial bioluminescence spectral distribution depends on the type of bacterium. The bioluminescent mushroom, *A. mellea*, emits green.

Dubois continued his studies of bioluminescence into the first 30 years of the 20th Century, with attention mainly to the luciferase and luciferin from the clam *Pholas*. He established that the luciferase indeed had properties of an enzyme and that the "luciferin" pholasin was a glycoprotein, that is a protein with one or more attached sugar residues. In modern times this glycoprotein would be renamed or reclassified, as a "luciferin binding protein". Only very recently has the genuine Pholas luciferin been identified (Chapter 8). Along with many researchers in this field, prominent are the two naturalists, E.N. Harvey at Princeton University in the USA, and Y. Haneda in Japan, both continuing to discover and identify specimens, and publishing into the second half of the century. The methodology mainly adopted by all, was of collecting and classification, hot-water cold-water extraction and reaction, and the oxygen requirement. In 1916, Harvey verified a hot plus cold water reaction of the firefly extract. He also made a puzzling finding, that a hot-water extract from parts of this insect other than the light organ, the "photophore", also produced bioluminescence with the firefly luciferase from the photophore. He mistakenly concluded, that this hot-water extract was also luciferin or some form of it, but the right answer did not come to light until 1947, with McElroy's discovery that the hot water extract was ATP, later shown to be a

required co-enzyme for the firefly bioluminescence reaction. The title of McElroy's paper was however, wrong asserting "The energy source for bioluminescence …" because the photon energy derives from the oxidation of the genuine firefly luciferin, but this mistake was corrected a few years later. ATP, but not firefly luciferin, is the factor stable in the hot-water extract, so it was the cold water extract that contained the luciferin as well as the luciferase.

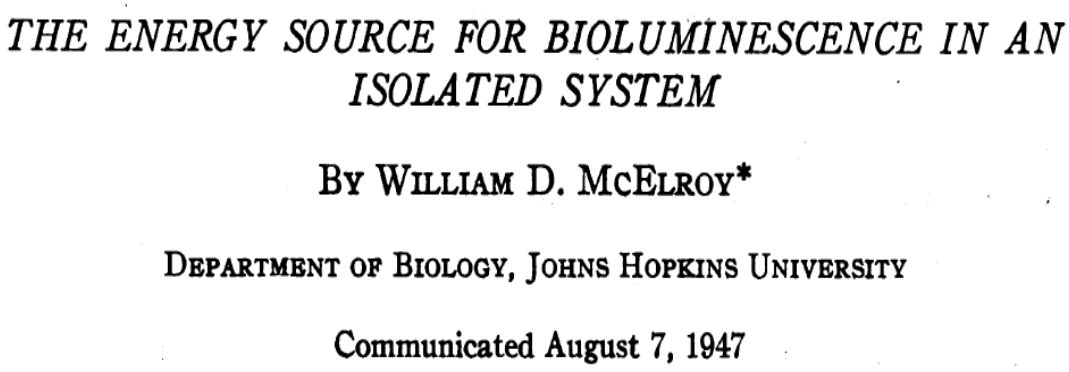

THE ENERGY SOURCE FOR BIOLUMINESCENCE IN AN ISOLATED SYSTEM

By William D. McElroy*

Department of Biology, Johns Hopkins University

Communicated August 7, 1947

Figure 2.4. ATP was first identified as a requirement for firefly bioluminescence but incorrectly attributed to be the energy source for the light.

Harvey was able to make bioluminescence extracts from many organisms, but not all. He obtained an active extract from the ostracod *Cypridina* and found it to be dialyzable, consistent with its luciferin being a small molecule. The "luciferin" from the clam *Pholas* was only slowly dialyzable, and by this time Dubois had also decided it was a protein and not a small molecule. The luciferin activities in all cases could be destroyed by oxidants suggesting they were reduced organic molecules. Little progress could be made on characterization of the luciferin chemical structures until 1933, when Anderson pioneered techniques for purification of the luciferin from *Cypridina*. He used multiple organic solvent extraction and derivatization by benzoylation, methods followed up by subsequent workers leading eventually by the 1950s of discovery by Shimomura in 1957, of conditions for crystallization, and later by others for its chemical structure characterization. Anderson also established quantitative methodology with the newly invented photocell and its incorporation in "luminometers", to follow the activity of luciferin by total light production and bioluminescence kinetics.

Harvey also reported an unanticipated result, that the bioluminescence of the jellyfish *Aequorea* was not diminished in the absence of air, as observed by Boyle in experiments with other bioluminescent organisms. Some other coelenterates also failed in this regard. This was another puzzle not answered for another 50 years. Another significant advance at that time was the recognition of bioluminescence reaction specificity. The luciferases and luciferins from the different types of organisms, mostly did not cross-react. We now know this is the general case except within the beetle family including fireflies, and some groups of coelenterates.

Attempts to obtain active extracts from the bioluminescent bacteria were without avail. However, starting in the mid-thirties, Frank Johnson (Princeton University), showed that the bioluminescence from bacterial cultures was a measure of overall metabolic activity. This idea goes back even again to Boyle, who reported on the inhibition of bacterial bioluminescence by the addition of "spirits of wine". Johnson made a number of investigations on the effect of narcotics, temperature, and high pressure, and in collaboration with the physical chemist Henry Eyring, showed how these effects could be interpreted on the basis of Eyring's Chemical Reaction Rate Theory. Although the nature of the physiological pathway was not yet elucidated, it was concluded that rate limiting steps leading to bioluminescence, were a major component of the overall metabolism of these cells. This conclusion continued to be strengthened when, in the 50's some of the same experiments, e.g., the effect of high pressure, could be carried out on the *in vitro* reaction with bacterial luciferase and reduced flavin. Bioluminescent bacteria became and continue to be, widely used for field assays, such as for toxic contamination of water sources. A trace of respiratory poison diminishes the bioluminescence intensity ("Do Not Drink").

3. **Bio**lu**minescence in the 1950s: Johns Hopkins and Princeton Universities, and Oak Ridge National Laboratory**

"Apparently there is no rhyme or reason in the distribution of luminescence throughout the plant or animal kingdom. It is as if the various groups had been written on a blackboard and a handful of sand cast over the names. Where each grain of sand strikes, a luminous species appears." E. Newton Harvey (1927).

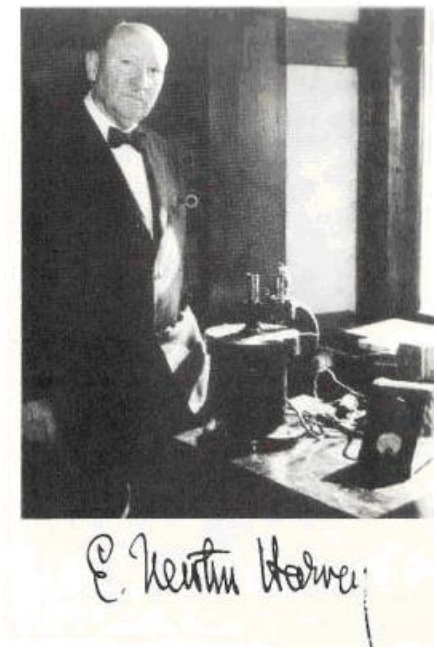

Figure 3.1. Professor E. Newton Harvey (1887-1959), Princeton University.

In the decade following 1950, it can be said that the foundation was laid for investigation of the biochemistry of bioluminescence. This was the result of a highly productive congregation of students and associates of Professor E. Newton Harvey, most of whom were at two universities in the North-East USA, Princeton and Johns Hopkins, and at the Oak Ridge National Laboratory in Tennessee. An important factor in any such study is the ready availability of biological material, and during the summer months fireflies are numerous and easily collectible in this area of the country. Mainly it was the pioneering work of Professor William D. McElroy and associates that established the biochemical pathway for firefly bioluminescence.

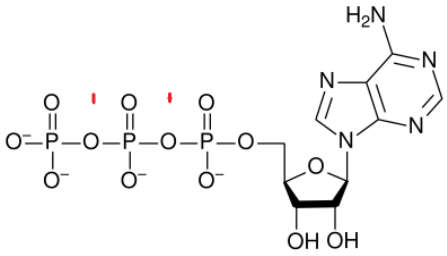

Figure 3.2. Adenosine triphosphate (ATP). The red arrows mark the two anhydride bonds that in the subject of Biochemistry, are called "high energy" bonds. The energy of hydrolysis from these bonds is coupled to drive many metabolic processes.

In 1941, Franz Lippman had shown adenosine triphosphate (ATP) to be the main energy source driving many cellular metabolic reactions. McElroy in 1947, identified ATP in the hot-water extract of firefly tails and named it the "luciferin", based on the classical definition that this extract produced light emission on addition together with Mg^{2+}, to the cold-water extract. Some argued that the title of the1947 paper (Fig. 2.4), stating ATP to be the energy source for the bioluminescence, had to be incorrect. From Planck's Equation, the energy equivalent of a photon of yellow firefly light (say at 550 nm), is around 52 kcal/mole, far in excess of the standard free energy available from ATP hydrolysis, about 7 kcal/mol:

$$ATP + H_2O \rightarrow AMP + PP + 7\ kcal,$$

where AMP is adenosyl monophosphate and PP (or PP_i) is inorganic pyrophosphate. Oxygen being another factor in the bioluminescence, would satisfy this energy requirement if the bioluminescence energy resulted from an oxidation of an undiscovered organic molecule, because most oxidation reactions are known to be highly exothermic.

Bernard Strehler, a student of McElroy, observed that the cold-water extract had a yellow color and showed this colored substance to be separable by dialysis from the high mass protein fraction, the luciferase. The absorption spectrum of the yellow dialysate had a major maximum at 350 nm and a fluorescence maximum at 530 nm. It qualified as the genuine firefly luciferin in that together with ATP and Mg^{2+}, its addition to the luciferase fraction generated the yellow bioluminescence. Furthermore, with the initial flash intensity (I_0) being a measure of the steady-state reaction rate, the luciferin, ATP, and Mg^{2+}, qualified as the true substrates, according to the Michaelis-Menten model of enzyme kinetics (Chapter 4). That means that, at a fixed luciferase concentration and excess of the substrates except one, say the luciferin, the I_0 increases linearly with added luciferin, until a point of "saturation", where it shows no further change with addition. However, there were a lot of complications needed to be resolved. One hydrolyzed product expected from ATP, the inorganic pyrophosphate (PP), was not detectable. Second, the fluorescence of the solution following reaction was greenish over a shorter wavelength than that of the firefly *in vivo* or *in vitro* bioluminescence yellow color. Also, the initial flash was quickly followed by a reduction to a lower constant light intensity, and there were effects on the light output on addition of various factors like

inorganic pyrophosphate, pyrophosphatase, coenzyme-A, phosphate, and chemically oxidized luciferin. The overall reaction was proposed to be:

$$E + LH_2 + O_2 + ATP + Mg^{2+} \rightarrow light + AMP + PP + L + \ldots.$$

where E = firefly luciferase, LH_2 = luciferin, a reduced organic molecule, and L = its product. The Mg^{2+} is generally found necessary for ATP reactions. Nowadays the abbreviation Luc is used for firefly luciferase.

By 1956 the firefly luciferase from *Photinus pyralis* was obtained highly purified by crystallization. It was freed from pyrophosphatase activity which now allowed verification of the PP as a stoichiometric product, meaning that it was equivalent to the amount of AMP formed. The luciferase protein was homogeneous, both in its overall ionic charge using electrophoresis and by mass determined by ultra-centrifugation. The mass obtained from the sedimentation coefficient, was around 100 kDa and it was concluded from other experiments that firefly luciferase was a dimer of two identical subunits. Many years later based on DNA sequence, the mass was corrected down to 61 kDa, and it was concluded that firefly luciferase was a monomer having a single luciferin binding site. Possibly these first results were confused by aggregation as firefly luciferase is a hydrophobic protein. The reaction sequence was suggested to have two steps, an "adenylation", that is formation of the AMP ester, then oxygen oxidation, finally to the oxidized product "oxy-luciferin" in its excited (fluorescent) state, from which the light is emitted:

$$E + LH_2 + ATP + Mg^{2+} \rightarrow E\text{-}LH_2\text{-}AMP + PP$$

$$E\text{-}LH_2\text{-}AMP + O_2 \rightarrow E\text{-oxy-luciferin} + AMP + light.$$

Product inhibition would explain why the initial flash of bioluminescence (I_0) is followed by the lower level of light intensity, with the steady glow kinetics mentioned above. In the next

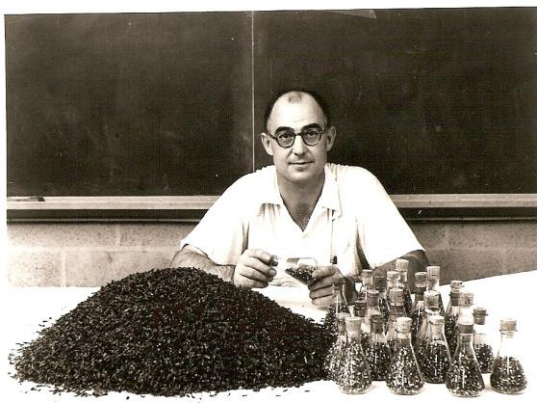

Figure 3.3. Professor William D. McElroy (1917-1999), Johns Hopkins University. "Firefly Mountain".

section the kinetics of bioluminescence reactions will be explained in more detail but, at the time of these first experiments, to rationalize the kinetics it was proposed that if the above two steps were rapid, a slower rate of release of products would not allow the enzyme to "turn-over", i.e., to catalyze another reaction. Initially therefore, all the luciferase would be available for catalysis giving the high I_0 value, followed by the lower light level corresponding to the slow release of products. Instability of the oxy-luciferin product frustrated attempts at its separation and chemical identification at that time.

Firefly luciferin was produced in crystalline form the following year, 1957. From 15,000 fireflies, 9 mg of crystalline luciferin was purified. In neutral solution the absorption had a major peak at 327 nm and a fluorescence maximum at 530 nm, compared with the *in vitro* bioluminescence maximum at 550 nm. No success was achieved in isolating the oxidized product oxy-luciferin having a fluorescence comparable to the bioluminescence spectrum that might better qualify it as the bioluminescence emitter. On reaction, the 327-nm luciferin absorption peak disappears and a product absorption around 380 nm rises. The small amount of available pure material precluded further chemical tests at that time.

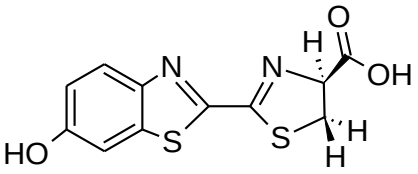

Figure 3.4. The chemical structure of firefly (beetle) D(−) luciferin as first published by White and collegues in 1961. The presently accepted configuration is t*rans*.

Having firmly established the above reaction sequence, the next task was to characterize the chemical structure of the firefly luciferin. This was achieved just a few years later, by Emil White and Frank McCapra, also at Johns Hopkins University. The proposed structure was verified by total synthesis. The structure can have two configurations that are mirror images called optical isomers, but only the D (−) optical configuration shown in Fig. 3.4, is active for bioluminescence. The L (+) optical isomer does not produce bioluminescence although it can undergo the adenylation, oxygen addition, and release of pyrophosphate in the presence of firefly luciferase. The structure of an oxidized luciferin, first called "oxy-luciferin" in the above equations, was also determined, but later found not to be the genuine product of the bioluminescence and therefore renamed "dehydroluciferin". Also in 1961, Howard Seliger and co-workers showed that the loss of absorption at 327 nm in the bioluminescence system, was accompanied by a rise of absorbance at 383 nm, the latter corresponding to the absorption of dehydroluciferin. Both firefly luciferin and dehydroluciferin free in aqueous solution, have high fluorescence quantum yields, around 0.7 at pH 8.5, with corrected spectral maxima at 535 and 544 nm respectively, both different from the bioluminescence spectral maxima in the range 562-565 nm, with either natural or synthetic firefly luciferin. Also however, the dehydroluciferin-AMP shows no fluorescence when bound to luciferase, and no fluorescence was discernible in the product of the bioluminescence reaction.

In 1959, Seliger measured the absolute bioluminescence quantum yield, i.e., number of photons produced per firefly luciferin reacted, to be almost unity, which implied that the chemical path was 100% for the light reaction, and that the bioluminescence emitting molecule would need to have the same unity fluorescence quantum yield as well as a fluorescence spectral distribution matching the bioluminescence. It was still many years later before the genuine reaction product, the true oxy-luciferin, was identified.

The second major advance in the field of bioluminescence at that time and coming from a neighboring geographical location, was the identification of the components required for bacterial bioluminescence. Strehler, then located at Oak Ridge National Laboratory, considering that bacterial luciferase should be a protein, transferred a culture of bacterial cells from their growth media containing 3% NaCl as in sea-water, into water without salt. As the bacterial cells contain a high salt concentration, in water they burst or osmolyze, passing their contents into solution. The cell walls were removed by centrifugation and the soluble protein, a crude bacterial luciferase, precipitated with acetone. The dried acetone powder was extracted with water and divided into two parts, one of which was boiled. The classical mixing experiment produced luminescence. On the knowledge from the *in vivo* studies of Frank Johnson at Princeton, that the *in vivo* bioluminescence is strongly linked to bacterial respiration, Strehler showed that reduced nicotine adenine dinucleotide (NADH; at that time this was called "reduced DPN"), a chemical known to be a central component in bacterial respiration, meaning those reactions involving oxygen to produce metabolic energy, greatly stimulated the bioluminescence from the bacterial extract. Simultaneous collaborative work of Strehler with J. Woodland Hastings, McElroy, and others at Johns Hopkins, showed that riboflavin phosphate (FMN; flavin mononucleotide) was a necessary and sufficient component and again with Strehler, that the NADH could be dispensed with altogether, and reduced flavin, $FMNH_2$ used instead. The function of the NADH as is well-known in metabolism, was apparently to reduce the FMN.

There was still a missing component in the extract that was then identified by Strehler and Milton Cormier at Oak Ridge, as a long-chain aliphatic aldehyde. McElroy, Hastings and Green, purified the bacterial luciferase several fold and the overall reaction was concluded to be:

$$\text{B-Lase} + FMNH_2 + \text{RCHO} + O_2 \rightarrow \text{light } (h\nu) + \text{FMN} + \text{RCOOH} + H_2O$$

where B-Lase here stands for bacterial luciferase, RCHO a long-chain aliphatic aldehyde, and RCOOH the presumed carboxylic acid product. In equations the symbol *hv* is commonly used to stand for light emission. Currently the symbol Lux is used for bacterial luciferase. Bioluminescence kinetics studies showed that $FMNH_2$ and RCHO were the luciferase substrates for the reaction. Cormier and John Totter at Oak Ridge, showed that the aldehyde was utilized in the reaction but that there was no loss of the flavin, qualifying the aldehyde as the true bacterial luciferin, on the definition that it is the reduced substance that on oxidation yields energy equivalent to a blue photon. They concluded this on measurement of the absolute bioluminescence quantum yield of each component under limiting amounts of each in turn. For each photon emitted, less than 0.3 molecules of FMN appeared to be lost, the

cycle of its reduction being achieved by NADH coupling. The FMN provided reducing equivalents only, and was essentially returned at the end of the cycle.

$$NADH + FMN + H^+ \rightarrow NAD^+ + FMNH_2$$

In contrast, about 20 molecules of aldehyde were utilized for each photon generated, i.e., the number of photons per aldehyde reacted, called the "quantum yield", was the inverse, 1/20 = 0.05. These results supported the above overall reaction pathway, with most of the flavin being returned at the end as FMN. This means, on the basis of the Stark-Einstein Law (Chapter 5), that the flavin ring is not decomposed to a different product in the light process. Bacterial bioluminescence is clearly much less efficient than the firefly.

With the involvement of $FMNH_2$ and O_2 in the process, it was considered that some type of peroxidation must be part of the chemical mechanism. There had been a number of mechanistic suggestions that formation of an aldehyde-flavin peroxide adduct, must be involved in the chemistry. Strehler showed that a weak chemiluminescence could be obtained by adding very concentrated H_2O_2 to riboflavin or FMN alone, and also that a purified aldehyde hydroperoxide added to the bacterial luciferase reaction containing FMN and NADH, generated strong light emission. After more than 50 years of research, a convincing chemical reaction mechanism of bacterial bioluminescence still awaits uncovering.

The bioluminescence system of the ostracod *Cypridina* had been a favorite of Harvey's from before the 1920s. He showed that the bioluminescence was O_2 dependent and that the Cypridina luciferin (recently renamed "cypridinid luciferin") produced bioluminescence only with luciferase from *Cypridina* itself, as well as the luciferase from other ostracods. In 1955 Fred Tsuji in Harvey's group at Princeton, reported on the spectral and other properties of purified cypridinid luciferin and in 1957, Osamu Shimomura in Japan, produced the cypridinid luciferin in a highly purified crystalline form. Shimomura remarked that his success was due to having freshly collected organisms that contained 10 or more times the active material than did the dried organisms available to the Princeton group but also, the discovery of crystallization condition was quite accidental. Forming crystals was essential for chemical characterization, but the cypridinid luciferin is extremely unstable in air probably the main reason that the structure was not finally solved until 1966. Last but not least to join the Princeton group, was Shimomura in 1959, to continue with Frank Johnson the studies of jellyfish bioluminescence.

Cypridinid luciferin bears no chemical structure similarity to the luciferins of bioluminescent bacteria or firefly. However, many marine bioluminescence systems do have related structures, the same ring system but differently substituted and generally, these remain specific for their corresponding luciferases in their bioluminescence reaction. Cypridinid luciferin was the first to be isolated in a pure state, but firefly luciferin had its chemical structure characterized first. The reason can be attributed both to the ready availability of the crude material from fireflies but also to the chemical stability of the firefly luciferin. Although the ostracods were also easy to harvest in quantity, the study of this bioluminescence system was frustrated by the ready air oxidation of the cypridinid luciferin. Arguably, the first luciferin to be isolated and structurally identified, was the long-chain

aliphatic aldehyde from the bacterial bioluminescence, but as this was a known chemical and not a novel natural product, the bacterial "luciferin" is usually not given priority in this regard. Some investigators suggest that bacterial luciferin should include both $FMNH_2$ and RCHO, but it seems more rational to classify the $FMNH_2$ as having a similar coenzyme activating function as ATP does in the firefly system. As will be described later, the $FMNH_2$ is proposed to activate the RCHO by transferring the oxygen to form a luciferase-peroxy-aldehyde, the key player for light production, like the luciferyl-adenylate in firefly bioluminescence.

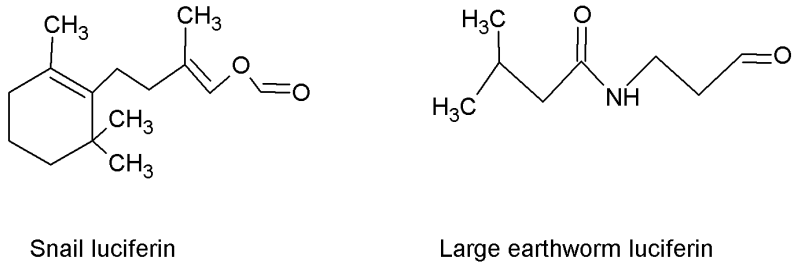

Figure 3.5. Luciferins of the limpet *Latia*, a freshwater snail and the common large earthworm *Diplocardia*, are both aldehydes.

Besides the luciferins of bacteria, firefly, and the several like cypridinid that are variations with a central imidazopyrazine ring (Chapter 8), in the past forty years only five new and distinct luciferin structures have been identified. Two are aldehydes, one from the fresh water snail *Latia* and the second from the common large earthworm *Diplocardia* (Fig. 3.5). The most recent ones besides another variation on imidazopyrazine, the Pholas luciferin (2009) that is a dehydrocoelenterazine, are a tetrapyrolle structure in the bioluminescent system of the dinoflagellates and krill (2005; Chapter 11), and in 2014 one from the small Siberian earthworm *Fridericia heliota* (Fig. 3.6, *Left*), which appears to be the product of biosynthesis from amino acid precursors tyrosine and lysine. Remarkable is that this luciferin from a different type of earthworm, is an ATP requiring bioluminescence system like firefly, as is also the glow-worm (Diptera) bioluminescence whose luciferin structure has not been determined. In 2015 the luciferin responsible for the bioluminescence of mushrooms was also identified (Fig. 3.6. *Right*). The biosynthesis of fungal luciferin appears to be by hydroxylation of its precursor, hispidin, a well-known metabolite in fungi. The fungal luciferase appears to be membrane-bound which will make it difficult to characterize.

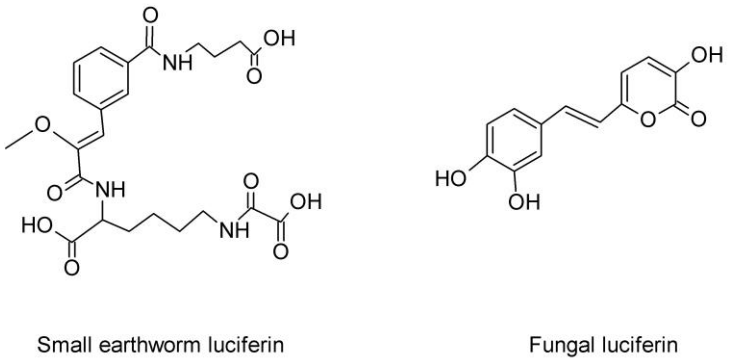

Figure 3.6. Two new luciferins: (*Left*) The Siberian earthworm, and (*Right*) mushrooms (fungi).

4. **Bioluminescence Kinetics**

"Theories have four stages of acceptance. i) this is worthless nonsense; ii) this is an interesting, but perverse, point of view; iii) this is true, but quite unimportant; iv) I always said so." J.B.S. Haldane (1953).

Biochemistry arose as a separate scientific discipline around the end of the 19th Century. There was a developing consensus among scientists that many properties of living organisms could be accounted for in terms of chemical reactions strongly aided by mysterious "factors" present in extracts of biological material such as yeast that had a remarkable effect of catalyzing specific chemical reactions. These factors were found to be proteinaceous in character and named enzymes ("out of yeast"). The major activity of biochemists for about the next fifty years, was toward solving the mechanism of enzyme catalysis primarily by the analysis of the kinetics of their chemical reactions. These catalytic "factors" only needed to be present in minute quantities much below the amounts of the chemicals in the reaction being monitored, and as catalysts they were released or "turned over" at the end of each cycle to be ready for another reaction round. Most enzymes were not available in chemical quantities which precluded the detection and characterization of intermediates by techniques available at that time.

In the literature, the statement is often found that bioluminescence is an enzyme catalyzed chemiluminescence but even though luciferase bears its name as an enzyme, the designation is questionable. Luciferase is not found necessarily to enhance the rate of chemiluminescence, but rather favors the deposition of the reaction energy into the first electronic state of the product. This is the same energy state as the longest wavelength absorption band of the product from which its fluorescence emission occurs. Thus, if the bioluminescence spectrum is the same as the product fluorescence, this is important evidence because it can lead to identification of the product chemical structure and give a clue as to the bioluminescence chemistry. A second critical property of most luciferases is, that within its binding cavity energy loss processes from the product excited state other than via radiation, are restricted. In other words, the product molecule bound to the luciferase must have a high fluorescence efficiency in order to account for a high quantum yield of the bioluminescence (see Chapter 5). The highest measured bioluminescence quantum yield is about 0.6 for one type of firefly luciferase (Chapter 9), so the fluorescence quantum yield of that product would have to exceed this value.

Up until the latter part of the 20th Century most enzymes were characterized by their kinetics. The standard enzyme kinetics scheme is the chemical equilibrium saturation model, adapted in 1912 by Michaelis and Menten and given the eponymous label. An enzyme (E) is considered to first bind a substrate (S) in a bimolecular reaction to form a complex (ES) that can reverse back or go forward by a unimolecular reaction. The complex (ES) is called the Michaelis-Menten complex, and reacts to the product (P), then on dissociation from E allows the enzyme to "turnover" and be available for another catalytic cycle.

$$E + S \underset{k_r}{\overset{k_f}{\rightleftharpoons}} ES \xrightarrow{k_p} E + P$$

The kinetics of bimolecular reactions usually has second order behavior, meaning that the rate of disappearance of reactants or appearance of product ES in the Michaelis-Menten kinetics model here, depends on the product of two concentrations, expressed by the differential equation:

$$\text{Rate}, \quad d\text{ES}/dt = k_f \text{E} \times \text{S}$$

with k_f called the second order rate constant, having units $M^{-1}s^{-1}$; in these and following equations, we let the letters stand for concentrations. Unimolecular reaction rates depend on only one concentration and follow first order kinetics:

$$d\text{ES}/dt = -k_p\text{ES}$$

and the first order rate constants k_p and k_r, have units s^{-1}.

An expression for the overall reaction velocity V, may be easily obtained by making the steady-state approximation, which assumes that the reaction to P (k_p) is slowest and therefore rate limiting, and that the ES complex is in rapid equilibrium with E and S. The steady state assumption means that the rates of formation and disappearance of ES are equal, then

$$k_f \text{E} \times \text{S} = k_r\text{ES} + k_p\text{ES}$$

and, after a few algebraic steps

$$V = V_{max}\,\text{S}/ (\text{K}_\text{M} + \text{S}).$$

This equation for Michaelis-Menten kinetics accounts for the observed saturation V_{max}, that is the maximum and constancy of the rate V after the substrate concentration has reached a certain value, $S >> K_M$ (Fig. 4.1). K_M is called the Michaelis-Menten constant, and can be evaluated from the point of half maximum velocity in Fig. 4.1.

$$\text{If}, \quad V/V_{max} = ½\,, \quad \text{then } K_M = \text{S}.$$

The definition of K_M is:

$$\text{K}_\text{M} = (k_p + k_r)/k_f = \text{K}_\text{D}\,,$$

which would be the same as the equilibrium dissociation constant K_D, provided $k_p << k_r$.

In the literature, K_M is often and confusingly called the “dissociation constant”, whereas an important experiment required to support the kinetics model is to determine K_D by a direct equilibrium measurement.

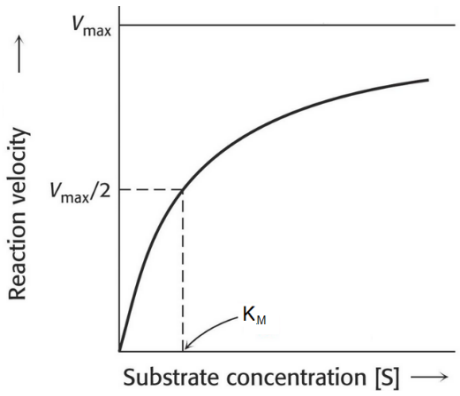

Figure 4.1. Michaelis-Menten enzyme kinetics. At a sufficient excess [S] the reaction velocity approaches a "saturation" value labeled V_{max}.

It is well known in the field of chemical kinetics that the mathematical analysis of a kinetics model rapidly becomes complex as the number of steps increases even slightly. Therefore, for the analysis of bioluminescence kinetics which we expect to be complex, we will first consider a simple "ABC" model, that of three irreversible steps of a consecutive reaction:

$$A \xrightarrow{k_A} B \xrightarrow{k_B} C$$

Assuming each step is a first order reaction with the initial concentrations of B and C being zero and the initial A = A_0, then the time evolution of the reaction component concentrations can be found by solving the following differential equations, with the condition that at any time they sum as:

$$A_0 = A + B + C$$

$$-dA/dt = k_A.A, \qquad \text{integration gives } A = A_0.\exp(-k_A.t)$$

$$dB/dt = k_A.A - k_B.B$$

$$= k_A.A_0.\exp(-k_A.t) - k_B.B, \quad \text{and}$$

$$B = k_A.A_0\{\exp(-k_A.t) - \exp(-k_B.t)\}/\{k_B - k_A\}, \text{ and}$$

$$dC/dt = k_B.B, \text{ and}$$

$$C = A_0\,[1 + \{\exp(-k_A.t) - \exp(-k_B.t)\}/\{k_B - k_A\}].$$

For the reader less expert in integral calculus various internet sources can be used to find integral tables: (http://www.wolframalpha.com/input/?i=definite+integral+calculator).

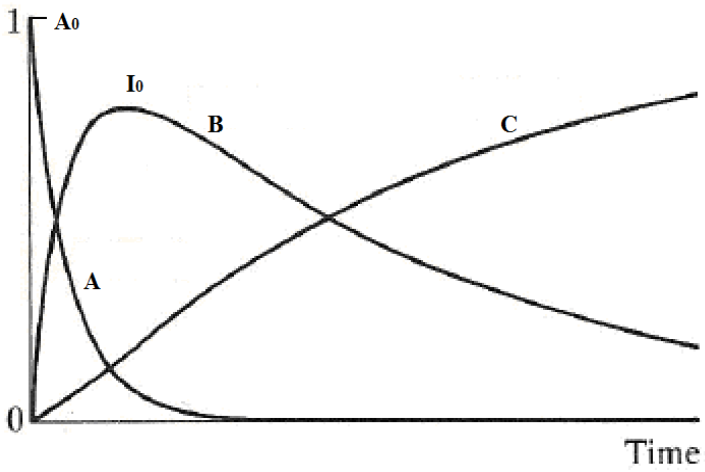

Figure 4.2. Time dependent concentrations of reaction components for the ABC model.

These above equations are "analytic" or "exact" solutions. Rather than obtain exact solutions for more complex models, it is usually more convenient to use a numerical analysis and Fig. 4.2 shows a computational result for the simple ABC case here. The concentration of component B rises to a maximum then decays exponentially to C, which rises in concentration at this same rate. In a bioluminescence reaction, the immediate product from B is the excited state designated as C*, but this has only a transient existence as the emission of bioluminescence on transition to the ground state C is at a rate $>10^9$ s^{-1}, much faster than the preceding chemical steps. The kinetics of the light emission intensity therefore will mirror the B kinetics, meaning that the chemical reaction kinetics should be the same as the bioluminescence kinetics. The reader will be relieved to know that there are many software packages available for modeling kinetics, e.g., "SigmaPlot".

At the time point where B is maximum corresponding to the initial bioluminescence intensity I_0, the concentrations are not changing and this is called the "steady-state". This means that at this time point, the differential of B is zero so that:

$$dB/dt = -k_A.A_0[k_A\exp(-k_A.t) - k_B\exp(-k_B.t)]/\ [k_B - k_A]$$

$$= 0$$

at the steady-state, meaning that

$$k_A\exp(-k_A.t) = k_B\exp(-k_B.t).$$

Solving for the time $t = t_M$ at the steady-state, I_0:

$$t_M = \ln(k_A/k_B)/\ (k_A - k_B).$$

In a bioluminescence reaction the light intensity reflects therefore the concentration of B, and at the steady-state the initial concentration of luciferin (A_0) can be obtained by solving the above equation for B:

$$\ln(B_{max} / A_0) = [k_B \ln(k_A / k_B)] / (k_A - k_B).$$

A second approach for complicated models is to make do with the "steady-state approximation". Two assumptions pertain, the first that the concentrations are constant (steady state) at the I_0 time point, and that one step is rate determining, e.g., $k_A << k_B$.

$$dC/dt = k_B.B = k_A .A_0 \exp(-k_A t), \text{ since } k_A << k_B \text{ , and } \exp(-k_B t) \sim 0.$$

Integration from $t = 0$ to $t = t$ gives:

$$C = A_0[1 - \exp(-k_A t)].$$

Bioluminescence kinetics as an investigative tool, may be said to only originate in the 1950s with the availability of the relatively purified components of the firefly and bacterial systems. However, the bioluminescence kinetics of these systems are not so simple, so the Ca^{2+}-regulated photoproteins will be discussed first being a good example of an "ABC" model, or better to call it an ABC* model. As the name implies, only two components, are involved in generating the bioluminescence:

$$Ca^{2+} + \text{photoprotein} \rightarrow h\nu.$$

The prototype is called aequorin named for the jellyfish *Aequorea* from which it was first discovered and purified in 1962. The kinetics features are similar for all other photoproteins in this class (Chapter 8). The semi-log plot in Fig. 4.3 is the Ca^{2+}-triggered bioluminescence from another photoprotein obelin. The bioluminescence "flash" triggered on manual addition of a solution of Ca^{2+} rises in less than 0.2 s, and decays in a closely exponential manner as evident by the straight line on the semi-log scale. The light intensity at the maximum in Fig,4.3A, is labeled I_0. This is the standard procedure for bioluminescence assays, a rapid mixing of the reaction components, recording the initial flash height I_0, and equating it to the concentration of the limiting component. The method of manual injection of an initiating component however, does not produce a true I_0 in the case that the initial reaction rate is faster than the manual mixing time, which cannot be less than around 0.3 s. This is the case for the Ca^{2+}-regulated photoproteins, the maximum light intensity after manual mixing, is lower than the I_0 obtained by using more recent techniques that utilize pressure driven stopped flow, having mixing times down to 1 ms. The exponential true rise rate of obelin bioluminescence using stopped flow is about 400 s^{-1} ($t_{½}$ =1.7 ms), and for aequorin it is somewhat slower, 115 s^{-1}. These rates differ among the types of photoprotein, but what is common is an independence on Ca^{2+}concentration for both rise and decay rates, and this is consistent with the consecutive model.

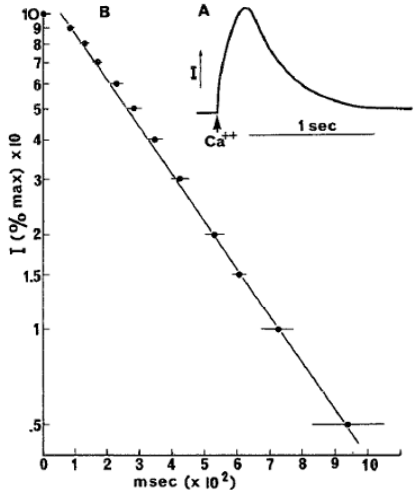

Figure 4.3. A. Flash obtained on rapid injection of Ca^{2+} into a solution of the photoprotein obelin. **B.** The semi-log plot shows that the decay of bioluminescence intensity after the maximum I_0 is closely exponential: I (%) = I (max) × exp(-kT); k = constant, T = msec (ms).

Bioluminescence is an extremely sensitive method for detection of a reaction component. Consequently, after the discovery of aequorin and that its bioluminescence was triggered essentially specifically by Ca^{2+}, it was considered that aequorin might be useful for measurement of low level Ca^{2+} concentrations, such as occur in biological systems. Aequorin has been widely and extensively employed in this regard, for over the subsequent 50 years from its discovery, and continues to be most popular, mainly because it was the first photoprotein to be applied for this measurement. For this application and also to elucidate the basic bioluminescence mechanism, the Ca^{2+} response of aequorin or other photoproteins, has to be calibrated as to the dependence of I_0 on Ca^{2+}concentration. In the consecutive model, the value of B_{max} or I_0, reflects the amount of the initial component A_0, or in the case of the photoprotein reaction, the added Ca^{2+} concentration. Photoproteins have an EF-hand structure with three Ca^{2+} binding loops (Chapter 12), and the question arises as to how many of these sites need to be occupied by a Ca^{2+} ion in order to trigger the bioluminescence, just one, two, or all three? The calibration task then is to observe the dependence of I_0 on the added Ca^{2+}concentration.

For technical reasons, the intensity is plotted as I_0/total light, labeled in Fig. 4.4 as L/L_{int}. The Figure 4.4 is a log-log plot to show up the large dynamic range or linearity on Ca^{2+} concentration, over almost three orders of magnitude. It also reveals that the sensitivity to added calcium ion concentration differs among photoprotein types, OL-obelin is the most sensitive and has the largest spread of linearity or dynamic range. In each case the slope is approximately 2.5, interpreted as a requirement of more than two bound Ca^{2+} for initiation of the reaction. We can write:

$$L/ L_{int} = \text{constant} \times [Ca^{2+}]^{2.5}$$

$$\text{Log } (L/ L_{int}) = \log (\text{constant}) + 2.5\log [Ca^{2+}].$$

The slope indicates that the kinetics order of the rate limiting step is fractional, 2.5. How can this be? It would arise from the presence of three binding sites having affinities depending on whether other sites are bound or not, e.g. Ca^{2+} to bare protein, to protein with one Ca^{2+} already bound, etc. A further complication is that the "binding" here is a kinetics parameter, the reaction kinetics has a greater than second order dependence, and the binding cannot be equated simply to an equilibrium constant.

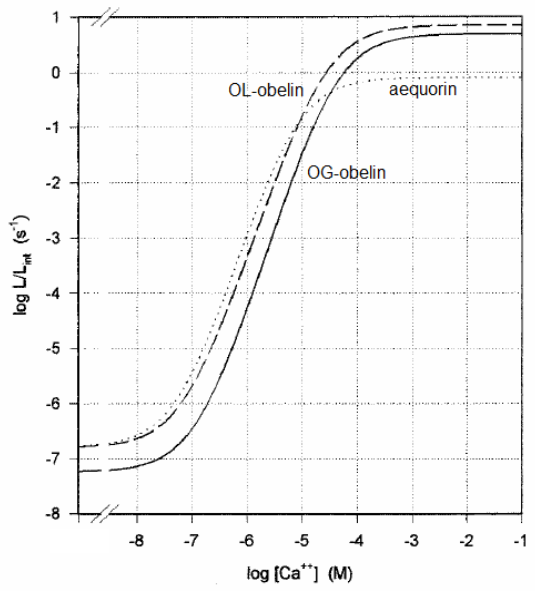

Figure 4.4. Light intensity triggered by Ca^{2+} addition to these photoproteins is linearly proportional on a log-log plot, to Ca^{2+} concentration over a wide range. OL, from *Obelia longissima*; OG, from *Obelia geniculata*.

This picture now brings up a problem about regarding this as a simple ABC* consecutive process in that the first step, the physical binding of the calciums to the photoprotein (P), is expected to be reversible. We will symbolize the protein with the first bound Ca^{2+} as A.

$$P + Ca^{2+} \leftrightharpoons PCa^{2+} = A$$

$$k_A << k_B$$
$$A \rightarrow B \rightarrow C^* \rightarrow C \text{ (final product)}$$

In order for the rise and fall rates to be independent of calcium ion concentration, the Ca^{2+} second order association equilibrium to PCa^{2+} must be rapidly established, and if k_A is the slowest rate in the system, the rise and fall rates of light intensity are insulated from the concentration levels of Ca^{2+}. Naturally, the equilibrium rate parameters are unverifiable as the presence of Ca^{2+} would trigger reaction and quickly remove the study subject.

Some reports of aequorin bioluminescence kinetics show that the slope in the log-log plot is closer to 2.0, which leads some investigators to the conclusion that two bound Ca^{2+} are

sufficient for triggering the reaction. Whether the slope is 2 or 2.5 might depend on solution conditions or other technical artifacts, so the matter cannot be settled by kinetics experiments alone.

The kinetics of firefly bioluminescence was the first to be given a detailed study even before firefly luciferase and luciferin were of good purity. The standard assay procedure as just mentioned, the one used in this study and for many other bioluminescence systems, is again by rapid manual injection of one component in excess into a glass vial containing a buffered solution of the luciferase, usually placed within an instrument for light measurement, called a luminometer that records the time-dependent light emission. This is sometimes humorously referred to the "squirt and flash" technique. Fig. 4.5 shows the bioluminescence intensity obtained following rapid manual injection of a solution of ATP and Mg^{2+}, into a pH 8 buffered solution containing firefly luciferin (LH_2) and firefly luciferase (Luc) under air. The luminometer records an immediate light flash with the intensity decaying more slowly than the rise of the flash. This record on a semi-log plot reveals that the bioluminescence intensity has a very fast rise and two slower decay rates, the semi-log scale again shows that both decay rates are exponential, that is with first-order kinetics. The flash height I_0, is proportional to the limiting concentrations of Luc or the substrates, and this is the basis of the extensive application of firefly bioluminescence for assay of ATP in biological extracts.

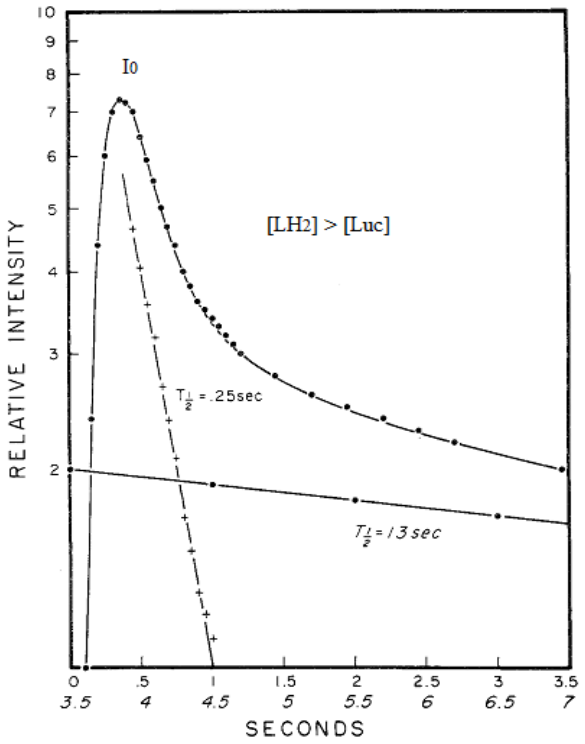

Figure 4.5. Addition of ATP in the firefly reaction shows both fast and slow decay of bioluminescence intensity. Luc = firefly luciferase, LH_2 = firefly luciferin. The line with filled circles are on the 0—3.5 s time scale.

The bioluminescence of the firefly reaction has been well established to occur in a sequence of steps some of which are irreversible:

$$\text{Luc} + \text{LH}_2 \rightleftharpoons \text{Luc-LH}_2$$

$$\text{Luc-LH}_2 + \text{ATP} + \text{Mg}^{2+} \rightarrow \text{Luc-LH}_2\text{AMP} + \text{PP} + \text{Mg}^{2+}$$

$$\text{Luc-LH}_2\text{AMP} + \text{O}_2 \rightarrow \text{Luc-LH}_2\text{O}_2 + \text{AMP}$$

$$\text{Luc-LH}_2\text{O}_2 \rightarrow \text{CO}_2 + \text{Luc-oxyLH}_2^{*} \rightarrow h\nu + \text{Luc-oxyLH}_2$$

$$\text{Luc-oxyLH}_2 \rightleftharpoons \text{Luc} + \text{oxyLH}_2$$

The symbol Luc- on the first line designates a non-covalent binding of the LH_2 to Luc. The initial or peak light intensity, $I_0 = 7.2$ units of relative intensity in Fig. 4.5, is a measure of the steady-state concentration of the luciferase bound adenylester Luc-LH_2AMP, and therefore the initial amount of active luciferase according to the ABC* model. That the bioluminescence kinetics also apparently fits the ABC* model can be rationalized in the same way as for the photoproteins, that the first step of the binding of the substrate luciferin if in fact it is a reversible equilibrium, is rapid and not rate limiting. The complex (Luc-LH_2AMP) is formed at a bimolecular rate contributing to the initial rate of rise of intensity, but rate information cannot be distinguished from the manual mixing rate in this type of experiment.

Following the maximum intensity, the linear decay on the log scale with half-life $t_{½} = 0.25$ s, is a pseudo-first order rate, probably that for the kinetics of molecular oxygen addition to form the AMP + Luc-LH_2O_2. In water at room temperature, the oxygen concentration is about 0.26 mM, which being in large excess can be considered constant over the reaction time. Usually luciferase and luciferin concentrations will be in the micromolar range. Consequently, the second order constant can be combined or "lumped" with the constant oxygen concentration, to form an apparent first order constant, as only the substrate concentration is time dependent. This oxygen addition step therefore, will have "pseudo-first order" kinetics. Oxygen addition forms a covalent complex, so this step will be irreversible and slower than the following decarboxylation reaction. About 1 s after the maximum in Fig. 4.5 the bioluminescence decay assumes a slower first-order rate, $t_{½} = 13$ s and, depending on the conditions of the experiment, this low level light can be almost constant for long times. Obviously this overall behavior is not consistent with the simple ABC* model. To account for this it was suggested that the product Luc-oxyLH_2 dissociates slowly preventing the luciferase being turned over in the final step. The slow light emission then reflects this rate of turnover or product release.

In the reaction following manual injection, the initial rise rate of bioluminescence intensity is again, an artifact originating from the time limitation for manual mixing, at least 0.3 s. Later experiments made in the 1970s used a pressurized stopped flow apparatus, and revealed the

faster rates of the earlier steps in the reaction of firefly bioluminescence. Modern instruments have mixing times or “dead times” even as low as 1 ms.

Fig. 4.6 shows the firefly bioluminescence signal from a stopped flow measurement using an apparatus with a mixing time of 5 ms. A solution of 0.2 μM of firefly luciferase was initiated with about a 100 times excess of the substrates LH_2 and ATP/Mg^{2+} under air. The sharper curve with a peak at about 1.5 divisions, is for a time scale of 500 ms/division, and the other curve is with 20 ms/division. The reaction is initiated at the first division, and it can be observed that in the broader curve there is a quarter of a division, about 25 ms, before the bioluminescence signal “turns on”, an induction time in other words. The peak intensity is reached at about 250 ms (< 0.6 division on the sharp curve) after initiating the reaction, and

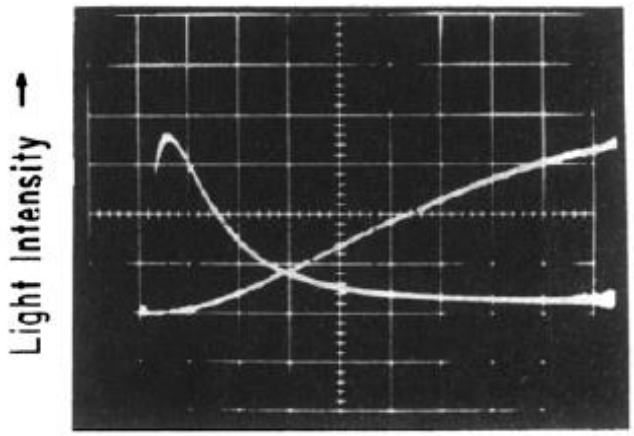

Figure 4.6. Rapid stopped-flow measurement of the firefly reaction. The time scales are 500 ms/division for the sharp curve and 20 ms/division for the other.

again its height is proportional to the concentration of luciferase, the limiting component in this experiment. In a second experiment, the reaction components were combined anaerobically (absence of air) and after a brief incubation, the reaction initiated with air-saturated buffer. The result is shown in Fig. 4.7, with the top panel (**a**) 100 ms/division, and lower (**b**), 10 and 20 ms/division. The 25-ms induction time is no longer seen. An aerobic experiment using LH_2-AMP in place of LH_2 still presented the induction period. It was proposed that this initial induction time before the appearance of bioluminescence, reflected a rate of a conformation change of the protein following the binding of substrate, so as to expose the bound LH_2-AMP for faster addition of molecular oxygen, followed by decarboxylation to the excited product that emits the light. This idea has been recently supported by determinations of the spatial structure of firefly luciferase, to be described in Chapter 12.

In 1984 the complementary DNA of the luciferase from *P. pyralis* was isolated, and from the predicted primary sequence, the true mass of Luc was determined to be 61 kDa. The first mass estimate made in 1956 of the crystallized native luciferase, was around 100 kDa, but later it was shown that under denaturing conditions, it divided into two equal subunits. A sedimentation study of the native protein showed a mass of 50 kDa at the lowest protein concentration, and also that it aggregated as the concentration increased. However, the specific activity measured by I_0/mg protein, did not depend on luciferase concentration. This is the reason that in these first studies it was concluded that firefly luciferase was a dimer, and a number of investigations of substrate binding parameters were interpreted based on that belief. Here we will reanalyze the data with the knowledge of the correct 61 kDa mass.

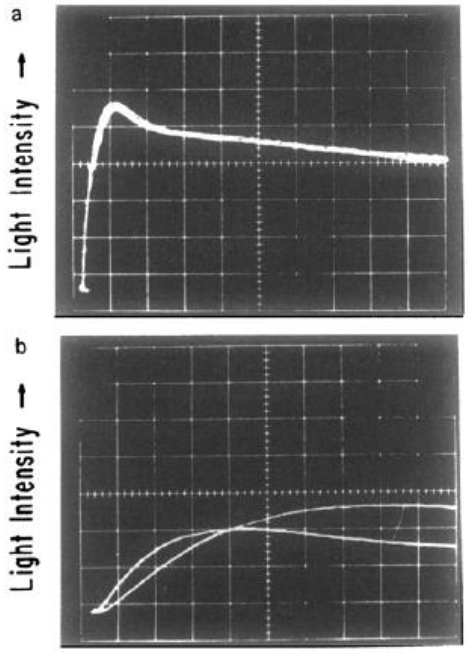

Figure 4.7. Stopped-flow study of the firefly reaction using very short time scales. **(a)** 100 ms/div. **(b)** 10 and 20 ms/div.

$$\text{Luc} + LH_2AMP \rightarrow \text{Luc-}LH_2AMP \quad \text{slow structural change}$$

$$\text{Luc-}LH_2AMP + O_2 \rightarrow \rightarrow \text{bioluminescence}$$

The simple Michaelis-Menten model was believed to fit well the steady-state kinetics of firefly bioluminescence modified by the slow turnover, until a more incisive examination was undertaken starting in the late 1960's. It is well known in the field that kinetics models are not unique, and need to be substantiated by direct measurement of component interaction. For example, in the biochemical literature we find the K_M often called the "dissociation constant", but this is incorrect, because the true dissociation constant K_D has to be measured directly by an equilibrium experiment:

$$A + B \leftrightharpoons AB, \qquad K_D = AB/(A \times B),$$

the letters again standing for their concentrations. A correspondence of K_M and K_D gives support to the validity of the kinetics model as representing the chemical steps.

The model is also one of pseudo-first order kinetics consistent with a bimolecular reaction. It is observed that the I_0 is linearly related to the concentration of each component. This can be shown by a plot of the Lineweaver-Burk equation, an inversion of the Michaelis-Menten enzyme velocity expression that conveniently allows linearization for manual computation:

$$V = V_{max}\, S / (K_M + S).$$

$$1/V = 1/V_M + (K_M /V_M)(1/S)$$

Fig. 4.8 is the result for LH_2 as substrate and I_0 as a measure of overall velocity, V. This Lineweaver-Burk expression arises from the first-order kinetics for LH_2 and similarly, the other substrates but again, there is an incorrect and common statement that there is "one binding site" for LH_2 in this case, when what is the case is that the light intensity is simply "first-order" in substrate concentration. We will now see how this has given rise to an unsolved Mystery in the field.

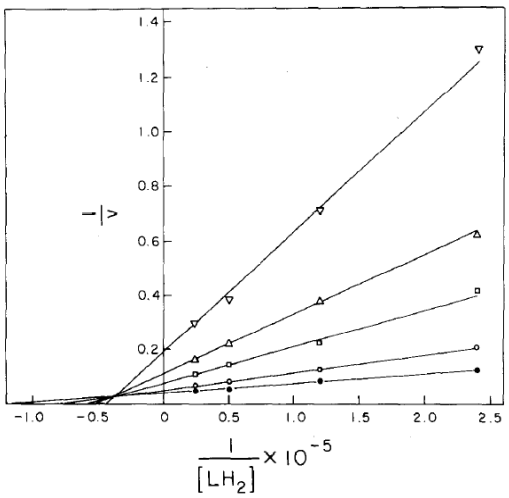

Figure 4.8. The Lineweaver-Burke plot of the firefly bioluminescence reaction. The Michaelis-Menten parameters can be conveniently determined from the intersections on the axes.

\

The number of binding sites and the dissociation constants for the firefly substrates were determined by equilibrium experiments and the techniques of dialysis, chromatography, and fluorescence, have all been applied. Unfortunately, the firefly luciferin is too unstable in air for a direct equilibrium study, so it has been assumed from the kinetics that there is in fact one luciferin "binding site" on firefly luciferase, the apparent origin of the confusion to be

demonstrated between equilibrium and kinetics. Dehydroluciferin, L, is a strong competitive inhibitor of firefly bioluminescence, also exhibiting first-order behavior. The kinetics model for competitive inhibition is:

$$Luc + LH_2 \rightleftharpoons Luc\text{-}LH_2$$

$$Luc + L \rightleftharpoons Luc\text{-}L$$

where the V_M can still be attained in the presence of the competitive inhibitor L, by just increasing the concentration of LH_2, and this kinetics property is interpreted simply as that both L and LH_2 must occupy the same physical binding site on Luc. That means that the stoichiometry of both must be identical. It was also found in the early studies, that luciferase also catalyzed the adenylation of L to LAMP but without light emission, and that LAMP is essentially irreversibly bound with a $K_D \sim 10^{-10}$ M, all these kinetics observations implying that L and LAMP must be binding at the same site as the genuine substrates, LH_2 and Mg-ATP.

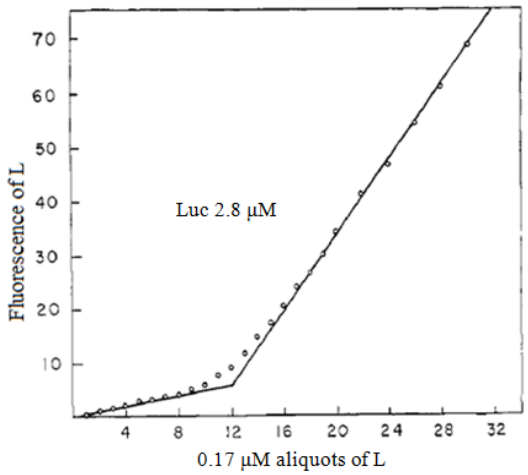

Figure 4.9. Fluorescence titration of dehydroluciferin (L) against firefly luciferase (Luc) allows the binding constants to be extracted.

Dehydroluciferin (L) is highly fluorescent in free solution but its fluorescence is quenched when bound to luciferase. A fluorescence titration provides an easy and direct experimental method for measuring the interaction. The result is 1.2 binding sites with an equilibrium K_D of 1-2 μM, not significantly different from the first-order bioluminescence kinetics inhibition constant K_i of about 1 μM. For LAMP on the other hand, there is no fluorescence either free or bound, so its binding has to be measured by a reverse titration. Fig. 4.9 shows increasing fluorescence on addition of aliquots of L to a mixture of Luc and excess ATP. LAMP is formed on L binding to Luc and a break point reveals the titration point, which is the concentration where no more L can bind and be adenylated. The break point is at a concentration of L 1.5 μM with Luc 2.8 μM. The result is the number of binding sites n = 0.6,

in contrast to the direct L fluorescence titration yielding 1.2 binding sites for L. Also, for luciferase with already bound Luc-LAMP, no further quenching of L fluorescence could be detected. Other equilibrium techniques gave similar results and the same "half-binding site" was found for the Mg-ATP, but about one binding site for ATP alone.

The puzzle of half-binding sites in the firefly reaction has yet to be resolved. Of course LAMP is not a participant in the bioluminescence, and the explanation may lie in the fact of Luc aggregation or dimerization with LAMP binding only to the dimer (Luc-Luc):

$$\text{LAMP} + (\text{Luc})_2 \rightarrow \text{LAMP-}(\text{Luc})_2 \quad \text{inactive,}$$

or a result of the protein conformational change in the reaction steps recently demonstrated in the structural study (Chapter 12). This discrepancy illustrates the ambiguity sometimes arising in correlating kinetics order and physical interaction. Where in the photoprotein case, there is fractional kinetics order, in firefly there appears fractional stoichiometry referred to in the pastliterature as "half binding sites".

The bioluminescence from the reaction of bacterial luciferase (Lux) with its substrates, is a broad blue-green spectrum with maximum around 490 nm. *In vivo* the substrates are reduced flavin mononucleotide ($FMNH_2$), tetradecanal, and oxygen, but with purified bacterial luciferase *in vitro*, other reducing agents can yield bioluminescence but with less efficiency than with $FMNH_2$. Aliphatic aldehydes (RCHO) with chain lengths seven and above are equally efficient, but differ in bioluminescence kinetics.

The bacterial luciferases from all the different types of bioluminescent bacteria, have homologous sequences and are dimeric, consisting of two non-identical subunits (α and β), with total mass around 78 kDa. The requirements for bioluminescence from all types of bacterial luciferase are the same, but their bioluminescence kinetics differ. No CO_2 is detected as a product, only the aliphatic acid (RCOOH) having the same chain length as the RCHO used. The overall light reaction is therefore written as:

$$\text{Lux} + FMNH_2 + \text{RCHO} + O_2 \rightarrow\rightarrow \text{Lux} + \text{FMN} + \text{RCOOH} + H_2O + h\nu\ (490\ \text{nm})$$

The flavoenzymes and flavoproteins occupy a large family of proteins having FMN (flavin mononucleotide; riboflavin phosphate) or FAD (flavin adenine dinucleotide) as coenzymes. Their spectral properties are very convenient for the application of stopped flow methods. In aqueous solution at pH 7, FMN has strong absorption bands at 375 and 445 nm and efficicient fluorescence with Φ_F 0.25 and λ_{max} 530 nm. FMN is not fluorescent in the bound state in most proteins including Lux, with the exception of the FMN-antenna protein (Chapter 13) and the LOV-blue light sensing proteins. The reduced state $FMNH_2$, has a single absorption band around 370 nm and no fluorescence.

The first stopped flow kinetics study of the reaction sequence in bacterial bioluminescence was made by J.W. (Woody) Hastings and Quentin Gibson in 1963. The aim was to uncover the steps within the double arrows in the overall reaction above. With excess substrates Lux does not turn over, as any excess $FMNH_2$ is oxidized to FMN by the dissolved oxygen in solution more rapidly than completion of the bioluminescence reaction on the luciferase.

These experiments additionally laid the foundation not only for a detailed investigation of the mechanism of this reaction, and also were seminal to the larger field of the biochemistry of flavoenzymes.

By ordering the addition and concentration of the substrates, Hastings and Gibson established the process as going through three intermediates all bound on bacterial luciferase:

$$FMNH_2 + Lux \leftrightharpoons Lux\text{-}FMNH_2 \qquad \text{Intermediate } \mathbf{I}$$

$$Lux\text{-}FMNH_2 + O_2 \rightarrow Lux\text{-}FMNHOOH \qquad \text{Intermediate } \mathbf{II}$$

$$Lux\text{-}FMNHOOH + RCHO \rightarrow Lux\text{-}FMNH\text{-}OOCH(R)OH \quad \text{Intermediate } \mathbf{III}$$

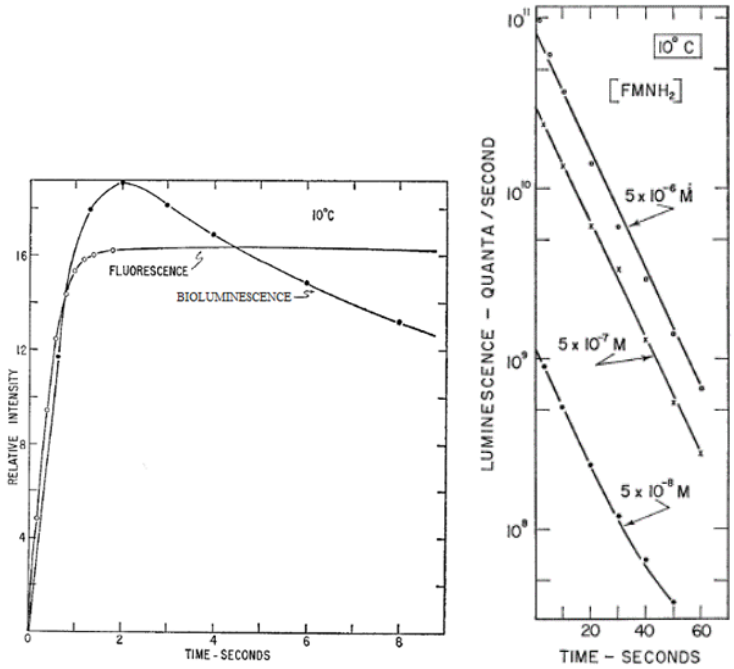

Figure 4.10. (*Left*) Rapid stopped flow mixing of $FMNH_2$ to bacterial luciferase and decanal. The fluorescence signal is Odue to free FMN. (*Right*) The decay of bioluminescence is closely exponential over many orders.

The left panel of Fig. 4.10 compares the kinetics of the bioluminescence and the fluorescence from free FMN, after rapid stopped flow addition of $FMNH_2$ in excess over AF-luciferase and decanal. The bioluminescence intensity achieves a maximum (I_0) at 2 s after the addition then decays in a closely exponential manner (right panel, semi-log scale) over two decades or more, consistent with an ABC kinetics model. With the $FMNH_2$ limiting, the I_0 is found proportional to the $FMNH_2$ concentration but the decay kinetics is unaltered. In a later more systematic study, this linearity of I_0 with $FMNH_2$ and the exponential decay, were shown to extend over more than four orders of magnitude. The fluorescence signal is due to the excess free FMN detected as fluorescence at 530 nm and both its rise time and that of the

bioluminescence, are seen be within the 5-ms mixing time of the stopped flow apparatus employed.

Intermediate **II** was proposed to be a complex of the luciferase-bound flavin with H_2O_2 and 25 years later this was proven by a Nuclear Magnetic Resonance (NMR) study, to be described in Chapter 10. Under conditions such as low temperature below 0°C, intermediate **II** can be stabilized for many hours. The identity of **III**, later proposed as a peroxyhemiacetal, is not established yet, except that the flavin peroxide and aldehyde as written above, remain bound to the luciferase. At this point the flavin coenzyme has already performed a function well known in flavoenzyme mechanisms, of transferring oxygen onto the substrate, here plausibly to form the corresponding FMNH-RCH(O)OOH, the candidate energetic precursor of the final aliphatic acid product.

A later systematic study of bacterial bioluminescence kinetics, concluded that the reaction was strictly first-order, and concluded that the luciferase had one "binding site" for $FMNH_2$, intermediate **I**. A new type of bacterial luciferase had been identified at that time, which showed remarkably different kinetics properties to the one used in the earlier kinetics study in Fig. 4.10. The luciferase used in Fig. 4.10 was from *Photobacterium* (*Achromobacter*) *fischeri* now labeled AF-luciferase, and the new one was labeled "MAV", later shown to be from a strain of *Vibrio harveyi*, VH-luciferase. The taxonomy of the bioluminescent bacteria has recently been revisited (Chapter 10) but I will use the original luciferase names here to reduce confusion. The kinetics of both types of luciferase under extensive variations of reaction conditions, displayed strictly first-order kinetics, again leading to conclusion of one "binding site". The analysis was based on the model above for the intermediates, namely the pre-equilibrium model or the Michaelis-Menten model for enzyme kinetics. But the strictly exponential bioluminescence decay demands an ABC model, and its irreversibility is not consistent with the intermediate **I** equilibrium above unless, as already argued for the Ca^{2+}-regulated photoproteins above, this equilibrium is established more rapidly than the irreversible steps that follow:

$$\mathbf{I} \rightarrow \mathbf{II} \rightarrow \mathbf{III} \rightarrow h\nu$$

The conclusion of a single binding site was also at odds with the determination of bioluminescence quantum yields for substrates and products. The quantum yield measures the number of photons produced per component utilized or produced in the overall reaction (Chapter 5). For the firefly case the quantum yield is high and it is safe to assume that there is only one chemical reaction pathway, the light reaction. Not so for bacterial bioluminescence and caution must be applied because these oxygen reactions are highly exothermic and competing reactions could be a pathway of major loss. In any case, it was found for both AF-VH-luciferase, under all reaction conditions with each component limiting in turn, the quantum yields for $FMNH_2$ and O_2 were only half those of RCHO, Lux, and an identified product H_2O_2. The absolute quantum yields were also luciferase type dependent but the one-half ratios were not, and the values measured in the same laboratory ranged for the aldehyde consumed from 0.05 to 0.1. The overall chemical stoichiometry from these quantum yield measurements therefore was concluded to be:

$$2FMNH_2 + Lux + 2O_2 + RCHO \rightarrow\rightarrow 2FMN + Lux + RCOOH + H_2O_2 + H_2O.$$

To account for the first order bioluminescence kinetics it is possible that there are competing reactions one for bioluminescence, the other a dark pathway, with the second bound $FMNH_2$ reacting directly with O_2 on the luciferase:

$$FMNH_2 + Lux + O_2 \rightarrow Lux\text{-}FMN + H_2O_2.$$

It would be fortuitous if both reaction rates were identical under all conditions to yield the constant quantum yield two times ratio. In fact, the kinetics of FMN appearance with excess luciferase and the $FMNH_2$ concentration limiting, was shown to be clearly biphasic with no contribution from the very rapid oxidation of free $FMNH_2$.

Analysis of the bioluminescence kinetics based on the Michaelis-Menten equation, recovered the K_M for $FMNH_2$ as about 1 μM for both VH- (MAV) and AF-luciferases. However, direct equilibrium experiments using both dialysis and chromatography methods, yielded the equilibrium K_D ~30 μM, another inconsistency with the kinetics if K_M is to be equated to K_D. The interpretation of a two-$FMNH_2$ stoichiometry and the equilibrium results was contentious at that time and generated much activity to try to resolve the issue. A fluorescence binding titration first indicated a single binding site for FMN which is fluorescent when free but quenched bound to luciferase, an experiment analogous to the one described for the LAMP-firefly study (Fig. 4.9), leading to a similar conclusion. This analysis revealed a single equilibrium binding site on Lux with K_D = 120 μM (3ºC). For the binding of $FMNH_2$, as it is not fluorescent either free or bound, a titration experiment was made using the circular dichroism (CD) change of the $FMNH_2$ as reflecting its bound state (Fig. 4.11), and the result again was a single binding site and K_D about 1μM, consistent with the kinetics result. A caution must be made here that a titration experiment must include demonstration of reversibility before concluding that the binding is truly an equilibrium. For weak binding such as for FMN, the K_D ~ 100 μM, and it is reasonable to assume that this is reversible, but it would be desirable and straightforward to test this by a dilution. For the stronger binding of $FMNH_2$, the reversible test is not feasible because of the technical difficulty of the $FMNH_2$ being prone to rapid auto-oxidation in the free state.

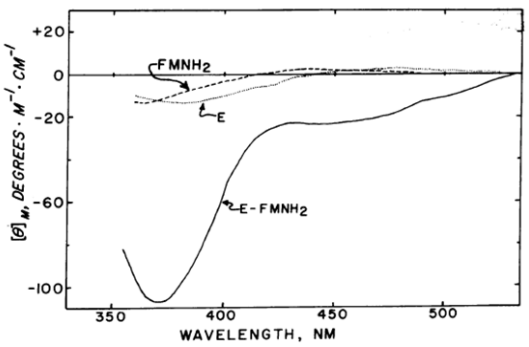

Figure 4.11. Circular dichroism (θ) of $FMNH_2$ free or bound, to VH-luciferase (E-$FMNH_2$ = intermediate **II**). E, is VH-luciferase alone.

The question of flavin binding sites was not finally resolved until later, from ^{13}C-NMR experiments and for FMN from the spatial structure (Chapter 12). One binding site was detected for FMN and two sites for $FMNH_2$. The nature of the $FMNH_2$ binding is different from FMN. One $FMNH_2$ is buried and is anionic, $FMNH^-$, with specific hydrogen bonding around the isoalloxazine ring to residues comprising the binding cavity. This would result in a tight binding and no doubt be reflected in a change in protein conformation and the circular dichroism. The second $FMNH_2$ apparently lies in a hydrophobic site on the protein surface without hydrogen bond attachments, and well might not display any significant CD change in its bound state. The binding constants for each were not able to be extracted from the NMR study, although it is assumed that the specific binding site is the point of reactivity. The question of the role of the second $FMNH_2$ in the bioluminescence if any, is also not answered at present.

Two approaches to resolving the reaction sequence in bacterial bioluminescence were reported in the early 1980's. The first was a comparison of the kinetics of bioluminescence with that of an intermediate having high fluorescence yield, $\Phi_F = 0.3$, appearing in the reaction mixture and the second, by comparing the bioluminescence kinetics with the sequence of absorbance spectral changes. The latter experimental approach enables suggestions about the chemical structures of intermediates involved will skill overcoming the technical difficulty in separating species with very similar absorption spectra that change with time. Both approaches supported that the reaction sequence consisted of distinct phases, and that the fluorescent transient species corresponding to one of the absorption intermediates, was the bioluminescence emitter.

Fig. 4.12 displays the time dependence of bioluminescence (dashes) and fluorescence (noisy line), both detected at 470 nm, after rapid manual addition of $FMNH_2$ to excess of the bacterial luciferase, oxygen, and tetradecanal. The apparatus constructed for these experiments allowed separation of the bioluminescence and fluorescence signals by chopping the excitation light. At the detection wavelength 470 nm and 10 nm slit width, only the fluorescence signal from the fluorescent intermediate will be detected, excluding any from free FMN (λ_{max} = 530 nm). Notice that the bioluminescence signal is on a log scale (*right panel*) and the fluorescence a linear scale (*left*). The high signal in the fluorescence channel at 1.8 s is due to excitation light scattering due to the turbulence of the mixing beginning at 1.0 s on this scale. Apart from that scattered light artifact, it is notable that there is little fluorescence signal at the same time point as I_0, i.e., 1.5 s after mixing. This fact is inconsistent with an ABC* model because such an excited product C* must form and have a

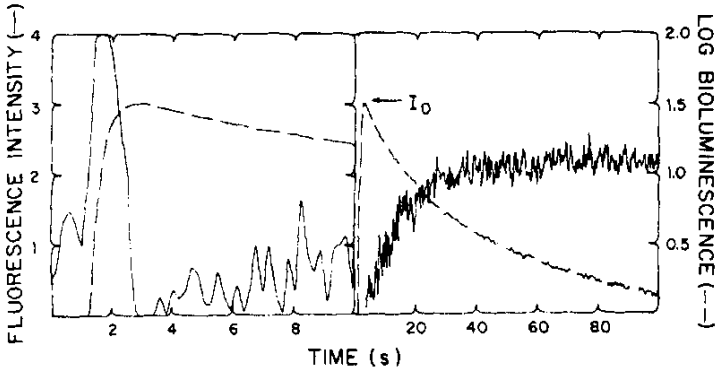

Figure 4.12. Fluorescent transient intermediate (full line, noisy trace) rises after the bioluminescence (dashes) maximum (I_0) from the reaction with VH luciferase. Fluorescence excitation 360 nm, detection 470 nm.

maximum also at the time of I_0, and decay concurrently with the bioluminescence signal. This so-called "Fluorescent Transient" does not reach a maximum (right panel) until the bioluminescence signal has decayed to less than 10% of I_0. The logarithmic scale reveals the complex decay of bioluminescence intensity which requires a three-exponential function for a precise fit:

$$I(t) = I_A\exp(-k_At) + I_B\exp(-k_Bt) + I_C\exp(-k_Ct),$$

where I(t) is the bioluminescence signal at time t. The rate constant and absolute intensities are:

$$k_A = 0.1\ s^{-1},\ k_B = 7 \times 10^{-3}\ s^{-1},\ k_C = 6.8 \times 10^{-4}\ s^{-1}$$

$$I_A = 62,\ I_B = 6.6,\ I_C = 1.0\ (10^{10}\ \text{photons/s})$$

Attention needs to be drawn to the fact that, on calculating the total bioluminescence emission under each component by the ration I/k, although the slow component I_C has the lowest intensity, about half the total light is contributed by this slowest process.

It is seen in Fig. 4.13 that the fluorescence and bioluminescence spectral distributions are indistinguishable, meaning that the fluorescent transient is indeed the bioluminescence emitter, at least for the slowest part of the reaction where the spectral distribution is conveniently scanned. It is not known what could be the excited state responsible for the bioluminescence at the beginning, say in the10 s after initiation when there is no fluorescence present. It was proposed that minor fluorophores, which are not separable from the natural luciferase, could be responsible. Evidence had been accumulating up to this study, that bacterial bioluminescence could be a "sensitized" chemiluminescence and therefore involves both a high energy intermediate plus the sensitizer, just like in sensitized fluorescence. The

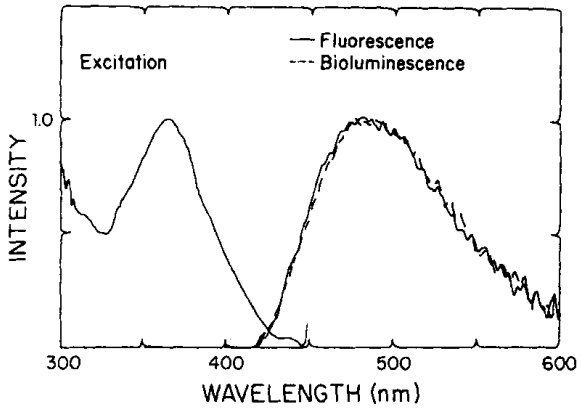

Figure 4.13. Excitation and fluorescence spectra (*full lines*) of the Fluorescent Transient in the bacterial luciferase reaction. The fluorescence spectrum is identical to the bioluminescence (*dash line*).

fluorophore, or the acceptor, may not be one necessarily part of the overall chemistry. We will elaborate mechanistic proposals in Chapter 10. Therefore, the bioluminescence intensity will depend on the concentration of two species, the energizer and the fluorophore. In the first part of the reaction, the energizer concentration is high but the fluorophore low resulting in the largest value for I_A; in the slow regime the reverse, although still of good overall bioluminescence efficiency.

The time evolution of the fluorescent transient fits well to an ABC model, with a rise rate $k_R = 6.6 \times 10^{-2}$ s^{-1}, and a fall rate $k_F = 3.3 \times 10^{-4}$ s^{-1} under the experimental conditions of Fig. 4.13. It turns out that it is not fortuitous that $k_C/k_F \sim 2.0$ as this two-times ratio holds for all variations of reaction conditions: concentration of reactants, temperature, and aldehyde chain length, tetradecanal, dodecanal, and decanal. Also, the activation energy for the slow bioluminescence and the fluorescent transient decay are the same. This two-times factor implies that the bulk of the bioluminescence, i.e., the slow and most of the intermediate, must appear via a bimolecular process, and in later studies it was found that the fluorescent transient of VH-luciferase is a dimer of two luciferase proteins having a mass ~160 kDa.

The bioluminescence kinetics here is clearly inhomogeneous and the model becomes quite complex in order to incorporate all the observations. It is further complicated by the fact that the overall quantum yield with respect to $FMNH_2$ in the VH-luciferase reaction as used here, is quite low, around 0.025, indicating that the bulk of the chemical kinetics might not represent the light path. In the firefly reaction the very high quantum yield, > 0.5, gives confidence that the overall chemistry corresponds to the light reaction. For bacterial luciferase there could well be side pathways that do not yield light, but these side reaction are omitted here for simplicity. The complete model accounts for all the data. It is well appreciated in the analysis of scientific data, that all observations can be incorporated into a suitably complex scheme but the simplest is always preferred (Occum's dictum). In this bioluminescence system this complicated scheme is the minimum required to account for the complex kinetics. The new symbol **IV** is introduced and is probably equated to the fluorescent transient itself.

III → light, component k_A

III → **IV**

III + **IV** → light, component k_B

IV + **IV** → light, component k_C.

Very recently, a stopped flow study coordinating bioluminescence and absorption spectral changes, reached a similar conclusion of an inhomogeneous kinetics picture (Fig. 4.14). There was observed an initial burst of light occupying the first few seconds, followed by a slower rate of light emission. As in the fluorescent transient experiments, the major part of the total light is under the slower phase of emission. It was postulated that the inhomogeneity is due to a small population of the luciferase being in a different state able to catalyze the reaction much more efficiently. Perhaps that is the protein-protein state of the intermediates shown by the fluorescence anisotropy experiments described in a later chapter. The question remains to be resolved.

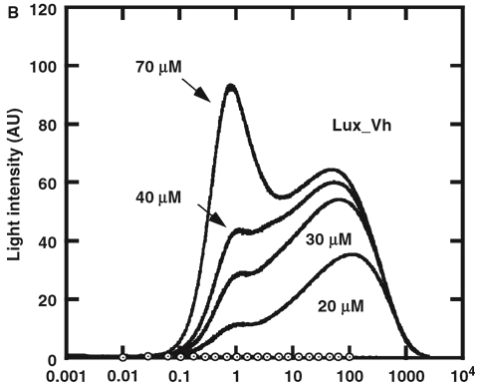

Figure 4.14. Bioluminescence kinetics from the bacterial VH-luciferase Lux-$FMNH_2$ (intermediate **I**) reaction with buffer containing concentrations of dodecanal indicated. There is an initial burst of bioluminescence followed by a complex slow phase.

Absorption spectral changes displayed the presence of several initial forms of a bound reduced flavin on reaction with dissolved oxygen without aldehyde. The sequence and rates of changes using VH-luciferase was suggested:

Lux-$FMNH_2$ + O_2 → **II** very fast (μs)

II → IIA ~ 0.1s, blue shifted

IIA → IIB ~ 1s

IIB → Lux-FMN + H_2O_2 ~500s → Lux + FMN ~2000s

Three distinct forms of the bound peroxyflavins were resolved by their absorbance spectra and proposed to result from conformation changes in the luciferase. The first form **II** had an absorbance maximum at 375 nm which proceeded to blue shift to 370 nm (form IIA), followed by an increased absorbance to form IIB having the same absorption maximum. Also from these experiments, the K_D for binding of $FMNH^-$ to VH luciferase was recovered, 11 μM (4ºC), similar to the earlier determined value of 33 μM (4ºC) by standard methods, and significantly different from K_M < 1 μM (22ºC) for the same type of Lux (VH-luciferase).

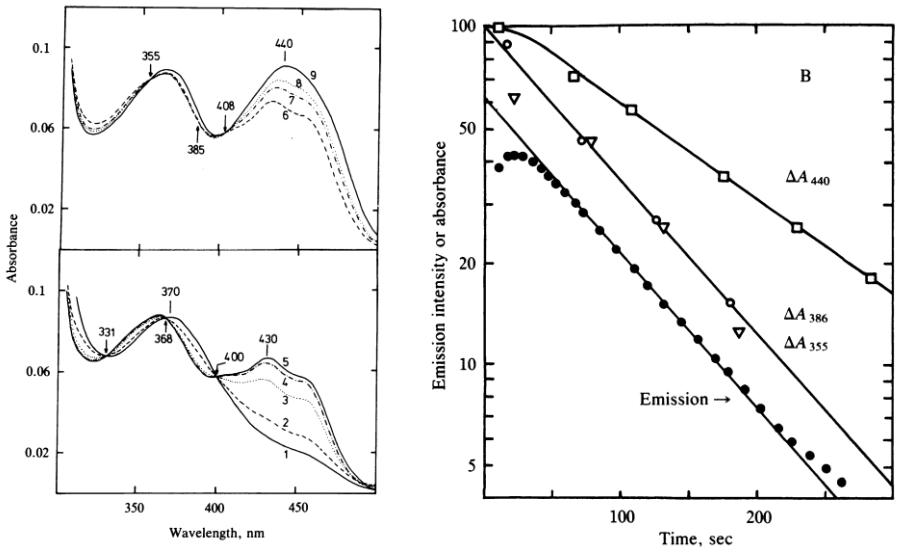

Figure 4.15. (*Left*) Absorbance changes after addition of decanal to VH-luciferase Lux-FHOOH (intermediate **II**). Curve 1, before mixing, 2, immediately after, and 3-8, 2-30 minutes after, and 9 after warming is the spectrum of FMN. (*Right panel*) The exponential decay of bioluminescence emission is the same as the conversion rate of the spectra having the isosbestic points at 355 and 385 nm, assigned as conversion of the peroxyhemiacetal (intermediate **III**) to the 4a-hydroxyflavin (Intermediate **IV**).

A second approach to trying to rationalize the bioluminescence kinetics, was to eliminate these initial steps by first isolating the luciferase-flavin hydroperoxide **II**, and then following bioluminescence and absorption kinetics on addition of decanal. Decanal is used because its reaction kinetics is slow allowing the time around 55 s required for scanning the absorption spectra. The spectra show clear isosbestic points, e.g., 331, 368 and 400 nm in the lower panel of Fig. 4.15 (*left*). Scan 1 is the first scan immediately after mixing and is close to the known absorption spectrum of **II** with a maximum at 372 nm and a shoulder at longer wavelength. Scans 2-8 are started over the next 2-30 minutes, and 9 is for the expected final product FMN. The precise isosbestic points allow some confidence in deconvolution to obtain an intermediate spectrum (360 nm absorption maximum) approximately corresponding to the excitation spectrum for the fluorescent transient (366 nm maximum) reported above in that fluorescent transient kinetics study. The right panel in Fig. 4.15 records the bioluminescence emission and shows that its closely exponential decay parallels that of the change in absorbance at 355 nm, a band attributed to the new intermediate.

This approach of using absorption spectrum shifts, has the advantage of recovering an intermediate spectrum, assigning its fluorescence as the origin of the bioluminescence and as the product of bioluminescence excitation, and proposing its chemical structure. However, the time resolution in these experiments did not allow detection of the initial stage (Fig. 4.15, *right*) where the bioluminescence is maximum but without the appearance of much of the fluorescent transient (FT) signal. The observations also did not extend to longer times where the final phase of reaction produces most of the bioluminescence photons. From these absorption data a simple linear ABC model was again proposed:

II + RCHO → **III** → FT* → FT + *hν* → Lux-FMN → Lux + FMN.

This model requires again that the appearance of FT fluorescence must parallel the bioluminescence excited state, FT*. The two-times decay ratio in the third phase of reaction furthermore, was excluded from consideration in this model.

Except for the very first experiments in 1963, the bacterial bioluminescence kinetics studies have all utilized the VH-luciferase from species of *Vibrio*. This type was chosen because of its slow kinetics also because of relative ease of isolation of the peroxy intermediate **II** and its property of being relatively easy to stabilize for measurement. Kinetics inhomogeneity possibly arises from the observation that the VH-luciferase-**II** undergoes protein-protein complexation not observed for the luciferase intermediates of PL-luciferase. Kinetics studies with these other types should be initiated and could well reveal a simpler picture.

5. **Quantum Yields**

Do not all fix'd Bodies, when heated beyond a certain degree, emit Light and fhine; and is not this Emiffion perform'd by the vibrating motion of their parts? Isaac Newton, *Opticks* (1704).

The measurement of quantum efficiency or quantum yield, is fundamental to the understanding of the mechanism of a chemical reaction involving the absorption or emission of light. The importance of this measurement is a direct consequence of the two "Laws of Photochemistry", the First Law formulated in the early 19th Century, is also called the Grotthus-Draper Law: "Only light absorbed in a chemical system is effective for a photochemical reaction to occur". The Second Law advanced 100 years later, the "Stark-Einstein Law" or the "Law of Photochemical Equivalence", states that: "For each photon absorbed only one molecule is activated for a chemical reaction".

This means that the photon participating in the light reaction, either in emission or absorption, has the same equivalence as the molecules in the sequence of chemical steps and therefore, must be accounted for in the overall stoichiometry just as the reactants and products must be. This equivalence is measured by the quantum yield, the ratio of the moles of light, i.e., einsteins, to the reactants or products involved in the chemical scheme. As a simple example, consider the combustion reaction of hydrogen and oxygen to form water. The stoichiometry is established from the material balance with knowledge of molecular weights and Avogadro's number, to determine the number of moles of each participant. The product yield is 2 moles of water from one of oxygen and two of hydrogen.

$$2H_2 + O_2 \rightarrow 2H_2O, \qquad 4g\ H_2 + 32g\ O_2 \rightarrow 36g\ H_2O$$

For a pure photochemical reaction the photochemical quantum yield (Φ_P) is:

$$A + h\nu \rightarrow A^* \rightarrow B \rightarrow C$$

Φ_P = (moles A consumed or C produced)/ einsteins absorbed

= (molecules of A or C)/ photons absorbed.

The einstein unit is defined as a mole of photons, $6.6 \times 10^{23}\ h\nu$.

If $\Phi_P = 1.0$, it means that for each mole of A consumed on absorption of one einstein, one mole of product C is produced. A quantum yield less than unity, i.e., non-equivalence, indicates the presence of competing pathways, possibly side reactions to yield other products. This is not unexpected as the absorption event places the target A into a highly energized state, consequently it can be very reactive. Some photochemical reactions have quantum yields greater than unity, interpreted as the result of the excitation inducing radical chain processes.

The light emitted from a bioluminescence process is the result of a chemical reaction of oxygen with a luciferin, a reduced organic molecule, bound within a luciferase protein

scaffold, the released energy being deposited into the first electronic singlet state S_1, of a product molecule. The light emission intensity as discussed previously, is a measure of the concentration of a rate-limiting intermediate, enabling the direct kinetics study as a first step in investigation of the reaction mechanism.

$$A \rightarrow B \rightarrow C^* \rightarrow C + h\nu$$

The quantum yield of chemiluminescence (Φ_C) or bioluminescence (Φ_B) is defined inversely from that for a photochemical reaction where photons are absorbed, against the emission of a photon in chemiluminescence. The total light then is one product of the reaction, and knowledge of the quantum yield is again essential to establish the stoichiometry, i.e., how many moles react and how many einsteins are produced.

Φ_C = total einsteins emitted/ (moles A consumed or C produced)

= photons emitted/ (molecules of A or C)

$= \Phi_Y \times \Phi_E \times \Phi_F < 1.0$

The overall quantum yield of chemiluminescence is considered a result of three separate efficiencies. In order to produce visible light, the reaction must release an energy called the "exothermicity", of 75 kcal/mol or more, and deposit this into the product in the same step as its formation to produce its excited state. For such a highly energetic reaction, the chemical yield (Φ_Y) is likely to be less than unity due side reactions from the highly energized product C* in the model above. It is also considered, that the excitation efficiency (Φ_E), the fraction of product produced in its excited state, is also unlikely to be unity. For this simple ABC model the spectral distribution of the emission would correspond to the fluorescence of C. Few molecules have a fluorescence efficiency (Φ_F) approaching unity, as non-radiative processes generally compete with the fluorescence emission. Also to be recognized, is that the deposition of chemical energy to excite C may not be as efficient as in the absorption transition, where every absorbed photon must generate a C*. Quantum yields for the light pathway in a chemiluminescence (Φ_C) or bioluminescence (Φ_B) therefore, being a product of these three efficiencies, must be less than unity. Some bioluminescence reactions have quantum yields up to 0.6, a few chemiluminescences are above 0.25 but most are below 0.01.

In order to measure the chemical equivalence of einsteins, there must be a way of measuring the photon in "absolute units". The reference photon is defined by the radiative emission from a "perfect Black-body". It is a common observation that a heated object radiates energy, a hot plate on a kitchen stove or a fireplace poker "red-hot", emitting both heat and the light visible to the eye. With highly improved spectroscopic methods in the 19th Century, the spectral distribution of such hot objects was determined to be broad with a maximum dependent on temperature (Fig. 5.1). The Sun for example, is an approximate black-body with a surface temperature of 5770 K, yielding a spectral maximum in the yellow-green, 502 nm. Experimental effort was put into constructing a perfect black-body device, one that as near as possible absorbed and re-emitted energy both with 100% efficiency. This device was basically just a box with a thoroughly blackened inside surface and a small aperture to

precisely define the cone of radiant emission. By the 1890s the black-body absolute spectral distribution had been measured with high accuracy.

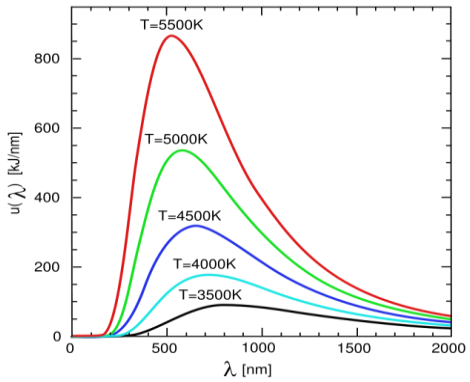

Figure 5.1. Temperature dependence of the black-body spectral distribution.

A theoretical understanding of such radiant emission was a subject of much interest to physicists at that time. The second half of the 19th Century was a period of great significance in the History of Science, culminating in a revolution in Physics, what we now refer to as the beginning of "Modern Physics", leading to a deep understanding of the nature of light initially due to the work of Planck and Einstein. The electromagnetic wave nature of light propagation had been well established by Maxwell by the 1860's. Up till around 1900, Maxwell's equations were the basis for many derivations for the black-body spectral distribution, mostly accounting well for the position of the maximum and the energy distribution at longer wavelengths. As already described in Chapter 2, these equations all failed to match the spectrum in some respect, particularly troubling was at higher energies the theoretical equations failed to have a short wavelength cut-off, that meant that the integrated intensity was infinite. In later years this was labeled "The Ultraviolet Catastrophe". In 1901, Planck decided to fix this difficulty with a postulate that the radiating atoms could only emit packets (quanta) of energy, and derived an appropriate expression for the spectral distribution with an arbitrarily inserted cut-off frequency.

This idea was contentious being quite arbitrary, and Planck himself thought he'd justify this cut-off postulate later, without his realizing the significance of the idea leading as it did to the beginning of Quantum Theory. The significance was apparently recognized by Einstein who hypothesized that light is composed of particles, these he suggested were equivalent to Planck's quanta, with energy given by the Planck equation, $E = h\nu$. Later, others suggested the term "photons" for Planck's quanta.

Chemiluminescence quantum yields are determined in absolute units with a photon detector having a calibration directly traceable to the black-body standard. This standard is usually maintained at National Standards Laboratories and carefully constructed to be as near as possible to a "perfect" black-body. For convenient detector calibration outside the National

facility, secondary Standard Lamps can be supplied, consisting of an incandescent tungsten light source precisely duplicating the black-body spectral distribution, at least over the visible range. It would seem to be easy to calibrate a chemiluminescence detector by simply placing it to view the light flux from the lamp, but severe technical problems need to be overcome.

From a 100-W tungsten lamp, at 30 cm and normal to the plane of the glowing tungsten filament, the 500-nm photon intensity in a band width of 10 nm, is about $10^{13}\,s^{-1}cm^{-2}$. An intensity in this range is appropriate for experiments in photochemistry. For calibration of a light source for photochemistry a secondary detector, usually a thermopile, which is a type of black-body detector, is calibrated from the standard lamp and then used to transfer the calibration to the photochemistry light source. A thermopile is a device containing a blackened surface in which is enclosed a thermocouple. As the surface heats on exposure to the light source, the temperature change generates a potential in the thermocouple, so this calibrates the light flux. Sometimes it is more convenient to use a chemical actinometer, a chemical system in which a photochemical change has been accurately calibrated separately with the standard lamp. Most popular is the ferrioxalate actinometer, which has a quantum yield for 366 nm radiation $\Phi_P = 1.26$, with an uncertainty ±0.03. The chemical actinometer method has an important advantage in that its reaction volume can made to match that of the system under study, so avoiding artifacts due to optical geometry. That means that the light flux and cone of acceptance exactly match.

Chemiluminescence intensity however, is many orders of magnitude below that of the usual tungsten lamp. This means that a standard lamp cannot be used directly to calibrate a chemiluminescence detector, which is usually a photomultiplier tube. A simple apparatus constructed for calibrating the photomultiplier is shown in Fig. 5.2. The flux from a standard lamp (L) is focused onto the entrance slit of a spectrometer in order to disperse the radiation into discrete wavelengths, and a thermopile (TP), which is a black-body detector, placed at the exit slit enables the absolute spectral response of the system to be determined. Then a substitution is used to calibrate a second source, much dimmer than the standard lamp. The light from the dim light source is then viewed by the photomultiplier, after further attenuation by use of density filters, finally to bring the flux into the linear range of the photomultiplier. The calibrated photomultiplier is then placed to view the reaction for quantum yield measurement. A simple set-up for this is shown in Fig. 5.3.

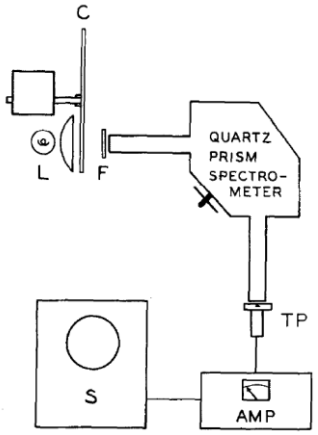

Figure 5.2. Spectrometer based system for absolute calibration of a thermopile detector (TP).

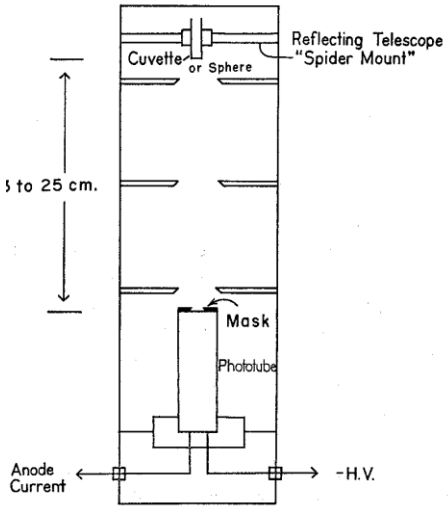

Figure 5.3. Measurement of absolute chemiluminescence quantum yields.

An aluminum reflecting telescope tube with a blackened inside surface, is convenient as it may come with baffles and a "spider mount" that can be used to hold the reaction container, a cuvette in this case, and at the bottom the mirror mount is reconfigured to hold the photomultiplier. The distance from the light source is such that the light intensity is a point source with inverse square behavior. The baffles prevent stray light and the photomultiplier is masked so only the central part of its face that should have uniform response, views the light source. The mask is also present when the photomultiplier is calibrated.

A critical optical artifact needs attention here, one generally unrecognized. Light emitted from a point source towards the cone subtended by the detector and contained in a medium of refractive index *n*, on exiting the plane window of a glass cuvette into air, will be refracted away from the detector cone by an amount n^2. Bioluminescence reactions are in water, so the correction factor $n^2 = 1.76$. For the photomultiplier calibration procedure, there is no

intervening medium except air, to the light source. If the source of light emission is close to the detector not at point source geometry, the correction factor is intractable. In theory, if a spherical container is used at point source geometry, there is no correction for refraction, but by filling the telescope tube with water the air-refraction correction 1.76 for the cuvette was verified, but found to be 1.1 for a spherical container. This is because such a container cannot a perfect sphere, as it has to be open at the top for adding the component initiating the reaction. The experimental setup in Fig. 5.3 was used to determine the quantum yield of luminol chemiluminescence, $\Phi_C = 0.0125$, with a tabulated root mean square (rms) uncertainty of ±0.0006.

With some sacrifice in accuracy, the alternative method using chemical actinometry can be used. This requires a spectrofluorimeter with known absolute spectral sensitivity. For this calibration the fluorescence spectral distribution of quinine is a well-accepted standard. The method has the advantage that the substitution of the actinometer, the quinine solution, and the bioluminescence reaction in equivalent cuvettes, takes care on any optical geometry mismatches as they are all in an aqueous solution. The excitation intensity is determined by the actinometer, and as the quinine fluorescence yield is also accurately known, $\Phi_F = 0.55$, the quinine fluorescence calibrates the detector absolutely. The luminol reaction replaces the quinine standard and the excitation light is then blocked, and the total chemiluminescence collected. Several reports using the actinometric methodology were in agreement with the earlier determined quantum yield for luminol of $\Phi_C \sim 0.01$ but with larger uncertainty, probably < 0.002.

The first measurement of a bioluminescence quantum yield was in 1957 for the bacterial bioluminescence. There had appeared some measurements of chemiluminescence efficiency before this time, but for bioluminescence it was only because the substrates $FMNH_2$ and aldehyde had been identified, that the measurement was meaningful. A photomultiplier was calibrated for absolute response for a spectral envelope with a maximum at 490 nm and a distribution over the same region as bacterial bioluminescence. The apparatus used color filters to restrict the spectral region and again, a thermopile to measure the total light from a secondary standard lamp, which was then substituted by a dimmer source. The thermopile was then replaced by a photomultiplier. Additional light filtering and shifting the photomultiplier to a greater distance, were used for further reduction of lamp intensity (Fig. 5.4). The reaction was carried out in a spherical container and AF-luciferase was used. The luciferase was not fully purified at that time and contained an additional activity of NADH-FMN oxidoreductase, but advantage could be taken of this activity to generate the $FMNH_2$ for bioluminescence as the determination of the quantum yield with respect to $FMNH_2$ directly was not practical, due to its rapid autoxidation.

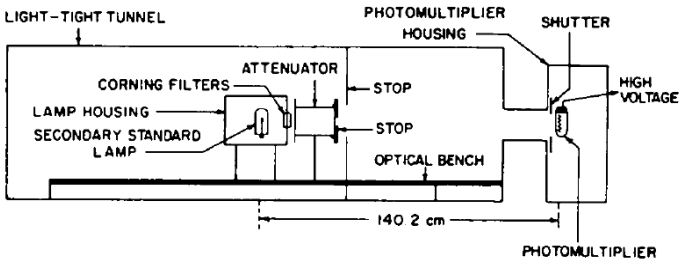

Figure 5.4. Bacterial luciferase quantum yield set-up for aldehyde utilization used by Cormier and Totter (1957).

The reaction scheme with the AF-luciferase preparation was:

$$NADH + H^+ + FMN \rightarrow NAD^+ + FMNH_2$$

$$FMNH_2 + RCHO + O_2 \rightarrow FMN + RCOOH + H_2O + h\nu$$

The aldehyde used was dodecanal and it was shown that the aldehyde was consumed, but the probable product dodecanoic acid was not identified at that time. The observation was that for every einstein of bioluminescence, 30 moles of dodecanal were lost, i.e., the quantum yield for dodecanal was 0.03 ± 0.01. For every einstein in emission generated from a mole of FMN after its reduction to $FMNH_2$, almost 100% of the FMN was recovered in the product. The quantitative result was Φ_B (FMN) > 3, meaning that FMN is not utilized in the light pathway, but turns over in the reaction to be used again by another NADH reduction step, according to the coupled reaction scheme above. The 30% uncertainty for the aldehyde value was estimated from the average for two AF-luciferase preparations. Otherwise the uncertainty was not systematically evaluated, but a conservative estimate would be greater than 30%. The quantum yield was calculated by integrating the bioluminescence intensity over an exponential decay of the bioluminescence, but only over the early times where it was apparently of a first order nature. As the much later bioluminescence-fluorescence kinetics study showed (Fig. 4.12), in this early period only about half the total light might have been generated, so that the aldehyde quantum yield was probably two-times low, and nearer to the recent estimates around 0.01 for AF-luciferase.

There have been a number of subsequent determinations of the quantum yield of bacterial bioluminescence. Some confusion has occurred through the use of secondary calibration standards that differ by a factor of about 2.5, so that for comparison here, the published values are adjusted to the result that would have been obtained by calibration based on luminol chemiluminescence. There is also some inconsistency arising from methodology, especially with regard to the Φ_B ($FMNH_2$). It is also apparent from results obtained in one laboratory with the same calibration protocol, that Φ_B depends on the bacterial type, AF-luciferase giving the highest values but still much below than that for the firefly. The Φ_B's listed next are all using dodecanal, but the value is generally independent of aldehyde chain length and some other solution variations. The highest values reported are for a single turnover of AF-luciferase, 0.12; decanal, 0.12-0.16; decanoic acid, 0.12; Intermediate **II**, 0.06 (based on FMN content). In the one laboratory a ratio of Φ_B about two times, was observed

for RCHO/$FMNH_2$, for three types of luciferase and three aldehyde chain lengths. As described before, the two-times ratio of aldehyde to flavin Φ_B's can be explained by the presence of two luciferase binding sites for $FMNH_2$, but it is otherwise not rationalized mechanistically.

In 1959, with the availability of purified firefly luciferin, the firefly bioluminescence reaction now qualified for quantitative measurement. The quantum yield determined with respect to firefly luciferin was 0.88, with tabulated uncertainties accumulating to an rms deviation of ± 0.28. Attention was carefully given to every uncertainty in the photometric calibration. The optical geometry was not point source but "close-up", to provide maximum detectivity owing to the limited availability of the pure natural firefly luciferin. The reaction was carried out in a one-inch diameter glass vial placed directly on the photomultiplier front face, and coupled to it with an oil so to eliminate at least theoretically, the refractive index correction discussed above. As a further precaution, the volume of reaction was reduced stepwise and the light yield extrapolated to infinite thinness. However, a few years later from the same laboratory, with point source geometry using the device constructed for the luminol investigation, the firefly luciferin quantum yield was determined as about one half the 0.88 value. The origin of this two-fold discrepancy was not pursued at that time due to concern that the luciferin used might have been racemized, as only the D-optical isomer is active for light production. Very recently, the firefly quantum yield has been redetermined with optically pure D-luciferin, and using the same luciferase from *P. pyralis*, and with two differently constructed setups, one with a carefully calibrated optical geometry and another having an integrating sphere for light collection (Fig. 5.5), which eliminates the refraction effect altogether (see also Table 1, Chapter 9). The calibrated geometry yielded Φ_B (luciferin) = 0.41 and 0.48, both with ± 0.07 uncertainty, and the integrating sphere 0.48; the luminol chemiluminescence quantum yield was also precisely confirmed in these recent studies.

The third bioluminescence class to be systematically studied by absolute radiometry, was that of marine systems that used chemically related luciferins, and the same overall chemistry. The luciferases of each system however, have no homology. The first type is from a crustacean *Cypridina* (*Vargula*) and its luciferin, now called cypridinid luciferin, reacts with molecular oxygen on the Cypridina luciferase, to produce a blue emission with maximum at 462 nm and Φ_B (cypridinid) = 0.30, and Φ_B (O_2) = 0.30, both with uncertainty of ± 0.04. With the same device the bioluminescence from the Ca^{2+}-regulated photoprotein aequorin purified from the jellyfish *Aequorea*, was measured. On triggering by Ca^{2+}addition, aequorin produces a blue bioluminescence with maximum around 465 nm and the determined Φ_B (aequorin) = 0.16. The calibration procedure of the photomultiplier was again with reference to the standard lamp yielding the absolute spectral response, and a spherical reaction vessel at a point-source distance was used. In later experiments a photometer setup calibrated against luminol reproduced the Φ_B (cypridinid luciferin) = 0.30.

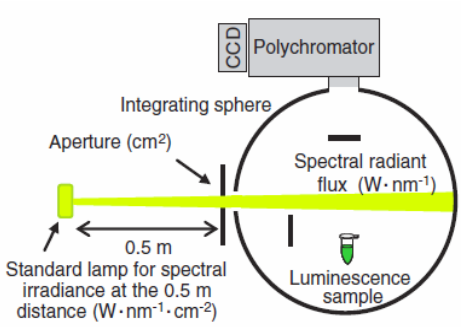

Figure 5.5. The **i**ntegrating sphere alleviates the optical geometry problem

Cypridinid luciferin is related to but less common than a widely occurring marine luciferin called "coelenterazine", named because it was first isolated from coelenterates such as the jellyfish. In the photoproteins, the coelenterazine exists as peroxy-coelenterazine derivative, stabilized within the protein cavity but able to be triggered for decarboxylation and light emission by the binding of calcium ions. Coelenterazine is also the substrate for the luciferase from the Sea-Pansy *Renilla*, and in that case has a bioluminescence emission maximum at 480 nm and Φ_B (coelenterazine) = 0.07 – 0.10. A critical observation was made here, that the inclusion of Renilla green-fluorescent protein (GFP) in the reaction, enhanced the Φ_B about three-fold along with a concomitant green shift of the bioluminescence spectrum to match that of GFP fluorescence, a maximum in the green at 509 nm.

The luminol chemiluminescence is now a generally accepted standard for absolute calibration of a luminometer. Since the first study in 1965 that reported the Φ_C traceable to the standard lamp and hence to the black-body emission, a number of independent measurements have verified this result mostly using the actinometric method that however, is less accurate. Recently the standard lamp approaches have verified the original Φ_C precisely. A conservative estimate of ± 20 % is suggested for a detector calibrated against the luminol reaction, carried out according to the strict protocol described in the literature.

The luminol method does not require any additional instrumentation for its application. It is a substitution standard, i.e., it can duplicate the optical geometry of the sample to be measured. Bioluminescence reactions are in aqueous solvent and one luminol chemiluminescence standard reaction is also in water, thus eliminating the refraction correction. The aqueous reaction produces a broad blue emission with maximum at 425 nm. The other luminol reaction is in DMSO, and has an emission maximum at 495 nm. The reactions in either solvent produce the same quantum yield, so if the spectral sensitivity distribution of the detector is not known or is only approximately known, the spectral overlap with the two different chemiluminescence reactions will provide an accounting for the difference. Additionally, the refractive index of DMSO is 1.48 compared to 1.34 for water, so this will yield for a square cuvette at point-source geometry, a signal reduced over the aqueous reaction by $(1.34/1.48)^2 = 0.8$. As the luminometer usually is constructed for close-up geometry, this refractive difference will provide a measure of the reliability of the optical

correction. Most chemiluminescence reactions are in organic solvent with3 refractive index closer to that of DMSO.

In the two luminol reactions there are precautions to ensure that maximum integrated light signals are reproduced, an additional cross-check that using the two reactions can give. The aqueous reaction is initiated with an injection of an aliquot of hemoglobin in buffer as a catalyst for decomposition of H_2O_2. Hemoglobin has absorbance in the same spectral region as the chemiluminescence emission, so its final concentration must be such as to avoid self-absorption reducing the escaping chemiluminescence. In DMSO, traces of water from the atmosphere reduce and slow the light emission, but this is generally not a problem if a fresh bottle of DMSO is opened. Commercial grade luminol of highest purity has been found to give the same Φ_C as synthesized luminol purified by sublimation. However, it is important to verify that the absorption spectrum and extinction coefficient of the luminol sample corresponds to the published values.

About the same time as the luminol chemiluminescence was measured, a radioactive liquid scintillation standard was made available and distributed for calibration of luminometers. It consisted of a hexane solution contained in a glass vial and was calibrated by actinometry and the fluorescence of tryptophan in aqueous solution. On comparing the light emission from the scintillation standard with luminol it was concluded that the latter calibration was about two times less. Comparisons made independently since that time, have averaged about a 2.5 times ratio. Quinine has been generally recognized as a preferred fluorescence standard being stable against photooxidation, and has a fluorescence distribution at longer wavelengths in the blue range comparable to that from most chemiluminescences. The scintillation standard however, is very useful for providing quick and easy rough calibrations, provided that it is recognized that the signal level needs to be adjusted by 2.5 ± 0.5 to correspond to absolute photons.

6. **Quantitative Molecular Spectroscopy**

The mechanisms of photochemical and chemiluminescence reactions have in common the central role of the electronic excited state of a target molecule. They differ in that photochemistry is concerned with the chemistry that happens after the creation of the excited state of the target, and chemiluminescence in both how the excited state is created and to a lesser extent what happens after. The target molecule in photochemistry is the one excited by the absorption of radiant energy, the theory of which is well understood having been developed over the last one-hundred years. Not understood is how the exothermicity from the chemical process, is deposited into the excited state of one of the product molecules, to result in radiant or fluorescence emission of the product.

"White" light is considered to correspond to the visual sensation of the black-body emission spectrum, such as from an incandescent tungsten filament at about 3000 K. White light is also produced by a mixture of the three "primary" colors, red, blue, and green. When white light of initial intensity I_0, passes through a solution of concentration c of some substance in a cuvette having a path-length l, an appearance of color in the exiting intensity I will result if one of the primary colors is subtracted by the substance. This subtraction or absorption say of a band in the red, would result in a blue-green color of I. An expression for absorption is the well-known Beer-Lambert Law:

$$I_0 / I = \log \varepsilon c l,$$

where ε is called the "extinction coefficient" and has units of $M^{-1}cm^{-1}$. The extinction coefficient is wavelength dependent, and in the condensed state its value is usually stated for the maximum of an absorption band. For example, FMN in water has ε (447 nm) = 12300 $M^{-1}cm^{-1}$. The absorption in the blue region results in its yellow color of flavins (Latin: *flavus*, yellow). The inverse is called the "Transmittance" T, and the "Absorbance" A, also "Optical Density" OD, and are defined as:

$$T = I/I_0 , \qquad OD = A = -\log T.$$

Quantum theory of molecular spectroscopy developed in the first half of the 20th Century, was based on the notion of the wave-particle duality of radiation. The particle part was the photon, and the wave part was the 19th Century classical picture of electromagnetic radiation as consisting of electric (***E***) and magnetic (***B***) field vectors, oscillating orthogonal (perpendicular) to each other and to the direction of propagation (***k***) (Fig. 6.1).

The quantum mechanical picture of a molecule, is of the atomic nuclei separated at the bonding distance within which are arranged the original atomic electrons, now occupying groups of energy levels called "orbitals". Thus, if a molecule encounters an electromagnetic radiation field, the electrons being negatively charged, will be forced into an oscillation and

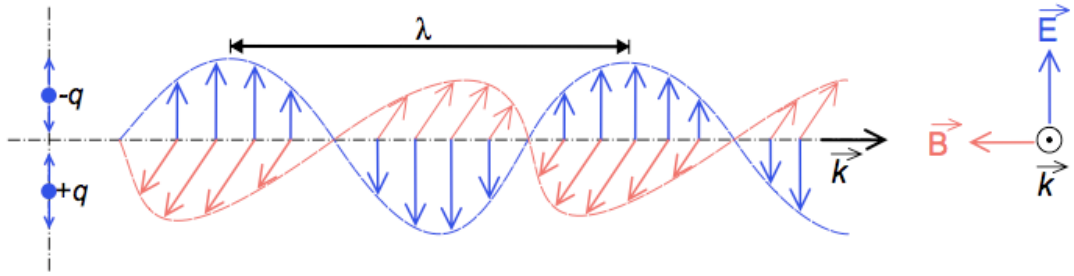

Figure 6.1. The photon wave consists of electric (**E**) and magnetic (**B**) field vectors oscillating orthogonal to each other. **λ** is the wavelength and ***k*** the direction of propagation.

depending on the energy of the electron, there could arise a coherence of the electronic oscillation with the radiation frequency. There will be a probability that the photon energy will be converted into an orbital energy excitation according to quantum theory. In other words, this is the quantum basis of absorption happening at particular wavelengths (λ), i.e., at frequencies (ν) corresponding to photon energies, according to the Planck relation for energy $E = h\nu = hc/\lambda$.

Among the rapid early developments of quantum theory, it is generally agreed that the Schroedinger Equation proposed in 1926, is the most notable. At this juncture, it was established that in the microscopic regime matter itself also needed to conform to the wave-particle duality. Schroedinger simply reformulated Newton's Second Law of Motion in a differential form:

Total energy of a system, ***H*** = kinetic + potential energies.

The "Hamiltonian" symbol ***H*** was adopted from its role in the earlier development of classical mechanics in the 19th Century. The Schroedinger time-dependent equation is a linear partial differential equation, partial because the energy is dependent on both time (t) and position (**r**) in 3-dimensions:

$$i\hbar\frac{\partial}{\partial t}\Psi(\mathbf{r},t) = \left[\frac{-\hbar^2}{2m}\nabla^2 + V(\mathbf{r},t)\right]\Psi(\mathbf{r},t)$$

where i is the imaginary number ($\sqrt{(-1)}$), *h-stroke* = $h/2\pi$, $\Psi(\mathbf{r},t)$ is called the wavefunction, dependent on both vector **r** and t, m is the mass of the electron in the usual case, the upside-down delta is called "del" and "del-squared" is the Laplacian operator, and V is the potential energy. Thus, the expression is just a wave equation formulation of the system energy, and is generalized but in a more obscure form as:

$$i\hbar\frac{\partial}{\partial t}\Psi = \hat{H}\Psi$$

where *H-carat* is called the "Hamiltonian Operator". The feature of the wavefunction formulation is that it has continuous solutions for the total energy, but some solutions have no time dependence, i.e., they correspond to "stationary waves". If you have the mathematical skills you can find these solutions, but an easier exercise is to solve the one-dimensional expression:

$$E\Psi(x) = -\tfrac{1}{2}[d^2/dx^2]\,\Psi(x) + \tfrac{1}{2}\,x^2\,\Psi(x)$$

or even better, go to an online demonstration so you can easily vary the parameters. The plot of the wavefunction is essentially the probability of finding the variable at each point on the x-axis (Fig. 6.2).
http://demonstrations.wolfram.com/QuantizedSolutionsOfThe1DSchroedingerEquationForAHarmonicOsc

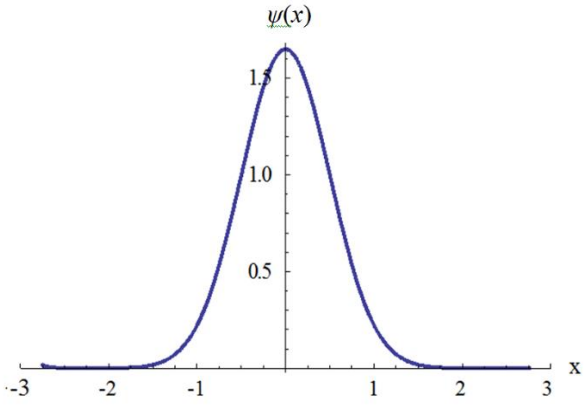

Figure 6.2. The values of the wavefunction $\psi(x)$ correspond to the relative probability of the electron being at each position on the x-axis.

This then, presents a way of determining an upper state energy of a system, which could correspond to the photon's energy resonant with the lower to upper state electronic transition in a molecule. The hydrogen atom consists of two members, an electron and a proton, and the Schroedinger equation predicts the energetic transitions exactly. Just as in classical mechanics, the three-body problem has no analytic solution, the wavefunctions for the hydrogen molecule and all more complex systems, must be determined by approximation (Chapter 14). Nevertheless, atomic gas-phase spectra which consist of sharp lines, can be calculated with good accuracy. For larger molecules in the condensed phase, even approximate calculations make great demand on computational speed and memory storage. There is recent interest in applying the methods of "computational chemistry" to understand chemical and biochemical excitation processes, but for bioluminescence excitation, as this take place within active cavities of proteins, there needs to be many approximations to make accessible calculations with available computational technology (Chapter 14). A popular

methodology currently in use is “Quantum Mechanics/ Molecular Mechanics” (QM/ MM), which combines the accuracy of QM with the speed of MM. For a biomolecular system

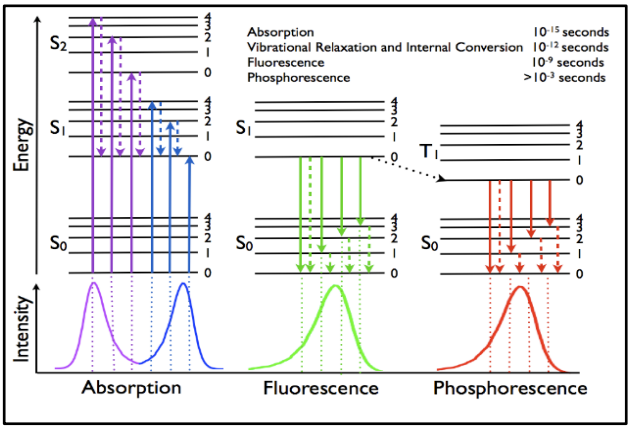

Figure 6.3. The Jablonski diagram summarizes energy level transitions.

the electronic energies in the active site are determined by QM and the rest of the protein having its energy minimized classically using MM. Recently, a QM/ MM computation of electronic distributions from hydrogen bonding in the active site of photoproteins explains their influence on spectral shifts of bioluminescence and fluorescence. In other examples these approaches have so far met with only limited success.

The next figure (Fig. 6.3) is called the Jablonski Diagram, a useful aid for describing energy transitions in atoms and molecules. In the lower panel of the figure, the spectral distribution of each transition is illustrated with the wavelength scale increasing to the right and the energy decreasing. The upper panel shows the energy transitions as vertical lines. Almost all molecules have lowest energy or ground states with all electrons paired, known as “singlet” states, and therefore designated in the diagram as S_0 for the zeroth level, S_1 for the next, and so on. Oxygen and nitric oxide are unusual in the electrons having parallel spins in the ground state, and such states are called triplet states. Normally, triplet energies are above S_0. They are labeled “T” in the Jablonski diagram. Superimposed on each state are slightly higher vibrational modes, the horizontal lines numbered 1, 2, 3, etc., although there are many more possibilities than just these few. The Born-Oppenheimer Approximation in the Schroedinger equation, allows a separate calculation of the nuclear wavefunction from the electronic wavefunction:

$$\Psi \text{ (total)} = \psi \text{ (electronic)} + \psi \text{ (vibration, rotation).}$$

These contributions of nuclear motion are symbolized as $S_{0,1}$ in the lowest vibrational ground state, $S_{1,1}$, the first vibrational state in the first excited electronic state, etc. According to the Franck-Condon Principle, transitions between electronic states are instantaneous in

comparison to nuclear motion, 10^{-15} s versus ~10^{-12} s; note that the shorter time is about the same as the inverse of the frequency of the photon field. The vertical lines represent the energy transitions, the full lines up for an absorption of a photon energy, or down for re-emission. These are called Franck-Condon transitions, and the upper level called the Franck-Condon State. The Boltzmann distribution function predicts that each level will lie in its lowest vibrational state at equilibrium. Thus, the leftmost transitions, full lines, symbolized by $S_{0,0} \rightarrow S_{2,4}$, will be immediately followed in the condensed state, by a rapid "cooling" by vibrational relaxation and also "internal conversion", represented by the dashed lines, and the molecule ends up at the lowest vibrational level of the first excited singlet state $S_{1,0}$. Internal conversion is a non-radiative process induced by collisions with surrounding molecules, and at room temperature this total equilibration time is of order of picoseconds (ps, 10^{-12} s).

The $S_{1,0}$ level is a stationary state in that it is stable for much longer times, typically more than nanoseconds (ns, 10^{-9} s). It transitions down to $S_{0,0}$ in two ways, a radiative rate (k_R) the full green down arrow manifest as fluorescence, competing with non-radiative loss (k_{NR}) (dash blue line), again through other interactions with the environment, resulting in its energy converted into heat. Then we can write the fluorescence yield as a ratio from the rates or probabilities of these two processes:

$$\Phi_F = k_R / [k_R + k_{NR}].$$

A third possible transition is "intersystem crossing", indicated by the dotted line down to $T_{1,0}$, the triplet state. The triplet in the absence of other interactions, is stable for long times, typically $>10^{-6}$ s. This is because the parallel to anti-parallel spin conversion needed to form the singlet ground state, is disallowed from quantum theory. Nevertheless, a radiative transition may eventually occur, the energy of the full red line appearing as phosphorescence. Again, the phosphorescence yield will result from the ratio of radiative to total triplet energy loss probabilities, combined with the initial probability of intersystem crossing.

The lower panel of Fig. 6.3 shows spectral distributions for each of these types of radiative transitions, absorption, fluorescence, and phosphorescence that might be observed for this molecule in the condensed phase. In contrast, in a dilute gas phase the spectra for a simple molecule consist of sharp lines, corresponding to each transition, e.g., $S_{0,0} \rightarrow S_{2,4}$, $S_{0,0} \rightarrow S_{2,3}$, etc. For a more complex molecular system, there will be many overlapping modes of vibration and rotation, resulting in "homogeneous broadening", the reduction or absence of structure in the spectral distribution. In the condensed phase, the aforementioned intermolecular collisions smooth out the distribution, and this is called "inhomogeneous broadening". The panel also demonstrates that each transition, either up or down, starts at the lowest vibrational level, but the most intense transition corresponding to the maximum in the broadened spectrum, can be at various vibrational levels of the final electronic manifold, e.g., $S_{1,0} \rightarrow S_{0,2}$, $S_{0.0} \rightarrow S_{0,4}$. The consequence is that emission spectra are found at longer wavelengths than the absorption, the difference in maxima called the "Stokes Shift".

Fig. 6.4 below, explains this phenomenon as a result from the Franck-Condon Principle with the result of a shift of the molecular electron distribution on excitation. Usually, there is an increase in dipole moment in the excited state manifold (E_1) over the ground state (E_0) and an

increase in bonding distance (q_{01}). It can be shown that for a simple diatomic, the electronic potential energy approximates an inverse Gaussian distribution, the full line in Fig. 6.4. The vibrational wavefunctions are the stationary brown waves at each vibrational level, and the zeroth level is seen to be most probable at the maximum of its wave amplitude. This is what the wavefunction means, that the transitions should have random probability. As the nuclear co-ordinate is "frozen" for the instantaneous transition times, the most probable absorption is $E_{0,0} \rightarrow E_{1,2}$, and for fluorescence $E_{1,0} \rightarrow E_{0,2}$. The maximum for the fluorescence spectrum therefore, will be at longer wavelength or lower energy, than for the absorption and is revealed as the Stokes shift.

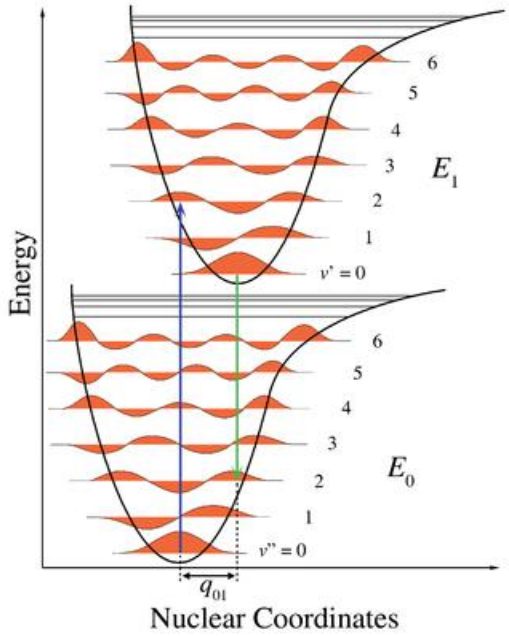

Figure 6.4. Franck-Condon transitions are most probable between the maxima of the vibrational wavefunctions.

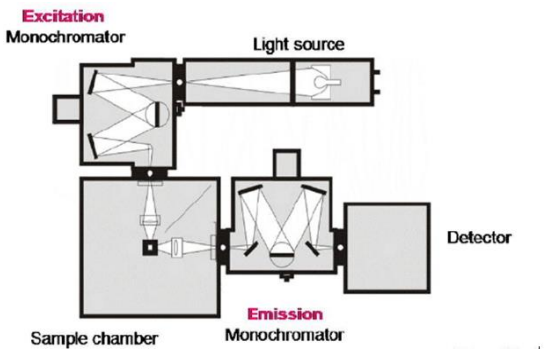

Figure 6.5. Modular spectrophotometer for fluorescence, or absorbance after a reconfiguration.

Experimental spectroscopy used in bioluminescence investigations ranges from the most basic to advanced techniques such as picosecond dynamic fluorescence. The basic requirements for all are a suitable light source, a method for spectral dispersion, usually a finely ruled diffraction grating, and a sensitive detector. Fig. 6.5 is an arrangement of the components for a fluorescence spectrophotometer. For an absorption spectrophotometer in the simplest arrangement, instead of the "emission" monochromator, the detector is placed in-line with the light beam entering the sample from the top "excitation" monochromator. Two light sources are used for absorption spectroscopy, a tungsten incandescent lamp to cover the visible region, and a hydrogen-deuterium lamp that provides higher intensity in the UV, 200-400 nm. As the grating is oriented by a motor, each wavelength passes the exit slit to illuminate the sample, and the transmitted intensity I recorded on the detector, usually a photocell along with the associated electronics required for display of the data. A reference measurement must be made to determine the initial intensity I_0 either by replacing the sample with a blank, or by incorporating double beam optics, so that the detector records only the intensity ratio, sample/blank, essentially equal to the transmittance, $T=I/I_0$. Some more modern absorption spectrophotometers utilize a linear charged-coupled device (CCD) detector. This enables all wavelengths to be collected simultaneously and there are no moving parts. The light source is positioned in place of the excitation monochromator and again, the inline transmitted beam focused onto the entrance slit of the emission monochromator and CCD detector. As there is no movement of the grating required, a CCD detector enables rapid collection of the complete spectrum important for application to stopped-flow kinetics.

A fluorescence spectrophotometer incorporates both monochromators as shown in Fig. 6.5, with the emission being detected at right angles to the excitation beam. In more expensive instruments a double monochromator is used on the excitation arm for reduction of stray light. The light source is usually a xenon lamp to provide much higher excitation flux in the UV. The fluorescence emission being isotropic, only a small fraction can be collected by the emission optics, and is further restricted by the slit width defining the wavelength interval of interest. Therefore the detector must be a photomultiplier having very high sensitivity. A CCD detector usually has insufficient sensitivity for fluorescence spectroscopy applications. Based on the earlier discussion, excitation into any absorption band will produce a fluorescence spectrum at wavelengths longer than the lowest absorption band. For detecting weak fluorescence, excitation of high intensity must be used, with care taken that this does not induce photochemical changes in the sample.

The construction of a monochromator is such that, as it is simpler to have the diffraction grating rotating linearly, the spectral intensity at each wavelength is collected with constant slit width in wavelength units, say 5 nm width at 400 nm, and the same width at 600 nm. Most publications present spectra for convenience as signal versus wavelength therefore, but these are not energy spectra that allow a theory-based analysis, i.e., that a single electronic transition should have a Gaussian energy distribution (Fig. 6.4). For sharp lines as in gas phase atomic spectra, it is correct to convert wavelength to frequency or energy by $\nu = c/\lambda$, but not for broad spectra as encountered in the condensed phase:

$$dv/d\lambda = -c/\lambda^2$$

$$I(v)\,dv = -c/\lambda^2 \times I(\lambda)\,d\lambda$$

These expressions enable the energy spectrum, $I(v)dv$, to be extracted from the wavelength spectra so it can be analyzed for its Gaussian parameters. Commercially available spectrophotometers usually come with software for doing such conversion. For presentation, it is usually the case that the energy is listed as "wavenumber" ($\bar{\nu}$) where:

$$\text{Wavenumber, } \bar{\nu}\ (\text{cm}^{-1}) = 10^7/\lambda \qquad \text{with } \lambda \text{ in nm}$$

$$\text{e.g., } \bar{\nu}\ (20{,}000\ \text{cm}^{-1}) = \lambda\ (500\ \text{nm})$$

An expression for finding the wavelength for maximum intensity for each type of plot is:

$$\lambda_m = \bar{\nu}_m^{-1}[1\text{-}0.36\times \text{FWHM}^2 \times \bar{\nu}_m^{-2}]$$

where FWHM is the full width at half the wavenumber maximum ($\bar{\nu}_m$). In some cases of broad spectra, λ_m and $\bar{\upsilon}_m^{-1}$ can differ by up to 7 nm.

Two accessory components are often utilized for fluorescence spectroscopy, one with a polarizer in the excitation path, the other a "T" configuration with an additional polarizer viewing the total emission (Fig. 6.6). This latter is useful for eliminating small instabilities in the excitation beam intensity while the grating is turning to scan the fluorescence spectrum, or more critically, if the emission signal is varying due say to a chemical reaction in the sample. This is a particular requirement if on measuring the spectrum of a bioluminescence reaction, the signal usually will be decaying over the time of several minutes required to scan the spectrum. The detector signal is then collected as a time-independent ratio. For polarization, the most expensive solution is to incorporate two Glan-Thomson prism polarizers, one in the excitation beam prior to its entering the sample, and the other between the sample and the emission monochromator. The polarization of fluorescence emission is determined by collecting the spectrum in two configurations of the excitation and emission polarizers.

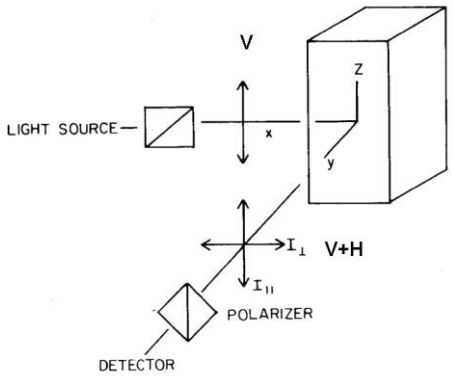

Figure 6.6. Collection of vertically (**V**) and horizontally (**H**) polarized fluorescence

The most probable orientation of a molecule for absorption is when its transition moment is parallel to the electric vector of the impinging photon. If the first polarizer after the light source is oriented to make the polarization of the excitation beam vertical (**V**) as indicated here, then the initial emission at right angles in the y-direction, also will be vertically polarized. However, the lifetime of the excited states of most systems is of the same order as that for rotational diffusion of the molecule, so that in the steady-state the output beam will have polarization components both vertical and horizontal (**H**), as indicated in Fig. 6.6. A parameter to define this polarization state is called the steady state anisotropy (*r*), where **V** and **H** are the emission intensities:

$$\text{Anisotropy, } r = (\mathbf{V} - \mathbf{H})/ (\mathbf{V} + 2\mathbf{H}) = 0.4 \text{ maximum.}$$

The maximum value not being unity, is due to the stochastic orientation of molecules in the sample, each having a transition moment component along the *z*-axis resulting in an average for the absorption probability.

A small molecule such as quinine has a rotational diffusion time less than nanoseconds, but its fluorescence lifetime is around 20 ns. Consequently, **V**~**H** and the steady-state fluorescence anisotropy will be near zero. Lumazine protein is a 21-kDa protein, an "antenna protein" functional in bacterial bioluminescence, and is so-named for short as it has a 6,7-dimethyl-8-ribityl-lumazine as a fluorescent ligand (Chapter 13). In solution the free lumazine derivative has a near zero anisotropy, but bound to the protein the anisotropy is greater than 0.35 (Fig. 6.8). This value is what can be calculated from the rotational diffusion of the lumazine protein as a whole, which leads to the conclusion that the lumazine is rigidly bound. On dilution for example, the lumazine to apoprotein equilibrium constant can be determined, from measurement of the loss of average steady-state anisotropy, the free lumazine having anisotropy about zero. Strictly, the chemical name "lumazine" means the central ring structure (Fig. 13.3). To avoid ambiguity, recent authors have suggested the name "ribolumazine" for the ligand.

A time-dependent or dynamic fluorescence study, requires the excitation light source to have sub-nanosecond duration, usually achieved with a pulsed laser. Fig. 6.7 shows a delta (~0.1 ns) excitation pulse and a following fluorescence having a decay time τ = 5 ns. The fluorescence signal F(*t*) at any time is proportional to the concentration of excited states, $S_{1,0}$. There is a random probability of removal of the excited state population given by the rates k_R + k_{NR}, so that the fluorescence decay function will be exponential:

$$F(t) = F_0 \exp(-t/\tau); \; F_0 = 1.0, \; t = \text{time in ns.}$$

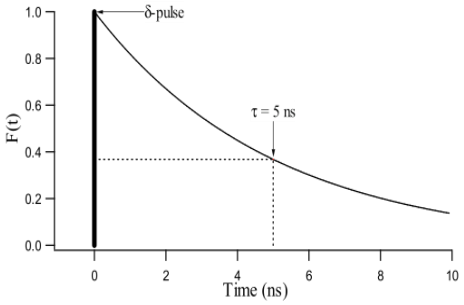

Figure 6.7. Decay of fluorescence after a subnanosecond excitation pulse (δ).

The fluorescence lifetime τ, is the time for the fluorescence to fall to 1/e of its initial value. The fluorescence half-life is given by, $t_{½} = 0.69 \times \tau$.

Dynamic fluorescence experiments have been applied to reveal excited state interactions, or again in the example of lumazine protein, the dissociation equilibrium of bound and free ligand. The fluorescence lifetime of free lumazine (τ_1) differs from when bound (τ_2), so that on dilution the decay of the total fluorescence signal will be a double exponential function:

$$F(t) = F_1\exp(-t/\tau_1) + F_2\exp(-t/\tau_2)$$

and the concentration ratio free/bound will be proportional to F_1/F_2.

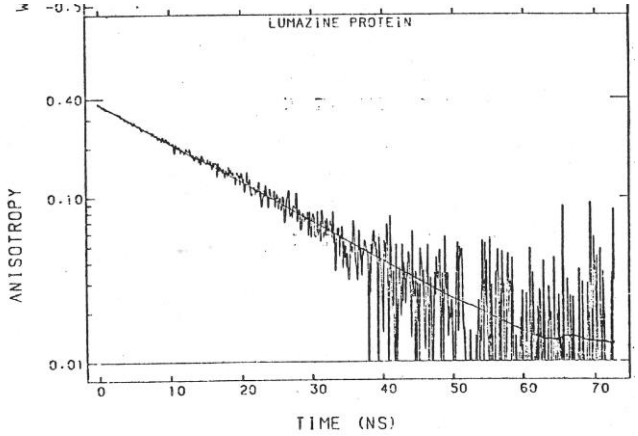

Figure 6.8. Semilog plot of the decay of fluorescence anisotropy of Lumazine Protein (22 kDa) at 2ºC. The straight line is a single exponential fit to the decay with φ = 18 ns, indicating a spherical rotator with the lumazine being rigidly bound.

Dynamic fluorescence anisotropy is also a technique applicable to studies of protein interactions, and has been utilized in bioluminescence studies. Following the initial excitation pulse, Brownian motion randomizes the transition dipole orientation at a characteristic time called the rotational correlation time, φ. From the theory of rotational diffusion, the rotational

correlation times for a sphere can be calculated. For example, in aqueous solution at 2ºC, a spherical shaped protein with 21-kDa mass, will coincidentally have a similar numerical value of the correlation time, $\varphi \sim 20$ ns. Fig. 6.8 shows the closely exponential anisotropy decay for lumazine protein at 2ºC with $\varphi = 18$ ns.

In its bioluminescence function, lumazine protein forms an equilibrium complex with bacterial luciferase (76 kDa), and the amount of free and bound lumazine protein will be revealed directly by fluorescence anisotropy decay analysis on the mixture. The result is a double exponential fit to the anisotropy decay:

$$r(t) = r_1\exp(-t/\varphi_1) + r_2\exp(-t/\varphi_2)$$

$$= 0.2\exp(-t/23) + 0.1\exp(-t/77)$$

Thus, the protein-protein equilibrium constant can be determined from $r_1/r_2 = 2$, meaning free lumazine protein to complex is in a two times ratio here. In the complex, the φ_2 is expected to be 23 + 76 ns, and the value found in the experimental analysis is only 77 ns, but actually this is within the uncertainty of the fitting analysis. We shall show later that this protein-protein complex anyway is too weak to account for the bioluminescence effects of lumazine protein, and the functional complex in reality is one with a luciferase reaction intermediate.

The explanation of inhomogeneous broadening can be extended to account for how the intermolecular environment affects excited state properties. Absorption of a photon usually results in shifts of electrons within a molecular system, resulting in an increase in dipole moment. Fluorescence spectroscopy of model compounds shows that in solvents of dielectric constant lower than that of water, the fluorescence spectrum is usually blue-shifted (Fig. 6.9). Simply, the S_1 energy level is raised because of the increase in the energy of Coulombic (electrostatic) interaction due to the lower dielectric constant. Solvent rigidity, for instance in a glassy environment, also induces blue shifts probably from inhibition of molecular relaxation. Such conditions as these are used to explain the effect on spectra on a ligand's binding within a protein cavity. Commonly observed changes are on spectral position, rotational relaxation times, and transitional probabilities.

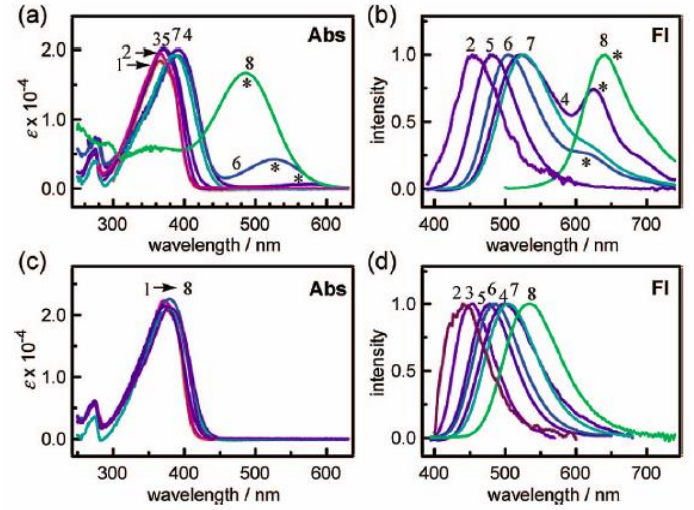

Figure 6.9. Effect of increasing solvent polarity on the absorption and fluorescence spectra of firefly dimethyloxyluciferin (*top*) and its 6'-methoxy derivative (*lower*). 1. p-xylene, 2. benzene, 3. chloroform, 4. DMSO, 5. acetonitrile, 6. 2-propanol, 7. methanol, 8. water. The asterisk indicates the 6'-phenolate form.

Characteristics of electronic excited states can also be perturbed by the presence of secondary molecules added to the system. The effects of additives fall into two types, the first a reduction of the fluorescence quantum yield, called "quenching", and the second usually a shift in the emission spectrum by a generalized process called "energy transfer". Attention needs to be drawn to the fact that "energy transfer" is just renaming of the spectral shift. There may or may not be any change in quantum yield.

The quenching mechanism is simplest to describe. If the quencher (Q) forms a weak and non-covalent complex in equilibrium with the subject fluorescent molecule (M), there should be no change in the electronic orbitals and consequently the same energy of the absorption transition $S_0 \rightarrow S_1$. In the excited state, if the complex has no fluorescence then any emission observed will be only from uncomplexed M* having an unchanged spectrum and lifetime. This is called "static quenching", and in Chapter 4 it has been shown how this has been applied to ligand-protein binding in the cases of firefly and bacterial luciferases. The equilibrium constant (K_A) can be extracted from such a study.

$$M + h\nu \rightarrow M^* \rightarrow M + h\nu_F \qquad \text{fluorescence } F_o$$

$$M + Q \leftrightharpoons MQ \qquad \text{fluorescence signal } F_Q$$

$$F_o / F_Q = 1 + K_A[Q]$$

This is called the "Stern-Volmer Equation" from which the MQ ground state association constant, K_A, can be recovered from a plot of fluorescence against concentration [Q].

A second fluorescence quenching mechanism involves an interaction in the excited state. As fluorescence lifetimes are in the range of nanoseconds, this time is sufficient for binary

collisions to occur at diffusion limited rates. Oxygen is well known as a quencher of fluorescent states, and in aqueous solution at room temperature its diffusional pseudo-first order rate of encounters is about $10^{10}\ M^{-1}s^{-1}$. A saturating concentration of oxygen in water is about $2\times10^{-3}\ M$, yielding a diffusion-controlled rate of interaction, $k_q[Q] = 2\times10^{7}\ s^{-1}$. The fluorescence lifetime in the absence of Q, is seen from the two-state energy diagram (Fig. 6.10) to be:

$$\tau_0 = (k_r + k_{nr})^{-1}$$

and addition of Q will decrease the lifetime to

$$\tau_q = (k_r + k_{nr} + k_q[Q])^{-1}$$

With some algebra we can write another Stern-Volmer equation for dynamic fluorescence quenching:

$$\tau_0/\tau_q = 1 + \tau_0 k_q[Q]$$

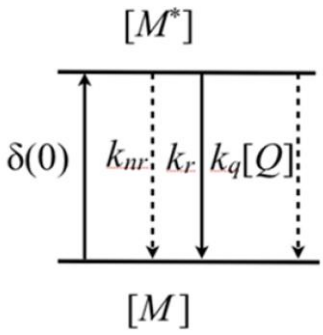

Figure 6.10. Dynamic quenching of fluorescence is equivalent to adding an additional non-radiative transition rate k_q.

For a fluorescence lifetime of 10 ns, a saturating oxygen concentration in water will reduce it by about 10%. Dynamic quenching is consequently distinguished experimentally from static by a reduction in the donor fluorescence lifetime, as well as the fluorescence quantum yield. Some fluorescent molecules also exhibit self-quenching at a sufficiently high concentration, and the mechanism can be either static or dynamic.

A common rationalization of dynamic fluorescence quenching is by electron transfer within the transiently formed encounter complex. In Fig. 6.11 LUMO, the Lowest Unoccupied Molecular Orbital of the excited donor $^1D^*$, is at a slightly higher energy level than HOMO, the Highest Occupied of the acceptor ^0A in the ground state. The Pauli Principle states that for a molecule in the ground state, the electron spins designated here by the up-down arrows, must be paired. That is, there should be no net electron spin but there are a few exceptions, in particular the oxygen molecule, which is a ground state triplet, and nitric oxide, a stable free radical. The picture in Fig. 6.11 is a simplified representation of the electron transfer process

within the collision complex where the electron in the first excited singlet (spin paired) LUMO state of the donor (^{1}D*), spontaneously transfers into the ground state LUMO of the acceptor ^{0}A. In the language of thermodynamics this is called "spontaneous", because it is a downhill or net exothermic (strictly, "exergonic") process. Contrarily, if the ground state HOMO and LUMO levels of ^{0}A are higher than ^{1}D*, then the roles are reversed, ^{0}A donates its electron from its ground state HOMO into the empty HOMO of ^{1}D* and the same radical pair is formed. No fluorescence emission occurs as the pair should rapidly diffuse out of the encounter complex "cage" in less than 10^{-9} s. Notice that the accepted electron in $A^{-\bullet}$ is drawn with its spin direction either up or down. Within the encounter the pair have a charge-transfer interaction that may delay a ready diffusional separation, leading to a possibility of radical annihilation back to an excited state, the triplet ^{3}D* if its level is low enough for the back transfer to be spontaneous. In Fig. 6.11 the singlet production would be endothermic and therefore less likely. In the next chapter this idea will be elaborated as it is the basis of one proposed mechanism of chemiluminescence excitation.

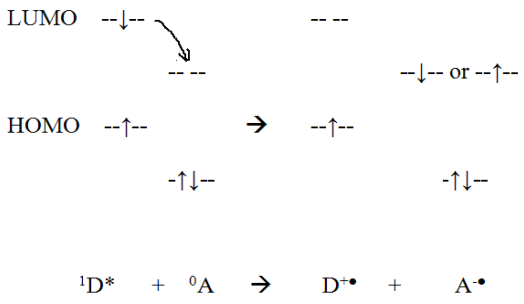

Figure 6.11. Electron exchange within the encounter complex leading to dynamic fluorescence quenching.

The second major class of excited state interaction is energy transfer, and is divisible into three sub-types essentially on the basis of the separation of donor and acceptor. The first is a

1. Trivial	D* → D + *hv* + A → D + A*	D—A > 100 nm
2. Dexter	D* + A → [D*--A] → D + A*	D---A < 1 nm
3. Förster	D* + A → D + A*	D—A = 1-10 nm

radiative process, and can be correctly labeled "fluorescence" energy transfer but sometimes it is called "trivial" because it is easy to explain. In the experimental measurement of the fluorescence spectrum of D, care must be taken that its absorption spectrum tail at longer wavelengths has an optical density that does not re-absorb some fluorescence, thereby distorting the fluorescence spectral distribution. A second molecular species A in the sample, could also by its absorbance and without having a specific interaction, absorb then contribute its own fluorescence and distort the original spectrum. These trivial energy transfers can be

avoided by keeping the optical density of all components below 0.1, and can also be determined as trivial as we will show, by having no effect on the donor fluorescence lifetime.

In the field of molecular spectroscopy, there are two general mechanisms of non-radiative electronic energy transfer, named for the seminal contributions of Theodore Förster (1946) and D. L. Dexter (1952). The Dexter Interaction is by an "encounter" forming an excited state complex called an "eximer", because it requires a close approach < 10 Å to enable overlap of donor and acceptor orbitals, and its efficiency has an exponential distance dependence. The overlap of orbitals results in electron exchange and although it is inherently quantum mechanical, an elementary pictorial scheme is visualized here in Fig. 6.12, which illustrates the operation of a donor in an excited triplet state ^{3}D* able to exchange an electron to populate a lower energy triplet state of a "sensitizer" or acceptor ^{0}A*.

Dexter developed his theory in connection with solid state luminescence, but it has been also applied to the case of concentration quenching of fluorescence (^{1}D*) in the liquid state, or the dynamic quenching by another molecule as discussed above:

$$^1D^* + {}^0A \rightarrow {}^0D + {}^0A + \text{heat, or} \rightarrow {}^0D + {}^1A^*$$

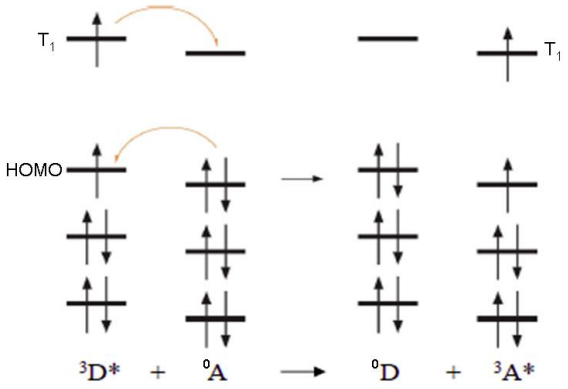

Figure 6.12. The Dexter Interaction within an encounter complex can lead to excited state formation.

The quencher or acceptor A, may or may not itself be excited, the latter to the triplet in Fig. 6.2. We will show later, that a Dexter mechanism also can be considered as the mechanism of chemiexcitation where the energetic intermediate going through its transition state is degenerate both structurally and energetically, with an excited state of the acceptor.

Förster Resonance Energy Transfer (FRET), results from a weak dipole-dipole Coulombic coupling of the $S_1 \rightarrow S_0$ transition moment of the donor to that of the acceptor $S_0 \rightarrow S_1$. It is called a "near-field" process because it has an inverse 6th-power dependence on the donor-acceptor separation, and although "weak", it can be effective up to around 10 nm, much less than the wavelength of the fluorescence if it were a radiative (trivial) transfer. In the literature, this is sometimes called "Fluorescence resonance energy transfer" but this is a

misnomer, as “fluorescence” is not transferred but only emitted at the end of the process. The preferred name attributes the seminal contribution of Theodore Förster who, in 1946 published a quantum mechanical analysis of this resonance coupling phenomenon. This property of “Sensitized Fluorescence” had been difficult to explain since its discovery in 1922. It was found that in a dilute vapor mixture of mercury and thallium atoms, excitation of mercury precisely at a wavelength in the UV where thallium does not absorb, produced a green fluorescence from thallium. The energy transfer had to be collisionless at the dilution used, because the collision rate was much less than the rate of deactivation of the S_1 state of the mercury. A quantitative accounting of this effect resisted many attempts by major names in the physics community, until Förster’s analysis of resonance coupling between two electronic oscillators, one the transition of a donor (D), and the other transition of an acceptor (A) the “sensitizer”. It is a non-radiative “near-field effect”, an important distinction from the trivial energy transfer, which is a “far-field effect”, where a photon emitted from the donor is simply absorbed by the acceptor at macroscopic separations.

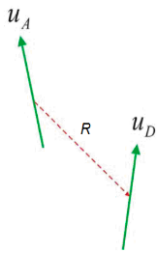

Figure 6.13. The donor (*D*) and acceptor (*A*) pair with randomly oriented transition dipoles.

Förster showed that for two molecules separated by more than their dimensions, their transition dipoles *u*, could exhibit coupling in resonance (Fig. 6.13). At a separation *R*, where the dipole-dipole coupling is weak and the approximations pertain, Förster derived the rate for energy transfer:

$$k_T(R) = \tau_D^{-1}(R_0/R)^6,$$

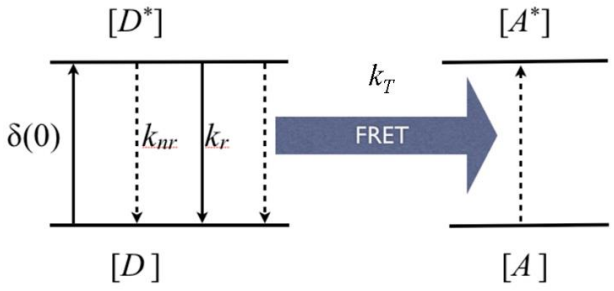

Figure 6.14. Resonance coupling between the transition oscillators introduces an additional non-radiative loss process k_T on D^*.

where τ_D is the donor radiative lifetime ($\tau_D = k_r^{-1}$), and k_{nr} is the non-radiative rate. As the transfer rate k_T is proportional to the inverse 6th power of the donor-acceptor separation, it is often used to determine distances of donor-acceptor separation in the range 1-10 nm. The separation at which the resonance transfer has a 50% probability over the donor fluorescence rate, is called the Förster or critical distance, R_0. It can be calculated using the spectroscopic properties of each molecule:

$$R_0^6 = \frac{9000 \ln(10) \kappa^2 \Phi_0}{128 \pi^5 N_A n^4} \int_0^\infty \frac{F_D(\sigma) \varepsilon_A(\sigma)}{\sigma^4} d\sigma$$

where κ^2 is a factor determined from the respective orientation of the *D* and *A* transition dipoles (Fig. 6.13.), Φ_0 is the donor fluorescence quantum yield, N_A is Avogadro's number, and *n* is the refractive index of the intervening medium. The integral in the above equation is the degree of spectral overlap (*J*, $M^{-1}cm^3$) between the area normalized (A = 1) donor fluorescence spectrum (F_D) and the acceptor absorption spectrum (ε_A) either on a wavenumber ($\bar{\nu}$ or σ) or wavelength (λ) scale:

$$J = \int_0^\infty \frac{F_D(\sigma) \varepsilon_A(\sigma)}{\sigma^4} d\sigma = \int_0^\infty F_D(\lambda) \varepsilon_A(\lambda) \lambda^4 d\lambda$$

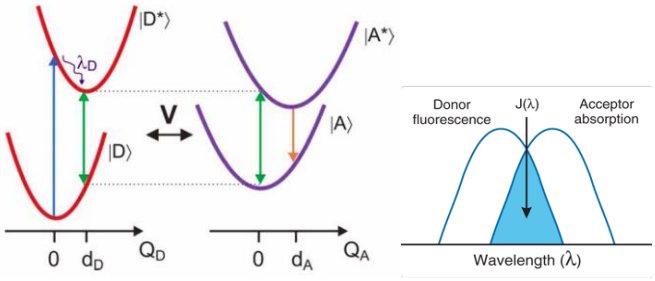

Figure 6.15. Resonance coupling between two electronic oscillators.

Fig. 6.15 illustrates by the blue shaded area, the overlap *J* in the case of these two molecular spectra. In later chapters we will show how the FRET mechanism accounts for bioluminescence color shifts in some systems.

In recent decades much activity in quantum spectroscopic theory, has resulted in a combination of the three energy transfer processes 1, 2, and 3, in a "Generalized Förster Theory". The upshot is that the three processes are essentially the same, only differing in the dominance of certain terms, and with the degree of separation of the partners. A simple picture is that for a radiative transfer, the separation has to exceed the wavelength of the photon. For the near-field and Dexter interactions, the transfer vehicle becomes a "virtual photon". We shall return to this aspect later but for the moment, the requirement for millimolar concentrations of participants in chemiluminescence of dioxetanones needed for

optimal Φ_C, indicates that a close interaction within collisional encounters is the case, and the Dexter mechanism of electron exchange therefore is a suitable vehicle for a basis of excitation theory. All three processes are relevant to the understanding of bioluminescence mechanisms.

Circular dichroism (CD) is another useful spectroscopic technique in characterizing proteins. The CD is measured as the difference in absorption of left-hand and right-hand polarized light. The value of this difference is usually very small, ~10^{-3} of the total absorbance but can be determined accurately with modern instrumentation. Nearly all molecules occurring in biological systems are optically active, for instance the amino acid residues constituting proteins except for glycine, are all L-enantiomers. Consequently, a polarized light beam passing through a protein solution will undergo a rotation. The vertically polarized light beam then can be resolved into two circularly rotating vectors with opposite rotations. Each will be transmitted through the solution differently giving rise to CD. The CD in the far-UV absorbance region 190-230 nm, arising from the amide links in the protein chain, is roughly diagnostic of the protein secondary structure, i.e., the percent of α-helix, β-sheet, and random coil. This had been a useful experimental result prior to the ability of crystallography to provide a high resolution spatial view of protein structures.

Fig. 6.16 shows the effect of binding of the lumazine ligand onto two different lumazine proteins. The circular dichroism in the 260-280 nm region is characteristic of the tryptophan and tyrosine residues in proteins. An interpretation of the observation that the CDs of the ligand around 420 nm are almost the same, is that the two lumazine proteins have very similar binding site structures. In this main absorbance band (415 nm) of the bound lumazine, the large negative circular dichroism indicates that the ligand lies in a very asymmetric environment, and this is confirmed by the spatial structure of lumazine protein determined more recently.

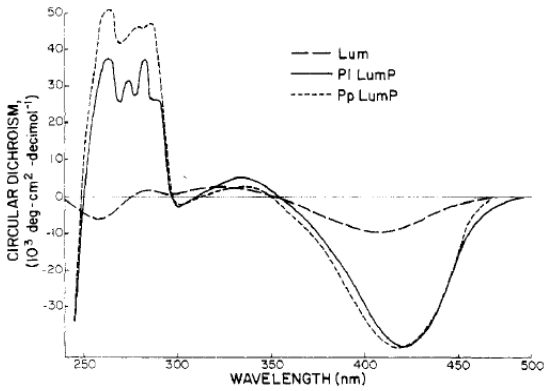

Figure 6.16. Circular dichroism of the lumazine derivative (Lum) free or bound on two types of lumazine protein (---, —). The binding site provides a very asymmetric environment compared to that in free solution (– –).

7. **Chemiluminescence**

Bioluminescence is a chemical reaction taking place on a protein where the chemical energy output, the “exothermicity”, is converted into light with a high efficiency and that accordingly, has evolved for maximum benefit for the fitness of the bioluminescent organism. In order to elucidate the chemistry of bioluminescence, investigation of the mechanism of the chemiluminescence of the various luciferins and their analogs in solution outside of the protein, has proven a fruitful approach. This is especially true in the case of the chemiluminescence models of the firefly and coelenterazine-type systems, but has been frustratingly elusive for providing any basis for understanding the mechanism of bacterial bioluminescence. A significant outcome of these research efforts extending over the last fifty years, has been a major commercialization of chemiluminescence and bioluminescence methods in analytical applications, particularly in biomedical research involving cellular imaging and clinical diagnostics.

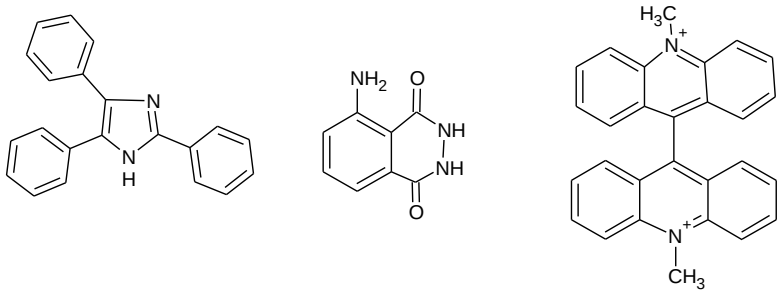

Lophine Luminol Lucigenin

Figure 7.1. The three “classical” and most studied chemiluminescence molecules.

The emission of light from a chemical reaction was first discovered in 1877 by Radziszewski who had synthesized lophine, triphenylimidazole, and observed a bright yellow emission on warming and exposure to oxygen. Albrecht in 1928, discovered the chemiluminescence of luminol, and in the 1930s the chemiluminescence of acridan derivatives such as lucigenin and acridinium esters was discovered, and subsequently investigated by many. In spite of continued studies in recent times, unearthing the chemiluminescence mechanisms of luminol and lophine have arguably proven fruitless, but in gratifying contrast much success has been achieved in the case of the acridans such as lucigenin. Consequently, acridan derivatives have been employed in many applications and are currently the basis of multibillion dollar industries. These three classical chemiluminescence reactions (Fig. 7.1) have chemiluminescence quantum yields only around 0.01, so do not present adequate models for the highly efficient bioluminescence chemistry.

The solution of a chemiluminescence mechanism first requires identifying the steps in the light reaction and whether or not these correspond to the observed overall chemistry. As these reactions are very exothermic, side reactions can often cloud the picture. If a major product

having the same fluorescence spectrum as the chemiluminescence can be trapped and identified, this is an important clue for identification of the light pathway. The kinetics of light emission is also important to be in correspondence to the chemical kinetics. The ultimate goal is to be able to identify a high energy intermediate that has sufficient breakdown energy to excite the product to its fluorescent state.

A landmark observation in this regard was made by Ed Chandross in 1963, of a very bright chemiluminescence from the reaction of oxalyl chloride with concentrated hydrogen peroxide (30%), in the presence of a highly fluorescent molecule such as 9,10-diphenylanthracene (DPA). If the fluorescent molecule was not present only a very weak bluish chemiluminescence was observed, but it was much stronger if DPA or other fluorescent compounds were added to the mixture. The enhanced chemiluminescent emission spectrum matched the fluorescence spectrum of the additive even though apparently, the chemical structure of fluorescer was not changed after the chemical reaction. This property would suggest the reaction to be a "sensitized chemiluminescence", by analogy with the phenomenon of sensitized fluorescence.

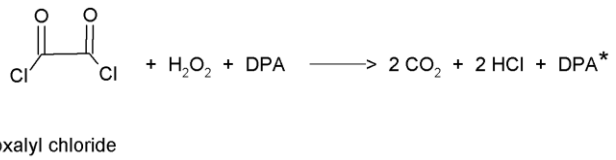

The commercial potential of this reaction was apparently recognized by Rauhut and associates at the American Cyanamid Company, who used it as the basis for development of the "light stick", a chemiluminescence that everyone is familiar with nowadays. Rauhut's group suggested that the chemiluminescence mechanism could involve peroxyoxalate, a dioxetanedione (**V**) (Fig. 7.2) as a "High Energy Intermediate" (HEI), the provider of the excitation energy for the fluorescence. This structure **V** with a highly strained ring system, can be seen to be equivalent to a carbon dioxide dimer, and its breakdown energy can be calculated to be more than enough to populate the S_1 state (*) of the fluorescent additive. A four-membered ring peroxide structure had also been proposed by McCapra in connection with his study of the mechanism of lucigenin chemiluminescence, and he also postulated the involvement of a dioxetane intermediate in firefly bioluminescence.

Concentrations in the millimolar range of the oxalyl esters and the fluorescent additive, are needed to achieve the highest Φ_C, a property implying requirement of a weak complex, reaction (3) (Fig. 7.2) and a Dexter-type interaction between the dioxetandione and the associated fluorescer, the "activator" as it is now called. It was proposed that within this complex, energy transfer occurs concomitant with concerted decomposition of the dioxetanedione to favor the reaction energy populating the excited singlet state S_1 of the fluorescer, from which the radiative transition generates the chemiluminescence spectrum. The energetic intermediate (**V**) is formed rapidly and appears to be metastable, with lifetime up to an hour at 25°C. The fluorescer apparently also catalyzes the breakup of the dioxetandione (**V**) because on its addition, the chemiluminescence intensity decays in minutes. The mechanisms of catalysis and excitation of the activator are still subjects of current investigations and will be described next.

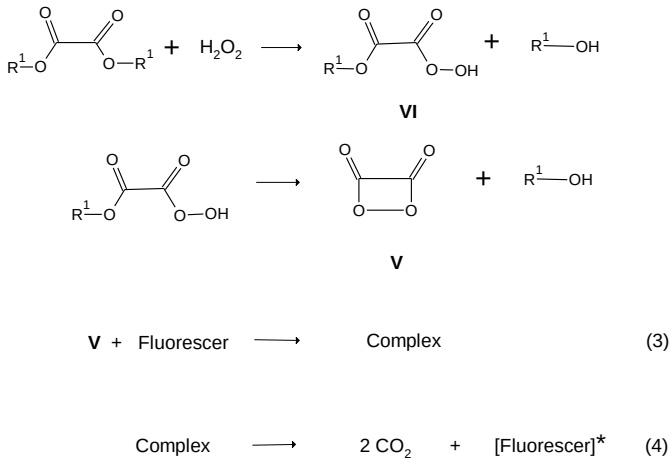

Figure 7.2. Oxalyl ester chemiluminescence developed for high quantum yield is the basis for the light stick (Cyanalum) chemiluminescence. (R^1 = alkyl) **V** is the dioxetanone high energy intermediale (HEI).

The Rauhut group used the quinine-fluorescence spectrometer technique for the first determination of the quantum yields of these reactions. The instrumental spectral sensitivity was calibrated using a Standard Lamp, and the absolute photon sensitivity by the ferrioxalate actinometry-quinine fluorescence yield protocol. For the oxalyl chloride reaction with DPA they determined $\Phi_C \sim 0.05$, but it could be increased to 0.13 by variation in reaction conditions, such as activator concentration and also by using rubrene as the activator. It was found to be further amplified to as much as 0.23 with the use of oxalyl esters having electron withdrawing substituents, especially chloride. More recently from a separate laboratory, a new recipe has been reported that yields $\Phi_C = 0.34$, and claimed to even approach $\Phi_C = 0.68$ if extrapolated to infinite activator concentration. This is the highest achieved for any chemiluminescence and now competes with the range 0.4-0.6 of the recently remeasured values for firefly bioluminescence. Both DPA and rubrene have almost unit values of Φ_F, meaning that the best Φ_E of chemiluminescence must be at least 0.3, i.e., 30% of the reaction of oxalyl ester excites the activator to its S_1 state.

Both the mechanism of activator excitation and the identification of intermediates, remain challenging tasks to this day. In addition to the peroxyoxalate **VI**, McCapra lists five more peroxy compounds all equally plausible as the excitation energy source, although the dioxetandione **V** is now generally favored.

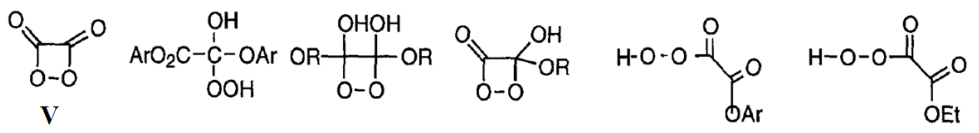

Figure 7.3. Peroxides postulated to be alternative excitation energy sources.

A description of some very recent work using NMR experiments will show the difficulty in trying to pin down the best HEI candidate. A brief introduction to the principles of NMR experiments is in Chapter 12 but although it is beyond the present scope to justify the NMR assignments here, a brief evaluation will be enough to show these as plausible. The experiments performed by the Barnett group, can be regarded as a "heroic" effort utilizing low temperature ^{13}C-NMR and did achieve good progress in characterizing the energetic intermediates.

Into uniformly labeled ^{13}C-oxalyl chloride in anhydrous deuterated tetrahydrofuran contained in an NMR tube, was added anhydrous H_2O_2 (30%) and DPA, all at -75°C. The concentrations were not reported, but would have to have been in the millimolar range to satisfy the low detectivity of a ^{13}C-NMR experiment. A bright blue chemiluminescence was visualized lasting more than 30 minutes. In a second test, the DPA was omitted but added after 30 minutes and the bright chemiluminescence again ensued. It was concluded that the energetic intermediate source necessary for excitation of the DPA to its S_1 state remained stable at -75°C over this 30 minute period. Visual intensity however, is very unreliable in forming any quantitative conclusion, due to non-linearity of the sensitivity of the eye.

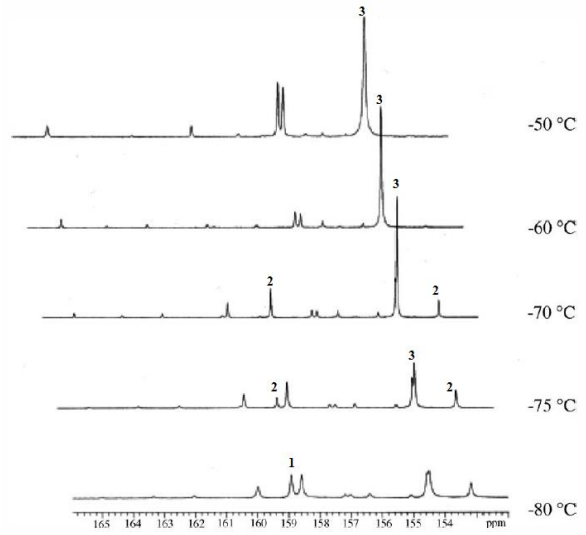

Figure 7.4. Low temperature ^{13}C-NMR experiments to detect intermediates in the DPA-oxalyl chloride chemiluminescence.

^{13}C-NMR measurements were obtained from the mixture at temperatures -80 to +20°C. In Fig. 7.4 the first scan at -80°C, shows a singlet peak marked 1, at a chemical shift 158.9 (ppm vs. TMS), and was assigned as from unreacted ^{13}C-symmetric oxalyl chloride, structure (1) in Fig. 7.5 below. The scan times were not listed but for ^{13}C-NMR experiments these are usually about 30 minutes in duration. Each scan in the figure is displaced left by 0.5 ppm for clarity of comparison. With a slight increase in temperature to -75 or -70°C, doublets (lines labeled

2) appeared at 153.9 and 159.3 ppm, assigned to the unsymmetric peroxy-oxalyl chloride, structure (2). These two signals disappeared above -60°C, with a singlet peak 3 developing at 154.5 ppm indicating another symmetric species, the dioxetandiones structure (3). This singlet peak 3 becomes more prominent as the temperature is raised and becomes broader above -60°C due to some dynamic exchange process, then disappears by -20°C. Two stable products were also assigned as CO_2 (125.6 ppm) and CO (184.5 ppm). Computational methods were employed to provide support for all assignments.

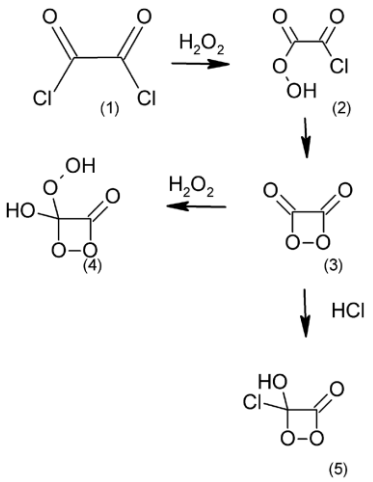

Figure 7.5. Pathway to the peroxyoxalate high energy intermediate, the dioxetandione (3).

These assignments received strong support from an EXSY (Exchange Spectroscopy) NMR experiment. The method of 2-D EXSY NMR reveals cross peaks under some conditions, between nuclear spins under slow exchange. The solution mixtures were as in the earlier ^{13}C-NMR experiments, with variable temperatures (-90 to +20°C) and the same reagent molar ratios. In Fig. 7.6, a cross peak circled at co-ordinates 164 ppm and 154 ppm, would arise from exchange between the dioxetandione (Fig. 7.7, D, 154.8 ppm) and peroxalic acid (C), the latter assigned to a singlet at 165.2 ppm. There is a discrepancy in the shift values between Figs. 7.6, and 7.7, apparently due to a calibration correction of about 1 ppm.

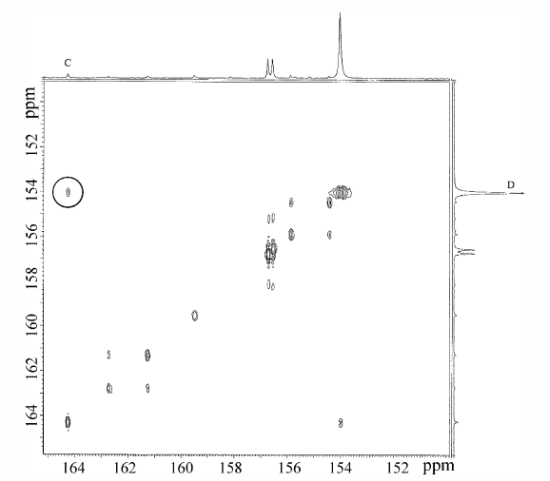

Figure 7.6. Two-dimensional EXSY NMR shows ^{13}C-^{13}C cross peaks.

Based on the previous ^{13}C-NMR experiment at various temperatures and the results from EXSY, the oxalyl chloride-H_2O_2 reaction intermediates and ^{13}C-shift assignments, were proposed to be as in Fig. 7.7.

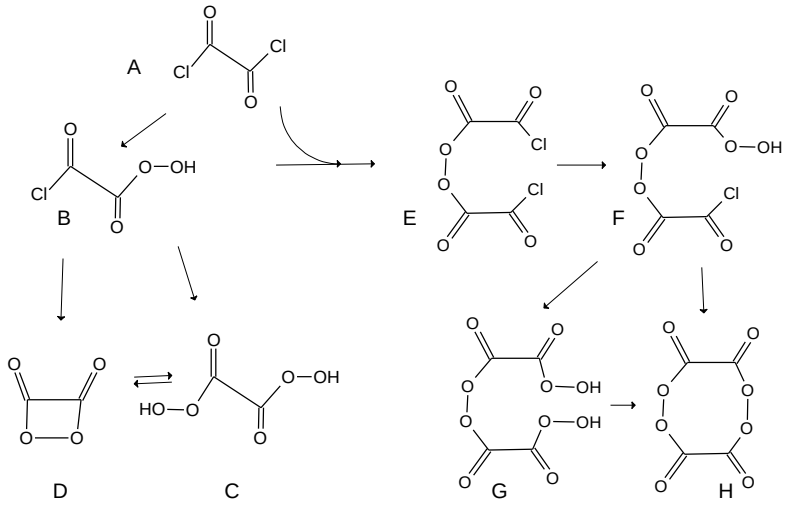

Figure 7.7. Complete assignment of the EXSY NMR experiment. A 159.0 ppm; B 154.1 and 159.4; C 165.2; D 154.8; E 155.9 and 162.8; F 156.8, 157.9, 155.9 and 162.8; G 156.8 and 157.9; H 160.3.

A more complete study would have been to compare the presence of the intermediates in the same reaction without the inclusion of DPA, which might allay the concerns of some critics. The uncertainty of identifying the reaction pathway to the high energy intermediate will be apparent now to the reader, and that it is a much unfinished business.

It has been known from the first reports that the oxalyl chloride reaction with H_2O_2 and fluorescent activator (DPA) even at room temperature, continues to produce chemiluminescence over many minutes. The inclusion of DPA can be delayed, and then its addition produces a very bright flash the intensity then settling to a lower level, corresponding to that from the standard system at that same time point. It was concluded that the "high energy intermediate" (HEI), the species responsible for direct excitation of the activator from its breakdown energy and generally believed to be the dioxetandione (peroxyoxalate), accumulates in the reaction mixture and decays separately over time.

Fig. 7.8 is from a detailed kinetics study of the reaction in ethyl acetate solvent at 20°C. The reactants are all at 1 mM except the DPA. The standard system includes DPA (0.2 mM) and the light emission continues for many minutes and has $\Phi_C = 0.1$ with respect to the amount of oxalyl chloride consumed, and after extrapolating to a saturating DPA concentration. In the delayed system, the DPA is added at 150 s, and in this experiment the light intensity is magnified about 10 times, then falls to the level of the standard system at that time point. At the highest DPA concentration the light intensity is magnified by almost two orders.

From a kinetics analysis of experiments having various molar ratios and temperatures (5-25°C), the rate and thermodynamic parameters were extracted assuming the following kinetics model:

reactants → → HEI → decay, $k_D = 9.6 \times 10^{-2}\ s^{-1}$

HEI + DPA → decomposed-HEI + DPA* $k_{CAT} = 3.6 \times 10^{3}\ M^{-1}\ s^{-1}$.

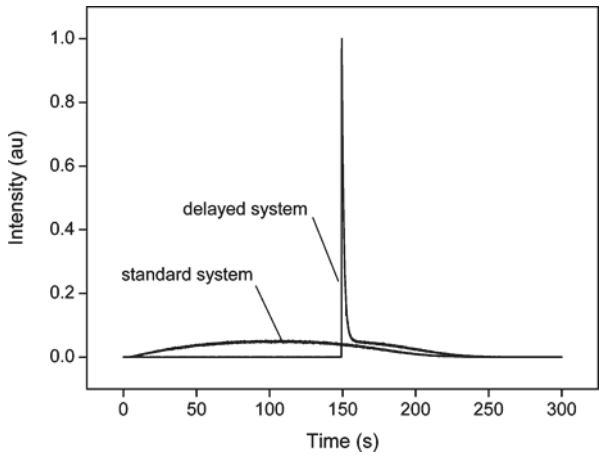

Figure 7.8. Delayed addition of the DPA shows stability of the high energy intermediate (HEI).

The chemiexcitation is assumed to be a bimolecular process in DPA concentration, and the catalytic rate constant k_{CAT} calculated from the intensity of the light flash using a variety of other activators, is found proportional to the activator reduction potential, consistent with the

proposal that an electron exchange mechanism is the basis of the chemiexcitation, an idea to be discussed in more detail later.

From the observed parameters, the maximum concentration of HEI in this standard system in the Fig. 7.8, is calculated to be only in the micromolar range, and extrapolating the linear temperature dependence of k_{CAT} to the very low temperatures and different solvent (THF) used in the ^{13}C-NMR study, the authors of the Fig. 7.8 study argue that the HEI would not be sufficiently stable to exist at millimolar concentration in the presence of DPA, and that the identification of HEI with any of the low-temperature NMR signals, is "highly improbable". It needs to be appreciated however, that although the sensitivity of ^{13}C-NMR experiments is only in the millimolar range, the disappearance of the signals above about -20°C, simply means that the concentrations fall below the detectivity limit and into the micromolar range at room temperature. Furthermore, bright chemiluminescence was observed at the -75°C temperature of the NMR study, and also after a 30-minute delayed addition of the DPA activator, although these observations monitored visually could be only qualitative. It will be important to resolve this discrepancy between the two experimental approaches, as the assignment of the HEI to the dioxetanone structure is basic to computational studies and mechanistic hypotheses. It may indeed require more heroic efforts.

Confirmation of the chemical structure and properties of dioxetanes was enabled by the landmark report from Kopecky and Mumford in 1969, of the synthesis of a stable derivative, tetramethyldioxetane (Fig. 7.9; $R_{0\text{-}4} = CH_3$). Although stable at room temperature, heating its solution caused thermolysis, and a bright blue emission ensued "enough to light up the room". A first conclusion of high chemiluminescence efficiency was incorrect because the

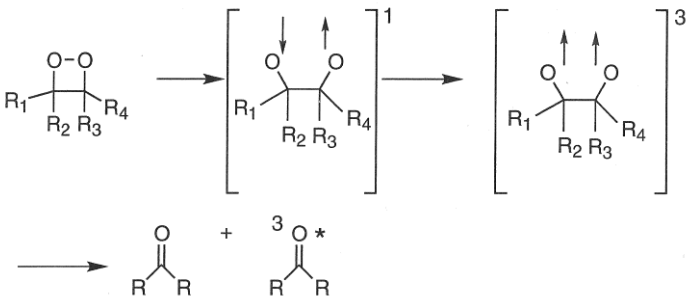

Figure 7.9. Thermolysis of tetramethyl dioxetane leads to high yields of triplet acetone (R= CH_3).

sample was at high concentration and the human eye has very high visual sensitivity. The Φ_C on thermolysis of alkyldioxetanes was accurately measured subsequently as less than 10^{-4}, but surprisingly, in the absence of oxygen which quenches triplet states, the ketone product such as the acetone from tetramethyldioxetane, was formed in its triplet state with efficiency more than 100 times higher than the singlet state. This triplet product is the origin of the bright blue chemiluminescence measured by the Φ_C. This conclusion raised the question

about how the ground state singlet dioxetane (Fig. 7.9, upper left), would proceed along its reaction co-ordinate to the transition state, with a homolytic split of the O-O bond therefore having to remain in a singlet state, and then to undergo efficient intersystem crossing into the triplet ground state of the transition state (upper right), then to fragment with one product in the excited triplet state thus violating spin conservation rules. The physical basis of such a chemical excitation mechanism still remains an active area of investigation.

In contrast to the intermolecular chemiluminescence system of the dioxetandiones (Fig. 7.5, structure 3) with an activator, firefly luciferin chemiluminescence is an intramolecular system, where the aromatic moiety, the apparent activator, is already covalently attached to the proposed high-energy luciferin dioxetanone (Fig. 9.4). It was considered by analogy that dioxetanes having fluorescent substituents might also have a high Φ_C, and effort was put into synthesis of such stable aryl dioxetanes. Some of these on thermolysis produced a blue chemiluminescence with remarkably high efficiency, $\Phi_C = 0.24$. With such an advance, an experimentally accessible model was established for detailed organic mechanistic investigation of intramolecular activation. This discovery also resulted in important commercial and research applications of chemiluminescent labels for immunodiagnostics, biological imaging, and gene expression in cells.

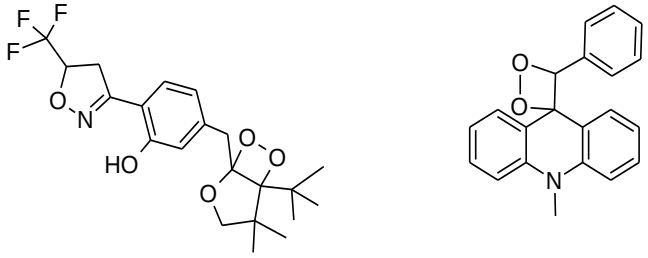

Figure 7.10. Two dioxetanes with highly efficient intramolecularly activated chemiluminescence (Φ_C= 0.24).

Chemiluminescence reactions in the condensed phase can be grouped into three classes: electrochemiluminescence, the linear organic peroxides, and ones with dioxetane intermediates. The general consensus is that only the last one is the most useful as a bioluminescence model, having the highest chemiluminescence quantum yields and involving oxygen.

The first class, electrochemiluminescence, does not involve oxygen, in fact oxygen quenches the light emission. In a mixture of two substances say A and B (Fig. 7.11), a weak light emission may be observed resulting from recombination of radicals, either as generated at electrodes or in some cases, from a chemical reaction as will be discussed next for the second class. An anion radical ($A^{\bullet -}$) generated at the cathode and a cation radical ($B^{\bullet +}$) at the anode, will undergo diffusional collision and the free electron spins (↓ and ↑) have a probability of annihilation with the immediacy of a Franck-Condon like vertical transition, the resultant exothermicity exciting one of the pair into in its S_1 level, B* in Fig. 7.11. The resulting

chemiluminescence will correspond therefore to the fluorescence of B. Electrolysis at the cathode deposits a free electron into the LUMO of A, the lowest unoccupied molecular orbital. At the anode, the result is a hole or an electron vacancy, in B's HOMO, the highest occupied molecular orbital. The proposal for the excitation process therefore, has a sound physical basis, electron-hole annihilation. This contrasts with the rather mysterious process

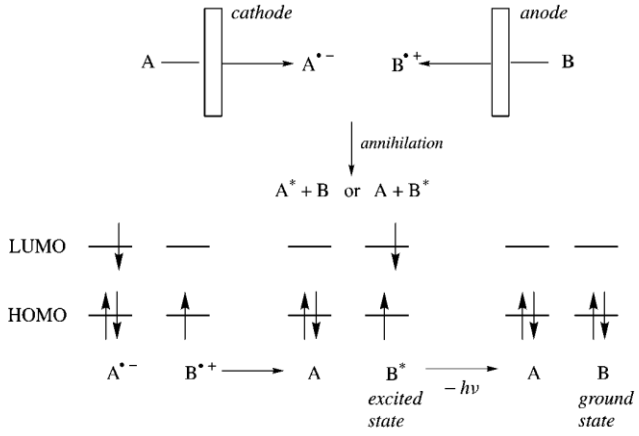

Figure 7.11. Electron transfer scheme for electrochemiluminescence that produces the excited state via radical annihilation.

mentioned above, of intersystem crossing considered to be involved in the chemiluminescence from thermolysis of tetramethyldioxetane (Fig. 7.9). If the radicals are generated at the same electrode under cyclic voltammetry, breakdown and loss of these very reactive radicals, which might occur during the diffusion time is minimized, and chemiluminescence quantum yields can be enhanced to an observed range up to $\Phi_C = 0.02$.

The second chemiluminescence class contains many reactions of aromatic organic molecules with oxygen. These are ones invariably involving linear peroxides as energetic intermediates, and being aromatic they will likely have products that are fluorescent. The chemiluminescence quantum yields in these cases are generally low, ranging from 0.01 even down to the detectability limit, 10^{-10}. In 1961 Henry Linschitz, postulated a radical annihilation process for the Zn-metalloporphin (ZnTPP) catalyzed oxidation of tetralin hydroperoxide that produced a "bright red" chemiluminescent (Fig. 7.12). He considered that the reactants would come together into an "encounter complex", which in the condensed phase could have a lifetime up to a nanosecond. His pictorial mechanism (Fig. 7.12) is shown where, within the encounter complex indicated by the square brackets, the peroxide oxidizes the ZnTPP, the electron indicated by the dot, leaving an electron hole, $ZnTPP^{+\bullet}$. If a dissociation of OH^- out of the complex takes place, an electron-hole hole annihilation will occur with the energy emitted as the red fluorescence of the zinc tetraphenylporphin

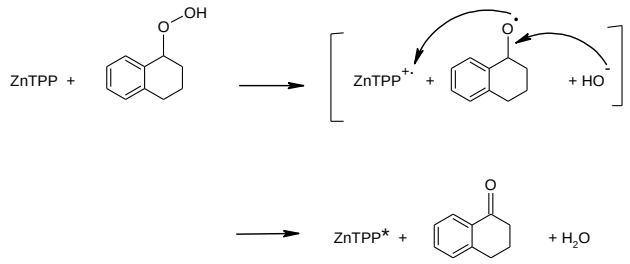

Figure 7.12. Electron exchange within an encounter complex.

(ZnTPP). The exit of OH^- would have to happen within the lifetime of the encounter complex. Although the mechanism is speculative it offers a convenient rationalization, and is similar to the idea proposed by G. Schuster in 1978 called "Chemically Induced Electron Exchange Luminescence" (CIEEL). CIEEL is a popular idea presently assumed to be generally applicable to chemiluminescence of linear peroxides, and probably in a modified form also to the cyclic peroxides. However, the chemiluminescence quantum yields of the first model reaction, that of diphenoyl peroxide, was found to be $<10^{-4}$, much lower than the 0.1 einsteins/mol first announced, raising the caution of attributing the light reaction to the overall chemistry. However, doubt has also arisen as to whether the experimental design necessarily requires the CIEEL pathway, as the intermediacy of cyclic peroxides in these reactions suggests a better excitation route. In the original formulation of the CIEEL hypothesis, the first step in the model diphenoyl peroxide chemiluminescence reaction, was proposed to be a one-electron oxidation from the peroxy group, that is a transfer of an

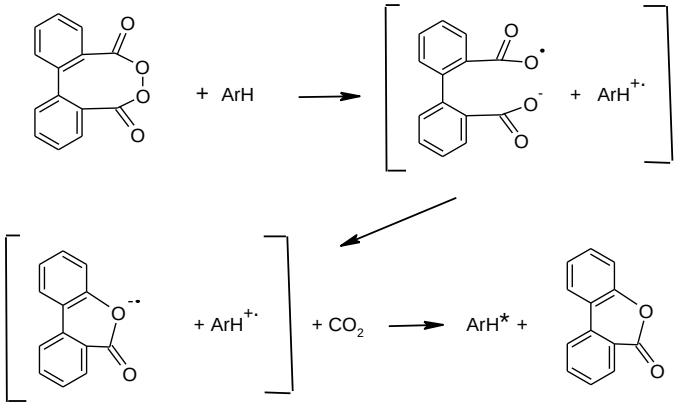

Figure 7.13. Chemically induced electron exchange luminescent (CIEEL) mechanism of excitation of a fluorescent activator (ArH) on breakdown of diphenoyl peroxide.

electron from an aromatic hydrocarbon (ArH) the "activator", into the O-O bond (Fig. 7.13). This being an endothermic process, it should be rate determining, and both the chemiluminescence intensity and decay rate should correlate with the oxidation potential of the activator, and such a correlation was presented in support of the CIEEL hypothesis.

However, Catalani and Wilson cast doubt on this conclusion on the grounds that their accurately remeasured Φ_C for this model reaction was only 2 x 10^{-5}, meaning that the kinetics could be controlled by some side path not directly reflecting the light step. Nevertheless, the basic idea of back electron transfer within the encounter complex remains very popular, and is incorporated in the suggestions also of dioxetane chemiluminescence, ones with much higher quantum yields (Fig. 7.14).

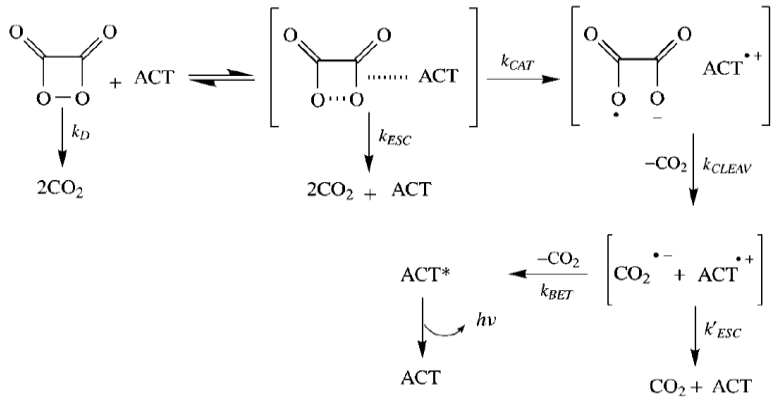

Figure 7.14. Back electron transfer within an encounter complex deposits the exothermicity to excite the fluorescent activator (ACT).

An electron transfer mechanism of dioxetandione chemiluminescence, received strong support from the fact that the Φ_C paralleled the reduction potential of the activator (ACT) in the oxalyl chloride intermolecular reaction, and of the aryl substituent, the fluorescent aromatic group, in the bicyclic dioxetane intramolecular activated chemiluminescence. The hypothesis illustrated in the scheme above (Fig. 7.14) for the activated dioxetandione case, was that a partial electron transfer or overlap to the O-O bond initiated bond elongation, eventually with full electron transfer, i.e., reduction, yielding some form of a radical anion and rupture of the C-C bond to produce CO_2, and then annihilation caused by a "Back Electron Transfer" (BET) to the ACT radical cation, resulting in excitation, ACT*. To obtain high Φ_C, the radical anion has to have a lifetime long enough for the electron transfer to be irreversible by allowing escape of one CO_2 fragment from the encounter prior to annihilation. More recently, the full electron exchange process has been folded into one of only partial transfer or a charge transfer mechanism, "Charge Transfer Initiated Luminescence" (CTIL), in which the full BET of CIEEL may be one extreme. The existence of the encounter complex containing the radical pair remains in dispute, and is the subject of many investigations and discussion in recent years.

A comprehensive review of the subject of efficient solution chemiluminescence is available in Adam (2006) (Chapter 15 **In Depth**). It contains a critical appraisal of the historical background up to that time, and presents cogent arguments for the original proposal of back electron transfer in the CIEEL mechanism, and the intermediacy of the dioxetandione in peroxylate chemiluminescence. The synthesis and usefulness as oxidants of organic

peroxides is also championed. A particularly useful summary of computational methods towards understanding the excitation mechanisms is also clearly given. The field of dioxetane chemiluminescence from the point of view of a photochemical mechanism, has also received other detailed reviews more recently. We will therefore mainly concentrate on some new developments in the last five years or so. Two groups are most active in this area, one led by M. Matsumoto, Kanagawa University in Japan, the other by W. J. Baader, University of San Paulo, Brazil. Each group has a particular molecular vehicle on which substitutions to produce different chemiluminescence spectra, efficiencies, and kinetics, can be tested. The aim from such model reaction studies is to understand the controlling factors favoring high efficiency and the tuning of chemiluminescence color.

The most recent reviews from Baader's group (2009, 2013, 2017) give a comprehensive discussion of the literature focusing on organic chemiluminescence and mechanism. The problems of chemiluminescence quantum yields and calibration measurements with secondary standards are examined, the luminol secondary standard utilized in their group compared with results from calibration with the scintillation cocktail and the actinometry-quinine fluorescence methods. Mechanisms of dioxetanone and dioxetandione chemiluminescence are given critical attention, and also the classic chemiluminescence systems, luminol, the acridans, and lucigenin.

Matsumoto and colleagues prefer the pictorial representation of a "charge transfer induced chemiluminescence", to describe the process of efficient intramolecular chemiluminescence energy transfer to the aryl substituent in the case of the dioxetanes. They suggest that CIEEL, as originally defined, is just one extreme case of charge transfer where for the former, a whole electron, i.e., initially a complete reduction of the aryl group, takes place. Also, there is some tendency in the literature to include both partial and full electron transfer in a revised definition of CIEEL. Emphasis is also made that the chemical mechanism is contentious, and a section on mechanism in the Matsumoto article (2004), is especially clearly readable and recommended.

Production of dioxetane chemiluminescence with a range of color, is a goal both from fundamental understanding and for applications. Matsumoto's group (2008) describe their results for color modulation and also in some cases, how the spectra do not necessarily correspond to the expected fluorescence of the product. The different spectral properties are shown to result from substitution variations and environmental conditions.

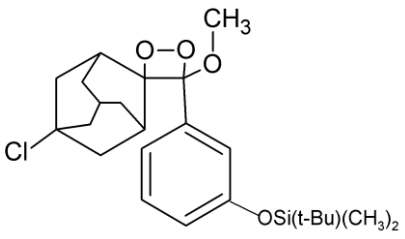

Figure 7.15. Schaap in 1987 discovered a stable dioxetane yielding very efficient intramolecular chemiluminescence on heating.

Paul Schaap is credited with discovering the first unambiguous example of dioxetane intramolecular activated chemiluminescence having high efficiency, $\Phi_C = 0.25$ and $\Phi_E = 0.57$, comparable to the efficiencies of bioluminescence reactions. The substituent on the left side of the dioxetane structure in Fig. 7.15, is called a spiroadamantyl and it renders the dioxetane stable at room temperature, making this chemiluminescence extremely convenient for investigation. Consequently, this dioxetane model has provided a basis for development of many variants with reactions of similarly high efficiency. For this first example having a siloxyl substituent, in the aprotic solvent DMSO the chemiluminescence is triggered by adding fluoride ion. With a phenol substituent likewise the chemiluminescence occurs on adding base. A phosphoryl substituted form (Fig. 7.16) was also discovered to be equally stable and has an advantage of being water soluble. It is triggered to the phenolate using the enzyme alkaline phosphatase, leading to a tremendous range of commercial applications, particularly in immunodiagnostics.

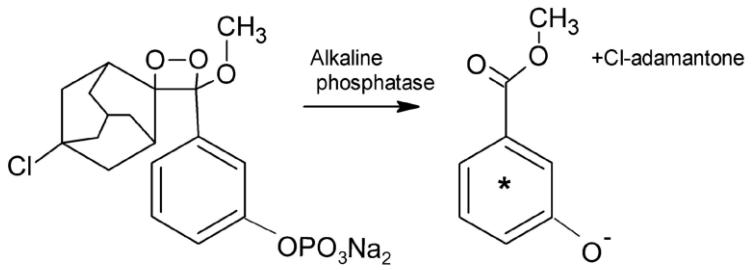

Figure 7.16. Phosphoryl substituted dioxetanes are chemiluminescent in aqueous solution and used in many model reactions as well as commercial applications.

Matsumoto's group has utilized this structural skeleton of Schaap for their investigation of the chemical mechanism of decomposition and energy transfer to the emitting product, with an eye towards expanding applications. In contrast to the triggered reaction of the siloxyl derivative in aprotic polar solvents where the Φ_C is very high, in aqueous solution it is much lower, $\Phi_C < 10^{-4}$ for the phosphoryl derivative triggered by base. Nevertheless, even with this low efficiency the sensitivity of detection devices easily overcomes this limitation.

Matsumoto's group (2001) synthesized a number of bicyclic dioxetanes having the same chemiluminescence emitter and similarly observed $\Phi_C = 0.1$-0.2 for the reaction triggered with tetrabutylammonium fluoride (TBAF) in the aprotic solvent acetonitrile, but the Φ_C remained below 5×10^{-3} for aqueous NaOH (Fig. 7.17). The inefficiency in aqueous solution was partly attributed to water quenching the fluorescence of the emitter as well as reducting the Φ_E. However, after another variation of substituents (Fig. 7.18), the aqueous chemiluminescence became remarkably enhanced, in one case ($R = CF_3$) obtaining $\Phi_C = 0.24$, about 50% that of the aprotic reaction. Other similar R-variants (structure 3) yielded a range $\Phi_C = 0.01 - 0.07$. In aqueous solution the product has $\Phi_F = 0.5$ and in acetonitrile 0.7, therefore accounting for most of the water/acetonitrile ratio of the Φ_C. Molecular orbital computations suggested that one important factor controlling the overall efficiency in

aqueous solution was the extent of hydrogen bonding at the carbonyl oxygen of the product emitter. The mechanism by which this could affect the Φ_E however, is not clear.

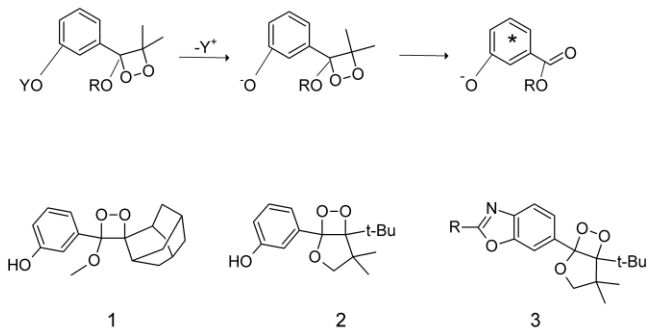

Figure 7.17. A series of dioxetanes having the same or similar emitter.

Another series of structures (Fig. 7.18) also produced high efficiency, an aqueous $\Phi_C = 0.18$, and 0.46 for the aprotic reaction, in the case of *R* = H, *X* = O. This last result leads to the highest excitation efficiency reported, $\Phi_E = 0.75$, a remarkable finding that merits reevaluation with reliably accurate photometric calibration. For all structures the change of Φ_C paralleled the Φ_F of the product, although not sufficiently to quantitatively account for differences in Φ_C's between aprotic and aqueous environments, or with the different substituents.

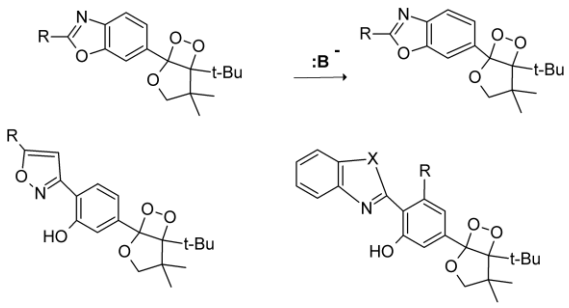

Figure 7.18. Dioxetanes that produce the highest excitation yields reported, $\Phi_E = 0.75$.

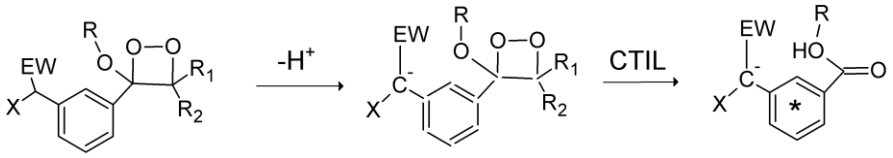

Figure 7.19. A carbanion induced dioxetane decomposition with an electron-withdrawing group (EW) generates chemiluminescence extending into the infra-red but with low efficiency even in DMSO. R = alkyl groups, CTIL is charge Transfer Induced Luminescence.

Watanabe et al. (2005) investigated the reaction of dioxetanes triggered by a carbanion (C^-) in place of the oxyanion electron-withdrawing (EW) group, e.g. –CN, rather than the phenolate in structures in Fig. 7.19. As the fluorescence of expected carbanion products is found at longer wavelengths than a phenolate product, such examples generate chemiluminescence spectra extending into the near infra-red, > 700 nm. For EW = CN, and X = methyl, the emission has a 758 nm maximum, but the Φ_C's are very low, 2 x 10^{-6}.

In the first study of his efficient dioxetanes, Schaap also shifted the chemiluminescence color by the obvious choice of having an aryl group with shifted fluorescence, e.g., a naphthalenyl in place of the phenyl substituent in Fig. 7.15. The chemiluminescence color shifted to longer wavelength corresponding to the fluorescence spectrum of the naphthalenate, >460 nm. Matsumoto and colleagues (2008a) reviewed the results of reactions of a series of dioxetanes

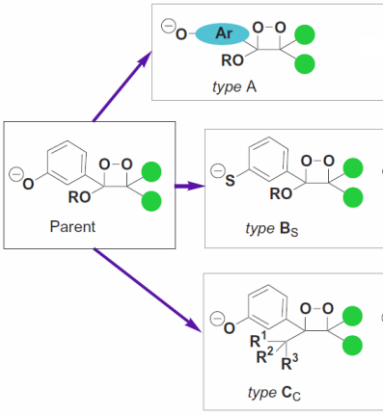

Figure 7.20. All chemiluminescence properties are affected by the nature of each substituent. The green balls are various substituents.

having color variants based on this same idea. As well as the emission color, both the Φ_C and the chemiluminescence kinetics depend on the nature of the electron-withdrawing group, the aryl substituent, and substituents on the dioxetane ring. The properties using a carbanion trigger are described in detail in this article therefore, and an aromatic thiol or amine are shown to also work. All these color shifted examples however, do not have the earlier bright Φ_C's. The TBAF triggered reactions in DMSO have an emission corresponding to the fluorescence spectrum of the diketo product, but there are some interesting exceptions that

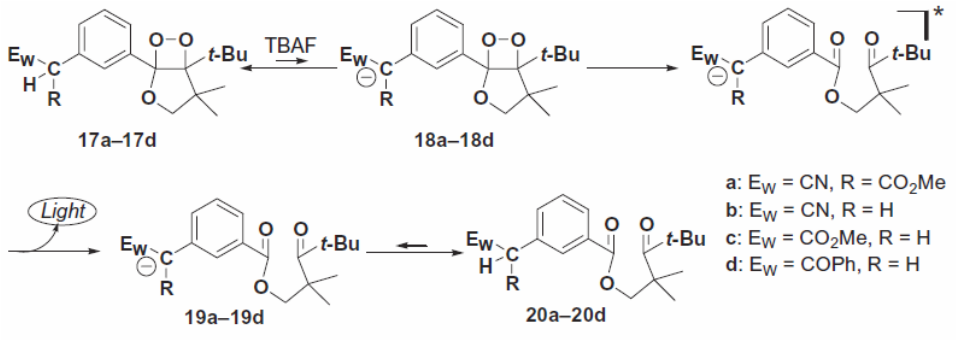

Figure 7.21. Carbanion triggered chemiluminescence may not generate the same spectrum as fluorescence due to the high basicity of the carbanion product.

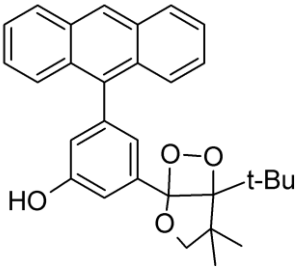

Figure 7.22. The chemiluminescence in a conformationally restricted medium may be shifted from the fluorescence of the final product. In DMSO this dioxetane has a chemiluminescence maximum at 709 nm but is blue shifted on triggering with K^+-butoxide in a crown ether.

might have relevance to an explanation of color shifts in many bioluminescence systems. For the carbanion triggered system, and depending on substitutions, the chemiluminescence emission can be in the far red, whereas the product fluorescence is yellow. This arises from the basicity of the carbanion which is around a pK ~ 25, and this is not accessible by fluorescence excitation. A second group of structures studied is biaryl substituted dioxetanes triggered in an anisotropic medium, specifically by a base enclosed in a crown ether (Fig. 7.22). Typically, for the anthryl-substituent (Fig. 7.23) in DMSO triggered by TBAF, the chemiluminescence maximum is 709 nm but in the presence of different types of K^+-t-butoxide crown ethers, it is blue shifted to 680-606 nm. A similar effect was also produced in dioxetanes with substituents that rendered them chiral. In the presence of optically active crown ethers each type of dioxetane isomer emits with a shifted spectrum.

The question of control of excitation efficiency is difficult to answer. For many structures examined there appears to be a synergy between Φ_E and Φ_F but it is not quantitative. A reduction of Φ_E by 1000x may not be accompanied by the same degree of Φ_F change. To probe this question, Matsumoto et al. (2011) synthesized several rotamer pairs of bicyclic dioxetanes that would produce the same fluorescent product from each of the pair. For the reaction in DMSO triggered by TBAF, rotamer pair **5b** produced the same chemiluminescence as the product fluorescence spectrum with Φ_F = 0.15 and a 598 nm

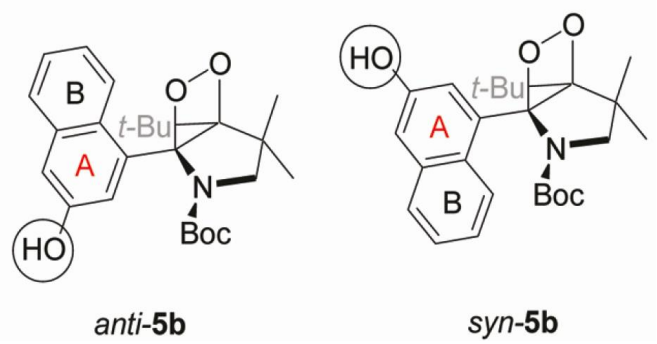

Figure 7.23. This rotamer pair produces the same chemiluminescence spectrum but with a 10-fold difference of Φ_C between *anti* and *syn*.

maximum, but Φ_C (*anti*) = 4.6 x 10^{-3} and Φ_C (*syn*) = 2.5 x 10^{-4}, with a similar change in kinetics decay constant. Results for several other pairs were similar, except with slight differences in emission spectra. Again, a concern with such low Φ_C reactions, is that differences might be the result of different chemical pathways, but here there was no evidence at least of different product yields. The authors suggested the excitation pathway for each rotamer could be sufficiently different as to lead to the observed changes. A time-dependent density functional theory computation showed different charge distributions around the dioxetane ring, which might favor a higher chemiluminescence efficiency for the *anti* structure, but they were cautious about any further interpretation.

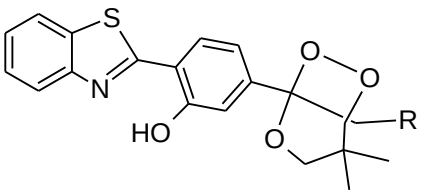

Figure 7.24. Thermodynamic parameters for chemiluminescence for this dioxetane show a higher barrier for thermal decomposition than for charge-transfer induced, with Φ_C = 0.25. Orientation of the aryl group (R) may be a factor controlling the excitation efficiency in charge-transfer.

Another question of excitation efficiency was about the well-known difference in thermal decomposition (TD) versus charge-transfer induced decomposition (CTIL), TD yielding triplet states and CTIL singlet. The structure in Fig. 7.24 (R = CH_3) has Φ_C = 0.25 for CTID in the aprotic solvent acetonitrile with TBAF as the trigger. Thermodynamic parameters were compared between the two decomposition reaction conditions, and the activation free energy $\Delta G^{\ddagger}$ for TD was about 120 kJ/mol, higher than for CTID, 80 kJ/mol. It was noted that the activation entropy $\Delta S^{\ddagger}$ for TD was not affected by the bulkiness of the R-group up to t-butyl, but for CTID it increased from about -47 entropy units for R = methyl, to zero for t-butyl.

The authors suggest that the thermodynamic parameters indicate a preference for proper orientation of the aromatic electron donor in the case of CTID but not for TD.

In an aprotic polar solvent like N-methyl-pyrollidone, by virtue of its being a strong proton acceptor, solvent-promoted decomposition (SPD) triggers bicyclic chemiluminescence reactions without the need for base addition. The Φ_C and spectra are the same as CTID. Contrasting with the R-group dependence of entropy for the CTID, the SPD term was a constant large negative value, not affected by the bulkiness (methyl to t-butyl) of the substitution. The suggestion was that SPD had a more demanding restriction on conformation than CTID.

Already described here was the study of Stevani et al. (2000), of the high Φ_C reaction of H_2O_2 with peroxyoxylate esters in the presence of a series of activators. The Φ_C in the range mostly 0.01-0.16 and the kinetics constants, were both dependent on activator concentration, and importantly, the individual values of Φ_C and k_{CAT} both correlated with oxidation potential of the activator. These authors concluded that the CIEEL mechanism in the oxalyl chemiluminescence was thereby strongly supported. Equally of course, the same mechanism of charge transfer, i.e., a partial or transient electron exchange, would be consistent with these data. It needs also to be noted that the S_1 level of the activator was also correlated with oxidation potential by Rauhut's group in 1969.

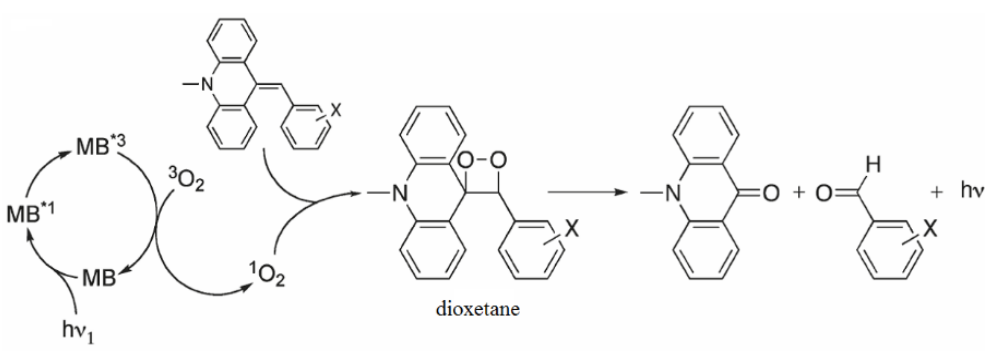

Figure 7.25. Singlet oxygen $^1O_2$ generated by methylene blue (MB) photosensitization adds across the double bond leading to the dioxetane. Subsequent unimolecular decomposition generates the excited state.

In a similar approach to investigating the dioxetane chemiluminescence, the Ciscato group (2010) claimed the first experimental evidence for intramolecular electron transfer in the catalyzed decomposition of a series of acridan derivatives; one example is shown in Fig. 7.25, the N-methylacridinium-1,2-dioxetane. The dioxetanes were not sufficiently stable for isolation but were confidently generated by methylene blue (MB) photosensitized generation of singlet oxygen ($^1O_2$), which is known to add with facility across double bonds as shown for the precursor in Fig. 7.25, leading to the formation of the metastable dioxetane. The Φ_C's were not accurately determined but estimated as in the 0.03 range. Activation parameters, chemiluminescence decay constants, and relative values for a series of X-substituents, again

revealed correlation with the activator oxidation potential. Recently however, this same group has found that dioxetane intermolecular activated reactions are generally inefficient with the glaring exception of the oxylyl chloride system. The reason for the high efficiency of intramolecular excitation as with Schaap's models (Fig. 7.15) and in bioluminescence systems, remains to be revealed.

8. **Marine Bioluminescence and Coelenterazine**

The luciferins from the firefly and the ostracod crustacean *Vargula* (formally *Cypridina*) *hilgendorfi*, were both finally purified in crystalline form by the mid-nineteenfifties, the latter after a long struggle going back to Harvey's investigations in the 1920s. There followed a "competition" among research groups to determine the chemical structures, and the first success was for the firefly luciferin in 1961, by Frank McCapra and Emil White at Johns Hopkins University. In 1966, the Cypridina luciferin (now called "cypridinid" luciferin) structure was solved by Y. Kishi in T. Goto's group at Nagoya University in Japan (Fig. 8.1). The discovery and structure of their bioluminescence products,

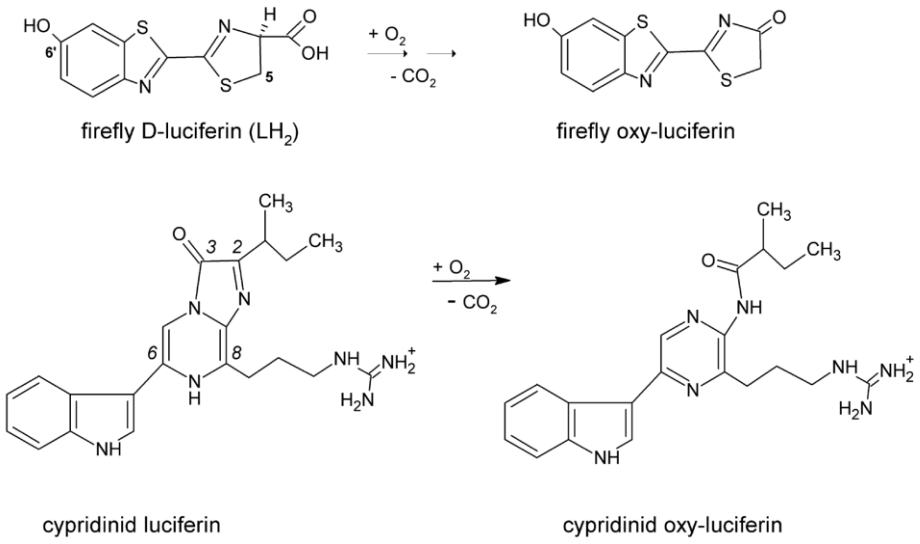

Figure 8.1. The first determined chemical structures of luciferins and their bioluminescence products (see Fig. 9.4) in later years.

the respective oxyluciferins and CO_2, followed in the next few years. An incentive in the determination of these two luciferin structures was that they were novel natural products whereas and not so challenging, the earlier discoveries for the bacterial bioluminescence system were the flavins and fatty aldehydes, already known as intermediates in bacterial metabolism. The long delay in elucidating the structure of cypridinid luciferin was due to its rapid oxidation in air. Although it had been successfully stabilized in the 1930s as a benzoyl derivative, it was another 20 years before its final purification in the crystalline state.

In both firefly and Cypridina bioluminescence systems, the overall light reaction is an oxidative decarboxylation, each requiring its specific luciferase for catalysis, the firefly luciferase or the unrelated cypridinid luciferase. An additional factor in the firefly bioluminescence was for ATP. The finding that these chemical structures were completely

different, accounted for Harvey's observation that these bioluminescence systems are specific, the luciferins and luciferases do not cross-react, a property also found for many but not all bioluminescence systems.

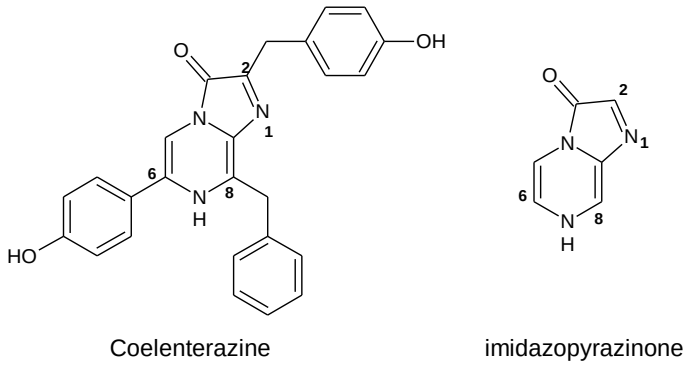

Coelenterazine imidazopyrazinone

Figure 8.2. Common marine luciferins are imidazopyrazinone derivatives.

The most common luciferin in marine bioluminescent organisms excluding the bacteria, is "coelenterazine", so named because it was first recognized as involved in the bioluminescence of a coelenterate, the jellyfish *Aequorea*, but subsequently found also to be the luciferin in the bioluminescence systems of distantly related organisms, some squid, shrimp, and fish, as well as the "Sea Pansy" *Renilla* that has been subject of very detailed investigation. Cypridinid luciferin and coelenterazine are seen to be derivatives of the same central ring structure, an imidazopyrazinone (Fig. 8.2). It is also apparent that the chemical structures of both are a fusion of amino acid fragments, arginine, isoleucine, and tryptophan, for cypridinid luciferin, and tyrosine and phenylalanine for coelenterazine. Feeding experiments with these amino acids isotopically labeled, confirmed that such an *in vivo* biosynthetic pathway exists in two organisms. There are also found some luciferins that are variations on the theme, for example a dehydrocoelenterazine for the bioluminescent squid *Symplectoteuthis*, in its photoprotein symplectin, and in pholasin from the clam *Pholas*, both of these bound through a sulfur link to the apophotoprotein (Fig. 8.3). These two photoproteins are not members of the Ca^{2+}-regulated class; pholasin is triggered by H_2O_2 to produce a blue bioluminescence and symplectin by Na^+ or K^+ with a yellow emission.

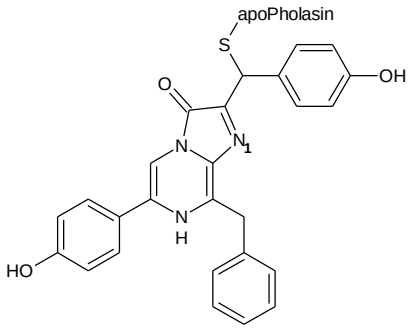

Pholasin

Figure 8.3. Pholasin from the clam (*Pholas*) contains dehydrocoelenterazine covalently bound to the apoprotein via a thiol link. Another photoprotein variant is symplectin found in a type of squid.

Following the discovery of the bright chemiluminescence from the oxalyl chloride reaction and the suggestion of high-energy cyclic oxygen intermediates, McCapra in 1964 proposed the involvement of dioxetanes in the lucigenin chemiluminescence and in firefly bioluminescence. His hypothesis was well supported a few years later by carrying out the reactions with isotopically labeled $^{18}O_2$ in place of the natural $^{16}O_2$. For the firefly luciferin, the label was quantitatively recovered in the bioluminescence products, one ^{18}O atom in the CO_2 released and one in the firefly oxyluciferin. The same labeling pattern was then found for the bioluminescence of cypridinid luciferin, and for coelenterazine in its bioluminescence reaction with the luciferases from *Renilla* and the deep sea shrimp *Oplophorus*, leading to a general acceptance that the high-energy intermediate should be the luciferin dioxetanone (Figs. 8.4 and 8.5).

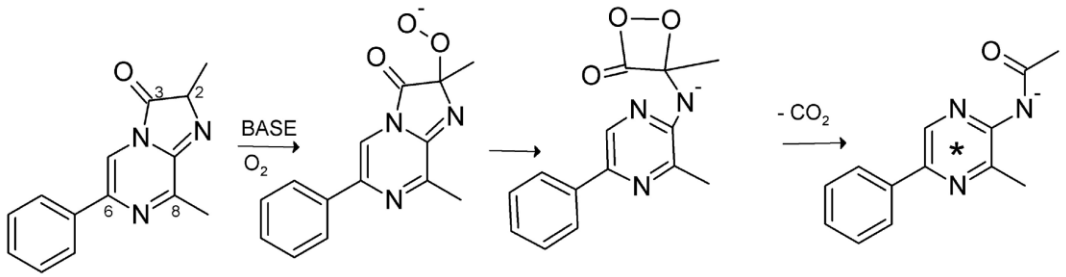

Figure 8.4. Chemiluminescence reaction sequence of an imidazopyrazinone derivative. Decarboxylation yields CO_2 and the amide anion in its fluorescent state (*).

In 1967, McCapra and Chang investigated the mechanism of the chemiluminescence of an imidazopyrazinone derivative (6-phenyl-2,8-dimethyl) as a model for the cypridinid luciferin bioluminescence reaction (Fig. 8.4). In the aprotic solvent DMSO the reaction is base catalyzed, spontaneously reacting with dissolved oxygen to produce an emission with maximum at 455 nm, the same as the fluorescence of the product amide anion. The $\Phi_C \sim 0.0003$ and $\Phi_Y = 0.89$, and the amide anion final product had $\Phi_F = 0.1$, giving confidence that the chemical and light pathways

correspond. Under this very basic condition with t-butoxide, the target of oxygen addition was proposed to be the C-2 carbanion, considering that the presence of the negative charge on C-2 would relieve the triplet oxygen spin restriction by spin-orbit coupling, facilitating the formation of the peroxy anion. Nucleophilic attack of the peroxyl anion to the C-3 position would then form the dioxetanone and its concerted decomposition, meaning simultaneous bond breaking, would produce the cypridinid oxyluciferin amide anion in its excited state, indicated by the asterisk in Figs. 8.4 and 8.5.

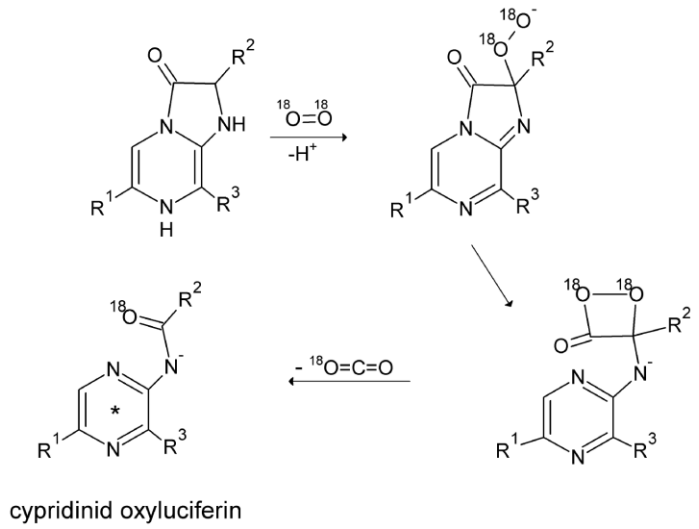

Figure 8.5. Labeling with oxygen-18 supports the intermediacy of a dioxetanone in cypridinid luciferin bioluminescence.

The Fig. 8.5 shows the points of ^{18}O labeling, and is the proposed bioluminescence mechanism for cypridinid luciferin, which having a high bioluminescence quantum yield $\Phi_B = 0.26$, and an almost quantitative cypridinid oxyluciferin product yield, $\Phi_Y = 0.86$, supports the proposition that the chemiluminescence and bioluminescence pathways correspond. Oxygen-18 labeling is consistent with the dioxetanone being the intermediate but this structure has not been directly observed, except that in the spatial structure of the Ca^{2+}-regulated photoproteins determined by X-ray crystallography, its precursor the 2-peroxycoelenterazine, is directly visualized by its electron density (Chapter 12).

No chemiluminescence of these imidazopyrazinones is observed in water as the product amide fluorescence is quenched, but in a strongly basic aprotic solvent DMF the amide anion is fluorescent $\Phi_F = 0.23$, and chemiluminescence $\Phi_C \sim 10^{-3}$ is observed. In the coelenterazine structure, the position corresponding to R^1 in Fig. 8.5, is p-hydroxyphenyl, and that p-hydroxy would be expected to be dissociated in the excited state of the product rather than the amide nitrogen as in the cypridinid reaction (Fig. 8.5), due to the excited state pK* for a phenolate being many units more acidic than the ground state pK, and furthermore much more acidic than the amide nitrogen. Coelenteramide and cypridinid oxyluciferin anions in non-aqueous solvents, show fluorescence spectra within the range of the bioluminescence spectra, but the identification of the point of negative charge for the coelenteramide case, has not been a matter of general agreement.

In water an extremely weak chemiluminescence of cypridinid luciferin and coelenterazine is observed accompanying decomposition. In the presence of bovine or human serum albumin however, a base-induced chemiluminescence of coelenterazine is measurable two or more orders of magnitude over that without the albumin. In water the product amides are non-fluorescent but bound in the luciferase environment both the neutral and anionic amides have $\Phi_F \sim 0.2$. It can be concluded that there must be specific interactions on the luciferase or the photoprotein binding sites that still remain to be understood, leading to enhancement of Φ_F and Φ_E, so as to account for the total Φ_B.

Coblentz in 1910, reported the *in vivo* bioluminescence of a *Cypridina* specimen to be broad with a maximum at 469 nm. In 1937, Eymers and van Schouwenburg measured the absolute bioluminescence spectrum from a specimen of *Cypridina*, and showed that the energy plot could be resolved into two Gaussian bands. On transforming their wavenumber plot (they used the symbol ν but the symbol used today for wavenumber is $\bar{\nu}$ (cm^{-1}), and ν is the preferred symbol for frequency (s^{-1})), to wavelength for easier comparison with later studies, the band maxima in Fig. 8.6 are at 466 and 548 nm, with the latter having about 50% intensity of the former. This observation of two bands was also found for the chemiluminescence spectra of purified cypridinid luciferin (Fig. 8.7), and suggests that this chemiluminescence is an appropriate model for the bioluminescence, with emission predominantly from the neutral amide excited state (λ_{max}= 466 nm) of cypridinid oxyluciferin. Fluorescence maxima of the neutral cypridinid oxyluciferin amide in solvents of different polarities, are in the range 453-463 nm.

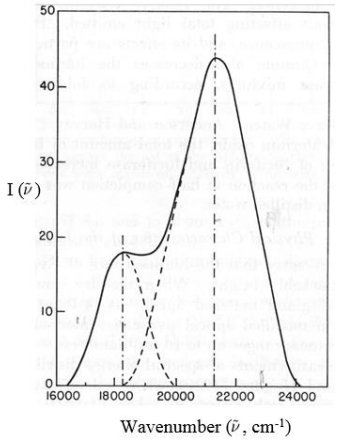

Figure 8.6. Absolute bioluminescence energy spectrum from a specimen of the ostracod crustacean *Cypridina*. Gaussian analysis resolves two bands. On a wavelength scale the maxima are 548 nm for the smaller and 466 nm for the larger band. The units of the abscissa here are wavenumbers (cm^{-1}) and the ordinate photons/wavenumber interval.

Goto's group in the late 1960's, reported on the fluorescence spectra of cypridinid oxyluciferin in the protic solvent diglyme with either a strong base, potassium t-butoxide, or a very weak base, a sodium acetate buffer at pH 5.6. In Fig. 8.7 (*left*) their spectra are plotted

adjusted to the same intensity maximum (normalized). To make the published figure more clear, numbers are inserted at the top to identify each spectral band maximum (nm); 350 and 421 are for the excitation and fluorescence of the presumed neutral amide of cypridinid oxyluciferin in diglyme/acetate, and 408 and 507 for the amide anion excitation and fluorescence in diglyme/t-butoxide. The 430 maximum is the chemiluminescence of cypridinid luciferin in diglyme/acetate and this spectrum therefore, being close to the 421-nm fluorescence of the product in the same solvent, is assigned as originating from the S_1 level of the neutral amide. With a cypridinid luciferin analog, an imidazopyrazinone having R^1 = phenyl (Fig. 8.5) in place of the indolyl (Fig. 8.1), in diglyme/acetate a bimodal chemiluminescence spectrum resulted (Fig. 8.7, *right*), with a main maximum at 355 nm corresponding to the fluorescence of unionized amidopyrazine, and a marked shoulder at 450 nm from the amide anion. The authors proposed that the chemiluminescence oxidation produced the anion as the initial excited state, but depending on the availability of a proton donor, it could be rapidly protonated to the neutral excited state. The involvement of a rate of excited state proton transfer was supported by using D_2O as solvent that would be expected to slow the rate and result in the observed larger anion contribution at 450 nm.

The proposal from Goto's report that the amide anion is the primary excited species and would undergo excited state proton transfer to the higher energy neutral level, is however doubtful on energetic grounds. It needs to be noted that these spectra from Goto's report are uncorrected, but in this spectral range the inaccuracy of the spectral maximum is small. The *in vivo* bioluminescence emission therefore, appears to be a mixture mainly originating in the excited neutral amide and with a lesser contribution from the excited amide anion.

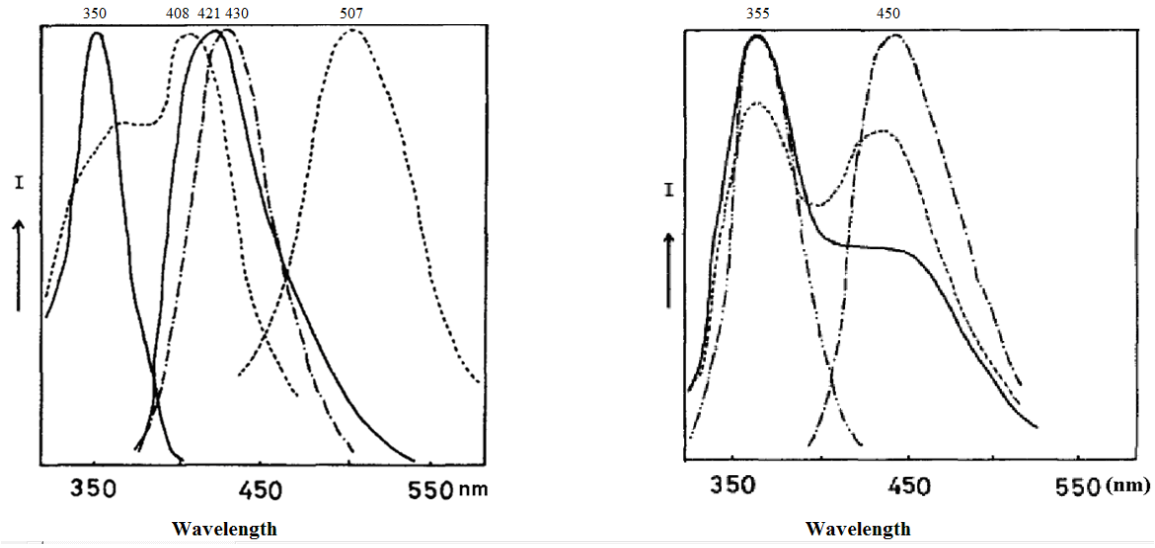

Figure 8.7. (*Left*) Fluorescence spectral maxima of cypridinid oxyluciferin amide in diglyme (421 nm –), diglyme plus acetate (430 nm –·–·), and diglyme plus butoxide (507 nm ···). (*Right*) Imidazopyrazinone chemiluminescence spectra in the weak base condition, diglyme plus acetate (355 nm –). It shows a shorter wavelength chemiluminescence band that originates from the neutral amide product and the longer wavelength from the amide anion. In D_2O the relative anion contribution is enhanced. I = fluorescence or chemiluminescence intensity. To reduce confusion in the published data, numbers to identify the maxima have been added along the top.

A more recent investigation of this same imidazopyrazinone chemiluminescence model reaction, employed low temperature to allow the intermediates to be trapped and identified by ^{13}C-NMR. Again, the interpretation of such NMR experiments will be described in a later chapter. The NMR experiments using a ^{13}C-enriched imidazopyrazinone model (Fig. 8.8, R^2 = p-methoxyphenyl) and after reaction with singlet oxygen ($^1O_2$) at low temperature (-95ºC) in methylene chloride, showed the existence of the 2-hydroperoxide substitution, and in a mixed solvent at -78ºC, the dioxetanone derivative itself was trapped and structurally identified. On warming to -50ºC, a chemiluminescence emission was observed having a maximum at 400 nm, but it shifted to a 475 nm maximum as the temperature rose to -10ºC.

It was proposed that the neutral dioxetanone derivative was less stable than the anionic dioxetanone, and that there were two pathways to the two excited products, with the de-protonation occurring in the upper pathway *prior* to the breakdown of the high energy dioxetanone (Fig. 8.8). Singlet oxygen is employed for the oxygen addition because it has no spin prohibition and reacts readily with the imidazopyrazinone and, depending on conditions, it will go via the upper pathway to the 2-hydroperoxy derivative or via the lower directly to the neutral dioxetanone. Under basic conditions, the neutral amide may lose a proton to join the upper route. Already mentioned is that the metastable 2-hydroperoxycoelenterazine intermediate has also been directly visualized in the X-ray structure of the photoproteins aequorin and obelin (Chapter 12). Hirano's group in 2008 made similar chemiluminescence model studies which revealed the influence of R^2 substituents (Fig. 8.8) on the acidity of the amide N of the product. This influence on the acidity of the N-1 will therefore result in the extent of protonation of the dioxetanone, and whether or not the neutral (400 nm) or anionic (475 nm) excited product is dominant.

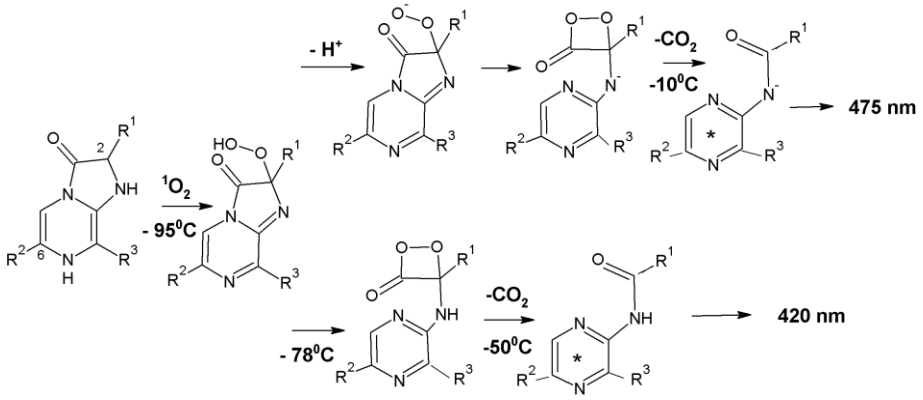

Figure 8.8. Chemiluminescence of an imidazopyrazinone derivative at low temperature reveals two pathways accounting for the two bioluminescence bands from *Cypridina* and the two chemiluminescence bands of cypridinid luciferin.

Coelenterazine is widely distributed among marine bioluminescent organisms, in addition to the ones already referred to, it has been identified as the origin of the bioluminescence in some comb jellies (ctenophores), copepods, and brittle stars. Coelenterazine has also been found in some non-luminous organisms, suggested by some that it has a metabolic function other than for bioluminescence. In some cases coelenterazine is found with a substitution, like a sulfate in extracts from the sea-pansy, and this derivative has been suggested to be a stabilized pre-luciferin.

Coelenterazine is found to participate in two classes of bioluminescence, one the classical luciferin-luciferase reaction and the other such as in the Ca^{2+}-regulated photoproteins. The overall decarboxylation chemistry is the same in both classes but in the photoproteins the property can be regarded as being that of a luciferase having in the first step, trapped a metastable intermediate, the 2-hydroperoxycoelenterazine derivative, so that the Ca^{2+}-triggered reaction now requires no external oxygen. This accounts for the failure of earlier investigators to find an oxygen dependence of the bioluminescence of aequorin extracts. We will discuss the coelenterazine luciferases first.

The coelenterazine luciferases from the different organisms are generally unrelated, in spite again of the fact of their catalyzing the same mechanism for the light reaction. Renilla luciferase has a mass of 34 kDa, the deep-sea jellyfish *Periphilla* 19 kDa, deep-sea shrimp *Oplophorus* 19 kDa, the copepods *Gaussia* 19.9 kDa and *Metridia* (isoforms) 18.4−24.2 kDa, and an artificially truncated Metridia luciferase 16.5 kDa, as some examples of the variants. This last with mass 16.5 kDa is remarkable, as it retains a high activity, includes a secretion sequence, and is exceptionally thermostable. Such properties would favor considerable usefulness in applications as a label for cell biology studies.

The bioluminescence quantum yields and spectra depend on the type of luciferase; the Φ_B range is 0.33 (*Periphilla*) to 0.1 (*Renilla*), and for the bioluminescence spectral maximum, 452 nm (*Oplophorus*) to 488 nm (*Metridia*). Model fluorescence studies conclude that the excited product coelenteramide anion is the origin of the bioluminescence emission, but is perturbed in each case by the different luciferase binding site environments. This explanation is supported by the fact that the fluorescence spectra of coelenteramide anions span a similar range in solvents of different polarity.

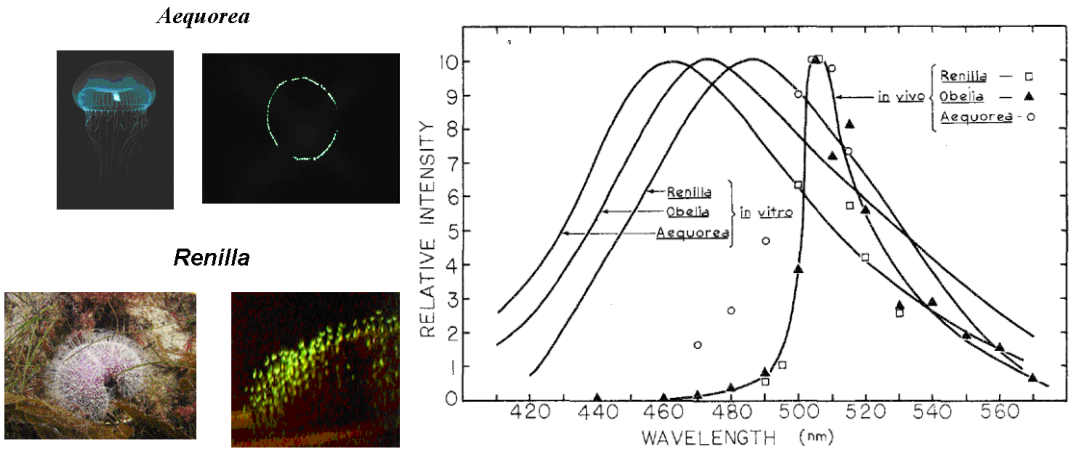

Figure 8.9. (*Left panel*)The presence of Green-fluorescent proteins in several marine organisms is the origin of the green color of the *in vivo* bioluminescence. The photos show the jellyfish *Aequorea* and the sea-pansy *Renilla* in room light (*left*) and the bioluminescence in the dark (*right*). (*Right panel*) The bioluminescence spectra from the *in vitro* reaction of the photoproteins or Renilla luciferase, is contrasted with the narrow green bioluminescence *in vivo*.

In almost all cases the bioluminescence from the animal is green, not in the blue 452−488 nm range found for the reaction of the purified system (Fig. 8.9, *right panel*). Johnson in 1966, suggested that the green bioluminescence *in vivo* was due to the presence of a "green protein" that Shimomura and he had observed earlier in extracts of the jellyfish *Aequorea*, and that the *in vivo* green emission was a "sensitized chemiluminescence". In 2008, Shimomura shared in the Nobel Prize for the original discovery of the green protein (Chapter 13). Subsequently, this proposal of sensitization was strengthened by an observation that in the reaction of partially purified Renilla luciferase, two overlapping bioluminescence spectra were resolved, one of the blue 480-nm distribution and the other of the green protein's fluorescence. Morin and Hastings in 1971, measured several *in vivo* bioluminescence spectra and showed these corresponded to the fluorescence spectral distribution of this "green-fluorescent protein" (GFP), and postulated that the GFP acted as an acceptor in a "Förster-type" mechanism, with the initial product, the excited coelenteramide anion being the presumed donor (Fig. 8.9, *right panel*). This idea was further strengthened a few years later from investigations of the Renilla system from Cormier and associates at the University of Georgia. Specifically, the Φ_B of the *in vitro* reaction of coelenterazine on Renilla luciferase was enhanced almost three times in the presence of Renilla GFP, concomitant with a shift of the bioluminescence maximum from 480 nm to 509 nm, the shifted spectral distribution exactly matching that of the Renilla GFP fluorescence (Fig. 8.10).

This suggestion of what we now call a FRET mechanism although reasonable, was based on the assumption that the probability of resonance coupling in a Renilla luciferase-GFP complex, exceeded that for the non-radiative loss so that all the excitation energy would be emitted via the GFP fluorescence. The enhancement of Φ_B was rationalized by the GFP having $\Phi_F = 0.8$, several times that of the product coelenteramide, $\Phi_F \sim 0.2$ (in DMF). However, this is not definitive proof as the overall Φ_B is a product of three efficiencies, and

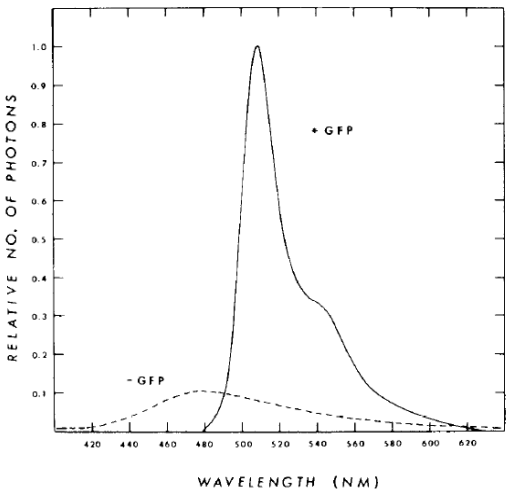

Figure 8.10. Bioluminescence emission from Renilla luciferin is shifted to the green on inclusion (+ GFP) of Renilla GFP accompanied by a three-fold enhancement of bioluminescence quantum yield.

FRET would have to be established by observing a decrease in the fluorescence lifetime of the donor. This is not practical in this bioluminescence system since the excited product donor has a too fleeting existence, and a direct fluorescence dynamics study here is frustrated by instability of the luciferase-bound product. More recent studies have substantiated that the FRET mechanism operates in some bioluminescence systems and this will be described in Chapter 13.

A second advance in knowledge in this field also came out of further investigations of the Renilla system. A coelenterazine-binding protein (CBP) could be purified from extracts. Again, CBP is unrelated in amino-acid sequence to the luciferases and a function suggested for it was for protection of the coelenterazine against auto-oxidation in free solution within the photophore of the Sea Pansy. The sequence of CBP revealed it to be in the class of EF-hand calcium-binding proteins, and in the presence of Renilla luciferase the addition of Ca^{2+} generated bioluminescence. It was first thought that the binding of Ca^{2+} released the coelenterazine into solution allowing it to freely diffuse to the luciferase, but a later study from E. Vysotski's group at the Russian Academy of Sciences in Krasnoyarsk, found that the bioluminescence intensity and the total light are both increased two-fold over that using coelenterazine alone. As well, the bioluminescence spectrum is slightly shifted if the CBP is used as the substrate over free coelenterazine (Fig. 8.11). It has therefore been proposed, that the bioluminescence reaction occurs within a luciferase-CBP complex and that the coelenterazine does not freely diffuse to the luciferase. It is speculated that for optimal efficiency, the Renilla reaction system *in vivo* should be a trimer of luciferase, CBP, and GFP. This result coming out of basic studies has important value for applications of this bioluminescence system in cell imaging. An analog called coelenterazine-v produces a yellow bioluminescence very suitable for imaging applications, but is too unstable to be used alone as a substrate unless it is bound within CBP.

The bioluminescence quantum yields for cypridinid luciferase and cypridinid luciferin (0.30), and Oplophorus luciferase with coelenterazine (0.34), indicate an excitation efficiency Φ_E almost unity, but Renilla luciferase with free coelenterazine is somewhat below this having

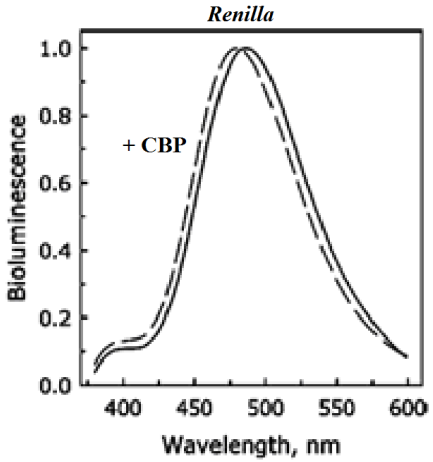

Figure 8.11. The bioluminescence from Renilla luciferase and free coelenterazine (–) is slightly shifted (——) using the coelenterazine binding protein (CBP) as substrate.

Φ_B only in the range 0.07-0.10, although it is two-fold enhanced using CBP as the substrate. In every case the product shows no fluorescence, explained by its being dissociated after the reaction as the amide product is non-fluorescent in aqueous solution. In an aprotic solvent such as DMSO, both amide products exhibit efficient fluorescence, for the cypridinid amide Φ_F = 0.3-0.4, and coelenteramide 0.2, for both the neutral and the coelenteramide anion. It is not likely that the Φ_B = 0.34 reported for the Oplophorus system, could exceed the coelenteramide Φ_F, and therefore in the first place, these quantum yields need to be remeasured with improved photometric accuracy. Solvent conditions also shift the fluorescence distribution for these products as well as other model compounds, over the range observed for the bioluminescence spectra with the different luciferases, 452-488 nm.

The active protein responsible for the bioluminescence of the jellyfish *Aequorea*, was first purified in 1962 by Johnson's group at Princeton. It was named "aequorin" and classified as a "Photoprotein" in that the bioluminescence was triggered just by adding calcium ions without any apparent requirement of oxygen, this last an observation first reported in fact by Harvey in the 1920s. It was suggested by Hastings and Gibson also in 1962, that a yellow chromophore tightly bound with aequorin, might be a luciferin hydroperoxide intermediate, but proof of its identity as a protein bound hydroperoxycoelenterazine, was only thoroughly established 40 years later through ^{13}C-NMR and the X-ray determined spatial structure of aequorin. Similar Ca^{2+}-regulated photoproteins as they are now called, have been detected in more than 26 different organisms, mostly coelenterates, and all have a mass in the range 22-26 kDa. The cDNA sequence determined for five of these photoproteins, shows that they belong to the larger class of "EF-hand" calcium-binding proteins, with three out of the four EF-hands having the required consensus sequence for calcium binding. Outside of the EF-

hand consensus, their sequences are not closely related. These five photoproteins are named for the genus following the aequorin example; from two other jellyfish, clytin (from *Clytia*) and mitrocomin (*Mitrocoma*), and from a hydrozoan, obelin (*Obelia*). Two others from the Ctenophera (comb jellies) have also been purified, mnemiopsin and berovin.

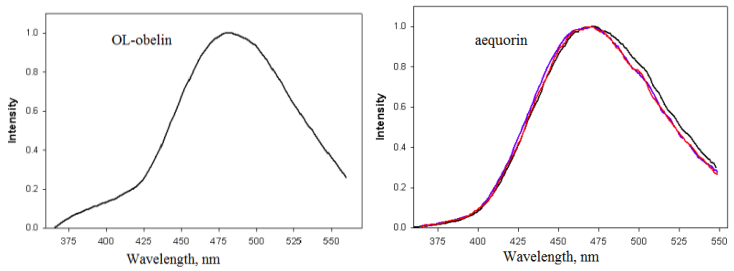

Figure 8.12. Ca^{2+}-triggered bioluminescence spectra from two types of Ca^{2+}-regulated photoproteins have different maxima and spectral shape. The product from aequorin has the same fluorescence spectrum (——) as the bioluminescence. OL = *Obelia longissima*.

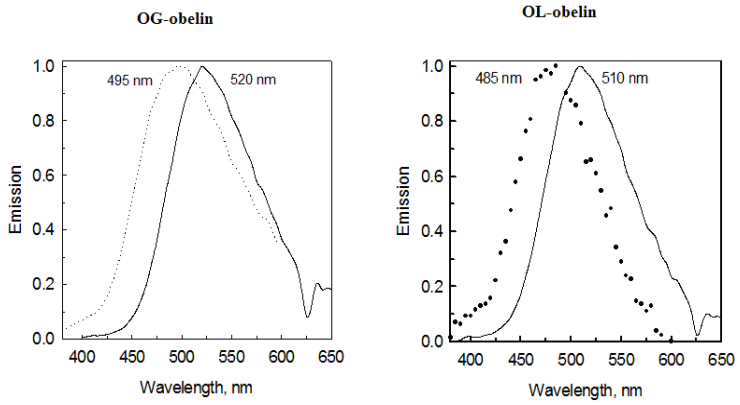

Figure 8.13. Bioluminescence (dots) of obelins from two species of *Obelia* have different spectral maxima (495 and 485 nm) and their product fluorescence (——) is at longer wavelength, 520 and 510 nm. OG = *Obelia geniculata*.

The addition of Ca^{2+} to a photoprotein triggers a blue bioluminescence emission with spectral maximum in the range 465−495 nm depending on the type. Aequorin shows $\Phi_B = 0.17$ consistent with the limit imposed by the $\Phi_F \sim 0.2$ of coelenteramide anion as determined in basic DMSO where it is relatively stable. The fluorescence spectrum of the aequorin and mitrocomin product bound coelenteramide anion, is the same as the bioluminescence with maxima in the range 465-470 nm. Unfortunately, its Φ_F has not been determined as it appears to dissociate quickly at least in the case of aequorin. The bioluminescence from obelins of various species is in the range λ_{max} = 475-495 nm, but their product fluorescence spectra are at a 25 nm longer wavelength than their bioluminescence maxima (Figs. 8.12, 8.13). The obelin product has Φ_F about 0.2, and although the bioluminescence and product fluorescence

spectra are different, the Φ_F of coelenteramide is unaffected in aprotic solvents of different polarity but the fluorescence spectra of the coelenteramide anion exhibit a wide range over the blue-green region. The obelins also show a small but significant difference from aequorin in their bioluminescence spectral envelopes. The shoulder at wavelength around 400 nm in the two types of obelin bioluminescence spectra, is not present in aequorin and mitrocomin bioluminescence, or in the obelin product fluorescence. From fluorescence model studies, this 400-nm band is attributed to the neutral form of coelenteramide. In the cypridinid bioluminescence this neutral amide contribution is dominant (Fig. 8.6).

An alignment of the primary sequences of aequorin and the obelin from *O. longissima*, is shown in Fig. 8.14. It reveals corresponding positions of α-helices (grey bars) A-H, that form the E-F hands (**I-IV**) characteristic of this class of calcium-binding proteins. Only E-F hands **I**, **III**, and **IV**, have the "canonical" amino-acid sequence (underlined), required for the binding of Ca^{2+}. The same correspondence or sequence homology, is found for all other Ca^{2+}-regulated photoproteins.

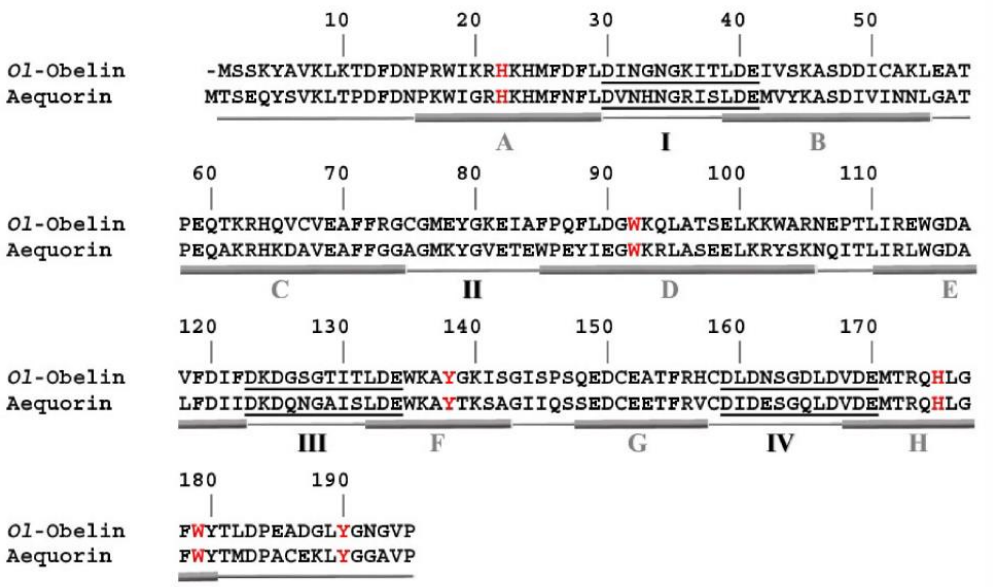

Figure 8.14. Alignment of the obelin and aequorin amino acid residue sequences using single letter abbreviations.

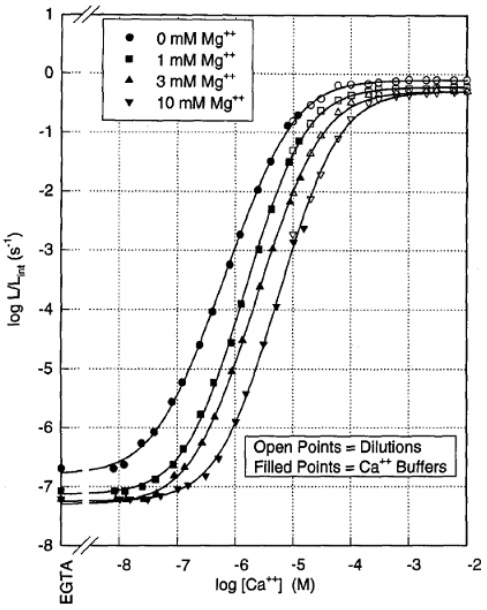

Figure 8.15. Light emission from aequorin is a very useful assay for cellular calcium. The log-log plot demonstrates the wide dynamic range but that a measurement must take account of possible physiological concentrations of magnesium which are inhibitory.

On rapid addition of Ca^{2+} to these photoproteins the bioluminescence rises to a maximum in 1-10 ms depending on the type of photoprotein. This has led to the wide application particularly of aequorin, for assay of intracellular Ca^{2+}; aequorin has been the most used as its discovery preceded that of the other photoproteins by more than 20 years. Fig. 8.15 shows the large dynamic range of the bioluminescence emission from aequorin plotted against Ca^{2+}concentration, and that physiological concentrations (> mM) of Mg^{2+}can be inhibitory. The slope of the line is > 2.0 and this as discussed in Chapter 4 (Fig. 4.4), has been interpreted as the bioluminescence requiring the binding of at least two Ca^{2+}ions. This of course, is just a kinetics interpretation. It is known from spatial structure, that each of the three EF-hand binding loop sequences binds a Ca^{2+}, but the binding affinities of each are not known. Ca^{2+} binding on each loop initiates a conformation change in the protein structure that probably transmits throughout (Chapter 12). In the description of the spatial structure, it has been shown that such changes would lead to alterations in the binding of the hydroperoxycoelenterazine ligand, leading to its destabilization and reaction to give light. The specific details of the photoprotein triggering mechanism are not yet known.

9. **Bioluminescence of Beetles**

"The glowworm shows the matin to be near

And gins to pale his uneffectual fire." William Shakespeare. (1601) Hamlet, Act I, scene 5.

There are a great many bioluminescent types identified within the class Insecta but only those in the order Coleoptera, the beetles, have received a detailed study of the biochemistry of their bioluminescence, probably because beetles are relatively larger than most insects and easier to collect in sufficient numbers. The firefly is actually misnamed because it too is a beetle not a fly whereas the true flies, of which there are numerous bioluminescent members such as the Australasian glow-worm, are in the order Diptera. The common North-American firefly *P. pyralis*, among the bioluminescent beetles has been the most studied in regard to its bioluminescence, due to its easy availability and location around the time intensive research was commenced late in the 1940s. The firefly belongs to the family Lampyridae, and there are only two other known families in Coleoptera with bioluminescent members Elateroidae, the click beetle, and Phengodidae, the railroadworm (Fig. 1.2).

The chemistry of the bioluminescence is the same among all the families of beetles, they all utilize the same substrates, firefly luciferin, ATP/Mg^{2+}, and O_2, but the bioluminescence properties such as spectra, differ among the species. The name "firefly" luciferin is commonly used although strictly, it should be called beetle luciferin. The variations in bioluminescence properties are especially noticeable in spectra, and the different colors are assumed to arise from perturbation of the excited state of the product through interactions within the binding site of the luciferase from each species, a question that is at the forefront of research at the present time. For example, even within the one family Lampyridae, Fig. 9.1 shows the range of spectral distributions from several species; *P. pyralis* has a yellow

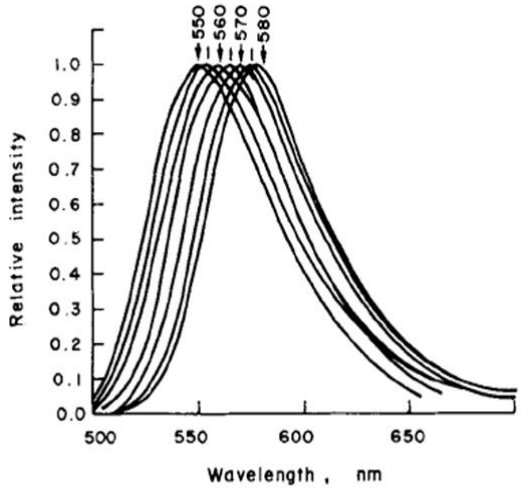

Figure 9.1. Bioluminescence emission spectra representative of the range of bioluminescence colors from several species of firefly all within the family Lampyridae, show absolute spectral maxima from 550 to 580 nm.

bioluminescence with spectral maximum at 562 nm, *P. scintillans*, orange with a 575 nm maximum, and *Photuris pennsylvanica* has a green bioluminescence color with a spectral maximum at 552 nm. It should be noted that the spectra shown are absolutely corrected but many published spectra are uncorrected for instrumental spectral sensitivity, and will not have a true spectral distribution, and will appear to have a few nm different spectral maxima from properly corrected reports. If it can be determined from a publication, uncorrected spectra will be labeled such.

Beetles of the other two families, Elateroidae and Phengodidae show bioluminescence colors ranging from green to red with spectral maxima 530−635 nm. Some species within these two families have two light organs (photophores) each emitting a different bioluminescence color, examples being the Jamaican click-beetle *Pyrophorus plagiophthalamus*, green and orange, and the South-American railroad-worm *Phrixothrix hirtus*, photophores along the sides giving yellow and the other one at the head, red (Fig. 1.2). The beetle luciferases from each species produce *in vitro* the same bioluminescence spectral distribution as *in vivo*. For example the natural luciferase purified from that species in Fig. 9.1 with maxima around 580 nm, gives the same *in vitro* bioluminescence spectral distribution. The same applies to the two recombinant luciferases from each photophore of the click-beetle, *in vivo* and *in vitro* both maxima at 539 nm, and the same for the other photophore, both at 571 nm, and the same situation for the railroadworm, 542 nm and 625 nm. As well as the variation over the spectral range, the bioluminescence quantum yields also differ (in Table 1, QY = Φ_B), with a decrease correlating with increase in spectral maximum; click-beetle green luciferase 539 nm, Φ_B = 0.61; Pyralis luciferase 562 nm, Φ_B = 0.48; and railroadworm red luciferase 625 nm, Φ_B = 0.15. Fig. 9.2 shows that spectral shifts can also result by mutation (Table 1). It is generally agreed that the reaction site in each luciferase differering in the amino acid residues comprising the cavity environment, gives rise to variations in the binding environment of the oxyluciferin, such as rigidity or effective polarity, which would account for the perturbation of the S_1 level of the bioluminescence product excited state.

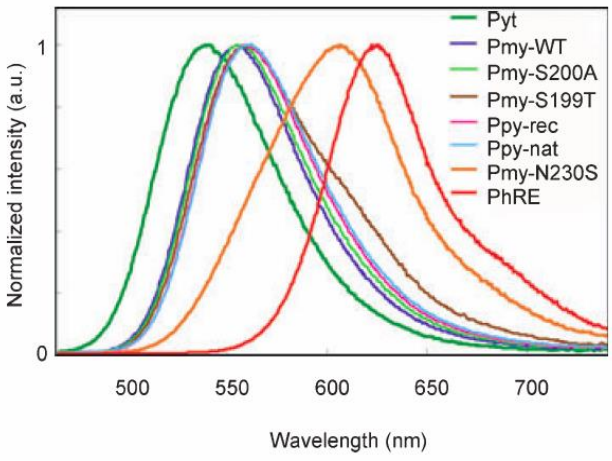

Figure 9.2. The range of *in vitro* bioluminescence spectra using luciferases from beetle species and some mutants. Ppy, *P. pyralis*; Pmy, *Pyrocoelia miyako*; PhRE, red light-emitting *Phrixothrix hirtus*; Pyt, green *Pyrearinus termitilluminans*.

Table 1. Bioluminescence maximum and quantum yield from beetle luciferases

Luciferase	λ_{Max}* (nm)	QY	± σ†
Pyt	539	0.61	0.019
PhRE	625	0.15	0.017
Pmy-WT	554	0.45	0.055
Pmy-N230S	606	0.21	0.0072
Pmy-S199T	559	0.48	0.056
Pmy-S200A	556	0.46	0.036
Ppy-rec	560	0.45	0.055
Ppy-nat	562 (566)‡	0.48‡	0.039‡

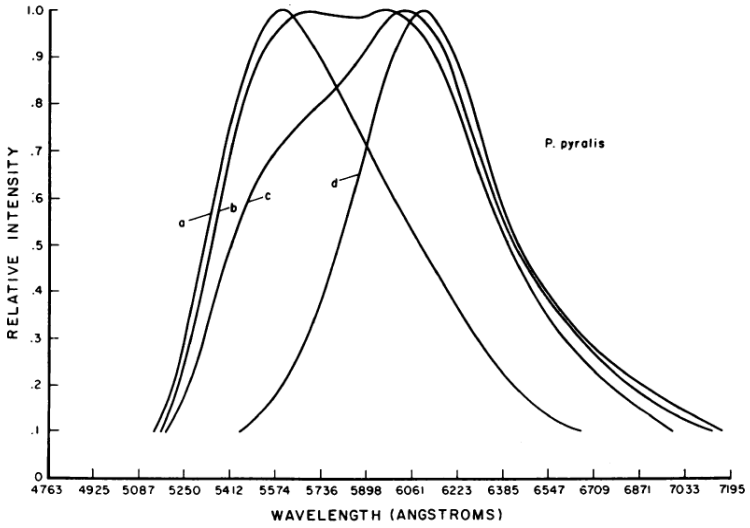

Figure 9.3. Spectral red shift of firefly bioluminescence induced by additives: (*a*) none, pH 7.6; (*b*) acid, pH 5.5; (*c*) Zn^{2+}; (*d*) Cd^{2+}.

Another observation that was if fact first reported about 200 years ago, was that the yellow bioluminescence from a firefly would turn red on warming. This is also seen in the *in vitro* reaction of Pyralis luciferase at elevated temperature, or by lowering the solution pH from its optimum 7.6 to around 6.0, or by the addition of cadmium or mercury salts (Fig. 9.3). A Gaussian analysis of the absolute spectral distribution from various species, for both *in vivo* and *in vitro* bioluminescence, concluded that on each luciferase, there must be potentially two excited state structures from which the emission could originate. One state would be responsible for the color range green through orange, presumably an environmental perturbation due to the binding cavity having differences in dielectric constant or binding rigidity among the types of firefly luciferases. Both solvent polarity and rigidity are well known to affect fluorescence spectra.

At higher temperature, acidic pH, or metal addition, it was proposed that this induced a conformational change that favors the second excited state of oxyluciferin, the one responsible for the red emission. This conclusion was based on the fact that the Gaussian parameters from each bioluminescence spectrum in the green−orange range, differed quantitatively from the red spectrum, meaning that the red emission must originate from a

different electronic state than the one responsible for green−orange. In Fig. 9.3 as example, even though this is a wavelength spectrum and not of the energy for which a Gaussian analysis can be correctly applied, it can be seen that the red spectrum is of narrower bandwidth (half-width = 62 nm) than the unperturbed normal spectrum (84 nm). This large red shift *in vitro* with acidic pH is only found with the luciferase from species of Lampyridae. A much smaller pH effect is observed in the reaction of click-beetle green luciferase.

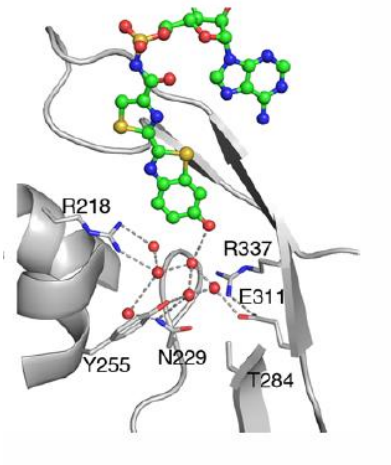

Figure 9.4. Protein associated water molecules (red balls) form an H-bond network to the luciferin-$O^{8'}$ and some cavity residues in the structure of Pyralis luciferase.

Figure 9.4 is the shows the basis for a recent proposal for one way the cavity site properties could modulate the bioluminescence color. *P. pyralis* and *P. scintillans* have a bioluminescence maximum at 562 and 575 nm, respectively (Fig. 9.1), and the same for their luciferases *in vitro*. The luciferase primary sequences are 89.8% identical, and a suspect residue that may be responsible for the difference in spectra is one occurring in the binding cavity, Tyrosine (Y255) in Pyralis luciferase and a Phenylalanine (F255) in Scintillans luciferase. On making the substitutions Y255F and F255Y the bioluminescence spectra were swopped. In the crystal structure of a luciferin analog bound to Pyralis luciferase (Fig. 9.4) it is seen that Y255 forms part of the cavity along with an H-bond network of protein associated water molecules, which in turn link to $O^{8'}$ of the luciferin. The substitution Y255F would clearly interfer with this network as the Phenylalanine lacks the H-bonding property.

The overall chemical mechanism of firefly bioluminescence (Fig. 9.5) was established with reasonable confidence by about 1970. It was almost entirely derived from study of the *in vitro* reaction with Pyralis luciferase. The intermediacy of a dioxetanone was supported by analogy with chemiluminescence mechanisms and the results of oxygen-18 labeling of the CO_2 product. At that time the product “Oxy-luciferin” could not be obtained in a chemically pure

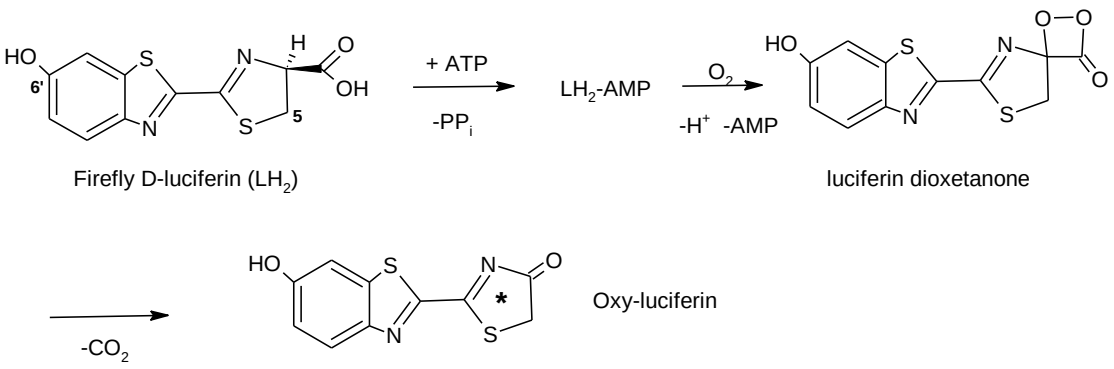

Figure 9.5. Overall steps in firefly bioluminescence; AMP is adenosine monophosphate; PP_i is pyrophosphate.

state due its chemical instability but there was sufficient physicochemical data to support the assumption that oxyluciferin was the excited state product. It has been 50 years after the structure of firefly luciferin was proven that firefly oxyluciferin was obtained in crystalline purity and definitive experiments could verify this assumption with certainty.

Within the active site of firefly luciferase the chemical mechanism leading to the dioxetanone involves first formation of a carbanion at the C-4 position (the chiral C in Figs. 9.5 and 9.6). A proximate basic residue (Luc-B:) such as a histidine would be needed to act as a proton acceptor. Molecular oxygen is a ground state triplet or equivalently a diradical, and it is generally believed that direct formation of the peroxy anion singlet state would be spin forbidden and therefore slow, except for the fact that the negative charge on the C-4 could relieve the forbideness due to spin-orbit coupling that mixes triplet and singlet states (see also Fig. 14.1).

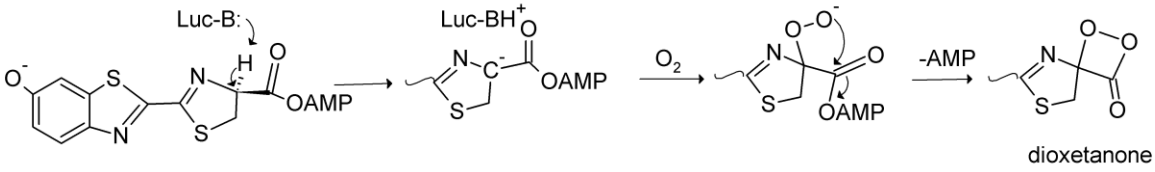

Figure 9.6. Firefly luciferin is deprotonated by a basic residue (B) in the luciferase (Luc) active site to favor the oxygen addition to the carbanion.

A recent study favors an alternate view that the oxygenation is a single electron process (SET) with a superoxide radical anion $\cdot O_2^-$ intermediary (Fig. 9.7). This is based on indirect evidence using a well-understood model reaction, the oxygenation of luciferin methyl ester in solution. A superoxide intermediate was trapped and identified unambiguously by electron paramagnetic resonance spectroscopy. Possibly the coelenterazine and bacterial

bioluminescence systems also proceed similarly through an anionic substrate and the superoxide radical, leading to the hydroperoxide intermediate.

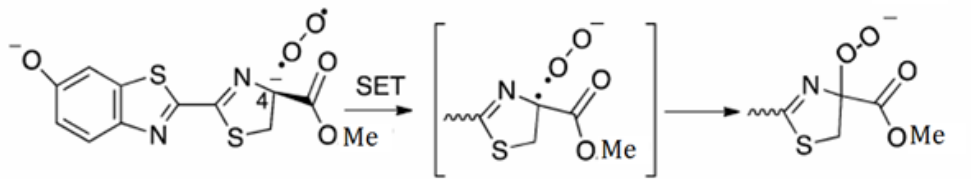

Figure 9.7. Oxygen binding to this firefly luciferin analog involves a superoxide anion intermediate (·O-O¯).

Firefly luciferase is seen to be a bifunctional enzyme (Fig. 9.5), the first catalytic activity being that of a synthase whereby firefly luciferin (LH_2) is adenylated at the carboxyl to form the AMP ester (LH_2-AMP) with the release of pyrophosphate (PP_i). The second activity is the addition of molecular oxygen followed by oxidative decarboxylation to the electronic excited state of oxyluciferin. Also to be noticed is that firefly D-luciferin is chiral at the C-4 position. The oxygen addition and bioluminescence only takes place if the luciferin is the D-enantiomer. The mirror image configuration of firefly luciferin, i.e., L-luciferin, also undergoes adenylation but no bioluminescence results. Strictly according to the definition, L-luciferin should not be called “luciferin” at all as it is not a substrate for generating bioluminescence.

Many derivatives of D-luciferin are bioluminescent exhibiting various properties of spectra, kinetics, and quantum yield. Of particular interest is the 5,5-dimethylluciferin derivative (Fig. 9.8), which generates a only a red bioluminescence color with Pyralis luciferase and also because the dimethyloxyluciferin product is more stable than oxyluciferin, thus allowing reliable study of its spectral properties. The bioluminescence from this derivative bears on the question of the identity of the emitter as will be shown.

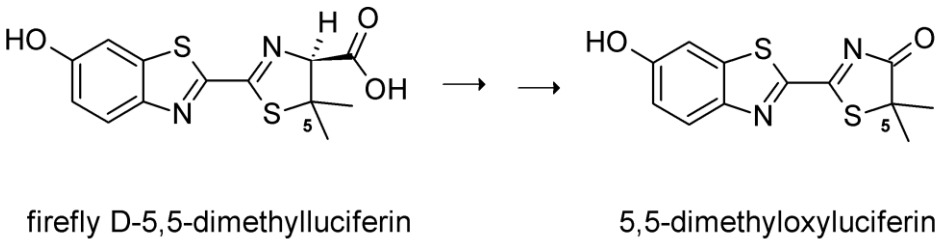

Figure 9.8. The firefly oxyluciferin analog with 5,5-substitution cannot undergo keto-enol tautomerism.

The definitive characterization of a chemiluminescence or bioluminescence reaction pathway entails identification of the reactants, isolation of the intermediate steps, isolation and identification of the reaction product, and proof that this is the primary excited species by showing correspondence of its fluorescence with the spectral distribution of the chemi- or bioluminescence. Although the chemical structure of the product firefly oxyluciferin had been plausibly established by the late 1960s as mentioned above, it was very difficult to prove this without question by quantitative study due to its chemical instability. First attempts to find a qualifying fluorescent product from the Pyralis luciferase-luciferin reaction were unsuccessful as the fluorescence of the final reaction mixture showed two bands shifted to a shorter wavelength than the bioluminescence. A kinetics study did show that the luciferin absorption maximum around 340 nm, decreased on addition of the ATP with a corresponding rise around 380 nm as expected for oxyluciferin absorption, and the rise rate was the same as the decay of bioluminescence intensity. The luciferase bound product was separated from unbound reaction products but again, although there now appeared only a single fluorescence band, its maximum at 525 nm was still about 40 nm shorter wavelength than the Pyralis luciferase bioluminescence maximum (562 nm). This fluorescence was suggested to be an artifact and assigned as from the decay product due to the chemical instability of oxyluciferin.

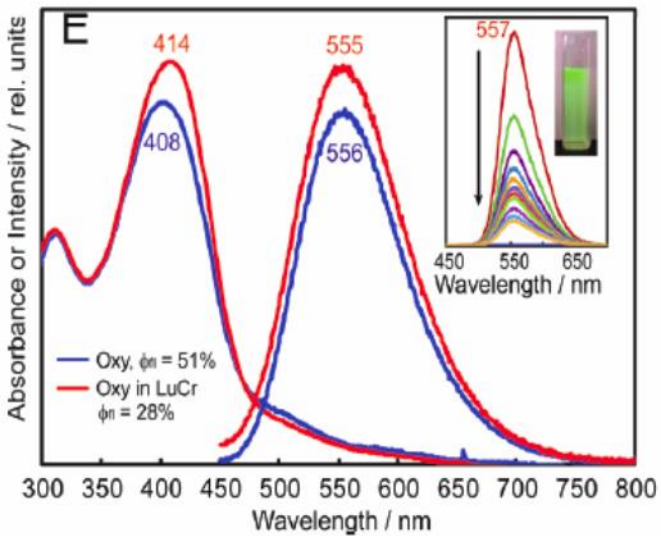

Figure 9.9. Absorption (left) and fluorescence (right) of firefly oxy-Luciferin (Oxy) in basic aqueous solution (blue) or bound to the luciferase (red) from *L. cruciata* (LuCr). The inset shows the bioluminescence as it decays over the reaction time with the corresponding decay of the product fluorescence due to instability of the oxyluciferin in solution. Spectra are uncorrected.

A recent study using Luciola luciferase from the Japanese firefly *Luciola cruciata* however, has demonstrated as shown in Fig. 9.9, that the fluorescence spectrum of purified oxyluciferin either free in basic aqueous solution (excitation at 408→556 nm fluorescence, blue line, Φ_F = 0.51) or complexed with Luciola luciferase (414→555 nm, red line, Φ_F = 0.28), has the same maximum as the bioluminescence spectrum (inset, 557 nm red line). The blue spectral

distribution is apparently broader (half-width = 107 nm) than the bioluminescence (60 nm) but quantitative evaluation is difficult as the spectra are apparently not corrected for instrumental spectral sensitivity. Evidently, the oxyluciferin product is more chemically stable after reaction and still bound within Luciola luciferase, unlike in the earlier investigations with Pyralis luciferase. A few years later the spatial structure was determined so surprisingly, these same solution conditions required to form crystals for the X-ray crystallography, must have allowed the bound oxyluciferin to be stable and unchanged.

Figure 9.10 shows that over the physiological pH region, the oxyluciferin structure exists in two neutral forms due to keto-enol tautomerism, and four anionic forms by acid-base equilibrium. Much attention has been given to identifying which form would be responsible for the green to yellow or for the red bioluminescence, by observing which has fluorescence spectral properties matching the bioluminescence. The neutral forms have a blue fluorescence and therefore can be eliminated from consideration. Until recently, the measurement of spectra was frustrated by the chemical instability of oxyluciferin. There is no doubt that the emitter is one of the anions but there are several possibilities, one of the three monoanions or the dianion shown.

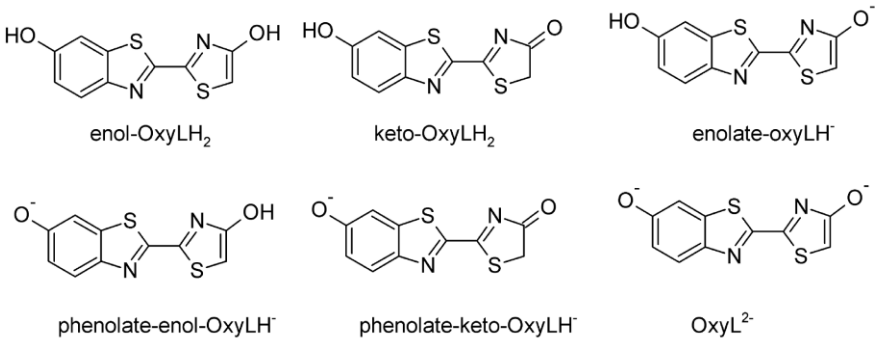

Figure 9.10. Ionic forms of firefly oxy-luciferin.

On the basis that bioluminescence is a chemiluminescence reaction taking place on a protein, considerable insight was first obtained from earlier studies of the solution chemiluminescence of firefly luciferin and its derivatives. Addition of a small concentration (0.005 M) of the strong base potassium t-butoxide to the luciferyl phenyl ester in the aprotic solvent DMSO, generated a red chemiluminescence with maximum at 629 nm (Fig. 9.11B). The phenyl ester was used for the DMSO studies because the AMP derivative has poor solubility. The base initiated reaction of firefly luciferin in water has a chemiluminescence maximum at 649 nm, the red shift over that in DMSO consistent with a lowering of the S_1 energy level due to the higher polarity of an aqueous environment. In either solvent, the product fluorescence was unstable but qualitatively at least, it did match the red bioluminescence spectrum. The 5,5-dimethylluciferyl phenolate gives only the same red chemiluminescence regardless of base strength. For the chemiluminescence of 5,5-dimethylluciferin (Fig. 9.8), the product 5,5-dimethyl-oxyluciferin is stable enough to allow a more quantitative fluorescence study. The spectral distribution of this fluorescence is indistinguishable from the chemiluminescence spectrum and also has the narrow bandwidth characteristic of the red bioluminescence

spectrum. As the dimethyl substitution does not allow keto-enol tautomerism, the firm conclusion is that the red bioluminescence must also originate from the keto form of oxyluciferin, the excited state of the phenolate-keto-OxyLH$^-$ (Fig. 9.10).

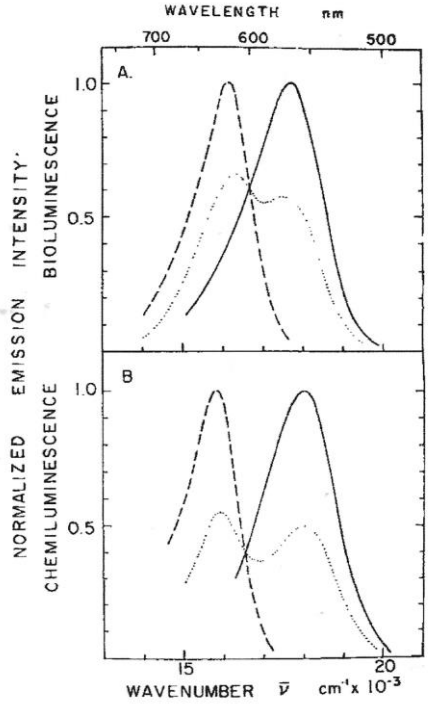

Figure 9.11. A. *In vitro* bioluminescence with Pyralis luciferase at pH 8.0 (———), pH 6.8 (⋯), and pH 6.0 (---). **B.** Chemiluminescence of luciferyl phenyl ester in DMSO with t-butoxide concentrations of 0.5 M (———), 0.05 M (⋯), and 0.005 M (---).

The 5,5-dimethylluciferin (Fig. 9.8) itself is not active for bioluminescence with luciferase because it does not undergo the adenylation step. The bioluminescence spectra have been collected using the synthetic substrate 5,5-dimethylluciferyl adenylate, which obviates the need for the ATP, using either Pyralis luciferase or the green click-beetle luciferase from *P. plagiophthalamus*. The green click-beetle luciferase reaction produced a red bioluminescence with maximum 624 nm (uncorrected), and the product fluorescence spectrum was the same, and both were similar to the red chemiluminescence in Fig. 9.11. Pyralis luciferase however, showed a yellow bioluminescence with maximum at 570 nm, almost the same spectrum as with natural firefly luciferin. It was concluded that the yellow excited state is neither the monoanion enolate-oxyLH$^-$ nor the dianion, but in all cases both red and green, the phenolate-keto-OxyLH$^-$, its S_1 level modulated by interactions within the luciferase binding site to generate the complete range of bioluminescence colors, green to red. This conclusion does not fit the criterion of a distinct electronic structure between the yellow and red excited states depending on the pH for example, as in the Pyralis luciferase reaction with natural firefly luciferin. Apart from the problem that the published spectra were not corrected for instrumental spectral sensitivity, it is apparent from Fig. 9.12 (right panel) that bandwidths of

the green (75 nm) and red (80 nm) click-beetle green luciferase bioluminescence spectra, are almost the same. Also, the bioluminescence quantum yield of its red bioluminescence is markedly reduced to only about 0.01, to be contrasted with 0.48 for the yellow bioluminescence of this luciferase with natural firefly luciferin. The same problem appears with the click-beetle green luciferase reaction with the 5,5-dimethylluciferin adenylate, the quantum yield being only a few percent of that with natural luciferin, 0.18.

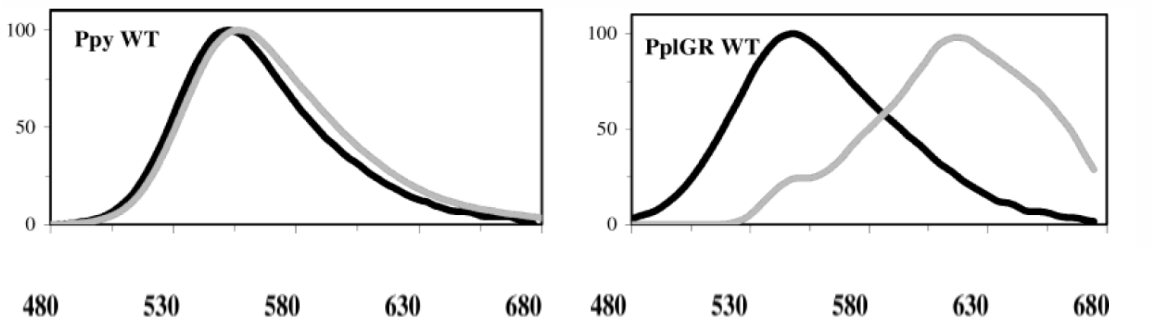

Figure 9.12. Bioluminescence with luciferyladenylate (*black*) or dimethyl-luciferyladenylate (*grey*), and (*left*) natural (WT) Pyralis luciferase, Ppy WT, or (*right*) the green luciferase from *P. phlagiothalamus*, PplGR WT.

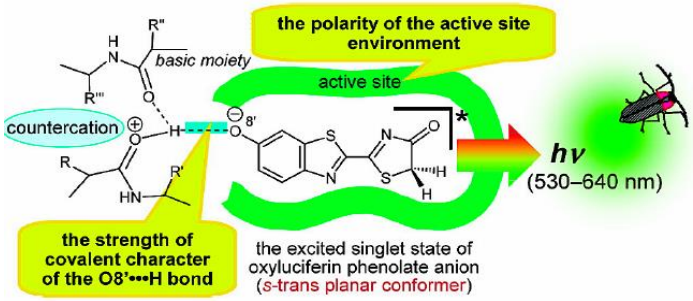

Figure 9.13. The S_1 level of the bioluminescence emitter, the phenolate-ketoOxyluciferin, is modulated by the polarity of the active site environment and the covalent character of the hydrogen bond to the phenolate oxygen, $O^{8'}$.

The chemical stability of the 5,5'-dimethyl-oxyluciferin made feasible a detailed spectral study to show how solvent perturbations could imitate interactions within the luciferase binding site, thus accounting for the whole bioluminescence spectral range, green to red. The conclusion that the keto anion is the emitter in all cases is summarized in the cartoon (Fig. 9.13). The fluorescence spectrum of 5,5'-dimethyl-oxyluciferin phenolate (the unsubstituted structure is shown within the green cloud) was observed to depend on both the strength of the base used in combination with the solvent polarity (Fig. 9.14). The fluorescence in the non-polar solvent benzene with the strong base tributylamine, had a maximum at 541 nm with Φ_F

= 0.82, but with a weaker base tetramethylguanidine, the maximum was at 570 nm with a reduced Φ_F = 0.25. The phenolate was not stable in water, so the most polar solvent used was methanol; the results were 630 nm and Φ_F = 0.1 for both strong and weak bases. It was proposed that in a non-polar solvent the phenolate is in a contact ion-pair with the counter cation, resulting in an increase in energy of the S_1 level. In a polar environment the Coulomb interaction is weaker and the base pair becomes separated.

The cartoon illustrates a plausible function for cavity amino acid residue side chains in this regard. The base-solvent perturbation does account for the complete green-red range of bioluminescence colors and the Φ_F values are also consistent with the Φ_B = 0.48 and 0.16 for the yellow and red emissions respectively with Pyralis luciferase, considering that the Φ_F could be enhanced in the luciferase binding site. There is also some bandwidth narrowing going from the shorter wavelength spectra (66 nm) to the spectra in the red range (52 nm).

The conclusion is that the overall keto structure is still a suitable candidate for the bioluminescence emitter in all cases, being electronically modified just by the nature of the charge situation at the 6'-phenolate position, meaning that it could be either a free anionic charge there on the $O^{8'}$ or a contact ion-pair with mixed ionic and covalent character. The results do not eliminate enols or enolates as the source of green to yellow bioluminescence of natural luciferin; as will be described next their fluorescence spectra also span the green to yellow range, but it is generally agreed that the red bioluminescence color with natural luciferin is from the excited state of the keto tautomer.

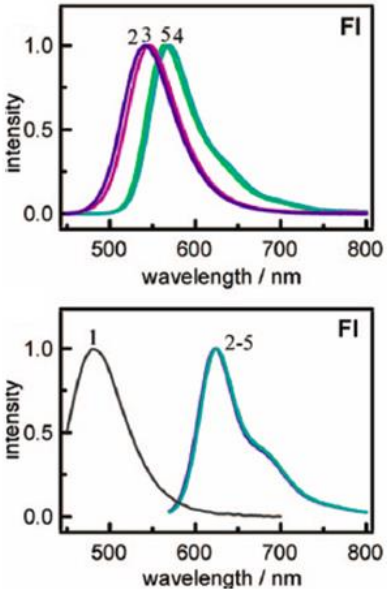

Figure 9.14. Fluorescence spectra (uncorrected) of firefly dimethyloxyluciferin in benzene (*top*) or acetonitrile (*bottom*) with added bases: **1.** none; **2.** TBA; **3.** BA; **4.** TMG; **5.** DBU.

This alternative view was developed from a similarly detailed study of the fluorescence of unsubstituted oxyluciferin itself. In 2009, oxyluciferin was prepared for the first time in crystalline purity and techniques were developed for its quantitative study. Its chemical stability was found to be enhanced by using solvents purged with nitrogen or argon to reduce oxygen to low levels with the result that the oxyluciferin anion is sufficiently stable for the

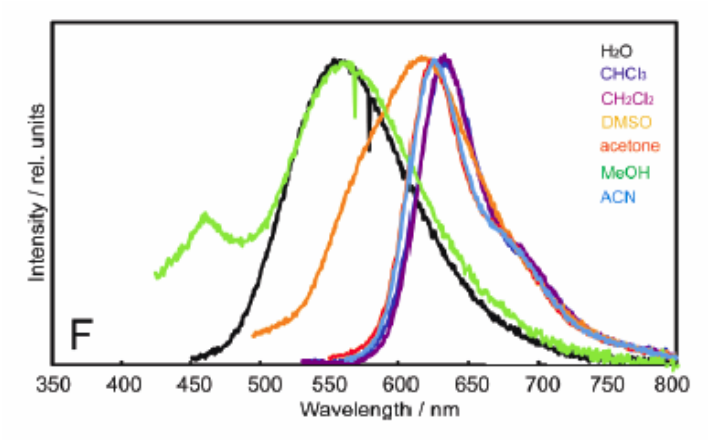

Figure 9.15. Solvent modulation of the fluorescence of firefly phenolate-keto-oxyLH$_2$.

many minutes needed for fast and accurate spectral measurement except again, a caution is that these spectra are not corrected. Fig. 9.15 shows the fluorescence spectra of oxyluciferin anion in solvents of various polarity or hydrogen bonding properties, using the same base tetrabutylammonium hydroxide. In water and methanol there is a good match for the yellow bioluminescence, maximum 555 nm. In the aprotic solvents acetonitrile (ACN) or chloroform ($CHCl_3$), the fluorescence is red and the spectrum also shows an encouraging decreased bandwidth (61 nm) over the yellow spectrum (108 nm). This narrowing is probably real but again, quantitative comparison is less than reliable as these spectra are apparently uncorrected for instrumental response. Some uncorrected spectral maxima and structural assignments are for each:

H_2O	559 nm	$\Phi_F = 0.42$	phenolate-enol-OxyLH$^-$or OxyL^{2-}
ACN	626 nm	$\Phi_F = 0.16$	phenolate-keto-OxyLH$^-$or phenolate-enol-OxyLH$^-$.

It is interesting to note that assignment of the red emitter as from the keto-phenolate anion and the yellow from the enolate dianion (OxyL^{2-}), was the original proposal made by White and coworkers in 1971. Their Gaussian parameters transformed here to a wavelength scale, are for the yellow bioluminescence from the Pyralis luciferase in vitro reaction carried out at its optimal pH of 7.6, a maximum at 558 nm (17,700 cm^{-1}) and FWHM 69 nm (2200 cm^{-1}). At pH 6.0 the bioluminescence is red, maximum 612 nm (16,150 cm^{-1}) and FWHM 64 nm (1700 cm^{-1}). The red emission is almost identical to the red chemiluminescence in basic DMSO just shown in Fig. 9.11, a maximum 624 nm (15,850 cm^{-1}) and FWHM 69 nm (1750

cm^{-1}). The yellow chemiluminescence is similar to the yellow bioluminescence with maximum at 549 nm (18,000 cm^{-1}) and FWHM 66 nm (2150 cm^{-1}) and the same parameters are evident for the fluorescence. Unfortunately, their report of a yellow chemiluminescence turned out later to be hard to reproduce.

In the mid-eighties, Pyralis luciferase was first cloned, this species chosen because of the detailed knowledge of the biochemical properties of this luciferase from the common North American firefly that had been accumulated over the previous 30 years. The nucleotide sequence was determined as encoding a single chain protein of 550 amino acid residues with calculated mass of about 61 kDa. This corrected the earlier estimate of the mass of around 100 kDa and also showed that it comprised only a single chain and not two subunits as earlier surmised. The expressed protein had identical bioluminescence properties as the natural Pyralis luciferase and contained no bound cofactors. Recombinant luciferases from many firefly species from different locations over the world, have been obtained in following years and their amino acid sequences found to be 67-98% identical to Pyralis luciferase. The variation in bioluminescence spectral maxima among these species (550-580 nm) evidently originates in these sequence differences, and uncovering the details and positive proof of this proposal is a matter vigorously pursued. The recombinant luciferases from the other beetle families, the Jamaican click beetle (Elateridae) and the railroad worm (Phengodidae), show lesser sequence similarity to Pyralis luciferase, about 50%, but are more similar among each other including to their isozymes. Some organisms within these last two families possess two photophores exhibiting different spectral emissions, the click beetle showing bioluminescence maxima for one photophore around 546 and the other 593 nm, and the railroad worm 546 and 623 nm (Fig. 1.2).

In the mid-nineties the spatial structure of Pyralis luciferase was determined by X-ray crystallography. This and bacterial luciferase were the first luciferase structures to be published. Over the past decade or more, the determination of primary and spatial structures, have led to much activity towards understanding the mechanistic details of the reaction arising from the nature of substrate and product interactions within the luciferase active site cavity. Discussion of the structural results will be reserved for a later chapter. With the availability of sequences from the many types of firefly luciferase, the interest was in the relationships among them with implications for the evolution of beetle bioluminescence. Also resulting was the practicality for point mutation to determine what changes in substrate and product interactions within the binding cavity might be responsible for the variation in spectral properties.

Early in these studies the similarity had been remarked upon, that the adenylation step is analogous to the activation of fatty acids by acyl-CoA (coenzyme A) synthases, and of amino acids by aminoacyl-tRNA synthetase for peptide bond formation generally in cellular metabolism.

$$\text{R-COOH} + \text{ATP}\ (Mg^{2+}) \rightarrow \text{R-C(O)-AMP} + \text{PP}$$

$$+ \text{HS-CoA} \rightarrow \text{R-C(O)-S-CoA}$$

$$\rightarrow \text{fatty acid synthase complex.}$$

Also tantalyzing is the that fact that luciferase also possesses a binding site for the common cosubstrate coenzyme-A, a property also involved in many adenylation reactions. On the basis of sequence similarity and structural homology, and an additional demonstration that beetle luciferase had a general acyl synthetase activity, luciferases have been grouped within what is called the "ANL superfamily" of adenylating enzymes. This synthetase function in cellular metabolism, is the initial step in extension of fatty acid chains and is present in all kingdoms of life. In the later chapter on spatial structure comparison, we will show how this catalytic relationship extends into the heart of the luciferase and synthetase biochemical mechanisms.

Following the availability of many beetle luciferase sequences, a comparison within the data bank was initiated aiming to detect an evolutionary origin of firefly bioluminescence. Homology with many of the acyl-CoA synthetases was detected implying a likely common ancestry. The high variation in amino acid residues among the luciferases suggested a more rapid evolution than for other enzymes, a result probably due to the fact that bioluminescence is not a mainstream metabolic reaction. The fossil record suggests a divergence of the bioluminescence beetles from other beetle families 150-200 million years ago. A remarkable recent finding is that two recombinant acyl synthetases from non-bioluminescent insects that showed no bioluminescence activity with firefly luciferin, could be converted to a "pseudo-luciferase" on single point mutation of a single serine residue. Although the bioluminescence level was only about 10^{-3} % of that with natural luciferase, the bioluminescence properties could be readily confirmed and had an emission spectral maximum around 610 nm (uncorrected).

This and accumulated evidence, gives strong support to a proposal that the evolutionary origin of beetle luciferase in insects was by gene duplication from an acyl-CoA synthetase. Firefly luciferin itself has not been identified as a metabolite in insects, so the evolution of bioluminescence would additionally have to entail co-evolution of a luciferin synthesis pathway, concomitant with the luciferase evolution. From the chemical structure it is seen that luciferin is some combination of two amino acid fragments, tyrosine and cysteine. In this regard, with a protein purified from the non-luminous fruitfly having an homologous sequence to luciferase, a structurally rigid synthetic firefly luciferin analog has been found to yield bioluminescence. This analog has no activity with genuine firefly luciferase. A speculation can be entertained, that an aromatic carboxylic acid say derived from tyrosine, might be prone to oxidation and be weakly chemiluminescent bound to the acyl-CoA synthetase, and this reaction could undergo adaptation, so that there would be co-evolution of a luciferin biosynthetic pathway as well as the synthetase-luciferase.

10. **Bacterial Bioluminescence**

The whole appearance of the ocean was like a plain covered with snow. There was scarce a cloud in the heavens, yet the sky...appeared as black as if a storm was raging. The scene was one of awful grandeur; the sea having turned to phosphorus, and the heavens being hung in blackness, and the stars going out, seemed to indicate that all nature was preparing for that last grand conflagration which we are taught to believe is to annihilate this material world. Captain Kingman reporting aboard the American clipper *Shooting Star*, South of Java (1854).

The marine bioluminescent bacteria are found throughout the world's oceans and in all environments, from the deep ocean functional at temperatures around 0ºC, to tropical waters where the surface temperature may exceed 30ºC. There are four marine genera that have received most study relevant to the bioluminescence mechanism, three are usually found specific for the light organ of the host, fish or squid, but can also occur free-living in sea water. The light production is continuous in the light organ but no luminescence is observed in the free-living state where they are at high dilution. The phenomenon of "milky seas" is believed to be from dense cultures of these bacteria growing on kelp or other run-off matter nearby ocean shores. This is because in culture these bacteria turn on their bioluminescence only after reaching a certain cell density, an observation that led to the important discovery of an "inducer molecule" that regulates the switching on of the *lux* operon, an observation initiating studies of "quorum sensing" in the physiology of some but not all types of bioluminescent bacteria. The operon is the sequence of genes in the bacterial genome, which in this case, is involved in the production of the several different proteins needed for the bioluminescence phenotype.

Classification of the bioluminescent bacteria has been an active field even starting in the late 19th Century and continuing to the present day, following the usual protocols based on morphology, staining, metabolic products, etc. Bacterial taxonomy in general is not a clear-cut procedure, and there has been an amount of shifting of names over the years that leads to some confusion on reading the literature. With use of the recent methods of phylogenetics, a more unambiguous classification has emerged, and these revised names will be explained next. Fortunately, the abbreviations for the types of bacterial luciferase most studied over the past 50 years can be retained here, as they still correspond to the revised classifications. The complete genome sequence of several types has been determined.

The bacterial luciferases from only five of the types have received detailed study from biochemical/biophysical aspects. These were chosen based on differences in properties such as bioluminescence emission spectra and kinetics, so as to isolate features of commonality. The requirement of $FMNH_2$, oxygen, and a long-chain aliphatic aldehyde for most efficient *in vitro* bioluminescence is universal, and it is safe to assume that the bioluminescence mechanism is the same for all. The bacterial luciferases from all types produce similar broad bioluminescence spectra *in vitro* with a type-dependent maximum in the range 490-505 nm. The detailed *in vitro* studies to be described here in this book are on the PL-luciferase from *Photobacterium leiognathi*, PP-luciferase from *P. phosphoreum*, VH-luciferase from *Vibrio*

harveyi (*campbellii*), AF-luciferase from *Alliivibrio* (previously *Photobacterium*, *Vibrio*, or *Achromobacter*) *fischeri*, and Y1-luciferase from *Alliivibrio sifiae* (previously *Photobacterium fischeri* strain Y-1).

The *in vivo* bioluminescence from the majority of these types of bacteria has a blue-green color, a broad spectrum with a type-dependent emission maximum in the range 490-505 nm. Some from the genus *Photobacterium* however, have *in vivo* emission maxima much bluer, towards 475 nm, and *A. sifiae* has a yellow emission with maximum at 542 nm (Fig. 10.1). These bioluminescence spectra shifted either to the blue or yellow, are due to the presence of an identified "antenna protein" purified from extracts of these types. Lumazine protein from species of *Photobacterium* is the origin of the shorter wavelength blue bioluminescence some having *in vivo* maxima as short as 470 nm, and the related Y1-protein is the antenna protein

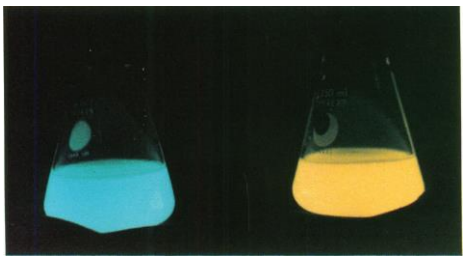

Figure 10.1. Growth cultures of (*left*) *P. phosphoreum*, and (*right*) *A. sifiae* (Y-1 strain). The different colors correspond to the fluorescence of the antenna protein in each type of bacterium.

originating the yellow emission from *A. sifiae*. Only one yellow type is known, but lumazine protein appears common to most species within the genus *Photobacterium*. *P. phosphoreum* is psychrophilic (cold loving) and the *in vitro* reaction intermediates with PP-luciferase are less stable even at 2ºC, than the intermediates from the mesophilic (moderate temperature) types like *P. leiognathi*. PL-luciferase intermediates can be stabilized for several hours at 2ºC, a very convenient property that favors quantitative investigation. *V. harveyi* is the common free-living type and VH-luciferase also produces metastable intermediates convenient for study, and therefore this type has received most investigation since its discovery in the late 60's. Strains of *V. harveyi* and *A. fischeri* have bioluminescence maxima around 495 nm and no antenna protein from these types has been discovered.

Elucidation of the chemical mechanism of bacterial bioluminescence has been frustrated by the lack of any convincing chemiluminescence model (McCapra, 2000). This has not inhibited numerous speculations however. For the firefly as well as the marine systems that use for example coelenterazine, much progress was achieved based on chemiluminescence studies of firefly luciferin or coelenterazine, usually reactions in basic DMSO, and useful insight was generated in spite of their low chemiluminescence yields that are often less than 0.01. All earlier studies of the bacterial reaction sequence therefore, have had to depend on kinetics and spectroscopy, and some of these results have already been outlined in Chapter 4.

These reports will now be expanded here in order to highlight any generally agreed conclusions or, if still under dispute, how resolution seems possible.

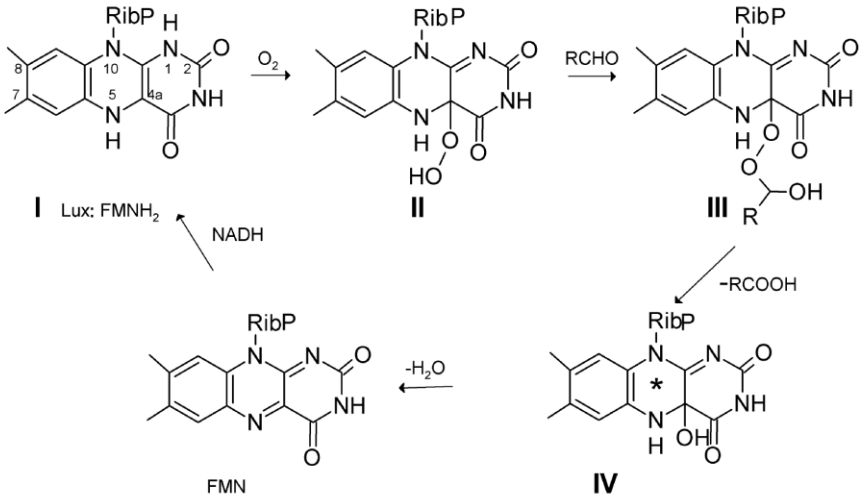

Figure 10.2. Linear mechanism of bacterial bioluminescence corresponding to the common flavoenzyme peroxidation pathway. RCHO is a long-chain aldehyde and RCOOH the corresponding acid. Lux is bacterial luciferase and the bold Roman numerals indicate that these structures are Lux-bound. In the cell, FMN is reduced by NADH on a reductase. RibP is ribityl phosphate.

The first kinetics study in 1963, revealed the presence of a metastable oxygenated flavin intermediate that was proposed at that time and now proven, to have structure **II** in Fig.10.2. Its absorption spectrum was consistent with its having an electron orbital distribution like reduced flavin $FMNH_2$, and in 1986 the structure was finally identified by NMR as the 4a,5-dihydro-4a-hydroperoxyflavin shown, and as being tightly bound to the bacterial luciferase. NMR also revealed that the flavin in Intermediate **I** is anionic at N(1). There is reasonable although circumstantial evidence, to suggest **IV** being the luciferase-4a-hydroxyflavin following the plausible suggestion for the **III** structure as a luciferase-flavin aldehyde peroxyhemiacetal, but these two suggestions have not been directly confirmed. In the early 70's, a metastable species was reported occurring in the reaction mixture as having the same fluorescence spectrum as the bioluminescence. In the early 80's this species later named the "fluorescent transient" (FT), was given a more quantitative study of its absorption and fluorescence spectra, plus the fluorescence and bioluminescence kinetics. The fluorescence state of intermediate **IV** was generally believed to be the origin of the bioluminescence. The detection and measurement of the fluorescent transient kinetics already described in Chapter 4, was among the first indications that the mechanism of bacterial bioluminescence was not by a linear mechanism but more likely to belong to the sensitized chemiluminescence class.

There have been many hypotheses advanced for the chemical mechanism leading to bioluminescence excitation but all fail in one respect or another, inconsistent with the biochemical data, the known chemistry assumed, or the absence of a model chemiluminescence having a promising light yield. In Fig. 10.2, the apparently direct

chemiluminescence step **III → IV***, continues to be presented in the literature as the excitation to give the model the appearance of completeness. It would be better to show this step with a double arrow shorthand, because a direct chemiluminescence process is inconsistent with the kinetics of the fluorescent transient **IV**.

McCapra (2000) reviewed the numerous mechanistic speculations in the literature and devised a new one with a role for protein association (Chapter13) leading to a sensitized mechanism (Fig. 10.3). The formation of the peroxyhemiacetal **III** is reasonable although again, there is no direct structural evidence for it. The equilibrium **II ⇄ III⇄ V** allows that the breakdown product, the aldoalkylperoxide **V**, may condense with a second **III** to form the aldehyde-peracid adduct, **VI**, a known chemistry. This Adduct then would proceed to the perester **VII** as the high energy intermediate having a known chemiluminescence analogy, whose breakdown proximate to the 4a-hydroxyflavin, leads to the excitation of this flavin.

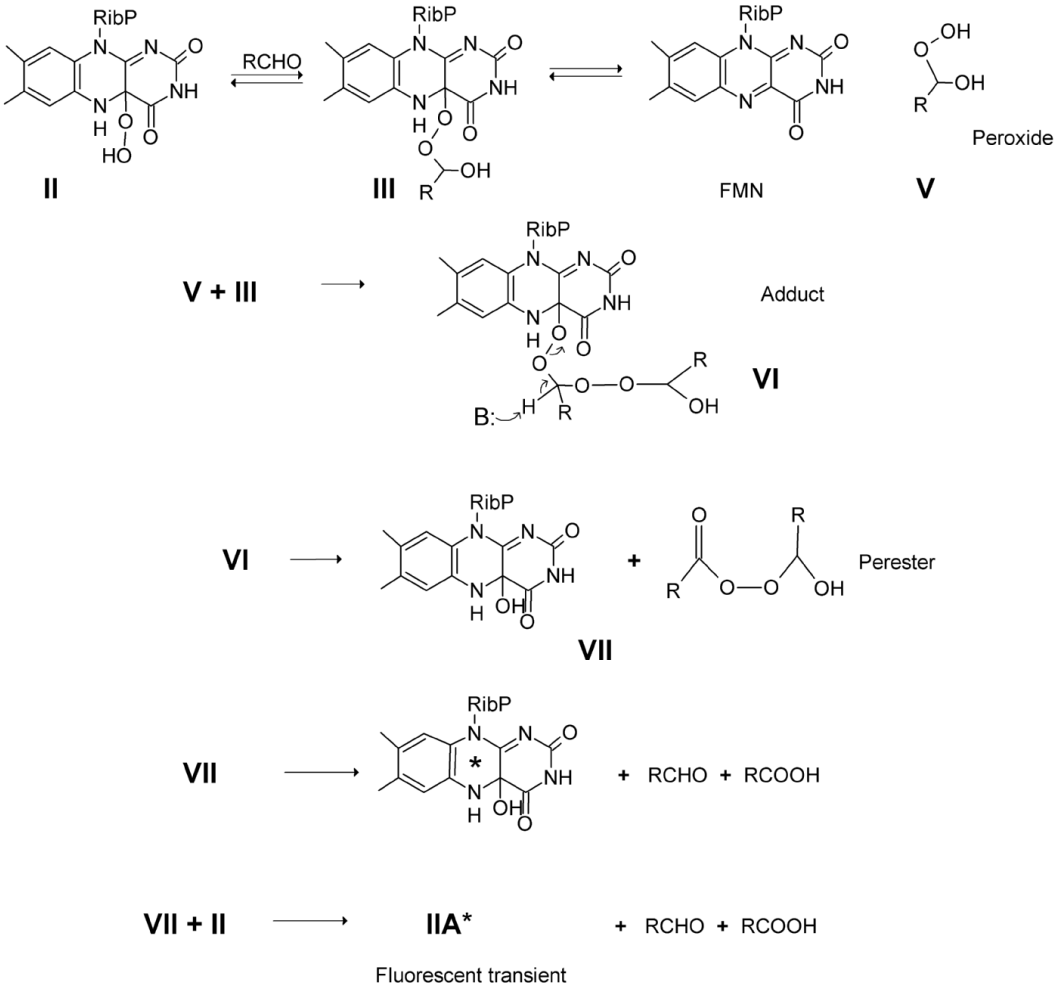

Figure 10.3. A non-linear mechanism of bacterial bioluminescence proposed by McCapra (2000) except with the emitter, the Fluorescent transient (Fig.4.13) identified as the luciferase photoflavin. B is an electron donor within the Lux binding site.

Unfortunately there are no examples of fluororescent 4a,5-dihydroflavins unless with an additional substition at the 5-position and rigidly bound such as in a glassy solvent at 77K. An alternate last line for excitation is added here to the McCapra mechanism in that in a Lux-Lux complex **VII-II**, the breakdown generates the same "luciferase photoflavin" (Fig. 13.6) observed on irradiation of **II** and found to have the same spectral properties as the Fluorescent transient intermediate in the bioluminescence reaction. This highly fluorescent photochemical product is labeled **IIA**. Such an acceptor role would also be provided by association with an antenna protein.

Scattered in the literature there are a number of observations that indeed suggest a complex pathway for the generation of excitation in bacterial bioluminescence. The series of steps observed for the fluorescent transient kinetics requires the pathway to be more complex than a simple A→B→C* model of direct excitation. In 1955, Strehler reported that the addition of crystalline pure hydroperoxydecanal (V) greatly stimulated the bioluminescence emission and in 1987, Watanabe and Hastings reported a similar result on addition of H_2O_2 to the intermediate **II**. Balny and Hastings in 1975 first reported that **II** was only weakly fluorescent but on continued irradiation in the excitation beam of the spectrofluorimeter it increased to $\Phi_F \sim 0.25$ with a slight blue shift to match the bioluminescence. More recently, the properties of this luciferase photoflavin have been extended more rigorously and shown to be same as for the Fluorescent transient. It would appear useful to follow up on these and other tests of the consistency of the McCapra hypothesis.

Published studies up to about the early 1990's have been extensively reviewed and details and back references can be extracted in these publications (Chapter 15). Recently, the use of modern biophysical techniques, NMR, X-ray crystallography, computation, and fluorescence dynamics, have proved to be productive tools for moving the subject in novel directions and elucidating more details of the mechanism of light production. Particularly, the observations of the kinetics of fluorescence and anisotropy decay in the nanosecond time domain for the bioluminescence proteins, have provided new insight, and give support for the idea of an energy transfer process operating in bacterial bioluminescence analogous to those marine bioluminescence systems involving the Green-fluorescent protein (Chapters 6, 12, and 13). The earlier investigations using kinetics and also to a certain extent molecular spectroscopy are indirect, but the recent more direct methods give unambiguous insight. However, it must be realized that the modern methods require milligram quantities of the subject proteins, only recently possible with the technology of cloning and advances in DNA sequencing that make it feasible to obtain an expression system that produces a correctly folded recombinant protein. This technology enables applications such as single point mutation, which is sometimes a critical requirement for growth of protein crystals that provide suitable X-ray diffraction.

11. **Dinoflagellates: "Phosphorescence" in the Sea**

The sparkling lights seen when sea water is disturbed is commonly called "phosphorescence", the name first given apparently by Charles Darwin in his logs from the H.M.S. Beagle voyage. It is not phosphorescence however, but a bioluminescence from marine plankton, mostly the dinoflagellates. The scientific term "phosphorescence" refers to the slow light emission following light absorption and distinct from a fluorescence transition $S_0 \rightarrow S_1$, and isdue to the $T_0 \rightarrow S_1$ transition from an excited molecule. Phosphorescence is familiar because of its many commercial applications, "glowing paint" for example. The "milky sea" phenomenon is a steady glow probably from bioluminescent bacteria, not the same origin as the flashes from the dinoflagellates.

Although the dinoflagellates were identified as the source of this bioluminescence in the 19th Century, there had been little attempt to investigate the biochemistry of this system until the 1960's. Most studies have been from the laboratory of Hastings at Harvard University. The bioluminescence is a standard luciferin-luciferase reaction in the presence of oxygen, and the emiision is a broad blue spectrum with maximum at 474 nm. The spectral distribution is the same as the fluorescence of the dinoflagellate luciferin itself, not its product (Fig. 11.1). Both luciferin and product structures are linear tetrapyrroles, and it is proposed that the absence of product fluorescence might be because it is quenched on release into solution, but not when bound in the luciferase. The mechanism of the bioluminescence is not known but supposed again to go by a peroxidic intermediate. Many of the dinoflagellates are photosynthetic and the similarity to the porphyrin closed ring structure of chlorophyll has been pointed out (Fig. 11.2).

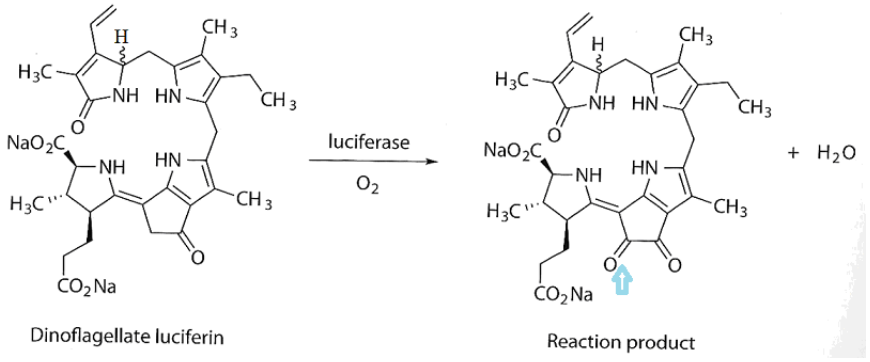

Figure 11.1. Dinoflagellate luciferin bioluminescence. The blue arrow indicates the product's new keto group. Krill luciferin has almost the same structure except with ~~OH.

Both for the *in vivo* system and for the *in vitro* reaction with the purified components that are extracted and stable at pH 8, the bioluminescence is triggered by slight acidification to pH 6. In some dinoflagellates there is a second 75 kDa "luciferin binding protein" identified as being involved in addition to the luciferase, but in others a homologous luciferin binding

sequence is present in the luciferase itself. The most studied luciferase is the one from *Lingulodium polyhedra*, and it is a 137-kDa protein, remarkable in that it consists of three contiguous and homologous domains, all equally catalytic. The one spatial structure determined is that of one of these domains. It consists of lid and barrel domains, the latter suggested to contain the luciferin binding, site although this is not proven (Figs. 11.3., 11.4.).

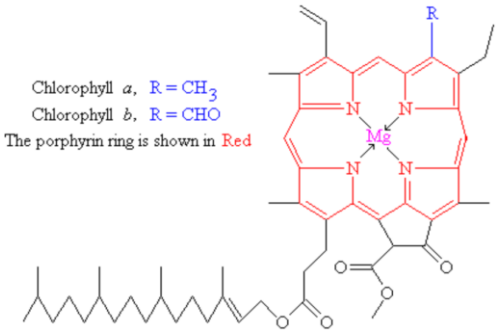

Figure 11.2. Chlorophyll is a pophyrin having a closed tetrapyrolle structure.

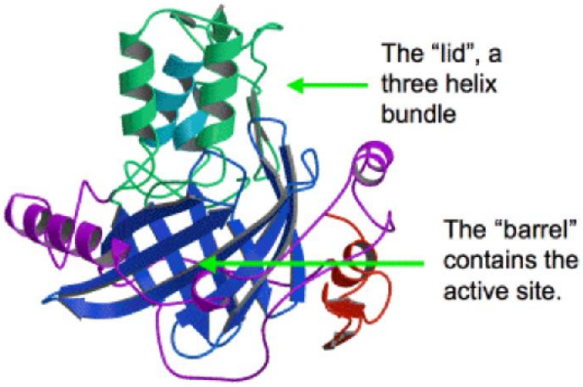

Figure 11.3. Spatial structure of one of the three domains of *P. polyhedra* dinoflagellate luciferase.

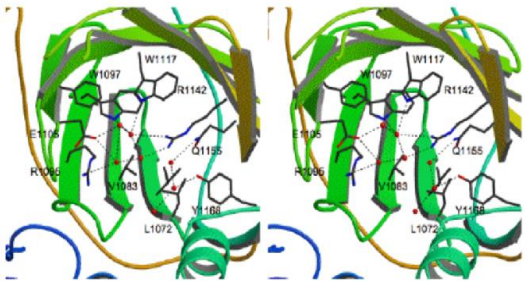

Figure 11.4. Stereoview ("cross-eyed") of the proposed luciferin binding site of dinoflagellate luciferase. The red balls are protein bound water molecules positioned where the luciferin could bind.

The pH control of the bioluminescence reaction lies in the properties of both the luciferase and the luciferin binding protein. Both are purified and stable in a pH 8 buffer, but the binding protein releases the luciferin on acidification to allow it to be available for the luciferase reaction. The activity of the luciferase at pH 6 is proposed from the spatial structure, to be due to the opening of a channel through the three-helix bundle at the top of the structure (Fig. 11.5). There are four histidine residues pointing into the channel, and assuming the usual pK = 6.5 for the histidine side group, at that pH there will be induced a conformation change and an opening of the channel that would provide a passage for the luciferin transport to the active site.

There are two properties of dinoflagellate bioluminescence *in vivo* that are distinct from other bioluminescent organisms. The luciferase and luciferin binding protein are packaged in intracellular organelles called “scintillons”. The scintillons may be separately purified and made to flash by acidification showing in this regard, the same bioluminescence properties as the separately purified system. In the organism the bioluminescence is under regulatory control. In the ocean at the surface, the light emission would have no value in daylight so the organisms exhibit a diurnal (daily) rhythm of bioluminescence, flashing only during the dark hours. If kept in culture under dim illumination, this rhythm persists for many days (Fig. 11.6).

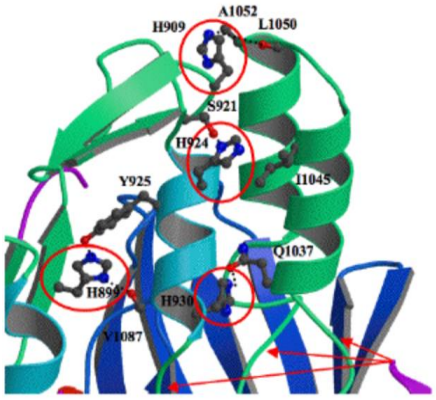

Figure 11.5. Proposed regulatory three-helix bundle showing the side chains of His residues. A conformation change induced by a change of pH to 6, is proposed to open the channel.

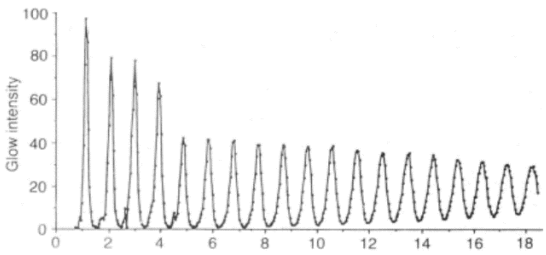

Figure 11.6. In dim light a circadian rhythm of bioluminescence from a culture of dinoflagellates persists for many days.

12. **Structural Biology**

"Light brings us news of the Universe." Sir William Bragg (1862-1942).

In the chemical sciences it has long been recognized that the spatial structure of molecules, the positions of their constituent atoms in space, is one determinant factor leading to chemical reactivity. From early in the 20th Century to realize this knowledge of structure, analysis of the X-ray diffraction from single crystals of the subject molecule has been the method of use. Supplementary to this in the last decades of the Century, has been Nuclear Magnetic Resonance (NMR) Spectroscopy. X-ray diffraction and NMR are still the only methods of determining spatial structure at the molecular level but have seen a great deal of advances in technology, so that they have become at the same time, very powerful but also very specialized. This means that nowadays, it requires collaboration with a specialist for maximum utility in gaining the particular knowledge for understanding the science at hand. Therefore, in this chapter a description of the basics of X-ray and NMR techniques will be briefly covered in order to give the student an understanding of the methodology, and for interpretation of the results relevant to a chemiluminescence mechanism or concerning a luciferase structure, as well as where the results have limitations for gaining the desired insight.

It is certainly the "Holy Grail" of biochemists to have the three-dimensional structure of their favorite protein. Such insight enables a view of the protein as a "machine", moving a small molecule around, changing its surroundings, catalyzing a process, and so on. The task for obtaining the spatial structure of macromolecules however, is not as straight-forward as for small molecules. Although tremendously successful with organic molecules, NMR for spatial structure is limited in size of the study subject, say to below a 30 kDa mass for a protein. We will show here however, that NMR finds great utility in identifying protein-ligand and in Chapter 13, protein-protein, interactions. The limitation of X-ray diffraction for proteins is that it requires growth of a single crystal of the protein with dimensions greater than 0.1 mm, and proteins are generally reluctant to cooperate in this regard. A currently developing technology is the X-ray Free Electron Laser (XFEL), which promises to overcome this limitation.

There is an abundance of web sites covering the physics that underlies NMR spectroscopy. The NMR phenomenon arises from a property of magnetic angular momentum possessed by the nuclei of atoms that have an odd mass number. The ones most commonly used for NMR in the chemical sciences are ^{1}H, ^{13}C, ^{15}N, and ^{31}P. Some NMR experiments relevant to bioluminescence mechanisms, have utilized ^{17}O and ^{19}F. This magnetic moment of a nucleus is a purely quantum property, but a classical analogy is of a spinning spherical body like a top having a surface charge, which is equivalent to a circulating current due to the spin, then from the Faraday law of electromagnetism a perpendicular magnetic moment will be produced. The quantum number is therefore called "spin" and it has only two values, spin up, **I** = +½, and spin down **I** = -½. In the absence of an external magnetic field both spin positions have identical energy. However, on imposition of a strong external static field (Fig. 12.1, B_0) the magnetic moment of the nucleus, say a proton, will prefer to orient parallel to the field having a lower energy, more stable than if oriented anti-parallel.

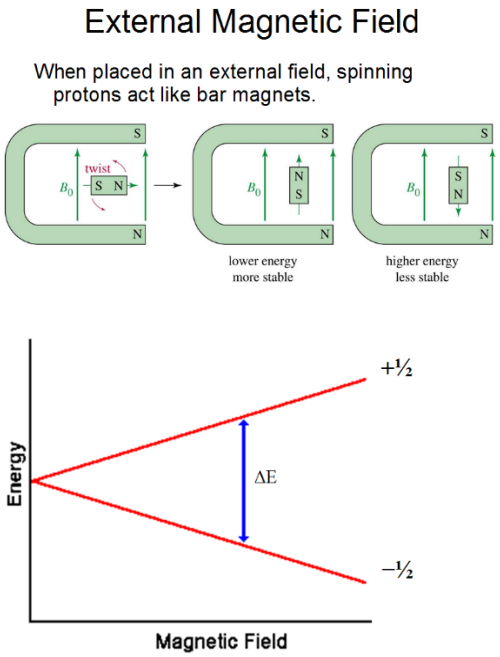

Figure 12.1. Imposition of a magnetic force (*top*) orients a bar magnet to two energy positions. (*Bottom*) In a similar way the proton energy level will be split by ΔE.

The principle of NMR Spectroscopy is simple in contrast to the often obscure methods that have been developed for its data collection. The energy difference between the two spin orientations is dependent on the strength of the external static magnetic field:

$$\Delta E = h\gamma B_0/2\pi = h\nu$$

where h is Planck's constant, B_0 the static magnetic field strength, and γ is the gyromagnetic ratio, which has a different value for each nucleus; for example for the proton

$$\gamma = 267.52 \text{ MHz/T},$$

where T is the static field strength in tesla (10^4 gauss). Since from Planck's Law, $\Delta E = h\nu$, then a photon of frequency ν may be in resonance, hence the term nuclear magnetic resonance, and if absorbed by the proton, will flip the spin pair to a non-equilibrium situation called an "excited" state. Note that this is a "nuclear excited state" not to be confused with an electronic excited state (Chapter 6). If the field is switched off, to attain equilibrium the same photon will be reradiated and can be detected by a radiofrequency receiver. NMR instruments are classified in frequency units, a common one is a "600 MHz NMR", just a standard way of specifying the static magnet strength for the proton flip, i.e.,

$$\nu = 600 \text{ MHz} = 267.52 \times B_0/2\pi$$

$$B_0 = 14 \text{ tesla},$$

and this is a very powerful magnetic field, the reason NMR instruments have to utilize superconducting magnets. Another way of stating this is that for this instrument, the resonance frequency for flipping a "lone" proton is $\nu = 14\gamma/2\pi = 600$ MHz. The NMR experiment entails scanning the sample in a range around this radiofrequency and finding out where absorption, i.e., resonance, occurs. This is like scanning an absorption spectrum for a molecule in solution with varying wavelengths or frequencies in the UV/visible region, except for the presence of the strong magnetic field and the very narrow line widths for the resonances, and a difference of many orders of magnitude in the photon frequencies applied.

Although the description above referred to the proton as "lone", obviously any molecule will contain many protons and the great utility of NMR is that each proton sits in a more or less different magnetic environment arising from the proximate electron density, say under the influence of a CH of an aldehyde, an oxygen of a hydroxyl group, etc. Through an accumulation of empirical observations of the NMR of many molecular structures, a proton resonance may be assigned to a specific part of the molecular structure, and one resonance might be identified as a methyl proton, another as an amide proton. Two factors that shift resonance positions are called "electronic shielding" and "scalar coupling", and these are responsible for the tremendous utility of NMR spectroscopy in chemistry. Fig. 12.2 shows the proton spectrum (^{1}H-NMR) of ethanol measured on a 600 MHz instrument.

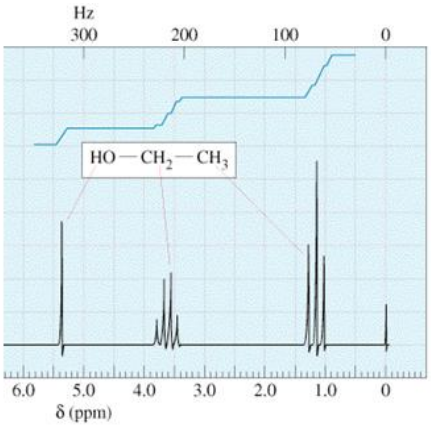

Figure 12.2. Proton NMR of ethanol reveals shifts (δ) in units of parts per million (ppm) characteristic of the electronic environment of each hydrogen.

Each type of proton experiences a different amount of magnetic interaction or "shielding" with the spins of the electron orbitals of the whole molecule compared to that of a "lone" proton, resulting in a minute difference in the magnetic field strength required for resonance or equivalently, a slight difference in the required frequency, ν, for resonance. From both theory and empirical evidence, the assignments of "chemical" shifts belonging to each proton resonance are as indicated in Fig. 12.2. The methyl protons are the most shielded and locate about 60 Hz less than the 600-MHz value of B_0. This is called a "downfield shift" and referring to the units of chemical shift (δ) in parts per million (ppm), methyl protons are generally found in the region around +1 ppm. Notice that "downfield" means a larger

numerical value in ppm units. The zero δ-shift is determined by including a reference compound, tetramethylsilane (TMS) in the sample, whose methyl protons are maximally shielded and therefore arbitrarily assigned a shift of 0.0 ppm. The methylene and hydroxyl protons are seen more downfield from the methyl ones.

Proton-NMR is determined in D_2O not H_2O as the deuterium nucleus has no spin so is not detected, and the concentration of H_2O protons would be many orders of magnitude greater than any protons belonging to the solute molecule. The number of protons at each shift is given by the integral under each indicated by the light blue line in Fig. 12.2. Also, there is seen to be a fine structure in two resonances. This is a through-bond effect called "J-coupling" resulting from the spin influence of a neighboring proton one or two covalent bonds away. Thus, the methyl resonance splits into three and the methylene five due to its five neighbors. The fine structure is easily seen for small molecules as the resonance line-widths are narrow. This fine structure depends on several factors, the field strength B_0, the exchange rate with solvent or other proton sources, and a "relaxation time" for the spin system. This last effect broadens the line-widths in larger molecular systems such as a protein-bound ligand. This is analogous to the influence of rotational diffusion in fluorescence anisotropy decay measurements as described in Chapter 6.

Another property of ^{1}H-NMR that makes it so useful is that almost 100% of the hydrogens have spin quantum numbers, or more correctly, the natural abundance of the even mass number and non-magnetic deuterium (^{2}H), is less than 0.02%. The same is the case for ^{19}F and ^{31}P but for ^{13}C and ^{15}N the spin natural abundance of these same nuclides is about 1% and 0.4% respectively. Also, the sensitivity for detecting resonances of ^{13}C and ^{15}N is low so that it is necessary for these experiments, to synthesize the subject molecule enriched with the isotope to be observed. The diagnosis of these ^{13}C-NMR spectra are along the same lines as for ^{1}H-NMR with the difference that the gyromagnetic ratios result in much larger values for the chemical shift, (δ).

NMR spectroscopy is extensively used for the elucidation of protein-ligand interactions. Information about the electronic perturbation of for example, FMN as a ligand on its binding to a flavoenzyme and the conformation changes in the protein, and changes in interactions that accompany its biochemistry, can be recovered in such studies. As a first example, here in Fig. 12.3 is shown the NMR spectra of flavodoxin, a redox protein with FMN as a ligand. To observe the ^{13}C-NMR of the FMN, it needs to be synthetically enriched with the isotope ^{13}C, otherwise its NMR spectrum would be swamped by the about 25 natural abundance ^{13}C-carbons of the 148 amino acid residues. The noisy baseline shown in the spectrum (Fig. 12.3) is due to this natural abundance protein contribution.

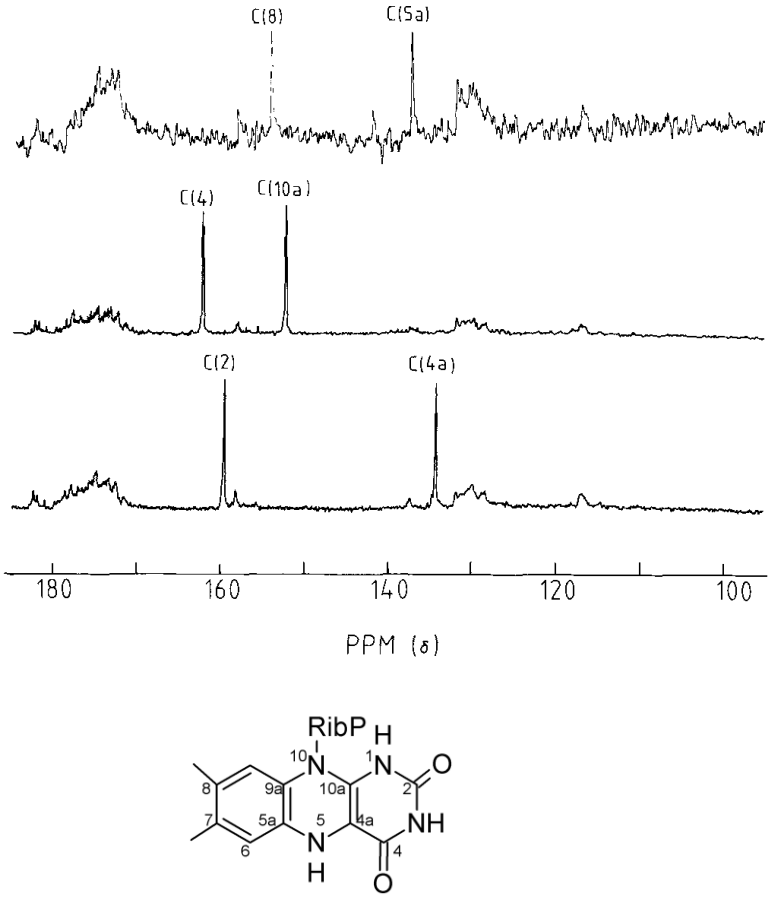

Figure 12.3. ^{13}C-NMR spectrum of apoflavodoxin reconstituted with different ^{13}C-enriched FMNs. RibP = ribityl-phosphate.

Compared to free FMN, in the bound state most resonances are downshifted, particularly the ones on the benzyl ring, free-bound, C(8) 151.7-154.0 ppm. C(2) and C(4) are hardly affected on binding and this is interpreted as the FMN in the bound state being as highly polarized as when free in aqueous solution, due to the hydrogen bonding of C(2) and C(4) with amino acid residues in the binding cavity being not so different from their bonding with H_2O in solution. It might be discerned also, that the resonances are broader than for the ^{1}H-NMR spectrum in Fig. 12.2, due to the slower rotational averaging of a ligand rigidly associated with the protein mass.

Next, in Fig. 12.4 is the ^{15}N-NMR for the fully ^{15}N-enriched lumazine derivative, free (A) and bound (B) to the lumazine apoprotein. The interpretation here is based on the observations of model compounds, that hydrogen bonding at these nitrogens N(1) and N(5), yields stronger upfield shifts than bonding to N(8) and N(3). Bound to the protein, the N(5)-shift is markedly upfield from the free solution value, attributed to a strong hydrogen bond, the hydrogen bond donor being one of the amino acid residues comprising the binding cavity. The N(3) has only a minor downfield shift, leading to the interpretation that the lumazine is much more polarized within the cavity than free in solution. The downfield shift of N(3) indicates a hydrogen bond donor property to an acceptor group in the binding cavity. Altogether, the lumazine protein binding cavity appears to be more polar than water. Note

again, that the bound state resonances are much broader than when free. These conclusions will be shown to be borne out in the X-ray spatial structure more recently determined for lumazine protein in the crystal state (Fig. 12.33).

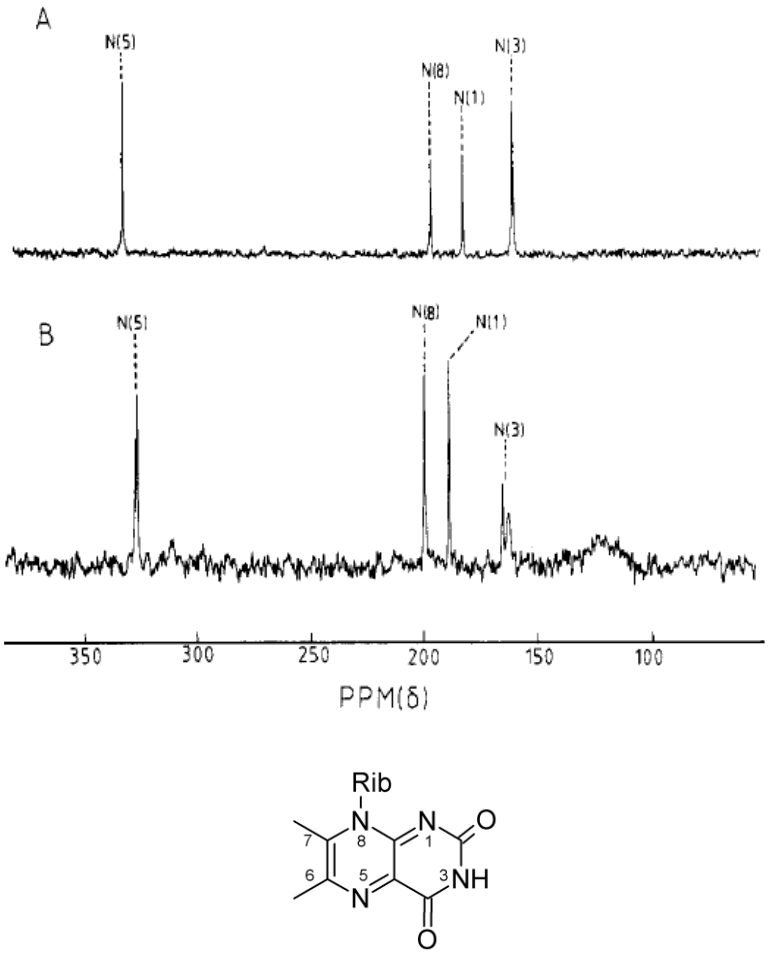

Figure 12.4. ^{15}N-NMR spectra of fully enriched [1,3,5,8-^{15}N]-6,7-dimethyl-8-ribityllumazine. (**A**) Free in buffer solution; (**B**) bound in lumazine protein. Rib = ribityl.

A ^{13}C-NMR study in 1985, identified the 2-peroxy-substituted coelenterazine (Fig. 12.5, right structure) as the substrate bound within the photoprotein aequorin. This was absolutely confirmed in the crystal structure determined a few years later in 2000. Apoaequorin was "charged" with synthetic coelenterazines enriched at the C(2)- or C(9)-positions, or alternatively at both the C(2) and C(9). The NMR result confirmed the proposal made many years earlier that oxygen addition formed the active ligand with a 2-oxy substitution. The ^{13}C-NMR spectrum (Fig. 12.5, *d*) is for the C(2)- C(9)-enriched coelenterazine in free solution. On the peroxidation within the aequorin binding cavity, the C(2)-carbon bonding would change from sp^2 to sp^3 and consequently, there is an upfield shift from the 129 or 130 ppm resonances, to 98 ppm. This assignment is verified in spectrum (*b*). Model studies assign the C(9)-resonance as the one shifted downfield to 148 ppm.

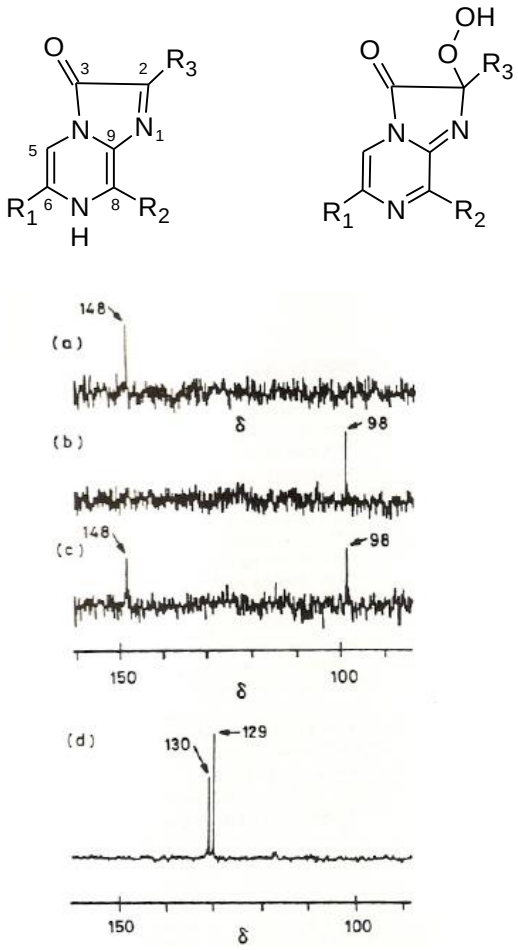

Figure 12.5. (*Top*) Coelenterazine and the proposed 2-hydroperoxy substituent. (*Lower*) ^{13}C-NMR (*d*) 2,9-^{13}C-enriched coelenterazine in free solution; (*a*) 9-^{13}C-coelenterazine; (*b*) 2-^{13}C-coelenterazine; (*c*) both, 2,9-^{13}C-coelenterazine.

A similar NMR study made contemporaneously elucidated the binding state of FMN and $FMNH_2$ on bacterial luciferase and in its bioluminescence intermediates. The results were that the initial bioluminescence intermediate (**II** in Chapter 4) was the bound 4a-peroxyFMNH as earlier proposed, and that on the luciferase before oxygen addition, there was a single binding site for FMN but two sites for $FMNH_2$, explaining the interpretation of a two-flavin stoichiometry from the earlier quantum yield study described in Chapter 5.

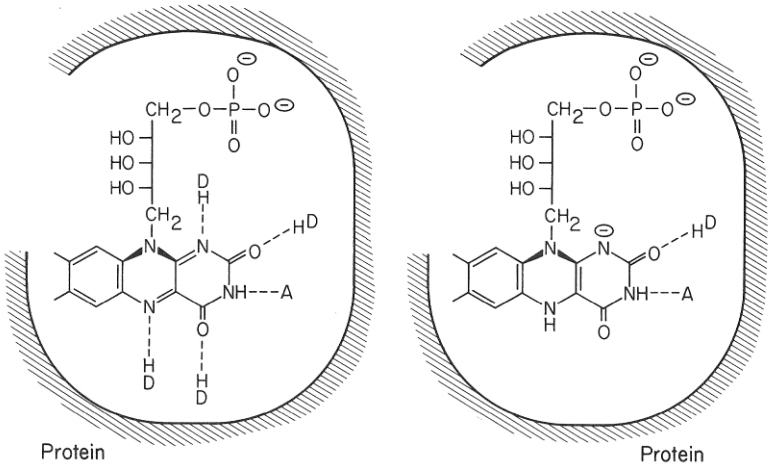

Figure 12.6. H-bond interactions of FMN and $FMNH^-$ in the binding site of bacterial luciferase derived from NMR experiments. The $FMNH_2$ is the anion in the bound state. D = hydrogen bond donor; A = acceptor; R = ribityl phosphate.

This second binding site for $FMNH^-$ must be a result of the conformational change of the luciferase earlier detected by the circular dichroism of $FMNH_2$ in the presence of luciferase (Fig. 6.16). An additional finding from the NMR is that it is bound as the N(1)-anion. Compared to the free state in aqueous solution, the FMN within the luciferase binding site has stronger hydrogen bonds to N(1) and N(5), but weaker ones to N(3) and the two carbonyl oxygens, as shown in Fig. 12.6. These conclusions are consistent with the spatial structure of FMN in the binding cavity obtained by X-ray crystallography more recently (Fig. 12.30).

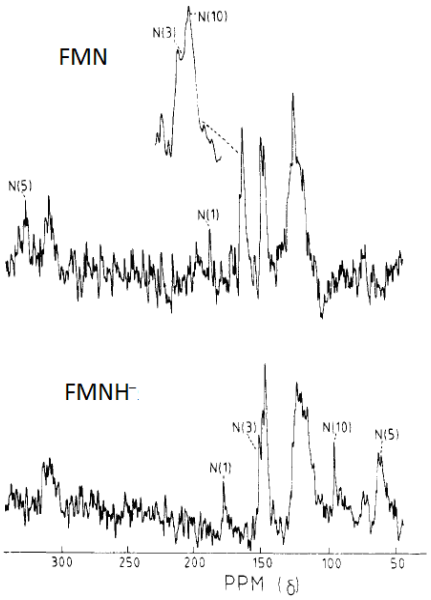

Figure 12.7. ^{15}N-NMR spectra of 1,3,5,10-^{15}N-enriched FMN and $FMNH^-$ bound within bacterial luciferase.

The ^{15}N-NMR spectrum of luciferase-bound FMN and FMNH$^-$ clearly shows the assigned resonances from the ^{15}N-enriched ligand lying on top of the signals from the natural abundance ^{15}N of the protein (Fig. 12.7). In the FMN spectrum, the broad width and weak intensity of the N(3) line, argues that its N(3) proton is exchanging slowly with the aqueous solvent, and that this part of the molecule is buried and not accessible to bulk water. In the protein, the N(5) and N(1) resonances are found about 10 ppm upfield from free solution, interpreted again as in the case of lumazine protein, of hydrogen bonding at these positions. The N(3) shift being downfield also suggests hydrogen bonding to the protein. In contrast, the bound FMNH$^-$ shifts are not much changed from FMNH$^-$ in free solution. As the FMNH$^-$ is clearly bound, it means that the protein interactions are not much different from the free state, except for the rigidity of binding.

In the ^{13}C-NMR spectra, it is more difficult to accurately separate those signals from the FMN carbons from the natural abundance carbon-13 of the protein. The technique adopted here is to take difference spectra, and as a first example it is seen that the C(6) resonance is clearly broad in both flavin oxidation states, whereas the methyl group at the 8-position having a narrow resonance, must be in a flexible condition, which would mean that the benzyl part of the flavin must be pointing towards the bulk water with the methyl group freely “waving” around (Fig. 12.8).

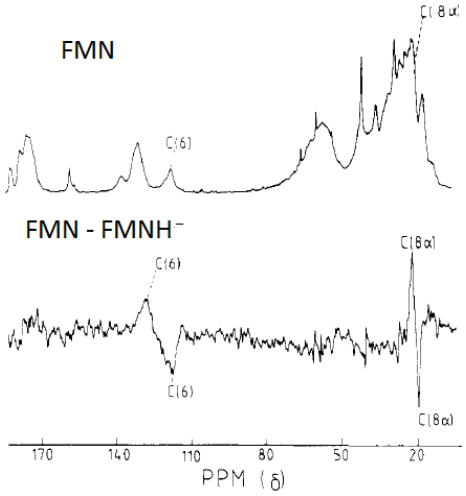

Figure 12.8. **^{13}**C-NMR spectra of 6,8a-^{13}C-enriched FMN and the FMNH$^-$ and their difference, bound within bacterial luciferase.

An unexpected finding was that the C(4a) resonance from the bound FMNH$^-$ was split, a doublet reflecting two FMNH$^-$s in different binding site environments. Both resonances 103.5 and 101.4 ppm in A (Fig. 12.9) are broad indicating rigidity of binding to the protein, but the 101.4 ppm shift is the same as for free FMNH$^-$ and it is more weakly bound as it is no longer seen after gel filtration, spectrum B. This is suggestive of a non-specific second binding site, perhaps in a hydrophobic surface patch. In spectrum C, which is the difference spectrum A-B, only the 103.5 ppm resonance remains, and is therefore specifically assigned

as belonging to the flavin in the bioluminescence catalytic site. The function of this non-specifically bound $FMNH^-$ is still not known. This second binding site is not seen for FMN so it must develop after the protein conformation change that accompanies the $FMNH_2$ binding.

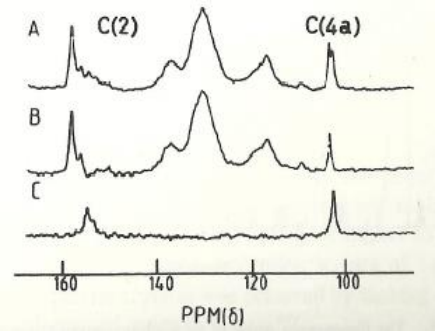

Figure 12.9. ^{13}C-NMR spectrum of 2,4a-^{13}C-enriched $FMNH_2$ bound in bacterial luciferase following oxygen addition at 0ºC. There is a splitting of the C-4a resonance and both lines decay slowly concomitant with bioluminescence potential (A-C).

The next Fig. 12.10 shows the spectrum following the oxygen addition to the luciferase-$FMNH^-$ complex and chromatographic separation of the luciferase-peroxyflavin (intermediate **II**, Lux:FMNHOOH). The most affected resonance is of the C(4a), shifted upfield to 82.5 ppm. Other resonances are only slightly affected, C(2), C(4), and C(10a), and all including C(4a), are close to that of a model compound having a C(4a) substitution. The 82.5-ppm resonance decays over a few hours corresponding to the loss of bioluminescence activity with aldehyde.

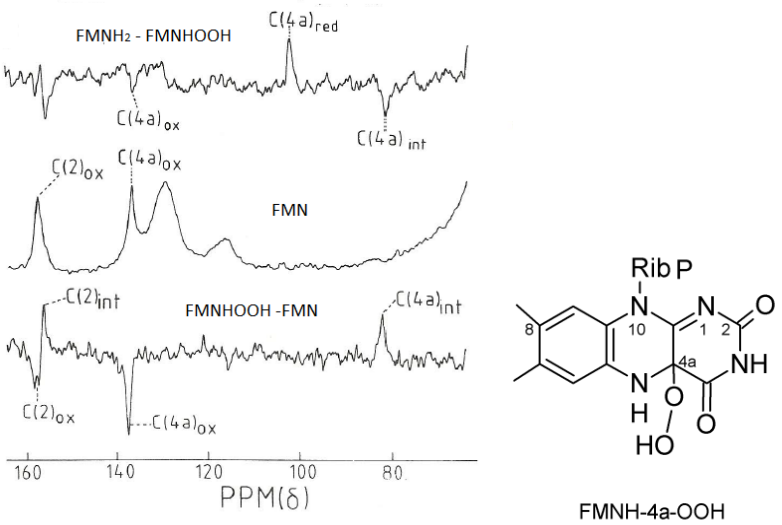

Figure 12.10. (*Top*) ^{13}C-NMR difference spectra between 2,4a-^{13}C-enriched and luciferase bound, $FMNH_2$ and FMNH-4a-OOH. (*Middle)* 2,4a-^{13}C-enriched FMN bound to luciferase. (*Bottom*) Difference between ^{13}C-NMR of luciferase bound FMN and FMNHOOH.

From the successful application of NMR to small molecule structure, the challenge to the NMR community naturally arose as to interpreting the total protein NMR spectra of macromolecules. This required new approaches, and from around 1980 to the present about 15% of protein structures in the Protein Data bank (PDB) have been determined by NMR. The photoprotein aequorin consists of 189 amino acid residues and its approximately 1000 protons would produce an impossibly crowded one-dimensional ^{1}H-NMR spectrum (Fig. 12.11). The same can be said for the about 200 ^{15}N's and the many more ^{13}C's. One solution among many to alleviate the crowding problem and the simplest approach is to spread the resonances out into two dimensions. The technical details of such multi-dimensional NMR experiments are beyond the scope of this chapter but a brief description of 2D-NMR may be adequate in this instance, just to appreciate the useful knowledge that can be recovered.

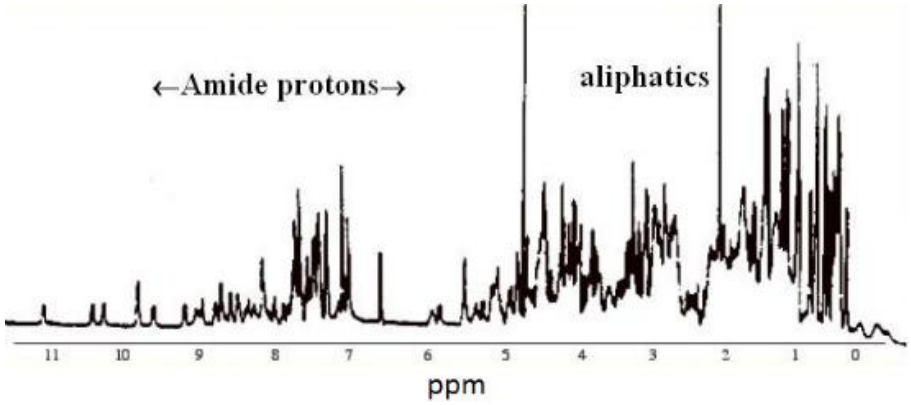

Figure 12.11. ^{1}H-NMR spectrum of a small protein is extremely crowded.

A favorite NMR experiment is “Heteronuclear Single Quantum Correlation” (HSQC). This first requires producing the recombinant protein fully enriched with ^{15}N, which is inexpensive compared to enrichment with ^{13}C that is required for many multi-dimensional NMR-experiments. ^{15}N-HSQC involves magnetization transfer between the heteronuclei ^{15}N and ^{1}H following the excitation pulse of appropriate duration, and adjustment of the time distribution of collection of the resonance signals. The result is a plot in two dimensions having the ^{15}N-shifts on one axis and proton shifts on the other. Each resonance indicated by the filled dots corresponds to one peptide bond N with its associated H.

The Fig. 12.12 is the ^{15}N-HSQC spectrum of aequorin, and one can count the about 188 spots corresponding to the number of amide protons in its 189-residue primary sequence. The resonances are quite spread out indicating an intact spatial structure, in contrast to a denatured state where they all become crowded together around 8.5/115 ppm. Some crowding also can be discerned here that might be interpreted as random coil content. Assignment to particular residues is labeled, and this had to involve more complex experiments and is not obtainable from ^{15}N-HSQC alone. The purpose of this study here was to determine the binding sites for Mg^{++}, which is an inhibitor of the Ca^{2+}-triggered

bioluminescence from aequorin. The conclusion was from the shifts (blue lines) of certain HSQC resonances that had been assigned to specific residues, that Mg^{2+} was bound into the loops of EF-hands I and III and not into all three loops known to be specific for the Ca^{2+} binding identified from the crystal structure (Figs. 12.15, 12.17). Also the strength of this Mg^{2+} binding was stronger to a third site loop in EF-hand III (Fig. 8.13), than to the loop in EF-hand I.

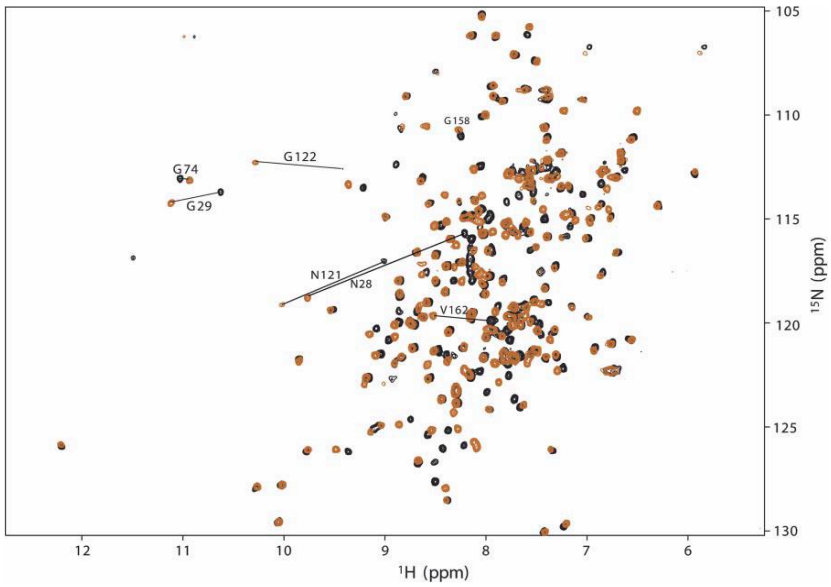

Figure 12.12. ^{15}N-HSQC spectrum of aequorin in buffer (brown dots) and in the presence of 10 mM Mg^{2+} (black). The blue line indicates a shift occurring on Mg^{2+} binding.

The PDB now contains 115000 protein structures the majority of which have been determined by X-ray diffraction. The major limitation for determining protein structure by this method is the necessity of having a single crystal, meaning that all the macromolecules are uniformly lined up in a repeating pattern that is necessary for generating a clear diffraction pattern. The observation and explanation of the diffraction of light goes back to the 19th Century. For visible light an interference pattern arises if separation of uniform scattering points is in the order of magnitude of the wavelength of the light. Diffraction at the atomic separation therefore requires X-rays that have wavelengths in the Å-range. A diffraction pattern is produced and is analyzed according to Bragg's Law, to reconstruct the separations d of the scattering points in Fig. 12.13.

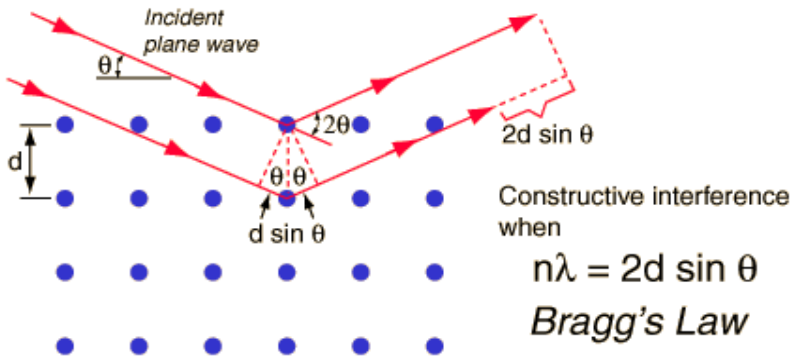

Figure 12.13. Scattering of radiation from repetitive points generates a diffraction pattern from which the separation d, can be recovered from Bragg's Law.

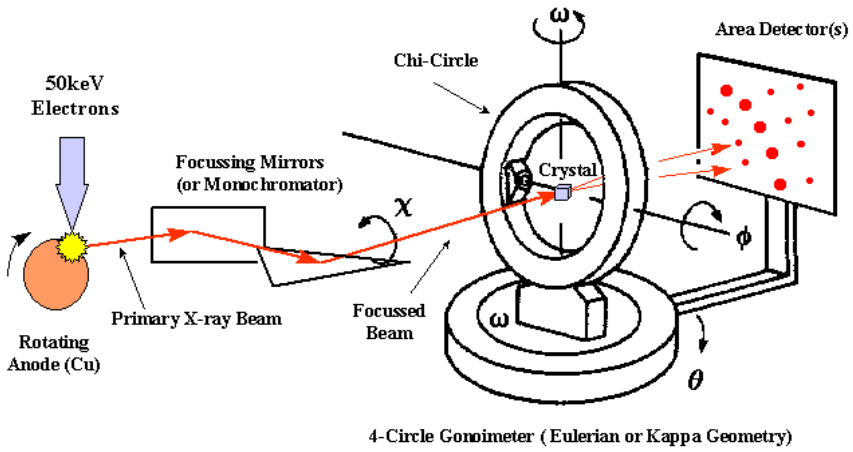

Figure 12.14. A protein single crystal held so as to be impinged by the X-ray is rotated at fixed angles to generate a family of diffraction patterns which can be analyzed to recover the positions of the scattering atoms.

The atoms of the protein must be within a single crystal of dimensions larger than the diameter of the X-ray beam. The crystal is kept at liquid nitrogen temperature and rotated, both conditions to prevent damage from the intense X-ray beam. Again, the technical details are not within the scope here and what concerns us is what the finally determined spatial structure reveals about a bioluminescence mechanism. At this present time, the available structures of relevance to our field are: the Ca^{++}-regulated photoproteins in various states, aequorin, obelin, clytin, and berovin; lumazine proteins; Renilla luciferases; Renilla coelenterazine binding protein; dinoflagellate luciferase subunit; bacterial luciferase and subunits; firefly luciferases; and many green-fluorescent proteins. The most detailed insight concerning mechanism has been obtained from the photoprotein structures, so these will be discussed first and in most detail.

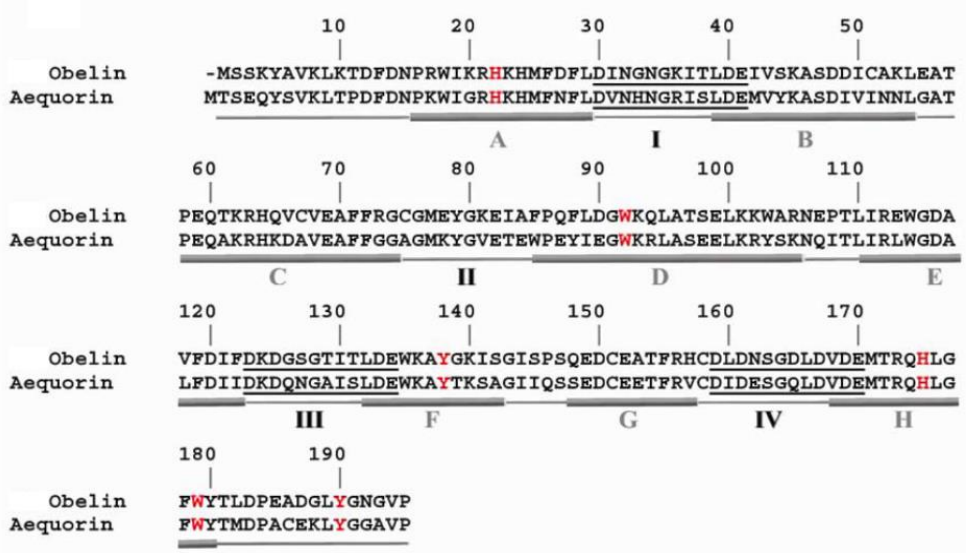

Figure 12.15. Alignment of primary sequences shows identity or similarity of many amino acid residues. The single letter abbreviation for the amino acids is used for conciseness.

It is a central doctrine in biochemistry that the primary structure, the sequence of the amino acid residues in a protein, determines its spatial structure and this is well borne out for the family of Ca^{2+}-regulated photoproteins. The opposite does not hold however. For example, the "bacterial luciferase structural family" includes a number of flavoproteins having homologous spatial configurations but most have quite unrelated sequence and function. If the amino acid sequences of aequorin and obelin are lined up as to make as many matches as possible, it is seen that many positions correspond (Fig. 12.15). These two photoproteins are regarded as having homologous primary sequences. All in the Ca^{2+}-regulated photoprotein class have a 75-95% identity in their primary sequence and it is expected that they all should have homologous spatial structure, so far found to be true.

The high resolution (~ 2Å) structures of aequorin and obelin determined by X-ray crystallography, were first reported in 2000. As just discussed, from the homology of their primary sequences, they are also predicted to be homologous in their three-dimensional structures as is evident in Fig. 12.16. The same spatial structural homology is found for the other photoproteins in this family. Also as predicted from primary sequence, the spatial structure of the photoproteins exhibits four "EF-hands", helix-loop-helix arrangements, indicated in the Figs. 12.15 and 12.17 by the Roman numerals. The parts of the primary sequence underlined by the grey cylinders in Fig. 12.15, are known from studies of the

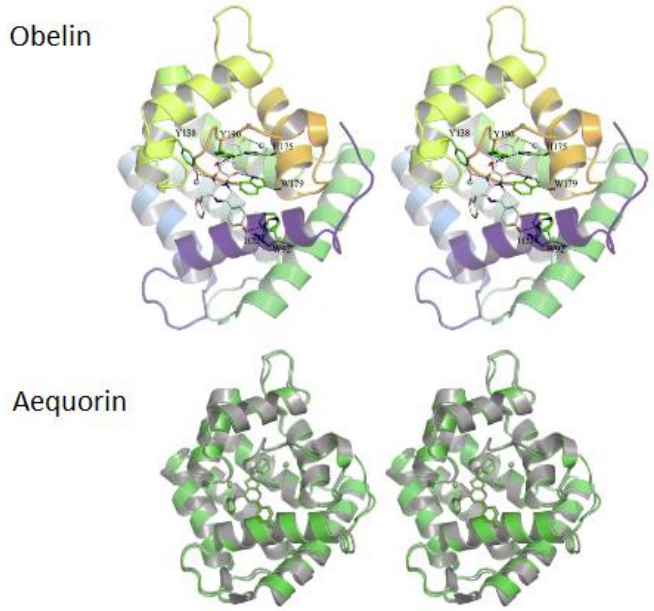

Figure 12.16. Stereoview ("cross-eyed") of the spatial structures shows structural homology.

structures many proteins, to spontaneously fold into a helix and each helix here, for example *A* in Fig. 12.15, is followed by a chain of residues, then another helix, *B* in this case, making what is called an "EF-hand", in Fig. 12.17 labeled **I**. These helices are drawn as spirals in pictorial representations of protein structures. EF-hands are a characteristic of the many members of the "superfamily" of Ca^{2+}-binding proteins, a great number of which are well characterized both in function and spatial structure. However, only the photoprotein sub-family possesses the bioluminescence function by virtue of its having the 2-hydroperoxy-coelenterazine buried and stabilized in a hydrophobic cavity, as pictured as the blue stick structure in Fig. 12.17**A**, and where it is primed for oxidative decarboxylation to generate the products CO_2 and coelenteramide in its S_1 state. Also well established for the superfamily, is that the Ca^{2+} binds into the loop part of the EF-hand, that loop sequence of 12 residues being quite specific for this binding, therefore called the "canonical sequence" for Ca^{2+} binding. This canonical sequence is only found here in EF-hands **I**, **III**, and **IV**, counting from the N-terminal marked **N** in the Fig. 12.17. Consequently, only three Ca^{2+}s can bind and from observations of bioluminescence kinetics, a minimum of two bound Ca^{2+}s appears to be necessary to trigger the reaction.

A Fourier analysis of the X-ray diffraction pattern of a molecule or macromolecule, recovers the electron density surrounding each atom scattering point, and into the total density pattern the molecular structure is fitted. In Fig. 12.17**B** part of the structure is amplified and selected to highlight the coelenterazine placed within the protein binding cavity surrounded by the interacting residues (green). A residue-ligand interaction is regarded as real if there is atom center to center separation less than 4 Å. Hydrogen bonds (brown dashes) are inferred

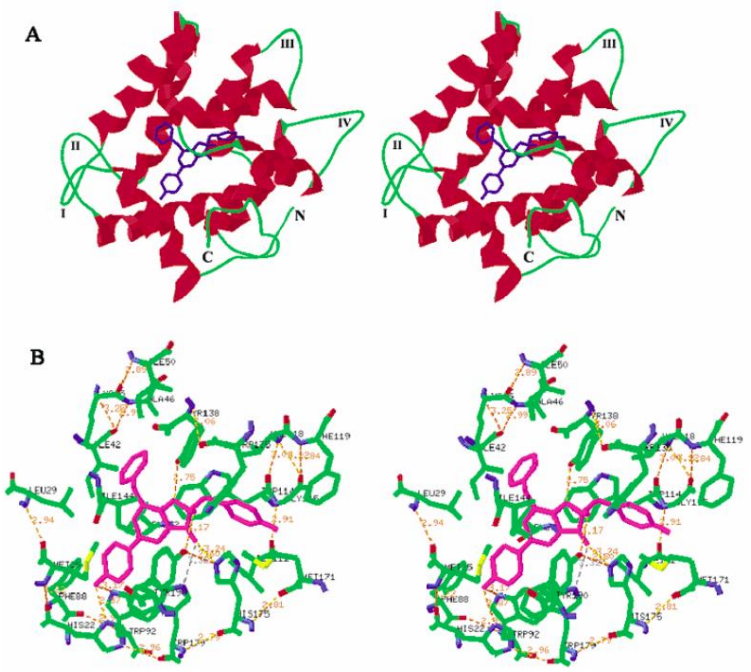

Figure 12.17. Stereoview of the obelin structure showing (**A**) the E-F hands (**I - IV**) and the coelenterazine (*blue*) in the binding cavity and (**B**) an amplified drawing to highlight the binding cavity and H-bonds (*yellow*).

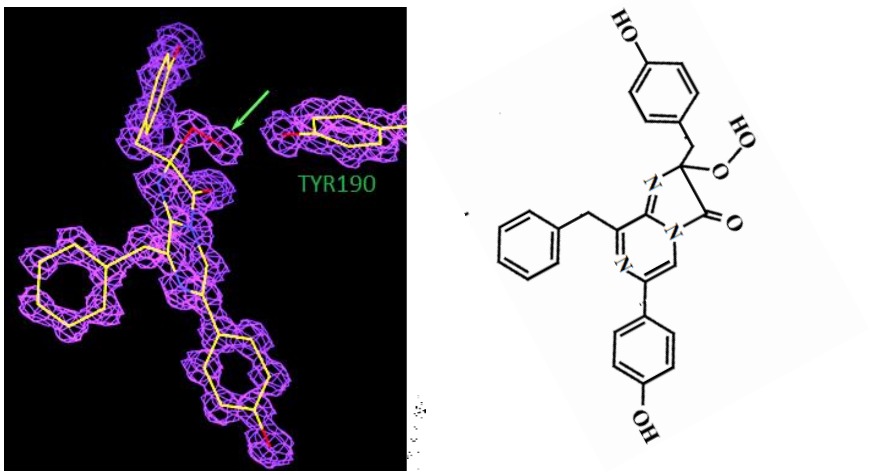

Figure 12.18. Electron density is recovered from the X-ray diffraction pattern. At extremely high "atomic" resolution (1 Å) the structure of the bound coelenterazine is revealed but with two additional densities (green arrow) interpreted as the 2-substituted peroxy (red sticks) group. There is an H-bond also to the Tyrosine residue hydroxyl oxygen (red stick).

and assigned if the purported donor and acceptor atoms are within 3.5 Å. The separation for covalent bonds is about 1.5 Å. Next, a very high resolution picture (Fig. 12.18) shows how the chemical bond structure of coelenterazine is fitted into the electron density in the photoprotein cavity region. Two important results are visualized here. The first is that there is extra electron density at the 2-position indicated by the green arrow, and on assigning this as

two oxygen atoms, it constitutes direct evidence that the ligand is the 2-hydroperoxy-coelenterazine, as proposed almost 30 years ago. The second result is that there is a Tyrosine residue, Tyr190 (Y190 in the sequence, Fig. 12.15), with its hydroxyl oxygen at hydrogen bonding distance from the second peroxy oxygen. As the hydroperoxycoelenterazine is very unstable in free solution, it is concluded that it is stabilized within the protein by this Tyrosine hydrogen bond.

It is helpful for visualization of these chemical interactions, to make a two-dimensional picture to show the atomic positions within the binding cavity. This picture is the basis of a "proton relay hypothesis" by which the binding of Ca^{2+} triggers the light reaction via the formation of the dioxetanone intermediate. In Fig. 12.19, the Y190 Tyrosine's hydroxyl oxygen is at hydrogen bond distance (dashed line) to both a Histidine side group, H175, as well as to the peroxy oxygen. The dashed lines are measured between the nitrogen and oxygen atoms as the hydrogen atoms do not show in X-ray patterns at this resolution. Donation of this hydroxyl proton to H175 as acceptor (step **1**) will then be compensated by a shift of the hydroperoxy proton onto the Y190 anion acceptor, and the coelenterazine peroxyanion will then undergo nucleophilic addition (step **2**) onto C(3) of the coelenterazine.

In the structure of the bioluminescence product, (Fig. 12.21, *right*), a water molecule (W2) possibly the one originally bonded to Y138 and H64 of obelin (Fig. 12.21, *left*), is seen to be relocated proximate to the N(2) anion of coelenteramide, and the tyrosine (Y138) is displaced towards the protein surface. Donation of a proton from this water (step **3**) would form the neutral dioxetane in the equilibrium **3A**. A mechanistic function for this water molecule has been indicated from the structures of the Y138F mutant. No bound water W2 is present before reaction but it appears again proximate to the N(2) anion in the product structure. According to the chemiluminescence model in Fig. 8.4, the oxidative decarboxylation occurs both from the neutral species and from the N(2) anion to produce respectively the neutral excited coelenteramide, the origin of the bioluminescence band with maximum around 400 nm, or the excited anion, the origin of the blue bioluminescence with maximum 470−495 nm, the value depending on the type of photoprotein. The reason for these spectral differences among the types is also now understood from the protein structure.

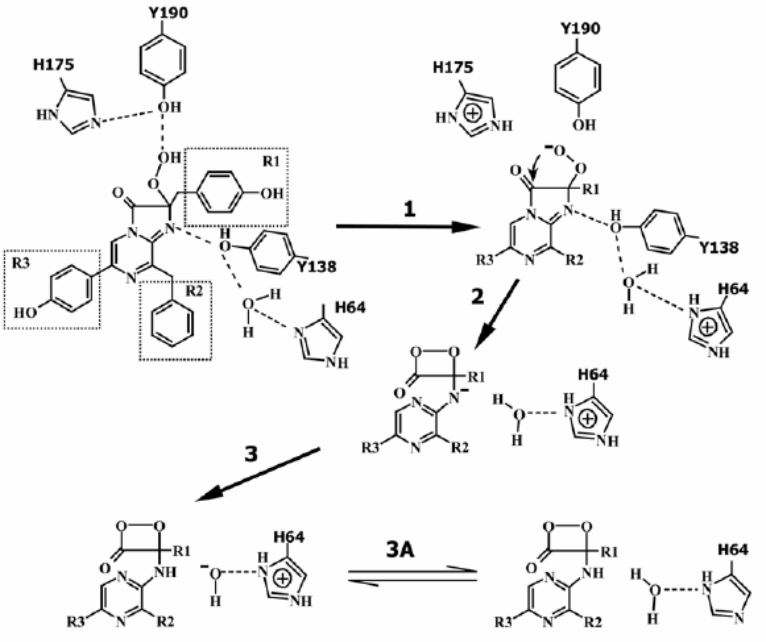

Figure 12.19. Two-dimensional representation shows the obelin cavity residues within about 4 Å of the ligand. The dashed lines are the inferred H-bonds.

The structure of Ca^{2+}-discharged obelin shows three calcium atoms coordinated in the binding loops and the product coelenteramide bound at the active site (Fig. 12.20, *left*). Amplification of the binding site region shows the shifts of residues including the water molecule already described in the two-dimensional sketch (Fig. 12.20, *right*). The green colors the loop-helix structure of EF-hand **IV** with its bound calcium, and is overlaid on the grey color of the structure prior to the Ca^{2+}addition. To accommodate the calcium in EF-hand proteins, the loop residues have to move so that the calcium is coordinated at a characteristic 2.4 Å distance, and it is evident here that this movement should also shift the Histidine H175 position, and thus could be the trigger of the postulated proton relay mechanism to generate bioluminescence.

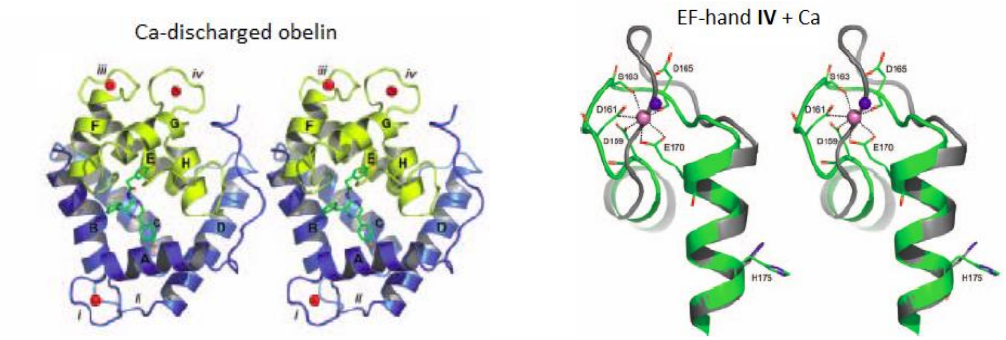

Figure 12.20. (*Left*) Stereoview of the spatial structure of obelin after Ca^{2+} addition and bioluminescence reaction showing the three bound Ca^{2+}s (*red balls*). (*Right*) magnified view of EF-hand **IV** shows the one Ca^{2+} (purple ball) in a characteristic bipyrimidal co-ordination.

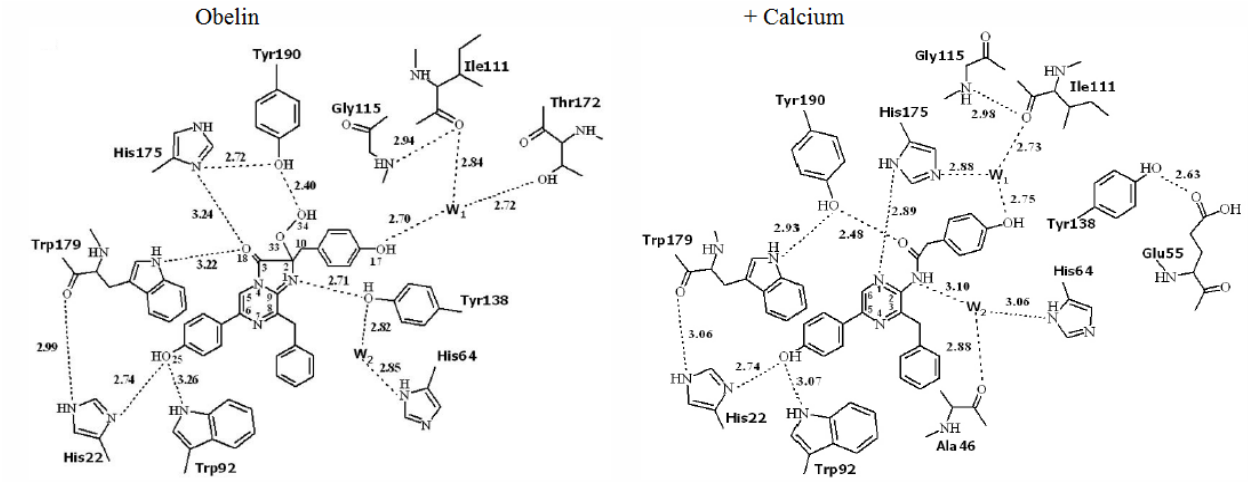

Figure 12.21. Two-dimensional picture shows the H-bond interactions (dots) around the 6'-(*p*-hydroxyphenyl) substituent of the peroxycoelenterazine in obelin and the coelenteramide after the bioluminescence triggered by addition of calcium.

The bioluminescence of aequorin and its product fluorescence have practically the same spectral distribution with a maximum at 465−469 nm. In contrast, the OL-obelin bioluminescence maximum is around 485 nm, but the product fluorescence is at a 25 nm longer wavelength and other photoproteins exhibit similar shifts. It was considered that the reason for these differences might be discovered by determining the spatial structure of the binding site and interactions therein. The two-dimensional picture (Fig. 12.21) shows that both before and after the addition of Ca^{2+} to obelin, the oxygen atom of the 6-(*p*-hydroxyphenyl) substituent of the pyrazine ring, subtends two hydrogen bonds, one to Histidine (His22) and the other to the imidazole N of a Tryptophan (Trp92). The structure of Ca^{2+}-discharged aequorin is not available, but aequorin before reaction (not shown here) has three hydrogen bonds to this equivalent oxygen from its Histidine (H16) corresponding in the sequence to obelin's His22, and to both Tryptophan 86 and Tyrosine 82. This Tyrosine 82 is equivalent to the position in obelin occupied by Phenylalanine 88. On the basis of this structural information, the approach of "Rational Mutation" was employed to see if shifting hydrogen bonds might alter these spectral properties. This approach has a great advantage in economy over making random mutations. In other words, the question posed was, what might happen if the Phenylalanine (F88) in obelin is substituted by a Tyrosine (Y), and Tyrosine (Y82) in aequorin by Phenylalanine (F)? Eureka, the natural (wild-type) aequorin bioluminescence maximum 469 nm, is shifted to longer wavelength, 500 nm on Y82F mutation, and the WT obelin 480 nm to shorter wavelength 453 nm, after the F88Y substitution (Fig. 12.22).

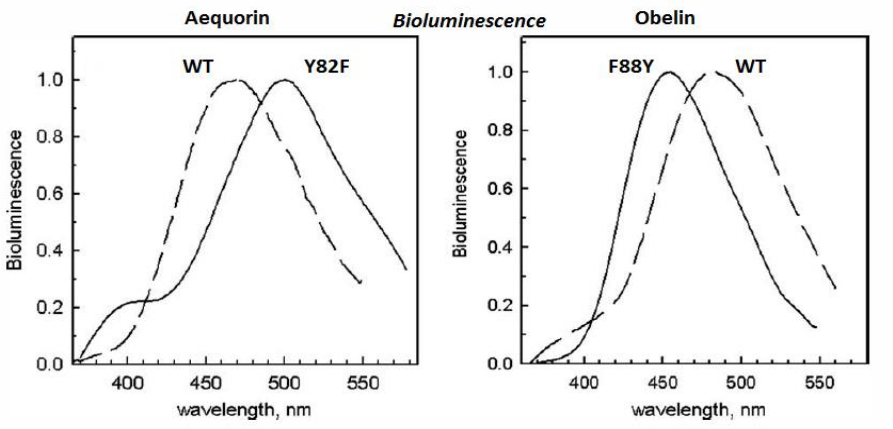

Figure 12.22. Rational mutation of aequorin shifts its bioluminescence maximum to a longer wavelength and the obelin to shorter wavelength. WT = wild-type (natural).

A similar direction of spectral shift is observed for the fluorescence of the bound coelenteramide in the Ca^{2+}-discharged protein mutants. For the WT aequorin product the fluorescence maximum is almost the same as the bioluminescence, 469 nm, but in the Y82F mutant it is at much longer wavelength 500 nm, with a prominent shorter wavelength band now present around 400 nm (Fig. 12.23).

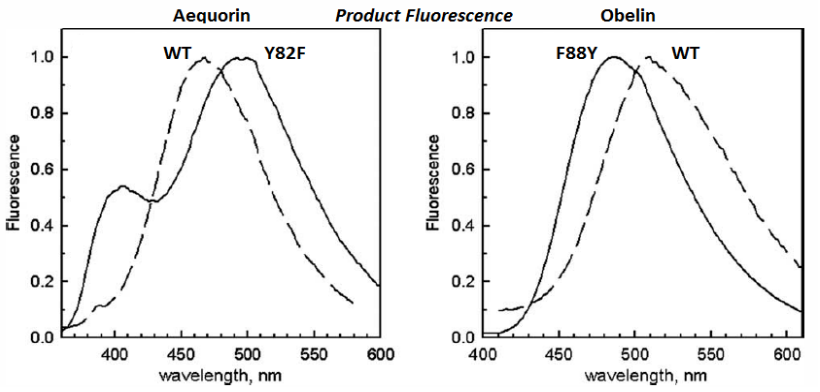

Figure 12.23. Rational mutation of aequorin and obelin shifts the product fluorescence.

Obelin WT product fluorescence maximum is 509 nm shifting to 487 nm in the F88Y mutant. The conclusion is that hydrogen bond interactions involving this 6-(*p*-hydroxyphenyl) oxygen

atom, are able to “tune” the emission spectra. The bioluminescence from F88Yobelin does not match that of aequorin WT meaning that there are environmental factors other than just H-bonding changes involved after mutation. These other factors might be revealed by X-ray crystal structure study of the mutants. In order to allay this fear, the spatial structures of F88Y obelin before and after reaction was determined and found overall to be closely the same respectively as the obelins. The only difference was in the H-bonding pattern connecting the 6-(p-hydroxyphenyl) group. In conclusion, on the basis of the present data, mutants can be constructed “intelligently”. A large range of bioluminescence colors from violet to green, a “Bioluminescence Rainbow”, has been constructed in this way (Fig. 12.24).

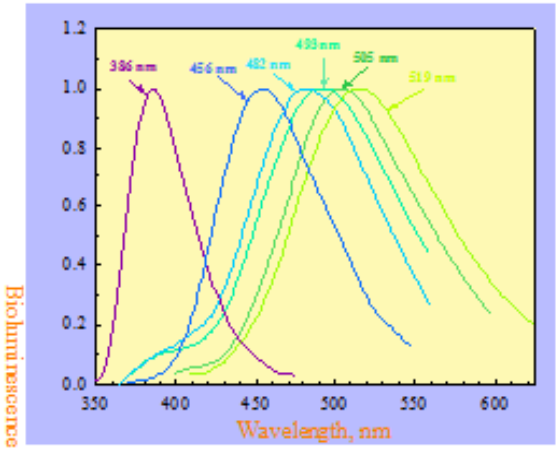

Figure 12.24. Variety of colors of photoprotein bioluminescence produced by rational mutation involving residues proximate to the 6-(p-hydroxyphenol) substituent of coelenterazine.

Photoprotein-GFP

Many organisms that utilize coelenterazine or related structures as the luciferin, exhibit a green bioluminescence not in the blue as observed from the *in vitro* reaction with the extracted and purified luciferin and luciferase, or from the photoprotein in its reaction triggered by Ca^{2+}. This green emission from the jellyfish *Aequorea* was first remarked upon in 1962 in a paper about the purification of aequorin. In a footnote it was mentioned that a “green protein” was also observed in the extracts, later renamed and the now famous “Green-fluorescent Protein” (GFP). A later study showed that the fluorescence of GFP was the same as the *in vivo* green bioluminescence from several types of organisms, including *Obelia*, *Clytia*, *Renilla*, and others, and it was proposed in the early 70’s that energy transfer of the “Förster-type” enabled the biochemically produced excitation energy to end up in the fluorescence state of GFP. Later studies on the Renilla luciferase system demonstrated the necessary complex between the luciferase and Renilla GFP and other evidence supporting this idea of a FRET process being responsible for the bioluminescence energy being emitted in the green.

Application of spatial structural determination and NMR, now provides direct evidence for a protein-protein complex between the photoprotein clytin and its cognate Clytia GFP. In this system FRET can be observed between the bioluminescence transition of the photoprotein donor and the $S_0 \rightarrow S_1$ transition of the GFP. The complex being weak is not amenable to crystal growth, so its structure is determined by a molecular docking computation with ^{15}N-HSQC mapping the shifts of known surface residues of the two structures that enables identification of the protein-protein interacting region, thus providing constraints necessary for a reliable docking computation.

As can be expected from its homologous primary structure, the determined clytin spatial structure is homologous to those of aequorin and obelin. Its bioluminescence is also triggered by addition of Ca^{2+} to produce a blue bioluminescence color with spectral maximum at 470 nm. Inclusion of Clytia GFP in the reaction at only micromolar concentration, shifts the bioluminescence spectrum to longer wavelength in a concentration dependent manner (Chapter 13). The finally shifted bioluminescence matches the narrow fluorescence spectrum of the GFP with maximum at 500 nm. On the basis that this shift is a result of FRET, the separation between the purported donor, the bioluminescence excited state and the acceptor GFP, needs to be <~100 Å, implying that the clytin and GFP must be associated, because at micromolar concentration they would have an average random separation of ten or more times this value. Using standard biophysical techniques, no complex of GFP with clytin was detected at a micromolar level and not even at higher concentrations if it had a K_D as much as ~ 0.1 mM. However, at above mM concentrations a calorimetric technique confirmed a weak complex does form with an estimated K_D ~ 1 mM.

It was concluded that the required FRET complex must be one transiently formed during the reaction. There is some kinetics evidence that the interaction does take place during an intermediate step. It seemed reasonable to assume that this FRET complex should have the structure determined from the docking of the crystal structures of the pair. The procedure adopted for determination of the docked structure of the complex, was first by assignment of chemical shifts in the ^{15}N-HSQC NMR spectrum of each protein partner, then observing "shifts of some shifts" that occurred when the two proteins were mixed at millimolar concentration. The crystal structures of clytin and Clytia GFP were already known and the NMR assignments were made by a series of experiments with ^{13}C- and ^{15}N-enrichments, standard procedures for the NMR structure determination, but the technical details are complicated and their explanation is beyond the scope of this book. The almost completely identified ^{15}N-HSQC resonances of clytin are shown in the Fig. 12.25. The blue lines are drawn to those resonances that undergo a significant shift when this ^{15}N-enriched clytin is mixed with unlabeled GFP. Three representatives, Alanine (A9), Valine (V10), and Lysine (K11), are shown in the amplified panels (Fig. 12.27), the black contours before and the blue after, adding GFP. The residues undergoing a shift on mixing can be identified from the spatial structure as lying in a surface region, therefore mapping the area of interaction of the clytin with the GFP.

The same experiment carried out with GFP ^{15}N-enriched and clytin not labeled, maps the surface region of the GFP partaking in its association with clytin. It is found that the GFP residues are for the most part acidic, i.e., negatively charged, and on the clytin surface basic,

positively charged. This means that an electrostatic interaction is driving the association. The structure of the protein-protein complex is then estimated by a computer program called "Haddock" that configures the pair in all possible geometries and calculates the energies of each complex mainly resulting from the elimination of surface solvation. The defined interaction sites are a critical constraint in accepting a minimum energy structure as being the true structure of the protein-protein complex. The GFP is a homodimer in solution so the complex must be tetrameric, a GFP dimer with two non-overlapping clytins. The donor-acceptor separation is 45 Å (Fig. 12.28) consistent with the observation of efficient bioluminescence FRET.

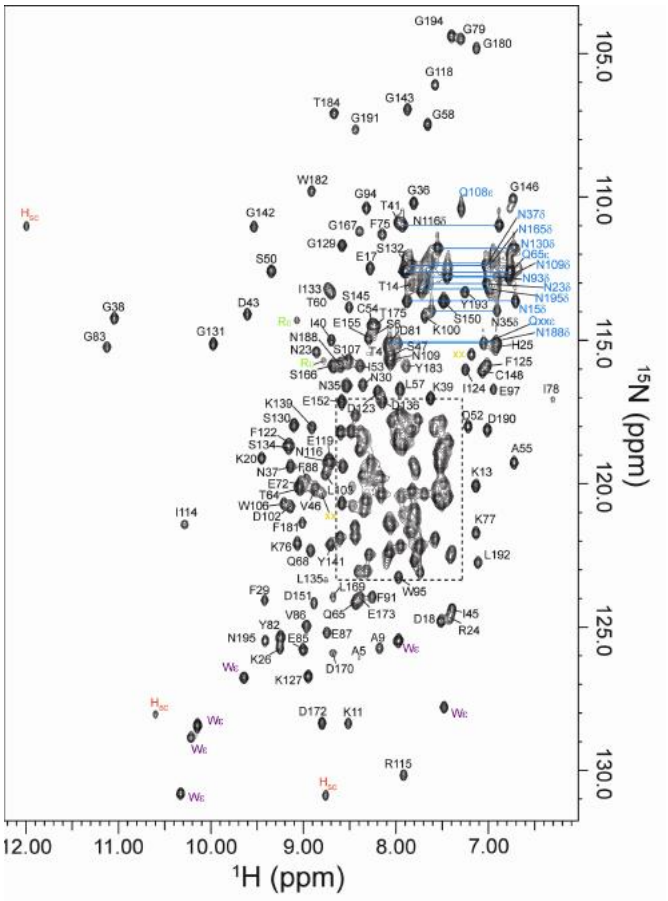

Figure 12.25. Assignment of the ^{15}N-HSQC NMR spectrum of the photoprotein Clytin.

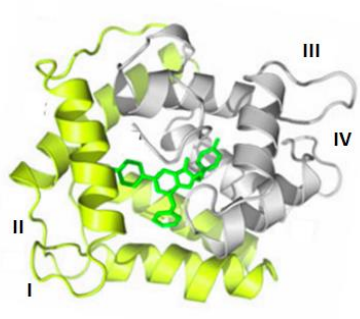

Fig. 12.26. Spatial structure of clytin is homologous to other photoproteins.

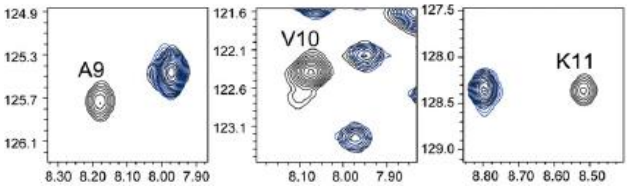

Figure 12.27. Representative ^{15}N-HSQC of several residues of Clytin (*black*) that shift (*blue*) after mixing with an excess Clytia GFP. These perturbed residues map the interaction site in the complex.

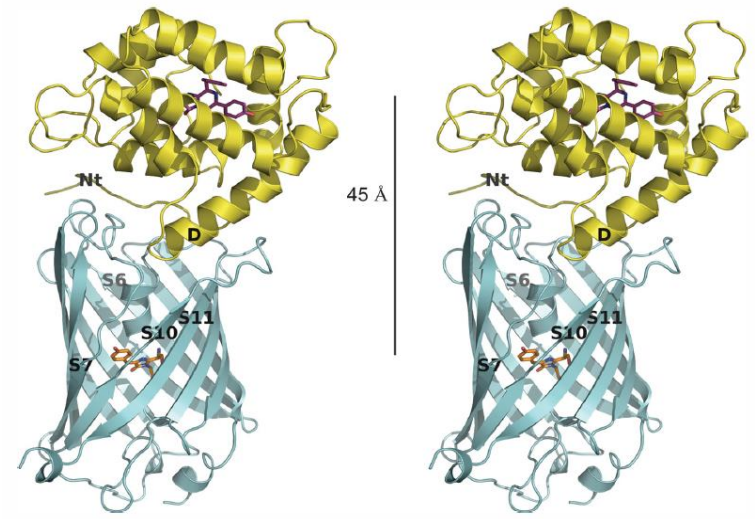

Figure 12.28. Stereoview of the of the Clytin-Clytia GFP complex constructed by computational docking using the known X-ray crystal structures of the individual proteins and the constraints of surface residues exhibiting a shift in HSQC on mixing the two proteins. In solution the complex would be tetrameric. This research was originally published by Titushin, M.S., Y. Feng, G.A. Stepanyuk, Y. Li, S.V. Markova, S. Golz, B-C. Wang, J. Lee, J. Wang, E.S. Vysotski and Z-J. Liu. NMR-derived topology of a GFP-photoprotein energy transfer complex, in the Journal of Biological Chemistry. 2010, 285: 40891–40900.

Bacterial Luciferase

The first X-ray crystal structures of proteins from bioluminescent organisms appeared in the period 1993-96. In 1993 the first structure determined was of the so-called "Non-fluorescent Protein" (NFP or LuxF), a flavoprotein produced by species of *Photobacterium* in a quantity comparable to luciferase itself. NFP is a 53-kDa homodimer with two tightly bound flavins on each subunit. The subunits have sequence homology to bacterial luciferase meaning that NFP should have a spatial structure resembling luciferase. More tantalizing, the NFP gene (*luxF*) lies within the bioluminescence operon (*lux*) of *Photobacterium* species. NFP has no luciferase activity, and no other function in the bioluminescence system or other enzymatic property has so far been uncovered. Bacterial luciferase itself had resisted crystallization at that time but NFP readily formed good single crystals, and with sequence homology to bacterial luciferase its structure therefore provided predictability for the structure of the luciferase, again on the basis that sequence determines structure. NFP has a $(\beta/\alpha)_7$ -barrel structure, i.e., a β-sheet followed by an α-helix seven-fold. Published in 1995, the determined structure of bacterial luciferase was very close to that predicted from the NFP structure, except having the canonical $(\beta/\alpha)_8$ -fold known as a "Triose Phosphate Isomerase" (TIM)-barrel fold. TIM-barrel folds are very common in protein structures. NFP binds on each subunit two FMNs substituted at the 6-position by a myristyl group, i.e., a tetradecanoic acid moiety. What is remarkable about this is that myristic acid is the product of the bioluminescence using the naturally occurring aldehyde tetradecanal as the luciferin. On each subunit one FMN is buried in the interface and the other in the vicinity of the N- and C-terminals. The luciferase structure at that time was without bound FMN so it had to be supposed that the binding site should be located analogously to the NFP FMN-binding sites, but which one, as luciferase has only one FMN binding site and it is only on the α-subunit of the heterodimer?

It has been mentioned above that there are now a number of flavoproteins known to be structurally homologous to bacterial luciferase. The bacterial luciferase structure was about the first to be determined so all these flavoproteins including NFP, are classified as belonging to the "bacterial luciferase structural family". The FMN binding site on luciferase was not known until recently but it is the same within the whole structural family including the N-, C-terminal sites in NFP. Structural homology between two proteins can be shown by a quantitative measurement calculated as the residual mean square (rms Cα) deviation of the average separation between the α-carbons of the amino acid residues in each chain, when the two proteins are optimally aligned.

The first line in the Table 2 (see Chapter 15) is the comparison of the original bacterial luciferase α-subunit paired with its recent structure having bound FMN. The 0.5 Å value for the rms Cα says that the tertiary structure overall is unchanged on binding FMN. A value below 3 Å is generally taken as clear proof of structural homology. Among the remainder of the flavoproteins in this family there is no sequence homology to luciferase. They need not be discussed anymore here except for the one abbreviated LadA:FMN, "Long-chain Alkane Monooxygenase:FMN complex" because this structure may help identify the aldehyde binding site in luciferase.

Table 2. The bacterial luciferase family. DALI comparison with the bacterial luciferase α-subunit

	Z-score	rms Cα (Å)	% id	# residues	PDB code
α-subunit+FMN	54.4	0.5	100	326	3FGC
β-subunit	40.1	2.1	31	320	1LUC-B
ADF	29.5	2.4	20	330	1RHC
SSUD	29.2	2.6	19	328	1M41
MER	28.5	2.7	23	321	1F07
LadA:FMN	27.1	2.8	15	433	3B9O
LLMONO	26.9	2.6	17	318	2B81
NFP	16.8	2.9	17	228	1NFP

The bacterial luciferase structure with FMN bound was determined by soaking the FMN into the luciferase crystals. The FMN is seen in Fig. 12.29 to be placed internally within the α-subunit, as predicted by a host of earlier studies. The FMN is located in a large cavity that has an opening to solvent. The FMN is in a planar conformation, non-covalently bound but with H-bonding to residues lining the cavity. The benzyl portion of the isoalloxazine ring points towards several hydrophobic residues, and the other end is in a more hydrophilic environment and interacting with two alanine residues, A74-A75, that have an unusual *cis* peptide bond (Fig. 12.30). Also, the sulfhydryl side group of the Cysteine 106 residue points towards the C(4a) position of the FMN. This may have mechanistic significance in that the peroxyflavin intermediate **II**, could be stabilized by being an endoperoxide having the cysteine side chain linked to the flavin. The nature of the FMN interactions illustrated here (Fig. 12.30, *right*), is in remarkably complete agreement with interpretations of the H-bonding from the earlier

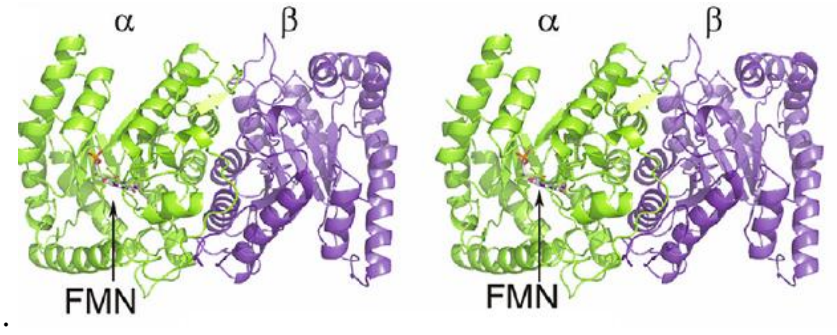

Figure 12.29. Stereoview of spatial structure of the bacterial luciferase α,β heterodimer showing the FMN (light blue) bound in the α-subunit.

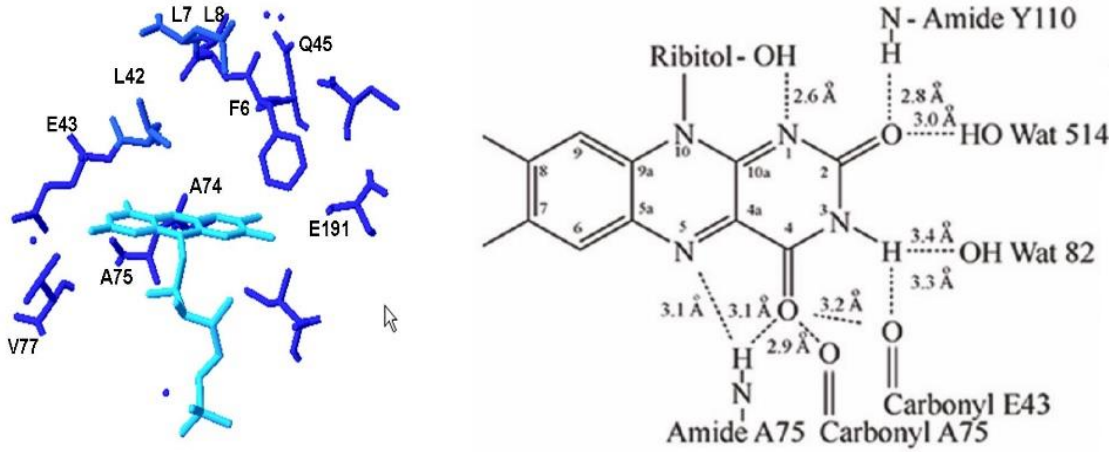

Figure 12.30. (*Left*) FMN (light blue) and the proximate residues (*dark blue*) in the bacterial luciferase binding cavity. (*Right*) H-bonding pattern of the bound FMN.

NMR study of luciferase in solution. Comparing Figs. 12.30 and 12.31 for bacterial luciferase and alkane monoxygenase respectively, it is seen that the FMN is very similarly interacting in each of the binding sites and also, faces in the same way towards a channel leading to the outside of the structure. In Fig. 12.31, a long-chain alkane (brown) is shown by modeling, to be accommodated in this channel. It would be an interesting project, although not definitive proof, to see if a long-chain aldehyde can be happily fitted into the luciferase channels comparable to the picture for alkane monooxygenase.

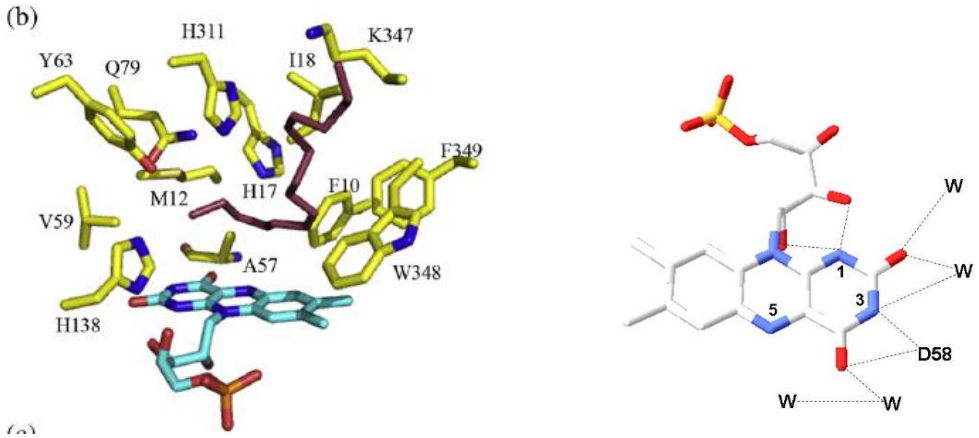

Figure 12.31. (*Left*) Active pocket of alkane monoxygenase with the FMN (blue) and the channel holding the long chain alkane (*brown*). (*Right*) H-bond interactions for the bound FMN. W = bound water; D = aspartate.

Lumazine Protein

The ligands of the lumazine proteins are readily interchangeable, the lumazine (6,7-dimethyl-8-ribityl-lumazine) in LumP by flavins, the riboflavin or FMN in the yellow-fluorescent Y-1 protein, by lumazine. Recently, recombinant apo-LumP from different species of *Photobacterium* has been recombined with these different ligands and their spatial structures determined (Fig. 12.32). As the primary sequence of LumP and the Y1-protein are homologous, they should also possess as can be seen, closely similar three-dimensional structures. The recombined holo-proteins have identical spectroscopic properties to the original native proteins.

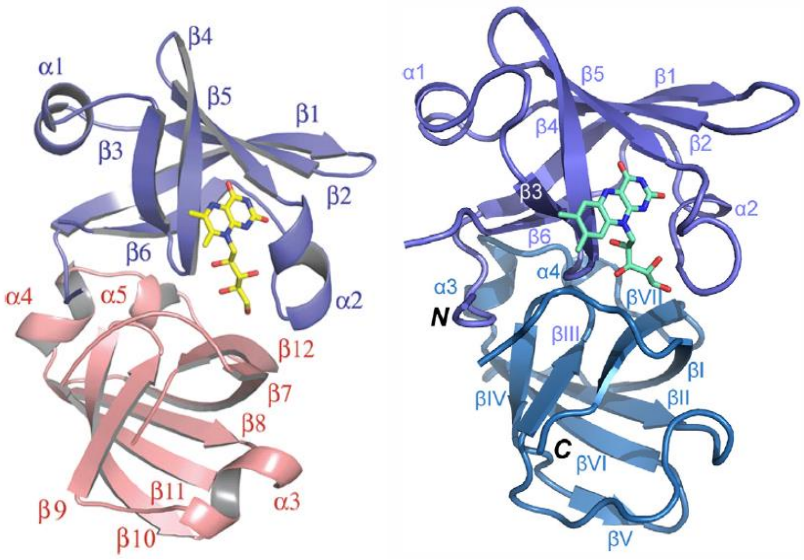

Figure 12.32. Structure of lumazine protein with the bound lumazine derivative (*yellow; left*) or riboflavin (*green; right*).

Lumazine protein consists of two domains having nearly identical β-barrel folds. The structure is unaffected by the nature of the ligand, the lumazine derivative, riboflavin, or FMN. The lumazine derivative is also a substrate for the enzyme riboflavin synthetase that consists of three identical subunits. These have primary sequence homology to lumazine protein, so it is not surprising to find also structural homology between these synthetase monomers and lumazine protein. A critical difference is that lumazine protein binds only one ligand in the N-terminal domain, whereas each synthetase monomer binds two lumazines, one each in the N- and C-terminal sites as required by the well-understood riboflavin synthetase mechanism. In both proteins the N-terminal binding sites are structurally identical but the C-terminal site in lumazine protein is blocked by a bulky side group from Histidine-145 that projects into the cavity and so prevents ligand binding.

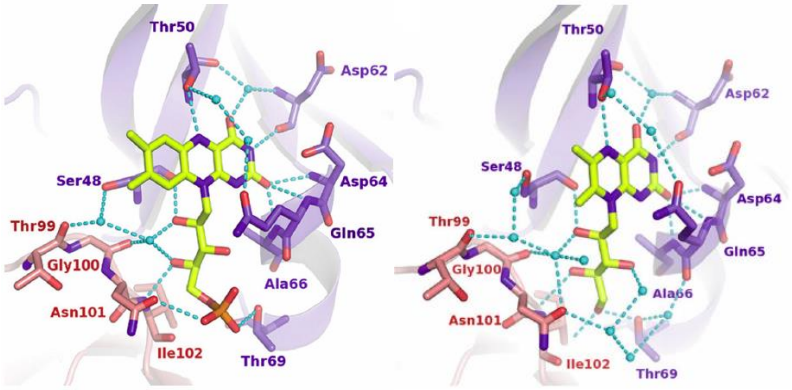

Figure 12.33. H-bond interactions in the binding site of lumazine protein to riboflavin (*left*) or lumazine (*right*).

The fluorescence properties of ligands bound in lumazine proteins, may be qualitatively rationalized by examination of interactions in the binding site. The lumazine derivative is buried in a hydrophobic pocket held in place by an extensive hydrogen bond network (Fig. 12.33). The fluorescence of the lumazine derivative in water has a maximum around 490 nm but in solvents of lower polarity it is blue-shifted towards that of lumazine protein itself. The opposite is found for flavins, less polar solvents cause a shift from about a 530 nm maximum to longer wavelength, although by only a few nanometers. The yellow fluorescence Y1-protein fluorescence maximum at 542 nm must be a result therefore, of additional interactions such as from the hydrogen bond network, although this network is not as extensive as for the lumazine in lumazine protein, explaining in part the weaker affinity of flavins for the lumazine apoprotein. Another distinctive property is the high fluorescence yield of the bound flavin compared to almost all other flavoproteins, which are usually hardly fluorescent.

There is a considerable amount of biophysical evidence to indicate that the mechanism causing these bioluminescence color shifts in the bacteria is by FRET via a weak dipole-dipole electronic coupling between the luciferase-produced excited state, possibly the “fluorescent transient” fluorophore, and the ligand of the antenna protein. There is experimental evidence for the formation of a lumazine protein-luciferase complex, and with the availability of their crystal structures, a computationally docked model has been produced (Fig. 12.34). A separation of only 10 Å between the sites proposed for the donor and acceptor, provides a very favorable circumstance for the Förster mechanism of bioluminescence color shift.

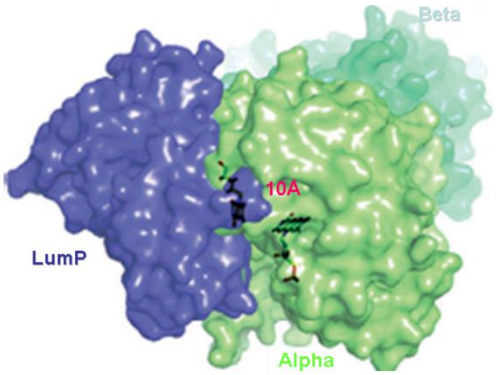

Figure 12.34. A computationally docked structure of lumazine protein and the α-subunit of bacterial luciferase suggests a 10 Å separation between the respective binding sites.

Firefly luciferase

The three-dimensional structure of firefly luciferase was first determined in 1996 and it was not surprising to find that it showed homology to the large family of adenylating enzymes including the acyl-CoA synthetases. These enzymes like firefly luciferase, also have a two-step mechanism (Fig. 9.4), an adenylation followed by the synthetase reaction or, uniquely for luciferase, the oxygen addition and decarboxylation that leads to bioluminescence.

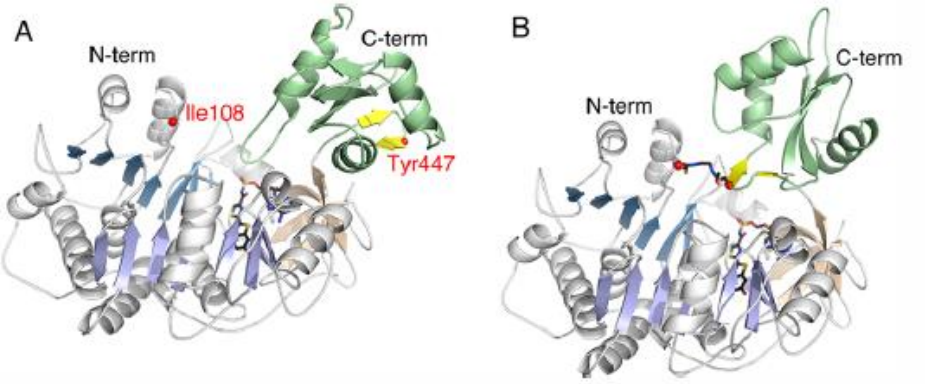

Figure 12.35. A. Two domain structure of firefly luciferase. The C-terminal domain appears to form a lid over the luciferin bound in the luciferase site. **B.** Chemically cross-linked luciferase reveals the second “capped” conformation.

The synthetases have a two-domain structure as shown here (Fig. 12.35) for the case of luciferase (**A**), with a large N-terminal domain and a smaller C-terminal domain, the latter potentially able to form a lid over the active site. The location of the active site in the 1996 luciferase structure was assumed to be the same as already detected for the synthetases and

this was verified in 2006 by two new luciferase structures, one containing a luciferin analog and the other the reaction products (Fig. 12.38). In 2012 Bruce Branchini and co-workers proposed that the two-stage mechanism for luciferase might be the same as for the synthetases. This mechanism is first a "domain alternation" where the adenylation takes place with the active site exposed (red line in Fig. 12.36), followed by a twist over (Fig. 12.34, **B**) through about a 140º angle to place the active site at the domain intersection, where the CoA ligation is catalyzed in the synthetase or for luciferase, the oxygen addition and decarboxylation take place.

To test this hypothesis the firefly luciferase was mutated at two positions. Isoleucine 108 on the C-terminal (Fig. 12.35, **A**) was substituted by cysteine (Ile108Cys), and on the N-domain the tyrosine 447 also by cysteine (Tyr447Cys). The bioluminescence activity of the mutant was almost the same as the natural luciferase (**A**, Fig. 12.35.), both the adenylation and oxidative functions were unaffected. A standard reagent used for cross-linking proteins is 1,2-

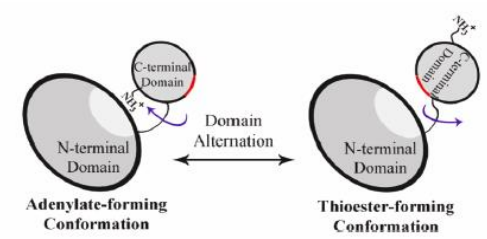

Fig. 12.36. Two domain alternation mechanism for a general adenyl synthase.

bis(maleimido)ethane that reacts with the sulfhydryl group of cysteine under mild conditions (Fig. 12.37). After verifying that both cysteines had been cross-linked, it was found that the adenylation function had been eliminated but the bioluminescence could be generated by using synthetic LH_2AMP. The crystal structure (**B**, Fig.12.35) proved that the cross-linked luciferase was indeed in the twisted conformation.

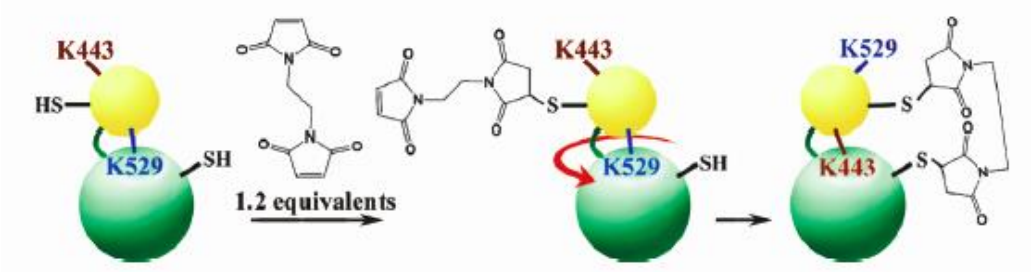

Figure 12.37. A cross-linking reagent 1,2-bis(maleimido)ethane is used to "freeze" closed the C-terminal luciferase "lid".

Firefly luciferase structures revealing the active site were first determined in 2006, one with a luciferin analog (DLSA) and a second with the products, oxyluciferin and AMP. As the true substrate itself would be short-lived being rapidly catalyzed to products, it is standard procedure in enzyme structure studies, to use an analog that is known to bind and to competitively inhibit the reaction. A two-dimensional picture of the active site of luciferase with the bound products is shown in Fig. 12.38. The aim of these studies was to determine what interactions might be responsible for spectral shifting, that is the range from blue to red observed for beetle bioluminescence colors.

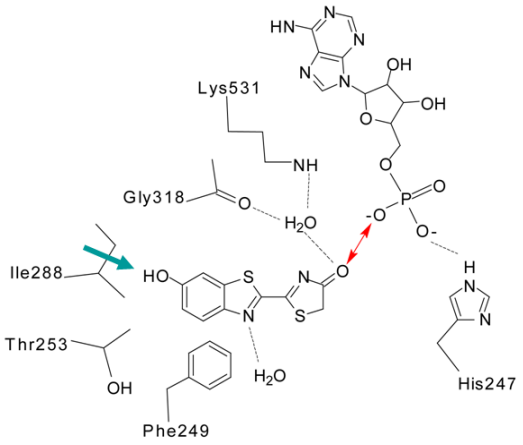

Figure 12.38. Two-dimensional diagram of firefly luciferase with oxy-Luciferin and AMP in the binding site. The red arrow suggest an ionic interaction at the keto position. The blue arrow indicates the shift of Ile288 from its original position with the bound substrate analog DLSA.

The products reside in the same binding cavity as the substrate analog DLSA, with the structural configuration hardly changed. There are small residue movements going from the bound analog to oxy-Luciferin indicated for isoleucine by the blue arrow, and of some other residues that also move into the cavity, so that overall the various shifts create a more hydrophobic environment for the product oxy-Luciferin. Thus, changes in hydrophobicity and/or ionic equilibria can qualitatively rationalize the green to orange spread of the firefly bioluminescence colors. There are many residue substitutions which affect the bioluminescence color, some quite far from the active cavity. Substitutions in the loop residues 220-235, which are nearby but not in contact with the substrate, have strong effects. It was suggested that these might open up the cavity to expose the excited product to an interaction with solvent. Direct evidence for this possibility is in a third structure obtained for mutated luciferase S285N, which produces red bioluminescence with firefly luciferin. The vicinity of the oxy-Luciferin is more open in the mutant than in the wild-type luciferase, more exposed to solvent, and with a more polar surrounding, all conditions known to favor a red shift of fluorescence spectra. A recent determination of structure of the luciferase from *Lampyris turkestanicus* reaches a similar conclusion of the importance of solvent accessibility to particular binding residues.

The valid criticism of these rationalizations is that the structure is for the open configuration. The chemical excitation catalyzed in the closed luciferase configuration produced the emitter in its excited state having a lifetime only a few nanoseconds, much too brief for any protein structural change. Therefore, determination of the true product interactions necessitates determination of the binding site interactions in the closed configuration.

13. **The Antenna Proteins. Bioluminescence FRET**

Lumazine Protein

The discovery of lumazine protein in 1978 resulted from the question of why the *in vivo* bacterial bioluminescence maxima from many *Photobacterium* species was around 475 nm, whereas the *in vitro* reaction using purified PP-luciferase from the same organism, had a maximum around 495 nm. The culprit was identified as a novel highly fluorescent protein first discovered in extracts of *P. phosphoreum*. This protein had a fluorescence spectrum matching the *in vivo* bioluminescence both in its spectral distribution and the maximum at 475 nm. Although the PP-luciferase *in vitro* bioluminescence had the usual maximum around 495 nm, inclusion of lumazine protein in the reaction mixture even at micromolar concentration, blue-shifted the bioluminescence spectrum to match the *in vivo*

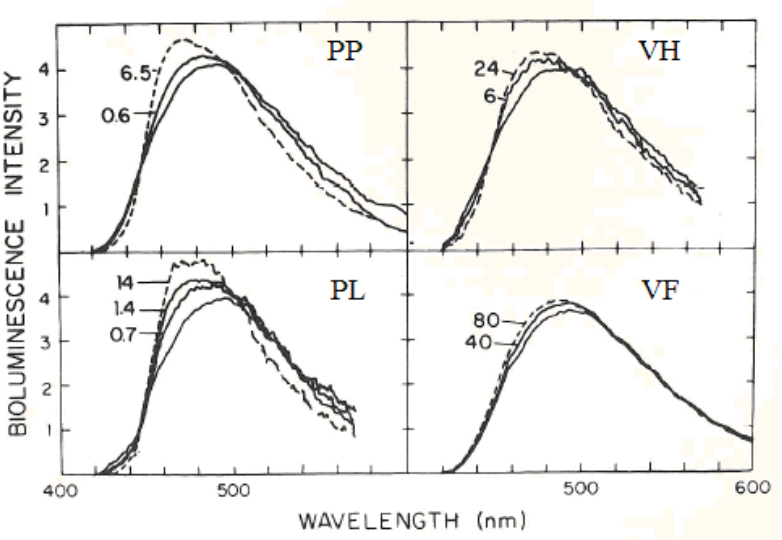

Figure 13.1. Inclusion of Lumazine Protein (μM) shifts the *in vitro* bioluminescence spectrum depending on the type of luciferase.

bioluminescence (Fig. 13.1). The shift was also accompanied by an effect on the bioluminescence kinetics (Fig. 13.2). This spectral shift appears to be general as the same property was observed for the bioluminescence using PL-luciferase, and also for the yellow fluorescence protein (YFP or Y1-protein) with the Y1-luciferase from this yellow bioluminescence bacterium, *A. sifiae*. In this last case, the Y1-luciferase *in vitro* reaction having the same blue bioluminescence as the other types with a maximum around 495 nm, shifted to longer wavelength on inclusion of the Y1-protein to a maximum at 542 nm, the same as the Y1-protein fluorescence and a match for the *in vivo* yellow bioluminescence spectrum of *A. sifiae*. Clearly, these fluorescent proteins are the origin of the bioluminescence apparently displacing the fluorescent transient in this role.

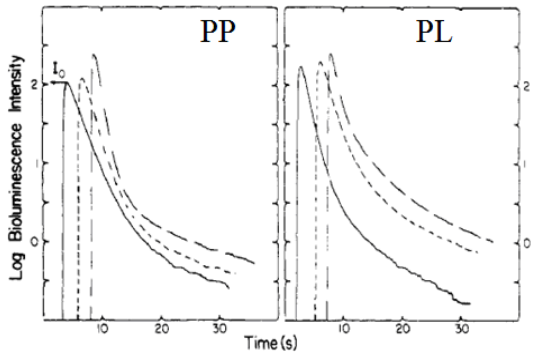

Figure 13.2. Inclusion of Lumazine Protein increases the bioluminescence intensity. (*Left*) PP-luciferase (*Right*) PL-luciferase.

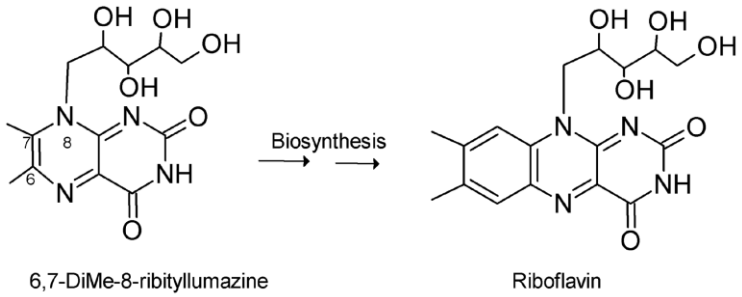

Figure 13.3. The similarity of structures of the riboflavin and the lumazine derivative is not surprising as the lumazine is the precursor of riboflavin (Vitamin B2) in its biosynthetic pathway.

The fluorescent ligand in the antenna protein from *Photobacterium* is 6,7-dimethyl-8-ribityl-lumazine, hence the shortened name “Lumazine Protein” (LumP) (Fig. 13.3). The yellow fluorescence protein is named the Y1-protein and its natural fluorescent ligand is a flavin, FMN or riboflavin. According to their apparent function of accepting energy and emitting radiation, they are called “antenna proteins” by analogy to the antenna proteins in the photosynthetic unit that operate in a reverse sense. These latter collect the impinging energy of sunlight photons and transfer it to the photosynthetic center. Determination of the amino acid sequences of Y1-protein and lumazine protein showed them to be closely related, i.e., homologous. Interestingly, as already mentioned in Chapter 12, the lumazine derivative is the precursor of riboflavin in its biosynthesis in bacterial metabolism.

Both antenna proteins, LumP and the Y1-protein, were observed to have kinetics effects as well as spectral shifts, specific for the type of luciferase (Fig. 13.2). The fact that the bioluminescence shift can occur at only micromolar concentrations, implies that there is a protein-protein complex involved in the reaction pathway, LumP–PP-luciferase or Y1-protein–Y1-luciferase. At micromolar concentrations the average separation in a free state of the two proteins would be more than 100 nm and these concentrations are too low for any trivial fluorescence transfer to be responsible for the spectral shift. Therefore, it seems that within a necessary complex the rate limiting step of bioluminescence is catalyzed and some type of energy transfer occurs to the antenna protein. Fig. 13.1 shows that only micromolar

concentrations of LumP are sufficient to shift the bioluminescence spectra of PP-luciferase and PL-luciferase, rather more for VH-luciferase, but for VF-luciferase the spectrum is hardly affected even at 80 μM. An empirical analysis assuming that the spectral shift corresponds to a protein-protein titration, results in an interaction constant K_i for PP-luciferase and PL-luciferase, 2-3 μ*M*, VH-luciferase 8 μ*M*, and VF-luciferase 180 μ*M*. Specificity for the luciferase type was also reported for the Y1-protein with K_i's in the same μ*M* range. The bioluminescence kinetics using PP-luciferase (Fig. 13.2, *left panel*) is unchanged in the presence of the PL-LumP (---) but markedly changed using PP-LumP (– –), and for the PL-luciferase both types of LumP increase the initial light intensity or flash height (I_0).

The formation of protein-protein complexes by these bioluminescence proteins are ideal subjects for investigation using fluorescence dynamics. The antenna proteins and the luciferase fluorescent transient intermediate (FT) are efficiently fluorescent and have relatively long (τ = 10-15 ns) and closely single exponential fluorescence decay lifetimes. Luciferase itself has no fluorescence in the visible region, only in the near UV around 330 nm from its tryptophan residues. Although of short lifetime, this intrinsic tryptophan fluorescence is still useful for fluorescence dynamics measurement. The 475-nm fluorescence maximum of the protein-bound lumazine ligand is found at 490 nm when free in solution. On dilution of lumazine protein therefore, the spectrum shifts to longer wavelength simply explained as due to the dissociation of the lumazine, and the fluorescence decay becomes a double exponential and can be accurately fitted with the free and bound lifetimes the amplitudes of which correspond to the concentrations of free and bound lumazine. After correcting for the respective Φ_F values, the equilibrium constant can be recovered. The binding is 1:1 with an equilibrium K_D = 0.05 μM at 4ºC.

The first fluorescence dynamics study was initiated with the expectation that efficient energy transfer would occur if the LumP and luciferase were in a preformed complex before reaction. The assumed donor species FT has a fluorescence decay lifetime of 10 ns and its excitation would be efficiently transferred to the acceptor LumP within the complex and not have to depend on the diffusive encounter rate between the two proteins or the rate of fluorescence decay of the primary donor species. The experiment then in the first instance, is to determine the mass of the proteins in their mixture using the rotational diffusion rate of the lumazine ligand as a probe. For this application using fluorescence anisotropy decay measurement, the protein-bound lumazine is an ideal intrinsic probe by virtue of its long fluorescence lifetime τ = 15 ns and Φ_F = 0.6, together with its rigid binding to the lumazine apoprotein, meaning that it rotates together with the whole protein. On forming a complex with luciferase, the rotator to which the lumazine is bound should change in mass from 21 to 97 kDa, and this will be clearly measureable by a change in the rotational correlation time, φ. The long fluorescence lifetime, τ = 15 ns, means that there will still be enough fluorescence intensity at times >100 ns to enable accurate measurement of anisotropy, *r*.

The theory of the hydrodynamics of macromolecules shows that a spherical rotator will have a monoexponential fluorescence anisotropy decay:

$$r(t) = r_0 .\exp(-t/\varphi)$$

where r_0 is the initial anisotropy and φ is the rotational correlation time. The rotational diffusion coefficient D_S for a spherical macromolecule is given by the Debye-Stokes-Einstein equation:

$$D_S = kT/(6\eta V)$$

where k is the Boltzmann constant, T the absolute temperature, η the viscosity of the solution, and V the volume of the molecule. It can be shown that

$$\varphi = (6D_S)^{-1}$$

and therefore, $= M_r(v' + h)/(RT)$

where M_r is the luciferase molecular weight, 77,000, v' is the partial specific volume calculated from the amino acid composition, 0.73 cm^3/g, h the degree of hydration ~ 0.2 cm^3/g, R the Gas Constant, and T the absolute temperature. Although proteins in general are not spherical, it is found that their anisotropy decay is always nearly monoexponential, appearing to rotate as a sphere by virtue of the associated waters of hydration in solution. A biexponential decay corresponding to rotation around two axes, is difficult to distinguish unless the correlation times are substantially different. Therefore, the theory of rotational diffusion of a fully hydrated macromolecule in aqueous solution at around (2ºC), results in a coincidental correspondence of the rotational diffusion time (φ) in ns units, with the molecule's mass in kDa. For example, LumP (21 kDa), has φ = 21.7 ns (2ºC), as shown in Fig. 13.4, which also shows the effect of increased temperature due to the decrease in viscosity of water, with a corresponding decrease to φ = 13.5 ns. Luciferase for example, with an axial ratio from its X-ray crystal structure of 1.5, also shows a single exponential decay of fluorescence anisotropy using the intrinsic Trp fluorescence as a probe (2ºC), φ = 61 ns, and also with an extrinsic probe, bound aminonapthlalene sulfonic acid, φ = 74 ns. The calculated value for luciferase from the diffusion equation above is 62 ns. The difference between the 61 and 74 ns values can be explained away but for the present discussion, the difference can be assumed to be not significant.

As already mentioned, the long fluorescence decay time for LumP is very valuable for these studies. If a protein-protein complex were to be formed then an expected φ ~ 100 ns for a LumP–luciferase complex due to their total mass, 97 kDa, should be accurately measurable as there still should remain sufficient fluorescence signal past the 100-ns mark. The first experiments carried out therefore, were to test a proposal that a LumP–luciferase complex should be preformed, and its extent of binding should correlate with the effect of LumP on the bioluminescence spectrum. In Fig. 13.5, the only fluorescent probe measured is that of the bound lumazine and in the top panel the free lumazine protein with φ = 23 ns, is seen to increase to 75 ns mixed with excess VH-luciferase. A completely associated LumP-VH luciferase complex should have φ ~100 ns, so the value of only 75 ns must reflect an average from an equilibrium mixture of free and bound. Dilution results in a decrease of this average φ and a simple analysis yields an apparent equilibrium K_D ~ 3 μM, lower than and not

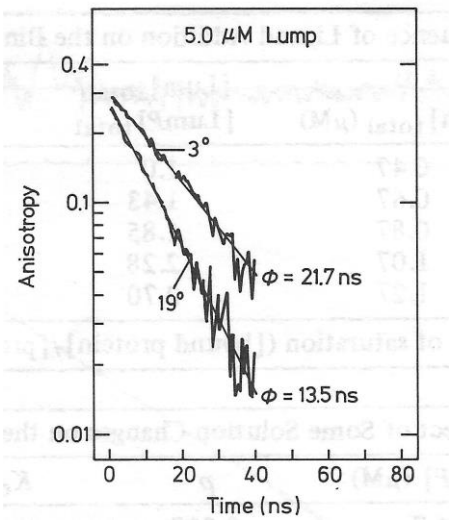

Figure 13.4. Fluorescence anisotropy decay of lumazine protein in aqueous solution is faster at higher temperature due to the lowered water viscosity. The line is the single exponential equation fit to the noisy data.

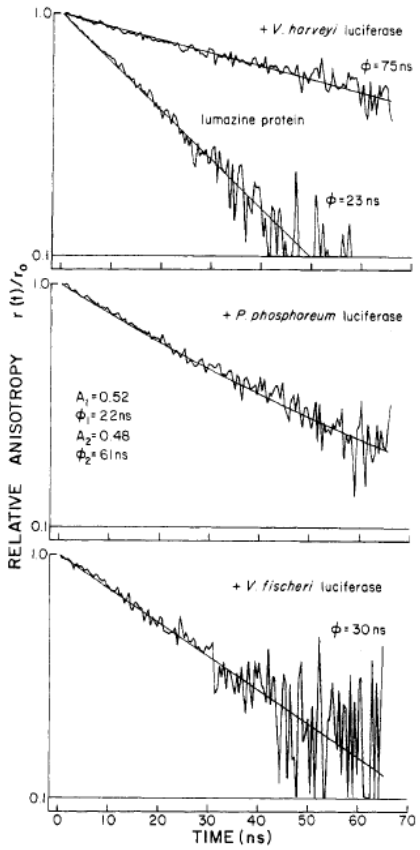

Figure 13.5. The fluorescence anisotropy decay of LumP alone (ϕ = 23 ns) is increased in the presence of VH- and PP-luciferases due to complex formation but hardly at all for AF-luciferase (*V. fischeri*) indicating no complex.

obviously correlated with, the observed K_i ~ 8 μM for the bioluminescence spectral shift. A more critical observation (Fig. 13.5, *middle panel*) is that with a large excess of PP-luciferase, the anisotropy decay is clearly biexponential but the recovered K_D ~ 1 mM, is markedly weaker than the bioluminescence shift with K_i of ~ 3 μM. That means that any preformed complex before reaction is not quantitatively correlated with the bioluminescence energy transfer in the complete reaction, at least in the PP-luciferase case. AF-luciferase (*V. fischeri*) hardly forms any complex and this is consistent with the lack of spectral shifting (Fig. 13.1). In none of the experiments does the addition of dodecanol or dodecanal have any effect; dodecanol is used as a luciferase intermediate stabilizing agent.

As a result of the negative result for PP-luciferase and also as found for later experiments with PL-luciferase, a revised postulated interaction had to be formulated, that the energy transfer complex must be one formed rapidly with a luciferase reaction intermediate. Efficient energy transfer needs a highly fluorescent donor and two luciferase-flavin species have this property, the fluorescent transient and and a high fluorescence form of the intermediate **II** luciferase 4a-peroxyflavin called **IIA** in Fig.10.3, a photochemical product formed by continued irradiation of **II**. Fig. 10.3 suggests that **IIA** and the fluorescent ttransient may be the same. These species have approximately the same properties for all the luciferases tested, AF, VH, PP, and PL. Dodecanol stabilizes these intermediates for many hours allowing for convenient separation and study. The intermediate **II** is weakly fluorescence and broad with a maximum at 500 nm (Fig. 13.6), and could be just a mixture of the decay product FMN and an amount of the photoproduct **IIA**. On continued irradiation for the fluorescence measurement, the long-wavelength part is eliminated due to photoreduction to $FMNH_2$, which then turns over to generate more **II** with an increase in intensity of the short wavelength contribution. The final photochemical product **IIA** has a fluorescence spectrum with a maximum around 495 nm similar if not the same depending on the report, as the bioluminescence in the case of VH-luciferase (Fig. 13.6).

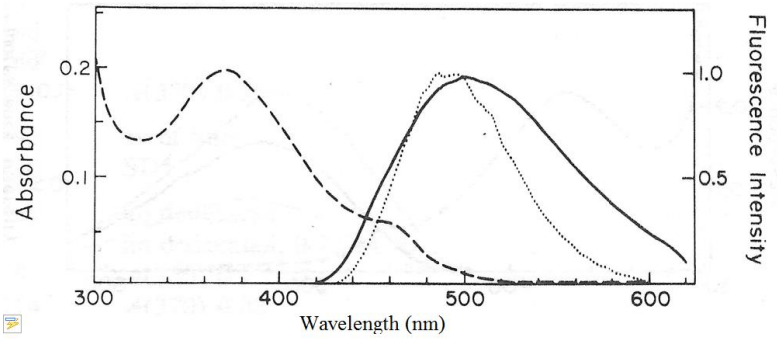

Figure 13.6. Absorption (---) and fluorescence (–) of luciferase 4a-peroxyflavin. After continued irradiation in the absorption band at 370 nm, the weak longer wavelength part of the fluorescence is reduced and a stronger final fluorescence spectrum remains overlapping the bioluminescence (…). Both fluorescence spectra are normalized.

The experiments on the fluorescent transients proved very fruitful. Fig. 13.7 shows that the decay of fluorescence anisotropy is closely a single exponential function for two types of fluorescent transient. The fluorescent transient from AF-luciferase (top panel) has φ = 140 ns, but the one from PL-luciferase has φ = 75 ns consistent with its mass of 77 kDa. The simple interpretation is that the AF-transient is a tight dimeric luciferase of ~150 kDa, and this was verified by a simple filtration experiment. The AF-FT preparation was retarded by a membrane filter having a 100-kDa cutoff but the PL-FT passed through, consistent with a monomeric 77-kDa mass.

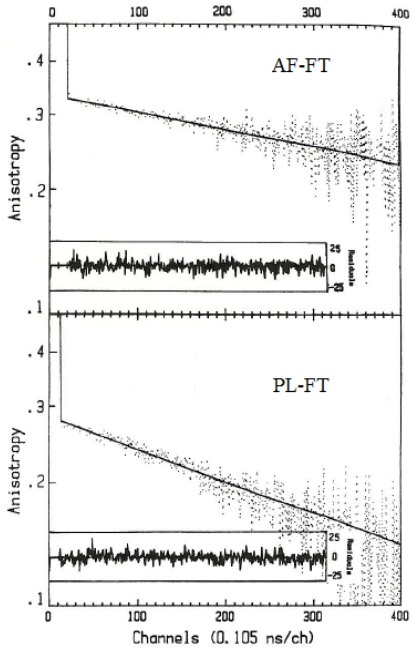

Figure 13.7. Fluorescence anisotropy decay of the Fluorescent Transients (FT) from AF- or PL-luciferases are precisely single exponential as shown by the constancy of the plot of the residuals. The rotational correlation times are ϕ(AF) = 140 ns; ϕ(PL) = 75 ns (2°C).

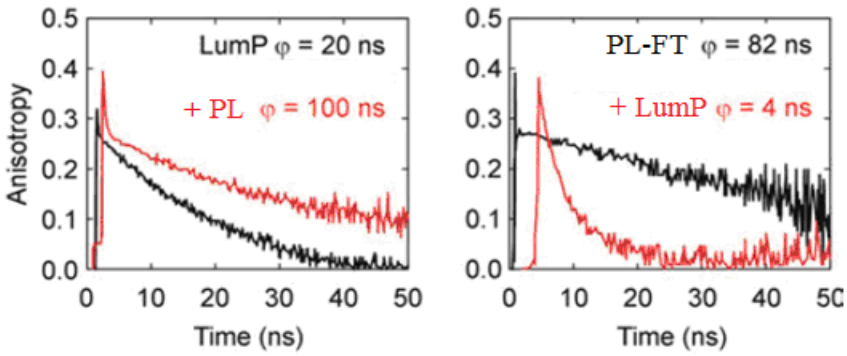

Figure 13.8. LumP and PL-luciferase form a weak protein-protein complex as revealed by the 100-ns decay time of the lumazine's fluorescence anisotropy (red line). With the PL-fluorescent transient (FT) a fast channel of anisotropy loss (red line, φ = 4 ns) is due to energy transfer FT* → LumP*.

A remarkably different result was obtained on inclusion of PL-lumazine protein with the PL fluorescent transient. A fast channel of anisotropy loss φ = 4 ns, is seen in the right panel of Fig. 13.8, attributable to FRET from the donor, the FT*, to the acceptor, the LumP. For the luciferase before addition of substrates (left panel), the longer anisotropy decay time of 100 ns indicates some protein-protein association but no energy transfer. The spike at earliest time is scattering from the laser pulse.

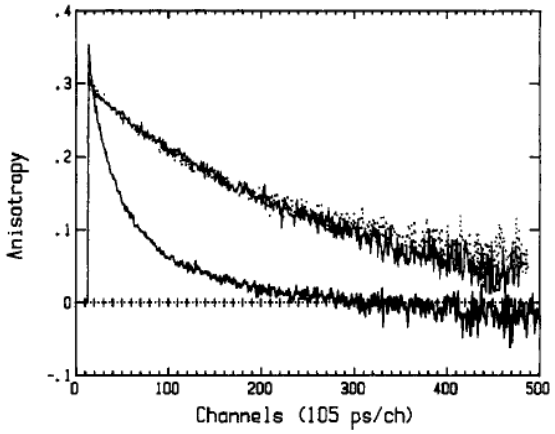

Figure 13.9. Lumazine protein induces a rapid anisotropy decay of the PL-FT (lowest line) but not from AF-FT or VH-FT (*upper heavy line and dots*).

Fig. 13.9 (*lowest line*), shows again that in the presence of lumazine protein, the anisotropy decay of the PL-FT contains a very rapid decay followed by a slower process. The biexponential fit is of a fast decay followed by a slow one. The latter is attributed to

$$r(t) = 0.1\exp(-t/3.1) + 0.22(-t/40)$$

uncomplexed fluorescent transient, its value distorted below the φ = 75 ns expected due to the computed fit being unrestricted, meaning that fixing it to a higher value, say 60 ns also gives an acceptable fit to the data. Anyway, the fast process certainly can be attributed to energy transfer clearly due to the weak dipole-dipole interaction of FRET, resonance coupling of the fluorescent transient $S_1 \rightarrow S_0$ and the bound lumazine $S_0 \rightarrow S_1$.

It has been shown that in the case of FRET within a macromolecule, the anisotropy decay function will be:

$$r(t) = A_1\exp(-2k_T/3.1) + A_2(-t/\varphi)$$

where k_T is the rate of FRET. For the fluorescent transients from AF- and VH-luciferases (Fig. 13.9, *upper heavy line and dots*), there is hardly any effect, undetectable FRET consistent with no spectral shift or just a weak amount of effect on the bioluminescence in these luciferase reactions. The Förster critical distance R_0, at which $k_T = k_D = 1/\tau_D$ where τ_D =

10.6 ns the fluorescence lifetime of the donor, is estimated from the spectral parameters to be 22 Å. So for $k_T = 10\ k_D$ the donor acceptor separation must be at least 15 Å.

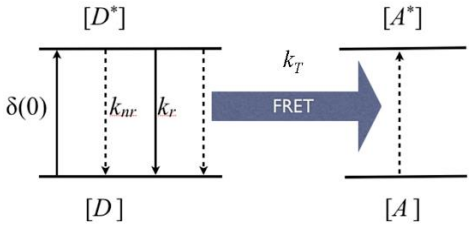

Figure 13.10. The probability of resonance coupling via FRET is represented by a rate k_T that is competitive with the radiative and non-radiative rates of the donor (D).

A more direct and accurate measurement of FRET is from the change in fluorescence intensity and lifetime of the donor (Fig. 13.10). Due to the greater separation of the relevant spectra, the donor-acceptor spectral overlap needed for the Förster equation can be determined more accurately for the yellow Y1-protein–Y1 luciferase system than the PL-system just described. Addition of the Y1-protein decreases the Y1-FT fluorescence signal and a fast fluorescence decay rate equated to k_T, appears in the decay. Fig. 13.11 shows a titration of the Y1-FT donor fluorescence signal at a wavelength of 480 nm where the Y1-protein fluorescence does not contribute, against additions of Y1-protein. The interaction is seen to have a close 1:1 stoichiometry. The Y1-FT fluorescence decay function for a concentration of 9 μM on addition of the Y1-protein (13 μM) is:

$$I(t) = 0.86\exp(-t/0.25) + 0.04\exp(-t/4.2) + 0.10\exp(-t/10.5).$$

The 4.2 ns lifetime is that due to a minor contamination of free FMN, the 10.5 ns is for the Y1-FT, and the 0.25 ns is k_T^{-1}. Plugging this 0.25 ns value into the Förster equation again with the known spectral parameters, yields a donor-acceptor distance about 20 Å. The same result was obtained from fluorescence decay using the combination of PL-FT and the yellow Y1-protein. It is remarkable that in this latter case, the $k_T = 4\ ns^{-1}$ is 10 times that for using the lumazine protein as acceptor, about the same as the ratio of spectral overlaps, in accordance with the Förster equation and giving good support for the postulated resonance coupling (Chapter 6).

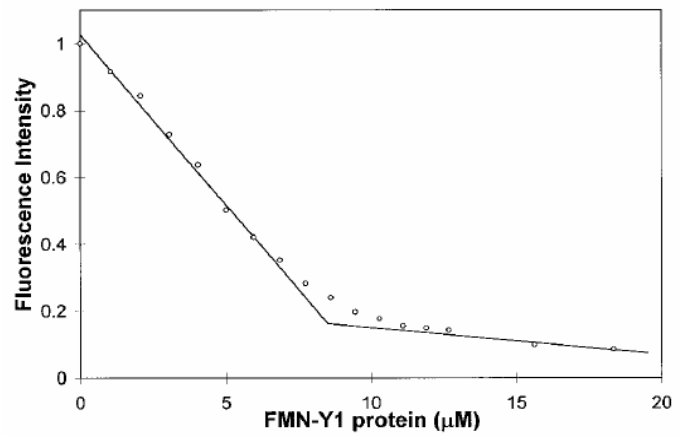

Figure 13.11. Titration of the fluorescence of Y-1 luciferase FT (9 μM) with FMN-Y1-protein shows a break around 9 μM consistent with 1:1 complex formation.

In summary, the antenna proteins found in the bioluminescent bacteria of the genus *Photobacterium*, lumazine protein, and the Y1-protein from the yellow bioluminescence bacteria *A. sifiae*, form complexes with fluorescent intermediates in the bacterial luciferase reaction. Within this complex the bioluminescence emitter, the fluorescent transient (FT) possibly a luciferase-bound 4a-hydroxyflavin, and the ligand of the antenna proteins, lumazine or FMN respectively, show weak resonance coupling of their excited electronic states, evidenced by the appearance of FRET between the pair. This property of FRET within the complex explains why the antenna proteins affect the bioluminescence spectra and kinetics at only micromolar concentrations. No or little spectral shift is observed in the reactions with AF-luciferase and VH-luciferase. Their fluorescent intermediates self-associate to dimeric complexes of two luciferase proteins and the antenna proteins do not interact with these luciferase dimers and consequently cannot engage in the coupling required for FRET. This accounts for the lack of bioluminescence shift in these cases.

It is evident that bacterial bioluminescence is a sensitized chemiluminescence distinct from the other well-investigated systems of the firefly or coelenterazine. The acceptor however, depends on the type of bacteria, those mainly from *Photobacterium* seem to prefer to use an antenna protein within a protein-protein complex, other types might use a fluorescent product of the reaction the FT being within a luciferase dimer containing the high energy donor. The picture is incomplete however; it is unfinished business.

Green-fluorescent Protein

The other antenna protein also occurring in marine bioluminescence systems, is the Green-fluorescent protein (GFP), probably the most famous protein in Science. The discovery of GFP by Shimomura in 1962, led to his award of a Nobel Prize in 2008 (Fig. 13.12). The fame of GFP however, is not because of the participation of GFP in bioluminescence where it was first identified, but because of the myriad applications of GFP as a fluorescent marker in

studies of gene expression, developmental biology, high-throughput screening, protein trafficking, imaging, clinical diagnostics, and additional commercial applications outside of Science. Reports on the role of GFP in bioluminescence are miniscule compared with those concerning its wide application, and a description of these is beyond the scope of our particular interest here, which is about the mechanism of function of GFP in bioluminescence systems.

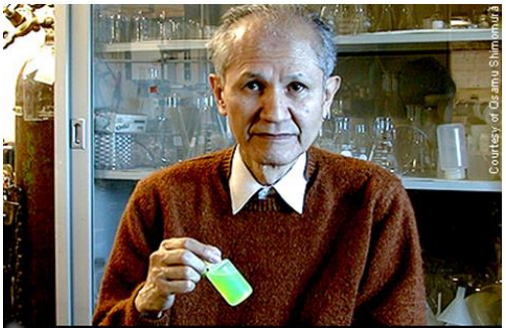

gure 13.12. Osamu Shimomura (1928-), Nobel 2008, Marine Biology Laboratory, Woods Hole, MA.

The fitness advantage of having a green emission for the many marine bioluminescent species is not known. Some organisms that utilize the same bioluminescence chemistry emit in the blue and lack GFP and to add to the puzzle, GFP-like proteins have been discovered in many other types of marine organisms that are not bioluminescent, corals, sea anemones, and others. Evidence has been presented that the function of these proteins in these non-bioluminescent animals is to lure prey. The GFPs occurring in bioluminescent organisms all have an efficient green fluorescence with type-dependent maxima in the range 497-509 nm. The fluorescence of the GFP-like proteins from non-bioluminescent organisms ranges from green into the red, with fluorescence efficiencies from almost unity to near zero. There are well over 200 entries for all the types of GFP in the Protein Data Bank. The spatial structures of GFPs form a distinct beta-barrel shape and they constitute a structurally homologous protein family. Despite this, the GFP structural family is another example of its members having weak identity of amino acid sequences.

The Renilla system provided the first convincing proof of GFP sensitized emission in an *in vitro* bioluminescence reaction, i.e., a “sensitized bioluminescence” so-called because it seemed to work on the same principle as sensitized fluorescence. Addition to Renilla luciferase of its luciferin, coelenterazine, generates a blue bioluminescence with a 485 nm maximum, but in the presence of only a micromolar concentration of Renilla GFP the bioluminescence spectral distribution becomes identical to the green fluorescence of GFP (Fig. 8.9). Also, there is an increase of Φ_B about three times over that in the absence of GFP. The Renilla luciferase bioluminescence shift was also shown to be specific in that GFP from other species within the genus *Renilla* worked, but GFP's from organisms more distantly related were less effective, and Aequorea GFP showed no effect at all at these micromolar concentrations. Interestingly, aequorin itself required more than 100 μM of its cognate Aequorea GFP to give the green bioluminescence *in vitro*. The same blue to green shift as in

the Renilla reaction is also found in the *in vitro* reaction of the Ca^{2+}-regulated photoprotein clytin (Fig. 13.13). Inclusion of Clytia GFP at only micromolar concentration produces a long wavelength shift of the bioluminescence spectrum towards the fluorescence of Clytia GFP itself. The effect here is also specific for the type of GFP, i.e., clytin bioluminescence is shifted by Clytia GFP but the closely related obelin needs a higher concentration of Clytia GFP to affect the same shift of its bioluminescence.

It is generally now agreed that in a bioluminescence system, GFP acts as an acceptor in a FRET process in which the luciferase or photoprotein product excited (S_1) state and the GFP ground (S_0) state transitions, are coupled in resonance within a protein-protein complex. According to the FRET equation again, several conditions must be met for FRET to be efficient (Chapter 6): substantial spectral overlap between the bioluminescence spectrum and the absorption spectrum of GFP, a strong fluorescence of the donor, a favorable orientation of the donor-acceptor transition dipoles, and a donor-acceptor separation usually of less than 50 Å. In the spectral shift experiments shown in Fig. 13.13, it is seen that the donor and acceptor are at only micromolar concentrations where their average separation would be greater than

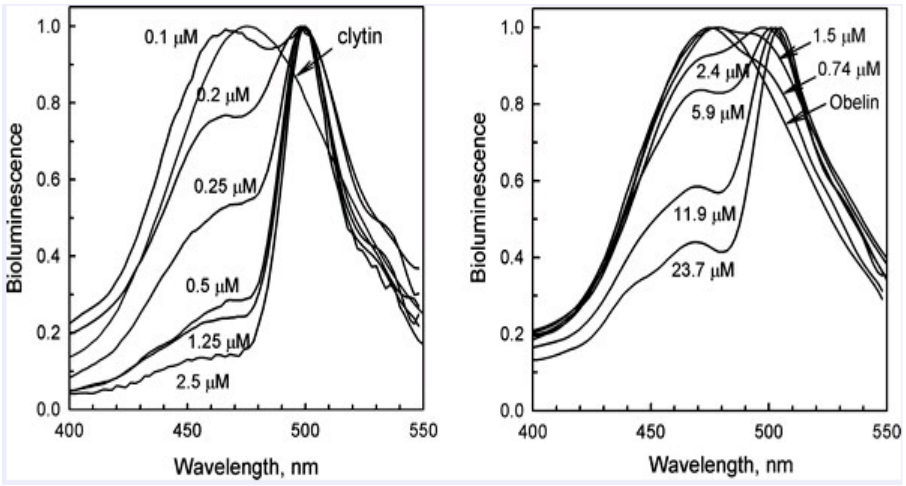

Figure 13.13. Inclusion of Clytia GFP shifts the photoprotein bioluminescence towards the fluorescence of GFP. Clytin (*left panel*) requires much smaller concentration of GFP to produce a noticeable shift than does obelin (*right panel*).

1000 Å were they not constrained within a protein-protein complex. The formation of such a complex has been indicated in the case of Renilla luciferase and its cognate Renilla GFP by a chromatographic technique called “Hummel-Dreyer gel filtration”. However, for clytin and Clytia GFP, no complex was observed with this same method. It is now known that a clytin-GFP complex is in fact formed but it is very weak, $K_D \sim 1$ mM (Fig. 12.28.), so the Renilla luciferase complex must be much stronger, but its K_D has not been determined. The question arises as to how such a weak clytin-GFP complex could be the one responsible for the FRET at micromolar levels, so it is proposed that GFP must have a stronger interaction with an intermediate in the reaction sequence. There is some circumstantial evidence to favor this idea in that if, using the computer-modeled spatial structure of the complex (Chapter 13), substitutions are made of residues in their sequences that are located within the protein-

protein interaction region, a decrease in the spectral shift effectiveness is found, implying a decrease in the reaction intermediate affinity for GFP. Another investigation was by stopped-flow which revealed that in the course of the <10 ms rise time of the bioluminescence after Ca^{2+} addition, the efficiency of bioluminescence FRET measured by the 510/470 nm intensity ratio increased at the same rate as the rise of bioluminescence intensity. This picture of a transient interaction is similar to that proposed for the binding of lumazine protein to a bacterial luciferase intermediate, and can be equally rationalized as being weak before reaction so as to allow unimpeded approach of substrates to the reaction site.

At this juncture we need to clarify again that in the literature, proposals about "energy transfer" have used terms that are imprecisely defined and lead to misunderstanding even today (Chapter 6). Consider the example of a spectrometer cuvette containing a solution of two different fluorescent molecules that are free in solution. Absorption of radiant energy into one of them results in its fluorescence emission that will be measured accurately by the spectrometer provided that the second molecule is sufficiently dilute. However, if the second molecule has an absorption spectrum that overlaps with the first fluorescence spectrum, the second molecule will be excited to its fluorescent state and the resultant emission spectrum will be a mixture of the two. This is genuinely a "Fluorescence Energy Transfer" because in fact, fluorescence itself is transferred. It is not sensitized fluorescence, it is a case of "far field" transfer, to be contrasted with the "near field" resonance condition that is the basis of FRET. Sometimes this far-field process is called the "trivial" transfer because it is so simply explained.

The FRET mechanism by which the antenna proteins transduce the bioluminescence exothermicity into their own fluorescence is, by analogy to the original observation of sensitized fluorescence, given the name "sensitized bioluminescence". In the recent literature reporting application methodology, the same idea is used to detect protein-protein interactions in cell systems for example, by labeling one protein with a luciferase and another with GFP. Again and misleadingly, the acronym BRET is used for "Bioluminescence Resonance Energy Transfer", which is incorrect because bioluminescence is not transferred, nor is it known if resonance transfer is precisely responsible. Note that in chemiluminescence systems, this spectral transduction is mostly by the Dexter mechanism.

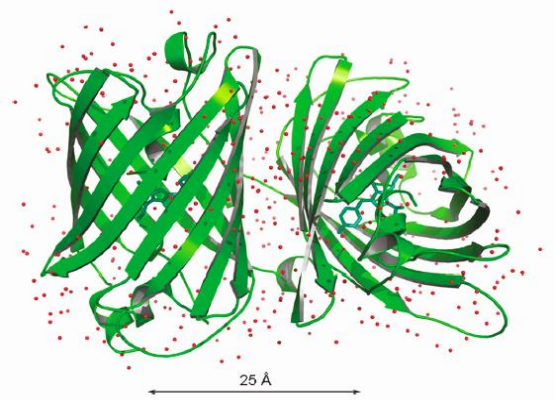

Figure 13.14. Structure of the Clytia GFP dimer showing the many protein bound water molecules (red balls).

The determined structure of Clytia GFP provides a good vehicle for testing the Förster equation. In the crystal as in solution, Clytia GFP is a dimer of mass 54 kDa (Fig. 13.14). The fluorescence decay is bi-exponential with a major (90%) component of 2.7 ns and minor one of 0.8 ns. The anisotropy decay also has two rotational correlation times, (20ºC) φ = 34 ns corresponding to the rotational diffusion of the 54 kDa dimer at this temperature, and a φ_T = 0.5 ns due to FRET between the two fluorophores. The 34 ns value is unchanged on dilution from 2 μM to 5 nM meaning that the dimer association is exceedingly strong. The red dots in the structure in Fig. 13.14 are the associated waters of crystallization and allow the reasonable assumption that the value to be taken for refractive index in the Förster expression, n = 1.6, should be the same as the one measured for a concentrated solution of amino acids. An analysis of anisotropy decay amplitudes yields a value for κ^2 = 1.08. Along with a measure of spectral overlap J, the Förster equation yields R_0 = 46 Å and R = 32 Å, the latter reasonably near the 25 Å separation observed in the crystal structure.

Anisotropy decay has already been shown to reveal protein-protein interaction in the bacterial bioluminescence system. The same measurement can be applied to find a possible complex with the clytin product, as only a very weak interaction with GFP was detected for the unreacted clytin, again far from the micromolar concentration required for the green bioluminescence spectral shift. Ca^{2+}-discharged clytin is fluorescent with a maximum at 510 nm but its absorbance maximum is at 340 nm and has no overlap with the GFP excitation band having a maximum around 470 nm. A tetrameric complex of two clytins and GFP dimer would have a mass of 76 kDa and therefore would show φ = 46 ns at 20ºC. Fig. 13.15 shows that the GFP φ = 33.6 ± 1 ns is not significantly increased even with 1000 times excess of Ca^{2+}-discharged clytin. There is no complex here, the same as with clytin before reaction.

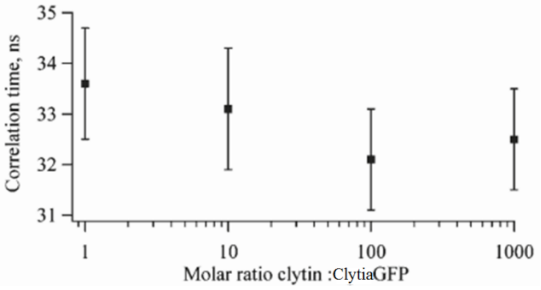

Figure 13.15. Addition of a great excess of Clytia GFP has no effect on the clytin rotational correlation time. The error bars are standard deviations of several measurements.

The conclusion has to be that the FRET complex has to be one with an intermediate in the light path, by analogy made to the one detected in the bacterial luciferase system. It is attractive to consider the computationally derived complex as the genuine structure in the bioluminescence FRET (Fig. 12.28). The spectral overlap is 1.3×10^{-13} $M^{-1}cm^3$ between the clytin bioluminescence and the absorption of Clytia GFP having a monomer extinction

coefficient of 64,000 M^{-1} cm^{-1} at 485 nm. Combined with the 45 Å separation of the donor and acceptor in the structure of the complex, and the fact that the GFP exists as a tight dimer, the consequence would be of a tetrameric structure binding two clytins and the donor-acceptor coupling should be very efficient. The energy from the clytin reaction should be quantitatively dumped into the fluorescence transition of the GFP. It remains to be established however, that the tight complex with the reaction intermediate does indeed form, and thus to be able to illuminate the picture.

14. Computational Bioluminescence

The recent and rapid evolution of fast computational technology underlies advances in many areas of Science. A few of these advances have been described here in earlier chapters, such as the statistical analysis of experimental data from bioluminescence kinetics and spectra, and the comparison of amino acid sequences among proteins, which extended to nucleic acid sequences, has expanded into the larger fields of "Bioinformatics" and "Big Data". In this chapter we will look at the present status of computational chemistry with the recent challenges of what can be called "Computational Biochemistry", the latest advances in computer technology allowing extension of computational chemistry to macromolecules.

Starting more than fifty years ago, *ab initio* methods were used to calculate the total energy of small molecular systems. By *ab initio* is meant that the properties taken for solution of the Schroedinger equation for a system were the charges on the nuclei and separately the electron orbitals. As the energy of a system of more than two interacting bodies cannot be solved analytically, this is the three-body problem mentioned before in Chapter 6, the method that has to be employed for molecular systems is that of "successive approximation". Initially each atom and its orbitals are positioned say, according to the spatial structure determined by X-ray crystallography, and the total energy, called the Hamiltonian ***H***, calculated considering the force field assumption, e.g., the Coulombic attractions and repulsions, the various strengths of bond stretching and bending, and the quantum mechanical correlations among the electronic orbitals. Then the atomic positions are perturbed slightly and ***H*** recalculated, and this repeated many times until achieving a lowest energy solution. This process is called "Self Consistent Field".

With the rapid improvement in computer power both in processing speed and the size of rapidly accessible memory storage, Computational Chemistry has become a well-matured sub-field of Chemistry. Both the structure and energy of complex chemical systems even as large as the coelenterazine molecule, can be calculated with good accuracy. Also computationally accessible, are structures and energies of intermediates occurring in reaction pathways, and even to the transition state complex itself, which is not amenable to direct experimental observation. The method of successive approximation is the same as employed for the gravitational N-body problem where the force field there is the gravitational attraction. The trajectory of the rocket vehicle carrying the Curiosity Rover from its liftoff, could be calculated with sufficient precision as to finally land it exactly on the intended site on Mars.

There are two approximations made initially to facilitate the solution of the Schroedinger equation for a multibody system. The first is the Born-Oppenheimer approximation, that the electronic motions of the electrons and nuclei can be determined separately then simply summed to give the total energy. The second is that the molecular orbitals (MO) can be constructed from a linear combination of atomic orbitals (LCAO) having certain coefficients (c). For example, for a diatomic molecule A-B:

$$\text{MO } \psi = c_A\psi_A + c_B\psi_B$$

Hartree-Fock theory (HF) is a simplified assumption that each electron experiences only a mean field from the remaining electron cloud. Higher levels of approximations such as “configurational interaction”, provide more accurate results but with greater demand on computational resources. For systems with not too many atoms, it is generally possible to obtain agreement between experimentally determined and computation molecular structure dimensions with ~1% accuracy, and other properties such as reaction enthalpies and free energies, dipole moments, infrared intensities and vibrational frequencies, with uncertainties all in the 2−5% range.

Density functional theory (DFT) is the most popular quantum mechanics method being less demanding than *ab initio* on computer resources. It is “functional” because the calculation requires starting from certain initial functions called “basis sets”, where it sets the number of electrons to consider and into which LUMO and HUMO orbitals they occupy. DFT makes use of average electron densities to obtain an initial guess for the orbitals. It is widely used for computational investigation for small molecules and is indispensable for large molecules. The computational effort for N atoms grows exponentially using *ab initio* quantum chemical techniques, whereas for DFT it increases only as N^3.

Semi-empirical methods are another approach to solving the Schroedinger equation. The known thermochemical data, e.g., heats of formation, are inserted into the calculation. For systems of N atoms, CPU and memory requirements for semi-empirical methods increase as ~ N^2 compared to *ab initio* up to ~ N^4. A software package GAUSSIAN is widely used for quantum mechanics computation as it incorporates many of these described approaches.

Advances in the field of computational chemistry allowed by availability of computer power and especially by the development of these software packages, has enabled the investigation of the properties of macromolecules, such as the spectral properties of protein ligands and pathways to enzyme catalysis; altogether we can call this field of study “Computational Biochemistry”. It is not within the scope of this text-book to provide expertise in this highly specialized and complex computational procedures, instead we will show examples of some results from studies of bioluminescence systems and mostly the ones involving coelenterazine. For a macromolecule a multiscaling procedure analogous to the Born-Oppenheimer approximation is used, separating the computation into two parts, an exact quantum mechanical computation for the small molecule of interest, a ligand or substrate like a luciferin, then subjecting this to perturbation by the electron clouds of the surrounding macromolecule whose spatial extent is determined by molecular mechanics (MM). This is a hybrid method called QM/MM, and is based on the assumption that the macromolecular system may be partitioned into an electronically important region requiring the QM treatment with the remainder, the surroundings acting only as an environmental perturbation. Studies using QM/MM have been made on the bioluminescence systems of bacteria, firefly, and the photoproteins. Commercial software packages for the MM computation having various force field assumptions are, AMBER, CHARMM, GROMUS, or OPLS-AA.

A number of computational studies of chemiluminescence and bioluminescence reactions utilizing the coelenterazine molecule have been made in the last few years. The questions addressed were about the initial step of the reaction of oxygen to form the stably bound 2-peroxy-coelenterazine, the conditions that stabilize this intermediate, the factors that lead to its decomposition to luminescence, the intermediates in the luminescence pathway, and the interactions that control the spectral properties of the final product coelenteramide. Quantum chemical calculations can provide information about electronic properties and energetics of unstable intermediates and transition states and thereby, may serve as essential and complementary insight for experimental interpretations. Explanations have been offered as to the origin of the observed spectral differences between photoprotein bioluminescence and the product fluorescence (Fig. 12.23). Some novel intermediates have been suggested for further investigation, and the role of hydrogen bonding as controlling emission spectra has been elucidated. Computational support has been given to identifying the longer wavelength blue bioluminescence band as originating from the 6-phenolate form of the product coelenteramide but with a conclusion contrary to that currently believed that the acting base, the proximate Histidine (His22 in obelin), is in the neutral state and not cationic.

An early study concerned the question of spin transitions required for the addition of molecular oxygen ($^3O_2$) which has a triplet ground state, onto the coelenterazine (an imidazopyrazine derivative, Im) to form the peroxide in a singlet ground state (^{1}Pox in Fig. 14.1), then its subsequent decomposition with high efficiency to the final product coelenteramide in its excited singlet state.

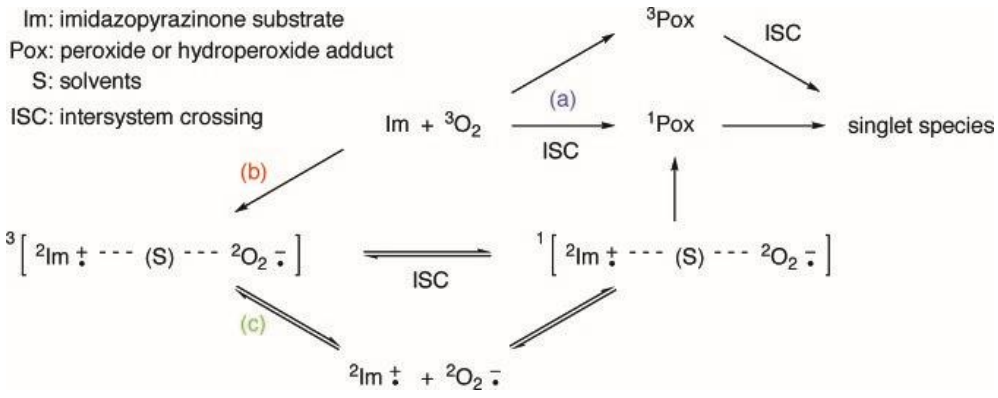

Figure 14.1. Three pathways to overcome the spin restriction inhibiting the reaction of triplet oxygen and an imidazopyrazine (Im + $^3O_2$). The top (*a*) direct production of triplet product ^{3}Pox followed by intersystem crossing (ISC) to the S_1 singlet species, is unlikely to be efficient. The lowest path (*c*) is the charge transfer superoxide route and does not involve intersystem crossing. A polar solvent (S) enhances separation of the radical pair which readily recombine to an overall singlet complex before chemical bonding.

Spin multiplicity changes from the initial triplet oxygen to the peroxide product in the singlet state, have to be accounted for in the course of the reaction. Numerical analysis showed the role of spin-orbit coupling in facilitating the molecular oxygen addition, involving the electron orbitals of the imidazopyrazinone (b). The middle process shows first an electron transfer to form the diradical pair remaining in the triplet state and separated by a polar solvent S. ISC changes the pair to a singlet followed by reaction to the peroxide ^{1}Pox. In the bioluminescence system this coupling would have to be regulated by the protein environment to inhibit intersystem crossing (ISC) to the ground state so as to allow maximum efficiency of generation of the singlet excited product coelenteramide in the overall reaction. The polarity of the environment, the anionic character, and the presence of hydrogen bonding as revealed by the spatial structure of the protein cavity, were shown to be important controlling features.

Electronic charge distribution around both the coelenterazine and the excited product coelenteramide support the assumption of the phenolate structure being the origin of the blue bioluminescence not the amide anion, because the N-1 position is more basic than the p-hydroxy of the 6-phenyl in both ground and excited states. As already concluded from observations of spectra of model compounds, the bimodal emission spectra originates from the neutral excited state of coelenteramide having a higher energy than the anion at wavelength maxima around 400 nm, the anion being responsible for the longer wavelength band. The small range of the anion peak wavelength among different types of photoproteins, was computed to be accounted for by the position of the proton, i.e., the degree of covalency over ionic character of the hydrogen bond from the 5-(p-hydroxy)phenyl substituent of the coelenteramide (CM) to the nitrogen of the proximate Histidine residue (His16 in aequorin, His22 in obelin, Fig. 14.2; also Fig.14.5).

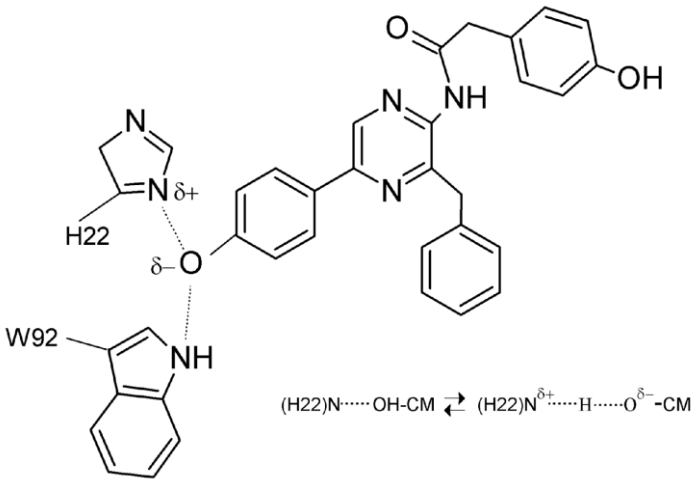

Figure 14.2. Ionic vs. covalency of H-bond accounts for the range of photoprotein spectra. CM is coelenteramide.

Figure 14.3 is the chemistry text-book picture for a chemical reaction pathway where for example, a diatomic molecule A−B separates into products A and B. The Reaction Coordinate can be equated to the A−B bond length for this simple model, but is designated as the degree of reaction for larger molecules. As the reaction proceeds the Gibbs free energy G reaches a maximum $\Delta G^{\ddagger}$ where the structure at this point is called the Transition State (TS). At this juncture there is a probability of either proceeding to products or returning to the reactant. A popular though naïve explanation of the mechanism of enzyme catalysis, is that the active cavity of an enzyme confines the structure and energy of the transition state to be degenerate with the product, i.e., having the same energy and structure as the product, thereby enhancing the probability of the forward reaction.

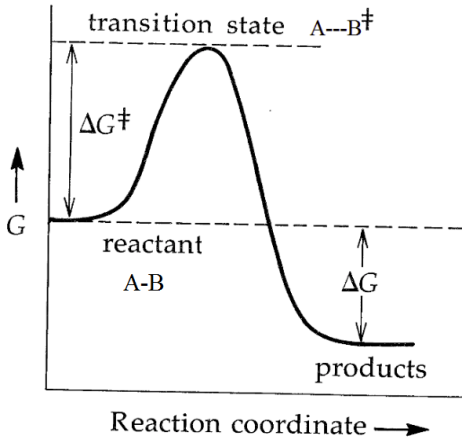

Figure 14.3. A simple picture of a chemical reaction where a diatomic A-B bond is energized until it reaches a transition state from which the stretched bond (A---B) breaks to go on to separated products or returns to the original diatomic. G is the Gibbs Free Energy and $\Delta G^{\ddagger}$ the energy barrier that has to be overcome to have a probability for forward reaction. The double dagger is the standard symbol for the transition state.

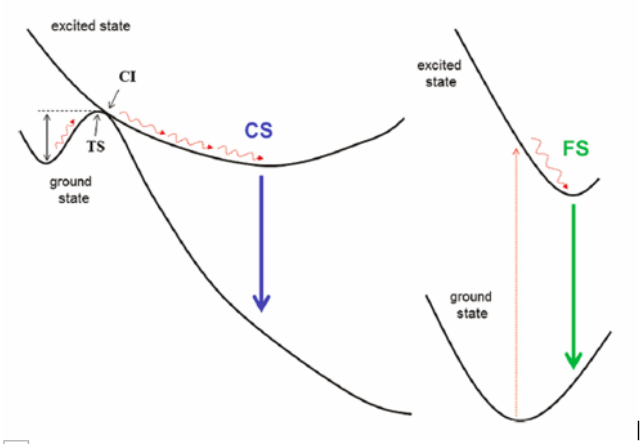

Figure 14.4. General scheme of the potential energy surface chemiluminescence (*left*) and fluorescence (*right*) emission. It shows that the initial chemiluminescence (**CS**) and fluorescence $S_{1,0} \rightarrow S_{0,0}$ (**FS**) states need not have the same emission energy. The transition state (**TS**) and conical intersection (**CI**) points related to the chemiluminescence excitation, are also shown.

This concept of transition state degeneracy is also employed to picture the mechanism of a chemiluminescence reaction. Fig. 14.4 the potential energy surface transition state (TS) intersecting the with the same co-ordinates as to be structurally and energetically degenerate with the excited state manifold of the product, and would have a good probability of crossing to this excited (S_1) chemiluminescence state (CS). The efficiency of the chemiluminescence emission then, is partly due to the partitioning of excited over ground state product manifolds indicated here in Fig. 14.3 by the intersection of the ground state and excited state potential energy envelopes at the point of TS, called a “conical intersection” (CI).

The decomposition pathway of the coelenterazine molecule was subject to a QM/MM computation with the intent of determining how the photoprotein cavity environment might enhance the probability of this crossing to the excited state. Three conditions were considered, first the molecule being only in a vacuum, second in a non-polar solvent to corresponding to the hydrophobicity of the photoprotein binding cavity, and third in a non-polar condition with inclusion of the influence of those amino acid side chains known from the spatial structure of the photoprotein to be interacting with the peroxycoelenterazine. These side chains are the ones from two triads of amino acid residues in obelin, Trp179 -Tyr190-His175 and His22-Trp92-Phe88, shown in Fig. 14.5.

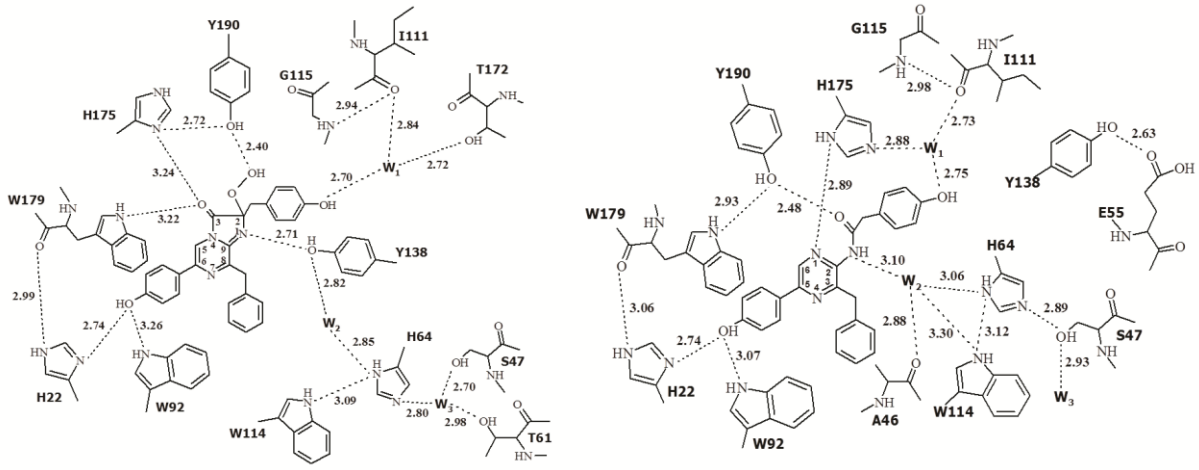

Figure 14.5. Hydrogen-bond (dashes) network of the binding cavity in obelin. The blue numbers are the separations for obelin before the bioluminescence reaction and the red for the fluorescent product as shown, all in angstroms (Å). For the computational study the neutral His175 that was only protonated on Nδ before the bioluminescence reaction was also protonated on Nε on the coelenteramide (red H). Other Histidine residues in the vicinity could also accept the leaving proton of the structure 2H in Fig. 14.7. The binding cavity is composed of the residues within 4 Å of coelenteramide.

The conclusion from this computation was contradictory to a previously accepted idea that the excited state ion pair or partial ion pair (Fig. 14.2) of the coelenteramide anion wss not formed, rather the His22 is in the neutral state and the hydrogen bond

proton must have migrated through a proton relay to one of the other Histidines within the binding cavity. One possibility is to the His175 (Fig. 14.5). This shows that the results of computation may lead to different conclusions depending on the approximations and other assumptions made for fitting the task into one's available computational budget. In the article in **In Depth** from Olivucci's group, it is pointed out that computational tools are not "Black Box", and considerable experience is vital in applying critical decisions that affect the validity of the model.

It was also shown that for the dioxetanone intermediate, external perturbation induces significant change in the energy levels of the transition state for homolytic splitting of the O−O bond. In the overall neutral state the transition state is 19.2 kcal/mol above the neutral dioxetane, whereas for the dioxetanone anion there could be an intramolecular charge transfer assisted splitting with this transition state only 7.8 kcal/mol above the anionic level. This charge transfer state is no doubt important for maximizing the bioluminescence efficiency. The anionic character could be assisted by either of the two amino acid triads shown in Fig.12.21.

Figure 14.6 is the computational result revealing three excited state structures following the decarboxylation of the coelenterazine dioxetanone, a conclusion based on the three energy minima along the reaction co-ordinate. The first "dimple" labeled CS, is small and it may be questioned whether it is a significant minimum considering the approximations that are involved in the QM/MM method. The red cross below the CS state is to reflect the calculation that the transition probability from this state is very small, so it is concluded that this transition could not contribute to the bioluminescence emission. The next minimum is labeled 2H* (Fig. 14.6) the neutral excited coelenteramide bioluminescence state (BS), the origin of the bioluminescence band with around a 420 nm maximum. Excited state proton transfer then forms the excited anion responsible for the natural blue bioluminescence with maxima in the 465-495 nm range depending on the type of photoprotein. The figure also indicates again, a possible difference in intersection of the fluorescence envelope (FS) and the BS. The alert reader might notice an error in Fig. 14.6 (taken from the reference), that the red emission line for 2H* BL representing the emission at shorter wavelength, should be larger than for the $2O^{-}$*BL. The FL emission is at an even smaller energy being at a longer wavelength than the BL in the cases of obelin and clytin.

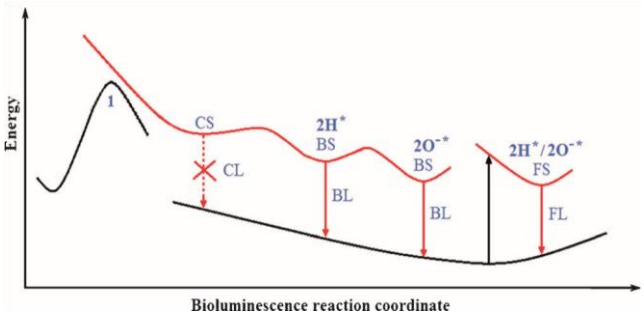

Figure 14.6. Schematic representation of the electronic states involved in the bioluminescence (BL) and fluorescence (FL) processes. The ground state is black and the first excited state is red.

It is proposed that this first excited intermediate CS is the coelenteramide diradical shown in Fig. 14.7. This would be consistent with the charge transfer nature of the transition state suggested in Fig. 14.5.

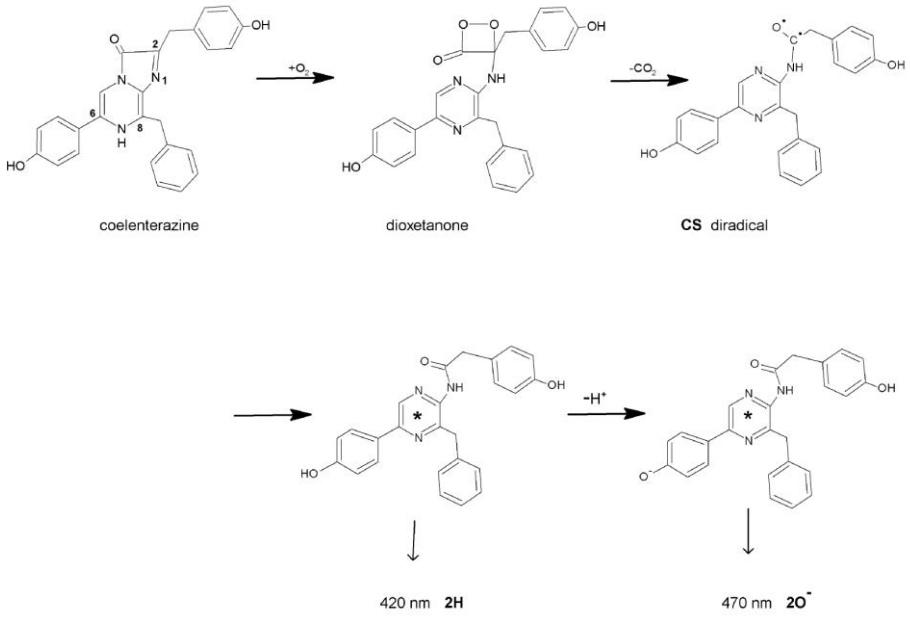

Figure 14.7. Bioluminescence reaction path of Ca^{2+}-regulated photoproteins is proposed to yield a primary diradical excited state **(CS)** which does not emit, followed by two excited products (*), the neutral coelenteramide **2H** and its phenolate **$2O^-$**.

This same computational approach has been applied also to the breakdown of the firefly anionic dioxetanone. A high level computation was performed for the molecule in vacuum and the result was consistent with an asynchronous mechanism. The classic CIEEL was discarded and the computationally preferred mechanism was a "Gradual Reversible Charge Transfer Induced Luminescence". The negative charge on the phenol ring becomes shared with the dioxetanone O—O bond which stretches first, therefore asynchronously to form a diradical, followed by stretching of the C—C bond. The computed CI intersects with the oxyluciferin S_1 potential energy function and the computed crossing efficiency is in the range of the observed bioluminescence excitation yield Φ_E. The reaction in vacuum therefore, is seen to be a believable model for the bioluminescence excitation in the firefly luciferase cavity.

Computational approaches have recently accounted for the high excitation yield of firefly bioluminescence and the possible oxyLH_2 conformations as well as interactions with protein bound waters within the active site, controlling the bioluminescence spectral shifts.

In summary, the remarkable success of computational chemistry engendered much enthusiasm for extending these methods to larger molecular systems, most recently to

Computational Biochemistry. We can mark this as the latest advance in technology mostly belonging to the 21st Century, which will provide much insight into this area of Science, which is the theme of this book. The first technological advance can be said to be the air-pump experiments of Boyle, and in the 20th Century the improved precision of spectroscopic methods, X-ray crystallography, and NMR.

At the present time a severe bottleneck arises because computational methods have to be pushed to the limits to be applied to macromolecular systems. Accuracy requires the QM part to be carried out with a high level computational method but along with the multitude of perturbations from the MM part, the computational cost becomes prohibitive. A compromise has to be made by using a lower level for the QM computation but then confidence in the results is lessened, especially in regards to calculations of spectroscopic properties or others involving rearrangements of electrons. There is little prospect that a desired orders of magnitude increase in computer speed, currently about 100 petaflops (10^{17} calculations-s^{-1}), to relieve this holdup, will be attained in the near future. A strong activity at present is "fragmenting", a multi-hybrid approach dividing the macromolecule up and computing the parts separately, thus allowing "parallelization" of the computation and getting around the "scaling" barrier, where the computational cost increases only linearly with the number of atoms instead of exponentially or greater. As with any new technology the interpretation of results and consequent predictions, deserve to be taken with due caution.

15. In Depth

Photobiological Sciences On-line is a source ebook maintained and continually updated by The American Society for Photobiology www.photobiology.info/#Biolum

Two recent hardcovers are:

Wilson, T., and Hastings, J.W. (2013) *Bioluminescence: Living Lights, Lights for Living*. Harvard University Press.

Shimomura, O. (2012) *Bioluminescence, Chemical Principles and Methods* (Revised Edition). World Scientific, Singapore.

Chapter 1. History. Bioluminescence and the Theory of Light

The content of this chapter is almost completely derived from the definitive and scholarly work of Harvey (1957).

Harvey, E.N. (1957) *A History of Luminescence from the Earliest Times until 1900*. The American Philosophical Society, Philadelphia.
https://archive.org/details/historyoflumines00harv

Needham, J., Wang, L., and Robinson, K.G. (1962) *Science and Civilization in China*, Vol. 4, Part 1 Physics, pp. 71−76. Cambridge University Press.

Lee, J. (2008). Bioluminescence: The first 3000 Years (Review). J Sib Fed U Biology 3:194−205. [PDF]. http://journal.sfu-kras.ru/series/biology/2008/3

Boyle, R. (1667) Obfervations and tryals about the Refemblances and Differences between a burning coal and Shining Wood. Phil Trans R Soc Lond 2:605−612.

Lee, J. (2009) A History of Bioluminescence. Photobiological Sciences Online (J Lee and KC Smith, eds.), American Society for Photobiology.
http://www.photobiology.info/HistBiolum/HistBiolum.html

Shapin, S., and Shaffer, S. (1985) *Leviathon and the Air Pump: Hobbes, Boyle, and the experimental life.* Princeton University Press.

Mythology. Reference to sea monsters also is found in ancient mythologies possibly also from genuine observations of bioluminescence. For example in the Talmud:

The body of the Leviathan, especially his eyes, possesses great illuminating power. This was the opinion of Rabbi Eliezer, who, in the course of a voyage in company with Rabbi Joshua, explained to the latter, when frightened by the sudden appearance of a brilliant light, that it probably proceeded from the eyes of the Leviathan. He referred his companion to the words of Job xli. 18: "By his neesings a light doth shine, and his eyes are like the eyelids of the morning" (B. B. l.c.). Wikipedia *http://en.wikipedia.org/wiki/Leviathan*

A TABLE OF THE CONDENSATION OF THE AIR

A	*A*	*B*	*C*	*D*	*E*	
48	12	00		$29\frac{8}{16}$	$29\frac{8}{16}$	*A A*. The number of equal spaces in the shorter leg, that contained the same parcel of air diversely extended
46	$11\frac{1}{2}$	$01\frac{7}{16}$		$30\frac{9}{16}$	$33\frac{6}{16}$	
44	11	$02\frac{3}{16}$		$31\frac{5}{16}$	$31\frac{13}{16}$	
42	$10\frac{1}{2}$	$04\frac{6}{16}$		$33\frac{8}{16}$	$33\frac{1}{7}$	
40	10	$06\frac{3}{16}$		$35\frac{6}{16}$	35	
38	$9\frac{1}{2}$	$07\frac{14}{16}$		37	$36\frac{15}{16}$	*B* The height of the mercurial cylinder in the longer leg, that compressed the air into those dimensions.
36	9	$10\frac{2}{16}$		$39\frac{6}{16}$	$38\frac{7}{8}$	
34	$8\frac{1}{2}$	$12\frac{8}{16}$		$41\frac{12}{16}$	$41\frac{8}{17}$	
32	8	$15\frac{1}{16}$		$44\frac{3}{16}$	$43\frac{11}{16}$	
30	$7\frac{1}{2}$	$17\frac{15}{16}$		$47\frac{1}{16}$	$46\frac{3}{6}$	
28	7	$21\frac{3}{16}$		$50\frac{5}{16}$	50	*C* The height of the mercurial cylinder, that counterbalanced the pressure of the atmosphere.
26	$6\frac{1}{2}$	$25\frac{3}{16}$		$54\frac{5}{16}$	$53\frac{10}{13}$	
24	6	$29\frac{11}{16}$		$58\frac{13}{16}$	$58\frac{3}{8}$	
23	$5\frac{3}{4}$	$32\frac{3}{16}$		$61\frac{5}{16}$	$60\frac{18}{23}$	
22	$5\frac{1}{2}$	$34\frac{15}{16}$		$64\frac{1}{16}$	$63\frac{6}{11}$	
21	$5\frac{1}{4}$	$37\frac{15}{16}$		$67\frac{1}{16}$	$66\frac{4}{7}$	*D* The aggregate of the two last columns, *B* and *C*, exhibiting the pressure sustained by the included air.
20	5	$41\frac{9}{16}$		$70\frac{1}{16}$	70	
19	$4\frac{3}{4}$	45		$74\frac{3}{16}$	$73\frac{11}{16}$	
18	$4\frac{1}{2}$	$48\frac{3}{8}$		$77\frac{1}{16}$	$77\frac{9}{13}$	
17	$4\frac{1}{4}$	$53\frac{11}{16}$		$82\frac{13}{16}$	$82\frac{4}{17}$	
16	4	$58\frac{3}{16}$		$87\frac{14}{16}$	$87\frac{3}{8}$	*E* What that pressure should be according to the hypothesis, that supposes the pressures and expansions to be in reciprocal proportion.
15	$3\frac{3}{4}$	$63\frac{15}{16}$		$93\frac{1}{16}$	$93\frac{1}{2}$	
14	$3\frac{1}{2}$	$71\frac{6}{16}$		$100\frac{7}{16}$	$99\frac{4}{7}$	
13	$3\frac{1}{4}$	$78\frac{11}{16}$		$107\frac{13}{16}$	$107\frac{7}{13}$	
12	3	$88\frac{7}{16}$		$117\frac{9}{16}$	$116\frac{4}{8}$	

Added to $22\frac{8}{5}$ makes

R. Boyle (1662) A defense of the doctrine touching the spring and the weight of the air. *New Physico-mechanical Experiments.*London. https://archive.org/details/lawsofgasesmemoi028650mbp

Chapter 2. Bioluminescence to 1950. Biology, Biochemistry, and Physics

Harvey, E.N. (1952) *Bioluminescence*. Academic Press, New York.

Johnson, F.H. (Ed.) (1955). *The Luminescence of Biological Systems*. American Association for the Advancement of Science, Washington, D.C.

https://archive.org/details/luminescenceofbi00nati

McElroy, W.D. (1947) The energy source for bioluminescence in an isolated system. Proc Natl Acad Sci USA 33:342−345.

Tsuji, F.I. (2010) Early history, discovery, and expression of Aequorea green fluorescent protein, with a note on an unfinished experiment. Microsc Res Tech 73:785−796. doi: 10.1002/jemt.20821.

Esimbekova, E., and Kratasyuk V. (2015) Analytical applications of luminous bacteria enzymes. Photobiological Sciences Online (J Lee and KC Smith, eds.), American Society for Photobiology. http://www.photobiology.info/Kratasyuk.html

Oba, Y., and Darrin D.T. (2014) Eco-Evo bioluminescence on land and in the sea. Adv Biochem Eng Biotech 144:3−36.

Branchini, B.R., Southworth, T.L., Salituro1, L.J., Fontaine, D.M., and Oba, Y. (2016) Cloning of the blue ghost (*Phausis reticulata*) luciferase reveals a glowing source of green light. Photochem Photobiol 93:473−478.

Chapter 3. Bioluminescence in the 1950s. Johns Hopkins and Princeton Universities, and Oak National Laboratory

McElroy, W.D., Hastings, J.W., Sonnefeld, V., and J. Coulombre J. (1953) The requirement of riboflavin phosphate for bacterial luminescence. Science 118:385−386.

Strehler, B.L., and Cormier, M.J. (1954) Isolation, identification, and function of long chain fatty aldehydes affecting the bacterial luciferin-luciferase reaction. J Biol Chem 211:213−225.

Strehler, B.L., and Totter, J.R. (1954) Determination of ATP and related compounds. Firefly luminescence and other methods. Methods Biochem Anal 1:341−356.

Green, A.A, and McElroy, W.D. (1955) Crystalline firefly luciferase. Biochim Biophys Acta 20:170−176.

Cormier, M.J., and Totter, J. (1957) Quantum efficiency determinations on the components of components of the bacterial luminescence system. Biochim Biophys Acta 25: 229−237.

Seliger, H.H., and McElroy, W.D. (1959) Quantum yield of the oxidation of firefly luciferin. Biochem Biophys Res Commun 1:21−24.

White, E.H., McCapra, Field, G., and McElroy, W.D. (1961) The structure and synthesis of firefly luciferin. J Am Chem Soc 85:337−343.

Shimomura, O., Johnson, F.H., and Saiga, Y. (1962) Extraction, purification, and properties of aequorin, a bioluminescent protein from the luminous hydromedusan, *Aequorea*. J Cell Comp Physiol 59:223−239.

Hastings, J.W. (2011) Progress and Perspectives on Bioluminescence: from Luminous Organisms to Molecular Mechanisms. In, *Chemiluminescence and Bioluminescence: Past, Present and Future* (Roda, A., ed.) Royal Society of Chemistry (London).

Oba,Y., Stevani, C.V., Oliveira, A.G., Tsarkova, A.S., Chepurnykh,T.V., and Yampolsky, I.V. (2017) Selected least studied but not forgotten bioluminescent systems. Photochem Photobiol 93:405−415.

Petushkov, V.N., Dubinnyi, M.A., Tsarkova, A.S., Rodionova, N.S., Baranov, M.S., Kublitski, V.S., Shimomura, O., Yampolsky I.V. (2014) A Novel Type of Luciferin from the Siberian Luminous Earthworm *Fridericia heliota*: Structure Elucidation by Spectral Studies and Total Synthesis. Angew Chem Int Ed 53:5566−5568. DOI: 10.1002/anie.201400529

Rodionova, N.S., Rota, E., Tsarkova, A.S., and Petushkov, V.N. (2017) Progress in the study of bioluminescent earthworms. Photochem Photobiol 93:416−428.

Kuse, M. (2014) Chromophores in photoproteins of a glowing squid and mollusk. Biosci Biotech Biochem 78:731−736.

Purtov, K.V., Petushkov, V.N., Baranov, M.S., Mineev, K.S., Rodionova, N.S., Kaskova, Z.M., Tsarkova, A.S., Petunin, A.I., Bondar,V.S., Rodicheva, E.K., Medvedeva, S.E., Oba, Y., Oba, Y., Arseniev, A.S., Lukyanov, S., Gitelson, J.I., and Yampolsky, I.V. (2015) The Chemical basis of fungal bioluminescence. Angew Chem Int Ed 54:8124–8128.

Tsarkova, A.S., Kaskova, Z.M., and Yampolsky, I.V. (2016) A Tale Of two luciferins: fungal and earthworm new bioluminescent systems. Acc Chem Res 49:2372−2380.

Chapter 4. Bioluminescence Kinetics

Atkins, P., and de Paulo, J. (2011). *Physical Chemistry for the Life Sciences*. 2nd Edition (Oxford, UK).

Markova, S.V, Vysotski, E.S., Blinks, J.R., Burakova, L.P., Wang, B-C., and Lee, J. (2002) Obelin from the bioluminescent marine hydroid *Obelia geniculata*: Cloning, expression, and comparison of some properties with those of other Ca^{2+}-regulated photoproteins. Biochemistry 41:2227-2236.

DeLuca, M., and McElroy, W.D. (1974) Kinetics of the firefly luciferase catalyzed reactions. Biochemistry 13:921−925.

Denburg, J.L., and McElroy, W.D. (1970) Catalytic subunit of firefly Luciferase. Biochemistry 9:4619−4624.

Strehler, B.L. (1955) Factors and biochemistry of bacterial bioluminescence. In, *The Luminescence of Biological Systems* (F.H. Johnson, Ed.) pp. 209−255. American Association for the Advancement of Science, Washington, DC, 1955. https://archive.org/details/luminescenceofbi00nati

Hastings, J.W., and Gibson, Q.H. (1963) Intermediates in the bioluminescent oxidation of reduced flavin mononucleotide. J Biol Chem 238:2537−2554.

Matheson, I.B.C., and Lee, J. (1983) Kinetics of bacterial bioluminescence and the fluorescent transient. Photochem Photobiol 38:231−240.

Suade, C., Nijvipakul1, S., Svasti1, J., Entsch B., Ballou, D.P., and Chaiyen, P. (2007) Luciferase from *Vibrio campbellii* is more thermostable and binds reduced FMN better than its homologues. J Biochem 142:539−552.

Chapter 5. Quantum Yields

Seliger, H.H., and McElroy, W.D. (1965) *Light: Physical and Biological Action*. Academic Press, N.Y.

Lee, J., and Seliger, H.H. (1965) Absolute spectral sensitivity of phototubes and the application to the measurement of the absolute quantum yields of chemiluminescence and bioluminescence. Photochem Photobiol 4:1015−1048.

Ando, Y., Niwa, K., Yamada, N., Irie, T., Enomoto, T., Kubota, H., Ohmiya Y., and Akiyama, H. (2007) Development of a quantitative bio／chemiluminescence spectrometer determining quantum yields: Re-examination of the aqueous luminol chemiluminescence standard. Photochem Photobiol 83:1205−1210.

Wang, Y., Kubota, H., Yamada, N., Irie, T., and Akiyama H. (2011) Quantum yields and quantitative spectra of firefly bioluminescence with various bivalent metal ions. Photochem Photobiol 87:846–852.

Chapter 6. Quantitative Spectroscopy

Seliger, H.H. (1978) Excited states and absolute calibrations in bioluminescence. Methods Enzymol 57:560-600.

Visser, A.J.W.G., and Rolinski, O.J. (2017) Photobiological Sciences Online (J Lee and KC Smith, eds.), American Society for Photobiology http://www.photobiology.info/Visser-Rolinski.html/

Parker, C.A. (1968) *Photoluminescence of Solutions*. Elsevier, Amsterdam.

Velapoldi, R.A., and Mielenz, K.D. (1980) A Fluorescence standard reference material: Quinine sulfate dihydrate. National Bureau of Standards, Washington, D.C. http://www.nist.gov/srm/upload/SP260-64.PDF

Chen, S.F., Ferré, N., and Liu, Y-J. (2013) QM/MM study on the light emitters of aequorin chemiluminescence, bioluminescence, and fluorescence: A general understanding of the bioluminescence of several marine organisms. Chem Eur J 19:8466−8472.

Visser, A.J.W.G., Vysotski, E.S., and Lee, J. (2010) Photobiological Sciences Online (J Lee and KC Smith, eds.), American Society for Photobiology. http://photobiology.info/Experiments/Biolum-Expt.html

Lee, J. (2017) Perspectives on bioluminescence mechanisms. Photochem Photobiol 93:389−404.

Chapter 7. Chemiluminescence

Baader, W.J., Stevani, C.V., and Bastos, E.L. (2009) Chemiluminescence of organic peroxides. In, *PATAI's Chemistry of Functional Groups*, pp.1-68. John Wiley, NY. DOI: 10.1002/9780470682531.pat0362.

Adam, W., and Trofimov, A.V. (2006) Contemporary trends in dioxetane chemistry. In, *The Chemistry of Peroxides*, Vol. 2 (Z. Rapoport, ed.) John Wiley, N.Y.

Augusto F.A., de Souza GA, Souza SP Jr, Khalid, M., and Baader W.J. (2013) Efficiency of electron transfer initiated chemiluminescence. Photochem Photobiol 89:1299−1317.

Augusto F.A., Frances-Monerris, A., Galvan, I.F., Roca-Sanjuan, D., Bastos, E.L., Baader, W.J. and Lindh, R. (2017) Mechanism of activated chemiluminescence of cyclic peroxides: 1,2-dioxetanes and 1,2-dioxetanones. Phys Chem Chem Phys 19:3955−3962.

Gunderman, K.-D., and McCapra, F. (1987) *Chemiluminescence in Organic Chemistry*. Springer-Verlag, Berlin.

Schaap, A.P., Handley, R.S., and Giri, B.P. (1987) Chemical and enzymatic triggering of 1,2-dioxetanes. Tetrahedron Lett 28:935−938.

Matsumoto, M., Mizoguchi, Y., Motoyama, T., and Watanabe, N. (2001) Base-induced chemiluminescence of 5-*tert*-butyl-1-(4-hydroxybenz[*d*]oxazol-6-yl)-4,4-dimethyl-2,6,7-trioxabicyclo[3.2.0]heptanes: chemiluminescence–chemiexcitation profile in aqueous medium. Tetrahedron Lett 42:8869–8872.

Matsumoto, M. (2004) Advanced chemistry of dioxetane-based chemiluminescent substrates originating from bioluminescence. J Photochem Photobiol C: Photochem Reviews 5:27–53.

Matsumoto, M., and Watanabe, N. (2005) Structural aspects of 1,2-dioxetanes active toward intramolecular charge-transfer-induced chemiluminescent decomposition. Bull Chem Soc Jpn 78:1899–1920.

Matsumoto, M, Tanimura, M., Akimoto, T., Watanabe, N., and Ijuin, H.K. (2008) Solvent-promoted chemiluminescent decomposition of a bicyclic dioxetane bearing a 4-(benzothiazol-2-yl)-3-hydroxyphenyl moiety. Tetrahedron Lett 49:4170–4173.

Matsumoto, M., Watanabe, N., Hoshiya, N., and Ijuin, H.K. (2008a) Color modulation for intramolecular charge-transfer-induced chemiluminescence of 1,2-dioxetanes. Chem Rec 8:213–228.

Ciscato, L.F.M.L., Bartoloni, F.H., Bastos, E.L., and Baader, W.J. (2009) Direct kinetics observation of the chemiexcitation step in peroxyoxalate chemiluminescence. J Org Chem 74:8974–8979.

Ciscato, L.F.M.L., Bartoloni, F.H, Weiss, D., Beckert, R., and Baader W.J. (2010) Experimental evidence of the occurrence of intramolecular electron transfer in catalyzed 1,2-dioxetane decomposition. J Org Chem 75:6574–6580.

Ciscato, L.F.M.L., Bartoloni, F.H., Colavite, A.S., Weiss, D., Beckert, R., and Schramm. S. (2014) Evidence supporting a 1,2-dioxetanone as an intermediate in the benzofuran-2(3H)-one chemiluminescence. Photochem Photobiol Sci 13:32−37.

Oliveira, M.A. de, Bartoloni, F.H., Augusto, F.A., Ciscato, L.F.M.L., Bastos, E.L, and Baader, W.J. (2012) Revision of singlet quantum yields in the catalyzed decomposition of cyclic peroxides. J Org Chem 77:10537−10547.

Catalani, L.H., and Wilson, T. (1989) Electron Transfer and Chemi-luminescence. Two Inefficient Systems: 1,4-Dimethoxy-9,10-diphenylanthracene peroxide and diphenoyl peroxide. J Am Chem Soc 111:2633−2639.

Bartoloni, F.H., Oliveira, M.A. de, Ciscato, L.F.M.L., Augusto, F.A., Bastos,E.L., and Baader, W.J. (2015) Chemiluminescence efficiency of catalyzed 1,2-dioxetanone decomposition determined by steric effects. J Org Chem 80:3745−3751.

Khalid, M., Oliveira, M.A., Souza, S.P. Jr., Ciscato, L.F.M.L., Bartoloni, F.H., and Baader, W.J. (2015) Efficiency of intermolecular chemiluminescence systems lacks significant solvent cavity effect in binary toluene/diphenylmethane mixtures. J Photochem Photobiol Sci A: Chemistry 312:81–87.

Bos, R., Barnett, N.W., Dyson, G.A., Lim, K.F., Russell, R.A., and Watson, S.P. (2004) Studies on the mechanism of the peroxyoxalate chemiluminescence reaction Part 1. Confirmation of 1,2-dioxetanedione as an intermediate using 13C nuclear magnetic resonance spectroscopy. Anal Chim Acta 502:141–147.

Bos, R., Tonkin, S.A., Hanson, G.R., Hindson, C.M., Lim, K.F., and Barnett, N.W. (2009) In search of a chemiluminescence 1,4-dioxy biradical, J Am Chem Soc 131:2770−2771.

Chapter 8. Marine Bioluminescence and Coelenterazine.

There's no such thing as a jellyfish. http://www.jellywatch.org/video

Ohmiya, Y., and Hirano, T. (1996) Shining the light: the mechanism of the bioluminescence reaction of calcium-binding proteins. Chem Biol 3:337−347.

Vysotski, E.S., and Lee, J. (2004) Ca^{2+}-regulated photoproteins: structural insight into the bioluminescence mechanism. Acc Chem Res 37:405−415.

Shimomura O. (2005) The discovery of aequorin and green fluorescent protein. J Micros 217:3–15.

Hirano, T., Takahashi, Y., Kondo, H., Maki, S., Kojima, S., Ikeda H., and Niwa H. (2008) The reaction mechanism for the high quantum yield of *Cypridina* (*Vargula*) bioluminescence supported by the chemiluminescence of 6-aryl-2-methylimidazo[1,2-a]pyrazin-3(7H)-ones (*Cypridina* luciferin analogues). Photochem Photobiol Sci 7:197–207.

Kuse M. (2014) Chromophores in photoproteins of a glowing squid and mollusk. Biosci Biotech Biochem 78:731−736.

Markova, S.V, Larionova, M.D, Burakova, L.P, and Vysotski, E.S. (2015) The smallest natural high-active luciferase: Cloning and characterization of novel 16.5-kDa luciferase from copepod *Metridia longa*. Biochem Biophys Res Commun. 457: 77−82.

Markova, S.V, and Vysotski, E.S. (2015) Coelenterazine-dependent luciferases. Biochemistry (Mosc) 80:714−732.

Burakova, L.P., Natashin, P.V., Markova, S.V., Eremeeva, E.V., Malikova, N.P., Cheng, C., Liu, Z-J., and Vysotski, E.V. (2016) Mitrocomin from the jellyfish *Mitrocoma cellularia* with deleted C-terminal tyrosine reveals a higher bioluminescence activity compared to wild type photoprotein. J Photochem Photobiol B: Biology 162:286−297.

Chapter 9 Bioluminescence of Beetles

Seliger, H.H., and McElroy, W.D. (1964) The colors of firefly bioluminescence: enzyme configuration and species specificity. Proc Nat Acad Sci USA 52:75−81.

Inouye, S. (2010) Firefly luciferase: an adenylate-forming enzyme for multicatalytic functions. Cell Mol Life Sci 67:387–404.

Branchini, B.R., Rosenberg, J.C., Fontaine, D.M., Southworth, T.L., Behney, C.E., and Uzasci, L. (2011) Bioluminescence is produced from a trapped firefly luciferase conformation predicted by the domain alternation mechanism. J Am Chem Soc 133:11088−11091.

Sundlov, J.A, Fontaine, D., Southworth, T.L., Branchini, B.R., and Gulick, A.M. (2012) Crystal structure of firefly luciferase in a second catalytic conformation supports a domain alternation mechanism. Biochemistry 51:6493−6495.

Branchini, B.R. (2013) Chemistry of firefly bioluminescence. Photobiological Sciences Online, (J lee and KC Smith eds.) American Society for Photobiology http://www.photobiology.info/Branchini2.html

Kaskova, Z.M., Tsarkova A.S. and Yampolsky, I.V. (2016) 1001 lights: Luciferins, luciferases, their mechanisms of action and applications in chemical analysis, biology and medicine. Chem Soc Rev 45:6048−6077.

Oba, Y., Branham M.A, and Fukatsu, T. (2011) The Terrestrial Bioluminescent Animals of Japan. Zoological Science 28:771–789. http://www.bioone.org/doi/full/10.2108/zsj.28.771

Viviani, V. (2009) Terrestrial Bioluminescence, Biological and Biochemical Diversity. Photobiological Sciences Online (J Lee and KC Smith eds.) American Society for Photobiology. http://www.photobiology.info/Viviani.html

Naumov, P., Ozawa, Y., Ohkubo, K., and Fukuzumi, S. (2009) Structure and spectroscopy of oxyluciferin, the light emitter of the firefly bioluminescence. J Am Chem Soc 131:11590−11605.

Ghose, A., Rebarz, M., Maltsev, O.V., Hintermann, L., Ruckebusch, C., Fron, E., Hofkens, J., Mély, Y., Naumov, P., Sliwa, M., and Didier, P. (2015) Emission properties of oxyluciferin and its derivatives in water: Revealing the nature of the emissive species in firefly bioluminescence. J Phys Chem B 119:2638−2649.

Mofford, D.M., Reddy, G.R., and Miller, S.C. (2014) Latent luciferase activity in the fruit fly revealed by a synthetic luciferin. Proc Natl Acad Sci USA 111:4443−4448.

Adams, S.T. Jr., Mofford, D.M., Reddy, G.S.K.K., and Miller, S.C. (2016) Firefly luciferase mutants allow substrate-selective bioluminescence imaging in the mouse brain. Angew Chem Int Ed. 55:4943 –4946.

Oba Y., and Schultz, D.T. (2014) Eco-Evo Bioluminescence on land and in the sea. Adv Biochem Eng Biotech 144:3−36.

Viviani, V.R., A. Simões, A., Bevilaqua, V.R., Gabriel, G.V.M., Arnoldi, F.G.C., and Hirano, T. (2016) Glu311 and Arg337 stabilize a closed active-site conformation and provide a critical catalytic base and countercation for green bioluminescence in beetle luciferases. Biochemistry 55:4764−4776.

Branchini, B.R., Southworth, T.L., Fontaine, D.M., Murtiashaw, M.H., McGurk, A., Talukder, M.H., Qureshi, R., Yetil, D., Sundlov, J.A., and Gulick, A.M. (2017) Cloning of the orange light-producing luciferase from *Photinus scintillans*−A new proposal on how bioluminescence color is determined. Photochem Photobiol 93: 479−485.

Amaral, D.T., Oliveira, G., Silva, J.R., and Viviani, V.R. (2016) A new orange emitting luciferase from the Southern-Amazon *Pyrophorus angustus* (Coleoptera: Elateridae) click-beetle: structure and bioluminescence color relationship, evolutional and ecological considerations. Photochem Photobiol Sci 15:1148−1154.

Chapter 10 Bacterial Bioluminescence

Lee, J. (1985) The Mechanism of Bacterial Bioluminescence. In, *Chemi- and Bioluminescence*. (JG Burr, ed.). pp. 401−437. Dekker, New York.

Wang, Z., Hervey, W.J.IV, Kim, S., Lin, B., and Vora, G.J. (2015) Complete genome sequence of the bioluminescent marine bacterium *Vibrio harveyi* ATCC 33843 (392 [MAV]). Genome Announc 3:e01493-14. doi:10.1128/genomeA.01493−14.

Ziegler, M.M., and Baldwin, T.O. (1982) Biochemistry of Bacterial Bioluminescence. In, *Current Topics in Bioenergetics.* (DR Sanadi, ed.) 12:65−113.

Baldwin, T.O., and Ziegler, M.M. (1992) The Biochemistry and Molecular Biology of Bacterial Luminescence. In, *Chemistry and Biochemistry of Flavoenzymes.* (F Müller ed.) Vol. 3. pp. 467−530. CRC Press, Boca Raton.

Lee, J., Matheson, I.B.C., Müller, F., O'Kane, D.J., Vervoort, J., and Visser, A.J.W.G. (1991) The Mechanism of Bacterial Bioluminescence. In, *Chemistry and Biochemistry of Flavoenzymes*. (F. Müller, ed.) Vol. 2. pp. 110−147. CRC Press, Boca Raton.

McCapra, F. (2000) Chemical generation of excited states. The basis for chemiluminescence and bioluminescence. Methods Enzymol 305:3-47.

Sheperd, P.T., and Bruice, T.C. (1980) Formation of a nonchemiluminescence excited state species in the decomposition of 4a-(alkylperoxy)flavins. J Am Chem Soc 102:7774−7778.

Kaaret, T.W., and Bruice, T.C. (1990) Electrochemical luminescence with N(5)-ethyl-4a-hydroxy-3-methyl-4a,5-dihydrolumiflavin. The mechanism of bacterial luciferase. Photochem Photobiol 91:629−633.

Lee, J. (1993) Lumazine protein and the excitation mechanism in bacterial bioluminescence. Biophys Chem 48:149−158.

Nemtseva, E.V., and Kudryaseva, N. S. (2007) The mechanism of electronic excitation in the bacterial bioluminescence reaction. Russ Chem Rev 76:91−100.

Wilson, T., and Hastings, J.W. (1998) Bioluminescence. Annu Rev Cell Dev Biol 14: 197−230.

Dunlap, P. (2014) Biochemistry and genetics of bacterial bioluminescence. Adv Biochem Eng Biotech 144:37−64.

Jiang, T., Wang, W., Wu, X., Wu, W., Bai, H., Ma, Z., Shen, Y., Yang, K., and Li, Y. (2016) Discovery of new substrates for *LuxAB* bacterial bioluminescence. Chem Biol Drug Des 88:197−208.

Brodl, E., Ivkovic, J., Tabib, C.R., Breinbauer, R., and Macheroux, P. (2017) Synthesis of α,β-unsaturated aldehydes as potential substrates for bacterial luciferases. Bioorg Med Chem 25:1487−1495.

Luo, Y., and Liu, Y-J. (2014) Bioluminescence and flavin mononucleotide fluorescence quenching of bacterial bioluminescence−a theoretical study. Chem Eur J 22:16243−16249.

Gozem, S., Mirzakulova, E., Schapiro, I., Melaccio, F., and Glusac, K.D. (2014) A conical intersection controls the deactivation of the bacterial luciferase fluorophore. Angew Chem Int Ed 53:9870–9875.

Lee, J. (2017) Perspectives on bioluminescence mechanisms. Photochem Photobiol 93:389−404.

Chapter 11 Dinoflagellate Bioluminescence: “Phosphorescence” in the Sea

Hastings J.W. (2009) Dinoflagellate bioluminescence and its circadian regulation. Photobiological Sciences Online (J Lee and KC Smith, eds.) American Society for Photobiology. http://www.photobiology.info/Hastings.html

Schultz, L. W., Liu, L., Cegielski, M., & Hastings, J. W. (2005). Crystal structure of a pH-regulated luciferase catalyzing the bioluminescent oxidation of an open tetrapyrrole. Proc Natl Acad Sci USA 102:1378−1383.

Chapter 12 Structural Biology

http://en.wikibooks.org/wiki/Structural_Biochemistry/Proteins/NMR_Spectroscopy

Table 2: http://ekhidna.biocenter.helsinki.fi/dali Holm L, Kaariainen S, Rosenstrom P, Schenkel A. (2008) Searching protein structure databases with DaliLite v.3. Bioinformatics 24:2780-2781.

Vervoort, J., Muller, F., Lee, J., Berg, W.A.M. van den, and Moonen, C.T.W. (1986) Identifications of the true carbon-13 nuclear magnetic resonance spectrum of the stable intermediate I1 in bacterial luciferase. Biochemistry 25:8062−8067.

Vervoort, J., Muller, F., O’Kane, D.J., Lee, J., and Bacher, A. (1986) Bacterial luciferase: A carbon- 13, nitrogen- 15, and phosphorus-31 nuclear magnetic resonance investigation. Biochemistry 25: 8067−8075.

Bergner, T., Tabib, C.R., Winkler, A., Stipsits, S., Kayer, H., Lee, J., Malthouse, P., Mayhew, S., Müller, F., Gruber, K., Macheroux, P. (2015) Structural and biochemical properties of LuxF from *Photobacterium leiognathi*. Biochim Biophys Acta 1854:1466–1475.

Malikova, N.P, Visser, N.V., Hoek, A. van, Skakun, V.V., Vysotski, E.S., Lee, J., and Visser, A.J.W.G. (2011) Green-fluorescent protein from the bioluminescent jellyfish *Clytia gregaria* is an obligate dimer and does not form a stable complex with the Ca^{2+}-discharged photoprotein clytin. Biochemistry 50:4232–4241.

Titushin, M.S., Feng, Y., Stepanyuk, G.A., Li, Y., Markova S.V., Golz, S., Wang, B-C., Lee, J., Wang J., Vysotski, E.S., and Liu, Z-J. (2010) NMR-derived topology of a GFP-photoprotein energy transfer complex. J Biol Chem 285:40891−40900.

Campbell, Z.T, Weichsel, A., Montfort, W.R., and Baldwin, T.O. (2009) Crystal structure of the bacterial luciferase/flavin complex provides insight into the function of the β subunit. Biochemistry 48:6085−6094.

Nakatsu, T., Ichiyama, S., Hiratake, J., Saldanha, A., Kobashi, N, Sakata, K., and Kato, H. (2006) Structural basis for the spectral difference in luciferase bioluminescence. Nature 440:372−376.

Lee, J., and Vysotski, E.S. (2011) Structure and Spectra in Bioluminescence, Photobiological Sciences Online (J Lee and KC Smith eds.) American Society for Photobiology, http://www.photobiology.info/Lee-Vysotski.html

Kheirabadi, M., Sharafian, Z., Naderi-Manesh, H., Heineman, U., Gohlke, U., Hosseinkhani, S. (2013) Crystal structure of native and a mutant of *Lampyris turkestanicus* luciferase implicate in bioluminescence color shift. Biochim Biophys Acta 1834:2729−2735.

Eremeeva, E.V., Berkel, W.J.H. van, and Vysotski, E.S. (2016) Transient-state kinetic analysis of complex formation between photoprotein clytin and GFP from jellyfish *Clytia gregaria*. FEBS Lett 590:307−316.

Chapter 13 The Antenna Proteins. Bioluminescence FRET

Lee, J. (1993) Lumazine protein and the excitation mechanism in bacterial bioluminescence. Biophys Chem 48:149−158.

Nemtseva, E.V., and Kudryasheva, N.S. (2007) The mechanism of electronic excitation in the bacterial bioluminescence reaction. Russian Chem Rev 76:1-100.

Titushin, M.S, Feng, Y., Lee, J., Vysotski, E.S., and Liu, Z-J. (2011) Protein-protein complexation in Bioluminescence. Protein & Cell 2:957–972.

Zimmer, M. (2011) Green fluorescent protein: A molecular microscope, Photobiological Sciences Online (J Lee and KC Smith eds.) American Society for Photobiology http://www.photobiology.info/Zimmer.html
http://www.conncoll.edu/ccacad/zimmer/GFP-ww/glowinggenes.html

Clegg, R.M. (2006) The History of FRET. In, *Reviews in Fluorescence* Vol. 3, (CD Geddes and JR Lakowicz, eds.) Chap. 1, pp. 1-45. Springer, New York..

http://www.photobiology.info/PDF/History%20of%20FRET.pdf

Haddock, S.D., and Dunn, C.W. (2015) Fluorescent proteins function as a prey attractant: experimental evidence from the hydromedusa Olindias formosus and othermarine organisms. Biol Open 4: 1094−1104. http://bio.biologists.org/content/4/9/1094.long

Eremeeva, E.V., Berkel, W.J.H. van, and Vysotski, E.S. (2016) Transient-state kinetic analysis of complex formation between photoprotein clytin and GFP from jellyfish *Clytia gregaria*. FEBS Lett 590:307–316.

Chapter 14. Computational Bioluminescence

Basic Introduction of Computational Chemistry. EMSL, Pacific NW National Laboratory. http://www.institute.loni.org/NWChem2012/documents/1_Basic_Introduction_of_Computational_Chemistry.pdf

Gozem, S., Melaccio, F., Luk, H.L., Rinaldi, S., and Olivucci, M. (2017) Learning from photobiology how to design molecular devices using a computer. Chem Soc Rev 43:4019−4036.

Ferrer, S., Ruiz-Pernia, J., Marti´, S., Moliner, V., Tuno´n, I., Bertra´n, J., and Andre´s, J. (2011) Hybrid schemes based on quantum mechanics/molecular mechanics simulations: goals to success, problems, and perspectives. Adv Protein Chem Struc Biol 85:81-142.

Allinger, N.L. (2011) Understanding molecular structure from molecular mechanics. J Comput Aided Mol Des 25:295−316.

Kamp, W. van der, and Mulholland, A.J. (2013) Combined quantum mechanics/molecular mechanics (QM/MM) methods in computational enzymology. Biochemistry 52:2708−2728.

Isobe, H., Yamanaka, S., Okumura, M., and Yamaguchi, K. (2009) Theoretical investigation of thermal decomposition of peroxidized coelenterazines with and without external perturbations. J Phys Chem A 113:15171–15187.

Morokuma, K. (2009) Theoretical studies of structure, function and reactivity of molecules. A personal account. Proc Jpn Acad, Ser B 85:167.

Navizet, I., Liu, Y-J., Nicolas Ferré, N., Roca-Sanjuán, D., and Lindh, R. (2011). The chemistry of bioluminescence: An analysis of chemical functionalities. ChemPhysChem 12:3064–3076.

Chen, S., Navizet, I., Lindh, R., Liu, Y., and Ferré, N. (2014) Hybrid QM/MM simulations of the obelin bioluminescence and fluorescence reveal an unexpected light emitter, J Phys Chem B 118:2896−2903.

Hou, C., Liu, Y.J., Ferré, N., and Fang, W.H. (2014) Understanding bacterial bioluminescence: a theoretical study of the entire process, from reduced flavin to light emission. Chemistry 20:7979–7986.

Luo, Y., and Liu Y-J. (2016) Bioluminophore and flavin mononucleotide fluorescence quenching of bacterial bioluminescence—A theoretical study. Chem Eur J 22:16243–16249.

Berraud-Pache, R., and Navizet, I. (2016) QM/MM calculations on a newly synthesized oxyluciferin substrate: new insights into the conformational effect. Phys Chem Chem Phys 18:27460−27467.

Yue, L., Lan, Z., and Liu.Y-J. (2015) The theoretical estimation of the bioluminescent efficiency of the firefly via a nonadiabatic molecular dynamics simulation. J Phys Chem Lett 6:540−548.

Ding, B-W., and Liu, Y-J. (2017) Bioluminescence of firefly squid via mechanism of single electron-transfer oxygenation and charge-transfer-induced luminescence. J Am Chem Soc 139:1106−1119.

Min, C-G., Silva, L.P.da, Silva, J.C.G. E. da, Yang, X-K., Huang, S-J., Ren, A-M, and Zhu,Y-Q. (2017) A computational investigation of the equilibrium constants for the fluorescent and chemiluminescent states of coelenteramide. ChemPhysChem 18:117–123.

Modeling software for chemists https://www.scm.com/

GAUSSIAN http://www.Gaussian.com/g_prod/g09.htm

16. Figure Attributions

Fig. 1.2. http://www.biotabiolum.ufscar.br/biota-biolum-project?set_language=en

Fig. 2.3. Spruit-van der Burg, A. (1950) Emission spectra of luminous bacteria. Biochim Biophys Acta 5:175-178.

Fig. 2.4. McElroy, W.D. (1947) The energy source for bioluminescence in an isolated system. Proc Natl Acad Sci USA 33:342−345.

Fig. 3.5. *Adapted from*: Shimomura, O. (2012) *Bioluminescence, Chemical Principles and Methods* (Revised Edition). World Scientific, Singapore.

Fig. 3.6. *Adapted from:* Petushkov, VN, Dubinnyi, MA, Tsarkova, AS, Rodionova, NS, Baranov, MS, Kublitski, VS, Shimomura, O, Yampolsky, IV. (2014) A Novel Type of Luciferin from the Siberian Luminous Earthworm *Fridericia heliota*: Structure Elucidation by Spectral Studies and Total Synthesis. Angew Chem Int Ed 53:5566−5568. DOI: 10.1002/anie.201400529

Fig. 4.3. Morin, J.G., and Hastings, J.W. (1971) Biochemistry of the bioluminescence of colonial hydroids and other coelenterates. J Cell Physiol 77:305−311.

Fig. 4.4. Markova, S.V., Vysotski, E.S., Blinks,| J.R., Burakova, L.P., B-C. Wang, and Lee, J. (2002) Obelin from the Bioluminescent Marine Hydroid *Obelia geniculata*: Cloning, Expression, and Comparison of Some Properties with Those of Other Ca^{2+}-Regulated Photoproteins. Biochemistry 41:2227−2236.

Fig. 4.5. McElroy, W.D., and Seliger, H.H. (1961) in *Light and Life* (WD McElroy and B Glass, eds.) p. 219. Johns Hopkins Press, Baltimore.

Figs. 4.6., 4.7. DeLuca, M., and McElroy, W.D. (1974) Kinetics of the Firefly Luciferase Catalyzed Reactions. Biochemistry 13:921−925.

Fig. 4.8. Denburg, J.L., Lee, R.T., and McElroy, W.D. (1969) Substrate-binding properties of firefly luciferase 1. Luciferin-binding site. Arch Biochem Biophys 134:381−394.

Fig. 4.9. Denburg, J.L., and McElroy, W.D. (1970) Catalytic Subunit of Firefly Luciferase. Biochemistry 9:4619−4624.

Fig. 4.10. Hastings, J.W., and Gibson, Q.H. (1963) Intermediates in the bioluminescent oxidation of reduced flavin mononucleotide. J Biol Chem 238:2537−2554.

Fig. 4.11. Becvar, J.E., and Hastings, J.W. (1975) Bacterial luciferase requires one reduced flavin for light emission. Proc Natl Acad Sci USA 72:3374−3376.

Figs. 4.12., 4.13. Matheson, I.B.C., and Lee, J. (1983) Kinetics of bacterial bioluminescence and the fluorescent transient. Photochem Photobiol 38:231−240.

Fig. 4.14. Suadee, C., Nijvipakul1, S., Svasti1, J., Entsch B., Ballou, D.P., and Chaiyen, P. (2007) Luciferase from *Vibrio campbellii* is more thermostable and binds reduced FMN better than its homologues. J Biochem 142:539−552.

Fig. 4.15. Kurfurst, M., Ghisla, S., and Hastings, J.W. (1984) Characterization and postulated structure of the primary emitter in the bacterial luciferase reaction. Proc Natl Acad Sci USA 81:2990−2994.

Fig. 5.2. Seliger, H.H., and McElroy, W.D. (1960) Spectral emission and quantum yield of firefly bioluminescence. Arch Biochem Biophys 88:136−141.

Fig. 5.3. Lee, J., and Seliger, H.H. (1965) Absolute spectral sensitivity of phototubes and the application to the measurement of the absolute quantum yields of chemiluminescence and bioluminescence. Photochem Photobiol 4:1015−1048.

Fig. 5.4. Cormier, M.J., and Totter, J.R. (1957) Quantum efficiency determinations on components of the bacterial luminescence system. Biochem Biophys Acta 5:229−237.

Fig. 5.5. Niwa, K., Ichino, Y., and Ohmiya, Y. (2010) Quantum yield measurements of firefly bioluminescence reactions using a commercial luminometer. Chem Lett 39:291−293.

Figs. 6.1, 6.3, 6.4. Visser, A.J.W.G., and Rolinski, O.J. (2010) Photobiological Sciences Online (J Lee and KC Smith, eds.) American Society for Photobiology. http://www.photobiology.info/Visser-Rolinski.html

Fig. 6.8. Visser, A.J.W.G, and Lee, J. (1980) Lumazine Protein from the bioluminescent bacterium *Photobacterium phosphoreum.* A fluorescence study of the protein-ligand equilibrium. Biochemistry 19:4366−4372.

Fig. 6.9. Hirano, T., Hasumi, Y., Ohtsuka, K., Maki, S., Niwa, H., Yamaji, M., and Hashizume, D. (2009) Spectroscopic studies of the light-color modulation mechanism of firefly (beetle) bioluminescence. J Am Chem Soc 131:2385−2396.

Fig. 6.16. Lee, J., O'Kane, D.J., and Visser, A.J.W.G. (1985) Spectral Properties and Function of Two Lumazine Proteins from *Photobacterium.* Biochemistry 24:1476−1483.

Figs. 7.3., 7.9., 7.12. McCapra, F. (2000) Chemical generation of excited states. The basis for chemiluminescence and bioluminescence. Methods Enzymol 305:3−47.

Figs. 7.4., 7.5. *Adapted from*: Bos, R., Barnett, N.W., Dyson, G.A., Lim, K.F., Russell, R.A., and Watson, S.P. (2004) Studies on the mechanism of the peroxyoxalate chemiluminescence reaction Part 1. Confirmation of 1,2-dioxetanedione as an intermediate using ^{13}C nuclear magnetic resonance spectroscopy. Anal Chim Acta 502:141−147.

Figs. 7.6., **7.7.** *Adapted from*: Tonkin, S.A., Bos, R., Dyson, G.A., Lim, K.F., Russell, R.A., Watson, S.P., Hindson, C.M., and Barnett, N.W. (2008) Studies on the mechanism of the peroxyoxalate chemiluminescence reaction. Part 2. Further identification of intermediates using 2D EXSY ^{13}C nuclear magnetic resonance spectroscopy. Anal Chim Acta 614:173−181.

Fig. 7.8. Ciscato, L.F.M.L., Bartoloni, F.H., Bastos, E.L., and Baader, W.J. (2009) Direct Kinetics Observation of the Chemiexcitation Step in Peroxyoxalate Chemiluminescence. J Org Chem 74:8974−8979.

Fig. 7.10. *Adapted from*: Matsumoto, M., Sakuma, T., and Watanabe, N. (2002) Synthesis of bicyclic dioxetanes bearing a 3-hydroxy-4-isoxazolylphenyl moiety: new CIEEL-active dioxetanes emitting light with remarkable high-efficiency in aqueous medium. Tetrahedron Lett 43:8955−8958.

Figs. 7.11., 7.14. Baader, W.J., Stevani, C.V., and Bastos, E.L. (2009) Chemiluminescence of Organic Peroxides. In, *PATAI's Chemistry of Functional Groups*, pp.1−68. John Wiley, NY.

Fig. 7.15. *Adapted from:* Schaap, A.P., Handley, R.S., and Giri, B.P. (1987) Chemical and enzymatic triggering of 1,2-dioxetanes. Tetrahedron Lett 28:935−938.

Figs. 7.16., 7.17., 7.18. *Adapted from:* Matsumoto, M. (2004) Advanced chemistry of dioxetane-based chemiluminescent substrates originating from bioluminescence. J Photochem Photobiol C: Photochem Rev 5

Fig. 7.19. Watanabe, N., Mizuno, T., and Matsumoto M. (2005) Intramolecular charge-transfer-induced chemiluminescent decomposition of 1,2-dioxetanes bearing a phenylmethanide anion. Tetrahedron 61:9569-9585.

Figs. 7.21.,7.22. *Adapted from*: Matsumoto, M., Watanabe, N., Hoshiya, N., and Ijuin, H.K. (2008) Color Modulation for Intramolecular Charge-Transfer-Induced Chemiluminescence of 1,2-Dioxetanes. Chem Rec 8:213-228.

Fig. 7.23. Matsumoto, M., Suzuki, H., Watanabe, N., Ijuin, H.K., Tanaka, J., and Tanaka, C. (2011) Crucial Dependence of Chemiluminescence Efficiency on the Syn/Anti Conformation for Intramolecular Charge-Transfer-Induced Decomposition of Bicyclic Dioxetanes Bearing an Oxidoaryl Group. J Org Chem 76:5006-5017.

Fig. 7.24. *Adapted from*: Tanimura, M., Watanabe, N., Ijuin, H.K., and Matsumoto, M. (2011) Intramolecular Charge-Transfer-Induced Decomposition

Promoted by an Aprotic Polar Solvent for Bicyclic Dioxetanes Bearing a 4-(Benzothiazol-2-yl)-3-hydroxyphenyl Moiety. J Org Chem 76:902−908.

Fig. 7.25. Ciscato, Luiz F. M. L., Bartoloni, F.H, Weiss, D., Beckert, R., and Baader W.J. (2010) Experimental Evidence of the Occurrence of Intramolecular Electron Transfer in Catalyzed 1,2-Dioxetane Decomposition. J Org Chem 75:6574-6580.

Fig. 8.3. Tanaka, E, Kuse, M, Nishikawa, T. (2009) Dehydrocoelenterazine is the Organic Substance Constituting the Prosthetic Group of Pholasin. ChemBioChem 10:2725-2729.

Fig. 8.5. Gunderman, K-D., and McCapra, F. (1987) *Chemiluminescence in Organic Chemistry*. Springer-Verlag, Berlin.

Fig. 8.6. *Adapted from:* Eymers, J.G., and van Schouwenburg, K.L. (1937) Enzymologia 3: 235.

Fig. 8.7. *Adapted from:* Goto, T., Inoue, S., Sugiura, S., Nishikawa, K., Isobe, M., and Abe, Y. (1968) Cypridina bioluminescence V. Structure of emitting species and its related compounds in the luminescence of Cypridina luciferin. Tetrahedron Lett 1968:4035-4038.

Fig. 8.8. *Adapted from:* Usami, K., and Isobe, M. (1996) Low temperature oxidation of coelenterate luciferin analog. Synthesis and proof of a 1,2-dioxetanone as a luminescence intermediate. Tetrahedron 52:12061−12090.

Fig. 8.9. (*Right panel*) Morin, J.G., and Hastings, J.W. (1971) Energy transfer in a bioluminescent system. J Cell Physiol 77:314−318.

Fig. 8.9. Ward, W.W., and Cormier, M.J. (1976) In Vitro Energy Transfer in *Renilla* Bioluminescence. J Phys Chem 80:2289−2221.

Fig. 8.11. Titushin, M.S., Markova, S.V., Frank, L.A., Malikova, N.P., Stepanyuk, G.A., Lee, J., and Vysotski, E.S. (2008) Coelenterazine-binding protein of *Renilla muelleri*: cDNA cloning, overexpression, and characterization as a substrate of luciferase. Photochem Photobiol Sci 7:189−196.

Fig. 8.14. Markova, S.V., Vysotski, E.S., Blinks, J.R., Burakova, L.P., Wang, B-C., and Lee J. (2002) Obelin from the Bioluminescent Marine Hydroid *Obelia geniculata*: Cloning, Expression, and Comparison of Some Properties with Those of Other Ca^{2+}-Regulated Photoproteins. Biochemistry 41:2227-2236.

Fig. 8.15. Illarionov, B.A., Frank, L.A., Illarionova, V.A., Bondar, V.S., Vysotski, E.S., and Blinks, J.R. (2000) Recombinant Obelin: Cloning and expression of cDNA, Purification, and Characterization as a Calcium Indicator. Meth Enzymol 305:223−249.

Fig. 9.1. Seliger, H.H., Lall, A.B., Lloyd, J.E., and Biggley, W.H. (1982) The colors of firefly bioluminescence-II. Experimental evidence for the optimization model. Photochem Photobiol 36:681−688.

Fig. 9.2. Table 1. Niwa, K., Ichino, Y., Kumata, S., Nakajima, Y., Hiraishi Y., Kato D., Viviani, V.R., and Ohmiya, Y. (2010) Quantum Yields and Kinetics of the Firefly Bioluminescence Reaction of Beetle Luciferases. Photochem Photobiol 86:1046-1049.

Fig. 9.3. Seliger, H.H., and McElroy, W.D. (1964) The colors of firefly bioluminescence: Enzyme configuration and species specificity. Proc Natl Acad Sci USA 52:75−81.

Fig. 9.4. *Adapted from:* Branchini, B.R., Southworth, T.L., Fontaine, D.M., Murtiashaw, M.H., McGurk, A., Talukder, M.H., Qureshi, R., Yetil, D., Sundlov, J.A., and Gulick, A.M. (2017) Cloning of the orange light-producing luciferase from *Photinus scintillans*−A new proposal on how bioluminescence color is determined. Photochem Photobiol 93: 479−485.

Fig. 9.7. Branchini, B.R., Behney, C.E., Southworth, T.L., Fontaine, D.M., Gulick, A.M., Vinyard, D.J., and Brudvig, G.W. (2015) Experimental Support for a Single Electron-Transfer Oxidation Mechanism in Firefly Bioluminescence. J Am Chem Soc 137:7592−7595.

Figs. 9.9., 9.10., 9.15. *Adapted from:* Naumov, P., Ozawa, Y., Ohkubo, K., and Fukuzumi, S. (2009) Structure and Spectroscopy of Oxyluciferin, the Light Emitter of the Firefly Bioluminescence. J Am Chem Soc 131:11590-11605.

Fig. 9.11. White, E.H., Rapaport, E., Seliger, H.H., and Hopkins, T.A. (1971) The chemi- and bioluminescence of firefly luciferin: An efficient chemical production of electronically excited states. Bioorg Chem 1:92-122.

Fig. 9.12. Branchini, B.R, Southworth, T.L., Murtiashaw, M.H., Magyar, R.A., Gonzalez, S.A., Ruggiero, M.C., and Stroh, J.C. (2004) An Alternative Mechanism of Bioluminescence Color Determination in Firefly Luciferase. Biochemistry 43:7255−7262.

Figs. 9.13., 9.14. Hirano, T., Hasumi, Y., Ohtsuka, K., Maki, S., Niwa, H., Yamaji, M., and Hashizume, D. (2009) Spectroscopic Studies of the Light-Color Modulation Mechanism of Firefly (Beetle) Bioluminescence. J Am Chem Soc 131: 2385-2396.

Fig. 10.1. Daubner, S.C., Astorga, A.M., Leisman, G.B., and Baldwin, T.O. (1987) Yellow light emission of *Vibrio fischeri* strain Y-1: Purification and characterization of the energy-accepting yellow fluorescent protein. Proc Natl Acad. Sci USA 84:8912-8916.

Fig. 10.3. *Adapted from:* McCapra, F. (2000) Chemical generation of excited states. The basis for chemiluminescence and bioluminescence. Methods Enzymol 305:3-47.

Figs. 11.1., 11.3., 11.6. Hastings, J.W. (2009) Dinoflagellate bioluminescence and its circadian regulation, Photobiological Sciences Online (J Lee and KC Smith, eds.) American Society for Photobiology.
http://www.photobiology.info/Hastings.html

Figs. 11.4., 11.5. L. Schultz, L.W., Liu, L., Cegielski, M, and Hastings J.W. (2005) Crystal structure of a pH-regulated luciferase catalyzing the bioluminescent oxidation of an open tetrapyrrole. Proc Natl Acad Sci USA 102:1378-1383.

Fig. 12.3. Vervoort, J., Müller, F., LeGall, J., Bacher, A., and Sedlmaier, H. (1985) Carbon-13 and nitrogen-15 nuclear-magnetic-resonance investigation on *Desulfovibrio vulgaris* flavodoxin. Eur J Biochem 151:49−57.

Fig. 12.4. Vervoort, J., O'Kane, D.J, Müller, F., Bacher, A., Strob1, G., and Lee, J. (1990) ^{13}C and ^{15}N NMR Studies on the Interaction between 6,7-Dimethyl-8-ribityllumazine and Lumazine Protein. Biochemistry 29:1828−1823.

Fig. 12.5. Musicki, B., Kishi, Y., and Shimomura, O. (1986) Structure of the Functional Part of Photoprotein Aequorin. J Chem Soc, Chem Commun 1986:1566-1568.

Figs. 12.6., 12.7., 12.8. Vervoort, J., Muller, F., O'Kane, D.J., Lee, J. and Bacher, A. (1986) Bacterial Luciferase: A Carbon-13, Nitrogen-15, and Phosphorus-31 Nuclear Magnetic Resonance Investigation. Biochemistry 25:8067−8075.

Fig. 12.9., 12.10. *Adapted from:* Lee, J., Matheson, I.B.C., Müller, F., O'Kane, D.J., Vervoort, J., and Visser, A.J.W.G. (1991) The mechanism of bacterial bioluminescence. In (F Müller, ed.), *Chemistry and Biochemistry of Flavoenzymes*, Vol. 2. Pp.110-147. CRC Press, Boca Raton.

Fig. 12.12. Ohashi, W., Inouye, S., Yamazaki, T., and Hirota, H. (2005) NMR Analysis of the Mg^{2+}-Binding Properties of Aequorin, a Ca^{2+}-Binding Photoprotein. J Biochem 138:613–620.

Figs. 12.15., 12.16, 12.19., 12.21. *Adapted from:* Vysotski, E.S., and Lee, J. (2007) Bioluminescent mechanism of Ca^{2+}-regulated photoproteins from three-dimensional structures. In, *Luciferases and Fluorescent proteins: Principles and Advances in Biotechnology and Bioimaging*. (VR Viviani, and Y Ohmiya, eds.) pp. 19−41. Transworld Research Network, Kerala, India.

Fig. 12.17. Vysotski, E.S., and Lee, J. (2004) Ca^{2+}-regulated photoproteins: structural insight into the bioluminescence mechanism. Acc Chem Res 37:405-415. **Fig. 12.18.** *Adapted from:* Liu, Z-J., Vysotski, E.S, Deng, L., Lee, J., Rose, J., and Wang, B-C. (2003) Atomic resolution structure of obelin: soaking with calcium enhances electron density of the second oxygen atom substituted at the C2-position of coelenterazine. Biochem Biophys Res Commun 311:433−439.

Fig. 12.20. *Adapted from*: Deng, L., Vysotski, E.S., Markova, S.V., Liu, Z-J., Lee, J., Rose, J., and Wang, B-C. (2005) All three Ca^{2+}-binding loops of photoproteins bind calcium ions: The crystal structures of calcium-loaded apo-aequorin and apo-obelin. Protein Sci 14:663−675.

Fig. 12.21. Stepanyuk, G.A., Golz S., Markova, S.V., Frank, L.A., Lee, J., and Vysotski, E.S. (2005) Interchange of aequorin and obelin bioluminescence color is determined by substitution of one active site residue of each photoprotein. FEBS Lett 579:1008-1014.

Figs. 12.25., 12.27., 12.28., 12.32. Titushin, M.S., Feng, Y., Stepanyuk, G.A., Li, Y., Markova, S.V., Golz, S., Wang, B-C., Lee, J., Wang, J., Vysotski, E.S, and Liu, Z-J. (2010) NMR-derived Topology of a GFP-photoprotein Energy Transfer Complex. J Biol Chem 285:40891−40900 (*Supplementary Information*).

Fig. 12.26. Titushin, M.S, Feng, Y., Lee, J., Vysotski, E.S., and Liu, Z-J. (2011) Protein-protein complexation in Bioluminescence. Protein & Cell 2:957−972.

Figs. 12.29., 12.30. Campbell, Z.T, Weichsel, A., Montfort, W.R., and Baldwin, T.O. (2009) Crystal Structure of the Bacterial Luciferase/Flavin Complex Provides Insight into the Function of the β Subunit. Biochemistry 48:6085−6094.

Fig. 12.31. Li, L., Liu, X., Yang, W., Xu, F., Wang, W., Feng, L., Bartlam, M., Wang, L., and Rao, Z. (2008) Crystal Structure of Long-Chain Alkane Monooxygenase (LadA) in Complex with Coenzyme FMN: Unveiling the Long-Chain Alkane Hydroxylase. J Mol Biol 376:453−465.

Figs. 12.32, 12.33.12.34. *Adapted from*: Sato, Y., Shimizu, S., Ohtaki, A., Noguchi, K., Miyatake, H., Dohmae, N., Sasaki, S., Odaka, M., and Yohda, M. (2010) Crystal Structures of the Lumazine Protein from *Photobacterium kishitanii* in Complexes with the Authentic Chromophore, 6,7-Dimethyl-8-(1-D-Ribityl) Lumazine, and Its Analogues, Riboflavin and Flavin Mononucleotide, at High Resolution. J Bacteriol 192:127-133.

Figs. 12.35., 12.36., 12.37. Sundlov, J.A., Fontaine, D.M, Southworth, T.L., Branchini, B.R., and Gulick, A.M. (2012) Crystal Structure of Firefly Luciferase in a Second Catalytic Conformation Supports a Domain Alternation Mechanism. Biochemistry 51:6493-6495.

Fig. 12.38. Nakatsu, T., Ichiyama, S., Hiratake, J., Saldanha, A., Kobashi, N, Sakata, K., and Kato, H. (2006) Structural basis for the spectral difference in luciferase bioluminescence. Nature 440:372-376.

Fig. 13.1. Lee, J. (1982) Sensitization by lumazine proteins of the bioluminescence emission from the reaction of bacterial luciferases. Photochem Photobiol 36:689−697.

Fig. 13.2. O'Kane, D.J., Karle, V.A., and Lee. J. (1985) Purification of Lumazine Proteins from *Photobacterium Leiognathi* and *Photobacterium phosphoreum*: Bioluminescence Properties. Biochemistry 24:1461−1467.

Fig. 13.4. Visser, A.J.W.G., and Lee, J. (1980) Lumazine Protein from the Bioluminescent Bacterium *Photobacterium phosphoreum.* A Fluorescence Study of the Protein-Ligand Equilibrium. Biochemistry 19:4366−4372.

Fig. 13.5. Visser, A.J.W.G., and Lee, J. (1982) Association between Lumazine Protein and Bacterial Luciferase: Direct Demonstration from the Decay of the Lumazine Emission Anisotropy. Biochemistry 21:2218−2226.

Fig. 13.6. Lee, J., O'Kane, D.J., and Gibson, B.G. (1988) Dynamic fluorescence properties of bacterial luciferase intermediates. Biochemistry 27:4862-4870.

Fig. 13.7. Lee, J., Wang, Y., and Gibson, B.G. (1991) Fluorescence anisotropy decay study of self association of bacterial luciferase intermediates. J Fluor 1:23−29.

Fig. 13.8. Titushin, M.S, Feng, Y., Lee, J., Vysotski, E.S., Liu, Z-J. (2011) Protein-protein complexation in Bioluminescence. Protein & Cell 2:957-972. This research was originally published by Titushin, M.S., Y. Feng, G.A. Stepanyuk, Y. Li, S.V. Markova, S. Golz, B-C. Wang, J. Lee, J. Wang, E.S. Vysotski and Z-J. Liu. NMR-derived topology of a GFP-photoprotein energy transfer complex, in the Journal of Biological Chemistry. 2010, 285: 40891–40900.

Fig. 13.9. Lee, J., Wang, Y., and Gibson, B.G. (1991) Electronic Excitation Transfer in the Complex of Lumazine Protein with Bacterial Bioluminescence Intermediates. Biochemistry 30:6825−6835.

Fig. 13.10. Visser, A.J.W.G., and Rolinski, O.J. (2017) Basic Photophysics. Photobiological Sciences Online (J Lee and KC Smith, eds.) American Society for Photobiology. http://www.photobiology.info/Visser-Rolinski.html

Fig. 13.11. Petushkov, V.P., Gibson, B.G., and Lee, J. (1996) Direct Measurement of Excitation Transfer in the Protein Complex of Bacterial Luciferase Hydroxyflavin and the Associated Yellow Fluorescence Proteins from *Vibrio fischeri* Y1. Biochemistry 35:8413−8418.

Fig. 13.13. Markova, S.V., Burakova, L.P., Frank, L.A., Golz, S., Korostileva, K.A., and Vysotski, E.S. (2010) Green-fluorescent protein from the bioluminescent jellyfish *Clytia gregaria*: cDNA cloning, expression, and characterization of novel recombinant protein. Photochem Photobiol Sci 9:757−765.

Figs. 13.14., 13.15. Malikova, N.P., Visser, N.V., Hoek, A. van, Skakun, V.V., Vysotski, E.S., Lee, J., and Visser, A.J.W.G. (2011) Green-Fluorescent Protein from the Bioluminescent Jellyfish *Clytia gregaria* Is an Obligate Dimer and Does Not Form a Stable Complex with the Ca^{+2}-Discharged Photoprotein Clytin. Biochemistry 50:4232–4241.

Fig. 14.1. Isobe, H., Yamanaka, S., Kuramitsu, S., Yamaguchi, K. (2008) Regulation Mechanism of Spin-Orbit Coupling in Charge-Transfer-Induced Luminescence of Imidazopyrazinone Derivatives. J Am Chem Soc 130:132−149.

Fig. 14.3. Roca-Sanjuan, D., Delcey, M.G., Navizet, I., Ferré, N., Li, Y-J., and Lindh, R. (2011) Chemiluminescence and Fluorescence States of a Small Model for Coelenteramide and Cypridina Oxyluciferin: A CASSCF/CASPT2 Study. J Chem Theory Comput 7:4060−4069.

Fig. 14.4. *Adapted from:* Chen, S., Navizet, I., Lindh, R., Liu, Y., and Ferré, N. (2014) Hybrid QM/MM Simulations of the Obelin Bioluminescence and Fluorescence Reveal an Unexpected Light Emitter. J Phys Chem B 118:2896−2903.

Fig. 14.5. Isobe, H., Yamanaka, S., Okumura, M., and Yamaguchi, K. (2009) Theoretical Investigation of Thermal Decomposition of Peroxidized Coelenterazines with and without External Perturbations. J Phys Chem A 113:15171−15187.

Fig. 14.6., 14.7. *Adapted from:* Chen, S., Ferré, N., Liu, Y. (2013) QM/MM Study on the Light Emitters of Aequorin Chemiluminescence, Bioluminescence, and Fluorescence: A General Understanding of the Bioluminescence of Several Marine Organisms. Chemistry 19:8466−8472.

18. AFTERWORD

This Book

One purpose of writing this as an e-book is to supplement a 5-video lecture course available at http://tube.sfu-kras.ru/video/1134/. As the book is open access it can readily be updated from time to time. This present version is dated May, 2017. A valuable on-line resource is *Photobiological Sciences On-line*, www.photobiology.info which covers the broad field of Photobiology and includes several modules on Bioluminescence. The book by Wilson and Hastings, *Bioluminescence: Living Lights, Lights for Living*, is highly recommended for an undergraduate text having particular emphasis on the Biology and Applications of bioluminescent systems. An extensive coverage of chemistry foundations as well as a great source of references can be found in the Shimomura book, *Bioluminescence, Chemical Principles and Methods*.

Bioluminescence is a very old science, the first written reports being from the Ancient Greeks. One theme emphasized in the present book is to show that progress in this field as well as for Science in general, the particular example being for understanding of this natural phenomenon of Bioluminescence, has been heavily driven by advancements in technology. First in the 17th Century were the inventions of the air

pump and the microscope. Later improvement in optics led to accuracy in spectroscopic measurements. The invention of the phototube and the photomultiplier less than 75 years ago, enabled quantitative measurements of bioluminescence. More recently, the methods of structural biology have given great insight into bioluminescence mechanisms. Dynamic processes have also been revealed using laser spectroscopy. The focus of this book is on Biophysics complementing the recent books more relevant to Biology and Chemistry mentioned above.

The Author

John Lee (b. 1935, Sydney, Australia) graduated from the University of New South Wales, B.Sc. (H1) in 1956, and Ph.D. in 1960, in the field of Nuclear Chemistry, the dissertation being published as "Positronium Chemistry" (1965) James Green and John Lee. Academic Press, NY.

In 1961 he took a position as Research Associate at Johns Hopkins University, Baltimore USA, and commenced investigation in the field of Bioluminescence under the tutelage of Howard H. Seliger. In 1969 he received an appointment in the Department of Biochemistry, University of Georgia, USA, and continued until 2006 retiring as Professor Emeritus (Biochemistry and Molecular Biology). Additional periods (1978-2012) were spent as a visiting scientist for research collaboration at Wageningen University, The Netherlands, The Siberian Federal University and Russian Academy of Science (Siberian Branch), Krasnoyarsk, Russian Federation, and the University of Sydney and Macquarie University, Australia. For 2000−2002 he served as President of the International Society for Bioluminescence and Chemiluminescence and currently is Co-Editor of Photobiological Sciences Online www.photobiology.info.